University of Glasgow

Peak Shaving Potential Using a Novel Flexible Two-Stage Heat Pump for Heating and Cooling

Thesis by
Narges Hassani Mokarram

Submitted in fulfilment of the requirements for the degree of Doctor of Philosophy at the University of Glasgow

James Watt School of Engineering
Systems, Power and Energy Research Division
University of Glasgow

May 2025

Abstract

Developing net-zero emission buildings is crucial, as the building sector is responsible for significant global energy consumption and greenhouse gas emissions. Governors have set a carbon-neutral target for 2050, mandating that all new constructions achieve net-zero emissions. This study introduces a thermal energy storage system integrated with a two-stage heat pump in a novel configuration, as heat pumps are considered a viable alternative to gas boilers.

The innovative, flexible two-stage heat pump has been analysed and compared with a baseline two-stage heat pump, as well as with both flexible and baseline single-stage heat pumps, under the same operating conditions. A control strategy was formulated based on heating duty, time of day, and storage tank status to enable the system to function in four different modes: 1) Normal operation, 2) Charging, 3) Discharging, and 4) Standby (Off). The weather data for heating systems in Glasgow and Birmingham, UK, were utilised to obtain variable hourly heating loads for a typical four-story residential building through IESVE software. A sinusoidal daily heating load profile was created to investigate the effect of heating load shape, maintaining the same maximum duty as the variable load derived from IESVE software. All proposed flexible cycles are named 1st configuration - *config. 1*, and the second flexible cycle in each model is named second configuration - *config. 2*.

Results indicate that the flexible two-stage system exhibits a 1.67% higher seasonal coefficient of performance (SCOP) with real variable loads and a 5.31% increase with sinusoidal loads. Furthermore, while the maximum price cut achieved was 2.1% with sinusoidal loads, the price reduction for real variable loads was less significant.

Additionally, this thesis introduces and thoroughly examines the novel configuration of the flexible two-stage heat pump system for cooling applications. Under identical operating conditions as far as possible, a baseline two-stage heat pump, a comparable flexible single-stage heat pump, and a second configuration of a flexible two-stage heat pump were compared and analysed alongside the newly proposed flexible two-stage heat pump. A control strategy was established to operate the system in four modes, normal operation, charging, discharging, and standby, based on cooling duty, time of day, and the status of storage tanks. Weather data for London/UK, and Rome/Italy, were used to acquire variable hourly cooling loads for a typical four-story residential building via IESVE software. The findings show that the flexible two-stage and single-stage systems achieved SCOP equal to

2.33% and 2.55% higher, respectively. Additionally, the heat pump demonstrated a higher SCOP and better flexibility in milder weather conditions, such as those in London, compared to Rome. Overall, the newly proposed system in this study shows superior performance compared to other similar heat pump systems.

In the third phase of this thesis, a techno-economic analysis was conducted on the two-stage flexible heat pump. An Al-extruded tube micro-channel evaporator and a corresponding condenser were designed for this system. The techno-economic analysis included calculating various economic parameters to assess the system's feasibility. Results indicate the system's economic viability, supported by calculated metrics such as Annual Profit (AP), Net Present Value (NPV), Period Payback (PP), Internal Rate of Return (IRR), and Multiple on Invested Capital (MOIC). The Al-extruded tube micro-channel heat exchangers achieved heat transfer rates of 106.28 kW for condenser and 76.34 kW for evaporator, with overall heat transfer coefficients of 1,790.8 W/m^2K and 1,011.8 $W.m^{-2}.K^{-1}$, respectively. The system demonstrates economic feasibility, with an NPV of £177,903, an IRR of 16.4%, and a payback period of 7.8 years. The total capital investment for 40 flats amounts to £163,880, yielding a MOIC of 2.08.

List of publications extracted from this thesis:

Published Journal Papers:

1. "Investigation on the peak shaving potential of a new flexible two-stage heat pump for Cooling"
   Narges H. Mokarram, Yiji Lu, Zhichao Zhang, Zhibin Yu (2025),
   Renewable Energy, Latest impact factor: 9.0.
   https://doi.org/10.1016/j.renene.2025.122882.
2. "Peak-shaving investigation of a novel flexible two-stage heat pump for heating"
   Narges H. Mokarram, Yiji Lu, Zhibin Yu (2025),
   Energy Conversion and Management, Latest impact factor: 9.9.
   https://doi.org/10.1016/j.enconman.2024.119236.

Submitted Journal Paper, currently under review:

3. Heat exchanger design and Techno-economic analysis of a two-stage flexible heat pump with thermal storage tank
   Narges H. Mokarram, Zhichao Zhang, Yiji Lu

Conference paper:

1. "Peak shaving feasibility investigation in a novel flexible two-stage heat pump for heating application", 1st International Conference on Net Zero Carbon Built Environment (ZCBE), 3rd to 5th July 2024, Nottingham University, Nottingham, UK.

Table of Contents

List of Tables

List of Figures

Acknowledgement

First and foremost, I would like to express my deepest gratitude to my former supervisor, Professor Zhibin Yu, for giving me the incredible opportunity to pursue my research and for supporting me through a school scholarship. I'm honoured by his offer, which opened a door for me to begin a new chapter of life in a different country, surrounded by a culture and academic environment that have deeply enriched my personal and professional growth. As someone deeply passionate about thermodynamics, having the chance to study at University of Glasgow - the historic birthplace of this field- has been nothing short of a dream come true.

Moving to the UK as a migrant from a different culture brought with it a unique set of challenges. The early days were often filled with self-doubt, homesickness, and moments of contradictory feelings. Yet, every struggle became part of the transformative process that shaped me, both as a researcher and as a person. I learned resilience, grew in confidence, and found my voice in a space far from home. This journey has taught me that dreams do not come easy, but with perseverance and the right support, they are indeed attainable.

After Professor Yu's departure from the university, I was fortunate to receive the guidance and support of Dr. Yiji Lu. I am sincerely grateful to Dr. Lu for stepping in with such dedication and care. His mentorship offered clarity, encouragement, and belief in my potential when I needed it most.

I am also immensely thankful to the University of Glasgow for providing a vibrant community, an inspiring atmosphere, and the beauty of a historic campus that became a true home away from home. The friendships that I formed and even lost here; all the bitterness and sweetness have fortified my inner strength during these years. Thank you to my fellow researchers and friends, who shared celebratory milestones, and everyday conversations that brightened even the hardest days.

To my beloved family in Iran, your unwavering love and belief in me have been a constant source of strength. Though miles away, your presence has been felt every step of the way. Your support has kept me grounded and motivated.

And finally, my heartfelt thanks go to the love of my life, David. Thank you for standing by me with patience, kindness, and boundless support through every challenge. Your love was my anchor when I doubted myself, and for that, I am endlessly grateful.

In the end, I humbly dedicate this research to Fariba and Sadegh, my Mom and Dad, the symbol of resilience, bravery and dedication in my life.

Author’s Declaration

Hereby, I certify that, unless noted otherwise, the thesis I have submitted for review towards the Doctor of Philosophy (PhD) degree from the University of Glasgow is entirely original with all contributions from others properly identified and acknowledged. I attest that this thesis has not been submitted, in whole or in part, for consideration towards another degree at this or any other institution. Furthermore, I affirm that I, the author, own the copyright to this thesis and that no quotation from it may be used without my express permission.

I confirm that the work was completed in compliance with the University of Glasgow's Code of Good Practice in Research. I certify that, where applicable, any co-authored material that was included into the thesis has been appropriately cited, and that no third party has altered this thesis in any way that goes beyond what is allowed by the University's PGR Code of Practice. I am aware that by submitting this thesis, I consent to its electronic deposit in the University of Glasgow Library through the Enlighten repository, and that it may be made publicly available in compliance with university policies.

Nomenclature

Parameter	*Explanation*	*Unit*
A	*area*	m^2
A_{cs}	*cross-sectional area*	m^2
A_{flow}	*Free flow cross-sectional area of air*	m^2
AP	*annual profit*	£
Bo	*boiling number* $Bo = \frac{\ddot{Q}}{\dot{m}_{ref} h_{fg}}$	-
C	*coefficient in the Lockhart–Martinelli parameter*	-
$\dot{C}_{CI}$	*Capital investment cost rate*	£ s^{-1}
c_{heat}	*Unit price of heat*	$p.Kwh^{-1}$
CRF	*Capital recovery factor*	-
comp	*Compressor*	-
Cond	*Condenser*	-
c	*hourly unit cost of electricity*	*Pence per hour*
c_P	*Specific heat at constant pressure*	$kJ.kg^{-1}.K^{-1}$
duty	*cooling duty of the system*	*kW*
D_h	*hydraulic diameter*	*m*
Diff	*Percentage Difference*	-
EXP	*Expansion valve*	-
evap.	*Evaporator in schematic figures*	-
G	*mass flux*	$kg\ s^{-1}$
h	*specific enthalpy*	$kJ\ kg^{-1}$
h_{fg}	*latent heat of vaporisation*	$kJ\ kg^{-1}$
h_{tp}	*Two-phase heat transfer coefficient*	$W\ m^{-2}K^{-1}$
H	*Height*	*m*
h	*specific Enthalpy*	$kJ.kg^{-1}$
i	*index*	-
i	*Nominal interest rate*	%
IRR	*Internal rate of return*	%
j	*J Colbourn factor*	-
K	*thermal conductivity*	$W\ m^{-1}K^{-1}$
L	*length*	*m*
L_C	*corrected fin length*	*M*
LMTD ΔT_{ln}	*logarithmic mean temperature difference*	-
L_{fus}	*fusion energy- energy needed to melt*	$kJ.kg^{-1}$
$m/\dot{m}$	*mass/Mass flow rate*	$kg/kg\ s^{-1}$
MOIC	*multiple of investment capital*	-
N	*system lifetime*	*Year*
N	*Number of (tubes, channels)*	-
NPV	*net present value*	£
N_{ch}	*Number of channels per tube*	-
N_{fin}	*number of fins*	-
N_{tube}	*number of Al-Extruded tubes*	-
n	*hours of the season*	*h (hour)*
P_H, P_F	*heated and wetted perimeter of the channel*	*m*
P_{crit}	*critical pressure*	*kPa*
P_R	*reduced pressure* ($P_R = \frac{P}{P_{crit}}$)	-

Pr	*dimensionless Prandtl number*	-
PP	*(Dynamic) period payback*	*Year*
PEC	*purchased equipment cost*	£
PCM	*phase change material*	-
Q	*thermal energy amount*	*kJ*
$\dot{Q}$	*thermal energy rate*	*kW*
$\dot{Q}_H$	*aimed heating load of the system*	*kW (Kilo Watt)*
$\dot{Q}$	*heat transfer rate*	*kW*
$\ddot{Q}$	*heat transfer flux*	$W\ m^{-2}$
$\ddot{Q}_H$	*Effective heat flux averaged over the heated/cooled perimeter of the channel*	$W\ m^{-2}$
$\dot{Q}_L$	*aimed cooling load of the system*	*kW*
R_t	*thermal resistance*	$K.W^{-1}$
Re	*dimensionless Reynolds number*	-
s_{fin}	*fin spacing (net difference between fin walls)*	*mm*
Su	*Suratman number* $(Su = \frac{Re^2}{We})$	-
SOC	*status of charging*	*% or -*
SCOP	*seasonal coefficient of performance*	-
T	*temperature*	℃
$T_{melt,PCM}$	*melting temperature of PCM*	℃
th	*thickness*	*m*
th_{fin}	*fin thickness*	*m*
T	*Operational hours in a year*	*h*
TCI	*Total capital investment*	£
$Q_{Max,PCm,th}$	*Theoretical maximum thermal capacity of the PCM tank*	*kJ*
x	*vapour quality*	-
X	*Lockhart-Martinelli parameter*	-
X_{tt}	*Lockhart-Martinelli parameter of turbulent liquid-turbulent vapour*	-
$\dot{W}$	*work Consumption*	*kW*
w	*Width of the Al-Extruded channel*	*m*
W_{ch}	*channel width*	*m*
We	*dimensionless Weber number,* $(We = \frac{G^2 d_h}{\rho_f \sigma})$	-
We^*	*modified Weber number*	-
U	*Overall heat transfer coefficient*	$W.m^{-2}.K^{-1}$
v	*specific volume*	$m^3.kg^{-1}$
V.	*opening and closing valves*	-
η_{is}	*Compressor isentropic efficiency*	*%*
ΔT_{app}	*approach temperature difference*	-
	subscripts	
atm	*related to Atmosphere-ambient*	-
c	*charging status*	-
d	*discharging status*	-
ini	*initial*	-
Max, th	*maximum theoretical amount*	-
tot	*total amount*	-
duty	*heating duty of the system*	*kW*
evap.	*Evaporator in schematic figures*	-
exp.	*Expansion valve in schematic figures*	-
Subscripts		-

0	*ambient*	-
1, 2, 3, …	*State points*	-
air	*Air-side related properties and parameters*	-
ann	*annular flow in channels*	-
cb	*convective boiling*	-
ch	*channel*	-
$cond\ (R_{t,cond})$	*conduction*	-
$conv\ (R_{t,conv})$	*convection*	-
g	*saturated gas state*	-
go	*gas only*	-
i	*inlet*	-
in	*inlet*	-
o	*outlet*	-
O&M	*Operating and maintenance (cost)*	-
L	*saturated liquid state*	-
Lo	*liquid only*	-
nb	*nucleate boiling*	-
non-ann	*non-annular flow in channels*	-
out	*outlet*	-
ref	*Refrigerant-side related properties and parameters*	-
sat	*saturated*	-
tp	*two-phase state*	-
tt	*turbulent liquid-turbulent vapour*	-
tv	*turbulent liquid-laminar vapour*	-
vt	*laminar liquid-turbulent vapour*	-
vv	*laminar liquid-laminar vapour*	-

Greek Letters

ΔT_{PP}	*Pinch Temperature difference*	-
ρ	*Density*	$kg.m^{-3}$
μ	*dynamic viscosity*	$kg.m^{-1}.s^{-1}$
ν	*kinematic viscosity*	$m^2.s^{-1}$
σ	*surface tension*	$N.m^{-1}$
$\emptyset$	*two-phase multiplier*	*(-)*
ϕ	*maintenance factor*	*(-)*
η	*Efficiency*	*%*
η_{is}	*isentropic efficiency*	*%*

Chapter 1 Introduction

Heating and cooling represent two fundamental energy-demanding requirements for household and industrial applications in all regions on Earth. On the other hand, energy usage trends are gradually increasing due to rapid population growth and the increase in living standards. This intensifies the greenhouse gas emission level and eventually exacerbates global warming and its long-term effects, climate change [1]. Building energy consumption is skyrocketing worldwide, with building heating and cooling energy consumption making up 54% of the building's overall energy consumption [2]. Most energy used for heating and cooling in residential and commercial buildings makes up 36% of the total energy consumed globally today [3]. Given that, the building industry is acknowledged as having a substantial impact on how human activity affects the environment [4]. For the Gulf Cooperation Council (GCC) countries (Bahrain, Oman, Qatar, Kuwait, UAE, KSA), annual water consumption will exceed 26 billion m^3, while the cooling demand is expected to be more than 36 million Rton (ton of refrigeration) until 2030 [5]. Regarding the other countries, the total cooling demand is expected to increase up to 5.8 EJ (Exa-Joule) in 2050, only for Asia, Latin America, India, and China [6]. In the European Union, the heating industry uses the most energy and produces the most carbon emissions. Nearly 50% of the Union's overall energy demand relates to this sector, with fossil fuels accounting for 75% of it [7]. While in 2017, just 10% of the world's heat demand came from renewable sources [8].

Regarding the environmental issues, around 80% of the energy used in European homes is used by heating systems to produce domestic hot water and space heating, which contributes significantly to building environmental emissions [9]. In the annual COP (Conference of the Parties to the United Nations Framework Convention on Climate Change), lots are discussed and achieved. The goals of decarbonisation by 2050 and a maximum 1.5 ◦C increase in ambient temperature have been set by the COP26 conference in response to the persistent global warming concerns. Also, in COP26, it was agreed that in 2024, international funding for the unabated fossil fuel energy sector should be discontinued by 34 nations and five public finance institutions. Trillions are being reallocated by central banks and private financial institutions to achieve global net zero by 2050 [10]. Decarbonisation of several energy-intensive industries is necessary to meet these grand goals.

In the UK specifically, household energy consumption is a significant factor in the current environmental and strategic supply of energy. 80% of domestic energy associated with space and hot water heating are being provided by electrical radiators or boilers fired with fossil fuels. The UK, as well, has passed legislation to achieve Net Zero by 2050 [11]. To achieve a carbon emission-free status by 2050, all new construction must be Net Zero-Energy Buildings (NZEBs) [12]. When greenhouse gases are created and removed from the atmosphere in equal amounts, the balance is called net zero. NZEBs have just moved from being studied to being used in practice [13]. Although the UK has made significant progress in the past ten years to decarbonise its industry [14], there are some challenges due to temporal changes, and quick dynamic responses (seasonal, weekly, and daily).

Among several possible solutions (such as hydrogen, biomass, heat pumps, and electrical heaters), electrically powered heat pumps are considered the most promising solution for decarbonising heating/cooling. Given that heat pumps are used in buildings, improving heat pump efficiency can directly address problems with building energy. Aligned with alterations of the traditional heating technology, the air source heat pump system is becoming increasingly popular [15]. According to the European Heat Pump Association's market forecast, heat pumps installed in buildings in gigawatt (GW) will increase from 1000 GW in 2022 to 6,500 GW by 2050 [16]. The Air-Source Heat Pump market worldwide is projected to grow by US$ 131.1 billion, driven by a compounded growth of 10.7%. Numerous recent studies have been conducted to increase heat pump efficiency, including using different refrigerants and suggesting innovative cycles [17].

Generally, a heat pump takes thermal energy or heat from the environment, such as soil, water, or air [18]. Among all heat pumps, air-source heat pumps are the most cost-effective option for householders. Utilising Air-Source Heat Pumps (ASHP) as a replacement for gas boilers would have some benefits, such as cost savings and emission reductions [19]. In the next section, more information is provided about the fundamentals of an air-source heat pump.

1.1 Fundamentals of Vapour compression cycle of a heat pump

A heat pump is a device that works based on vapor compression cycle - also known as Reverse Rankine Cycle. In the heating mode, It transfers heat from a low-temperature source to a higher-temperature sink by means of external work, most commonly via a closed vapor-

compression cycle comprising a compressor, condenser, expansion device, and evaporator. Fig. 1.1 shows a schematic figure of a simple single-stage heat pump. In the compression step (1 to 2 in Fig. 1.1), saturated or slightly superheated vapor is raised to a higher pressure and temperature – ideally in an isentropic process (entropy constant) - so it can reject heat to the sink [20]. In the condenser (the sink), the high-pressure vapor rejects heat isobarically (pressure constant) and condenses to liquid, often followed by mild subcooling (process 2 to 3 in Fig. 1.1) [21]. The liquid then undergoes throttling in the expansion valve, an isenthalpic, irreversible process (enthalpy constant) that lowers pressure and temperature to produce a liquid–vapor mixture (process 3 to 4 in Fig. 1.1) [22]. In the evaporator, the refrigerant absorbs heat at low pressure and typically leaves slightly superheated (process 4 to 1 in Fig. 1.1) to protect the compressor [21].

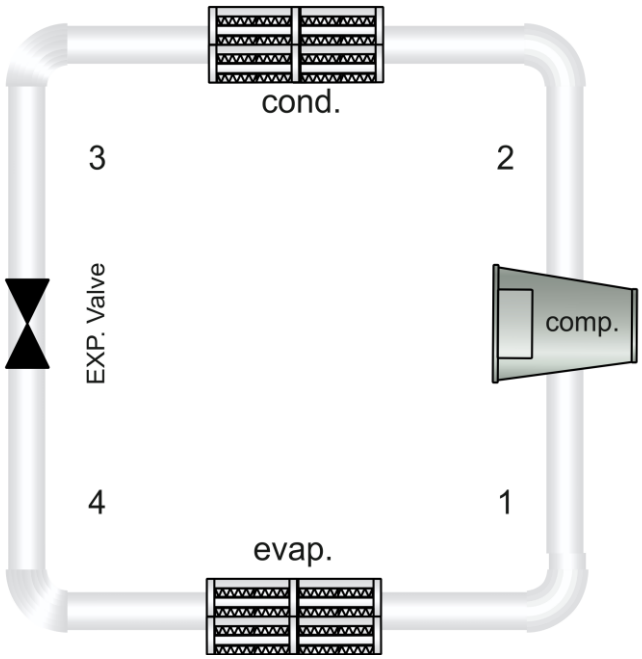

Figure 1.1 Schematic figure of a single stage heat pump

Performance is measured by the coefficient of performance (COP) for heating equals to the aimed/provided heating load (Q_H) or cooling load (Q_L) divided by the input work (work consumption of the compressor) (W_{in}), as shown n Eq. 1-1.

$$\text{COP}_{\text{HP}} = \frac{Q_H\ (Q_L)}{W_{\text{in}}} \qquad \textbf{Equation 1-1}$$

which exceeds unity because the provided heat Q_H includes both the extracted heat from environment and the input work done by the compressor. In the next section, thermodynamic viewpoint of an ideal and a non-idea heat pump cycle are elaborated. As any process in thermodynamics, the processes happening in a heat pump can be idealized to simplify the

simulation/calculations or can be viewed as realistic as possible within the thermodynamic rules.

1.1.1 The non-ideal vapor compression cycle

Practical vapor-compression heat pumps differ from ideal ones due to irreversibility which is visible on a T-s diagram. The reason is that entropy is generated in every process in the real world's chemical/physical processes. Fig. 1.2 shows a T-s diagram of an ideal and non-idea vapor compression cycle, the running cycle of a heat pump device. 1-2-3-4-1 cycle resembles the ideal vapour compression cycle, while 1`-2`-3`-4`-1` shows the non-ideal one. The state points of Fig. 1.1 are matched with the state points in Fig. 1.2. However, the pressure drops of heat exchangers have not been considered here.

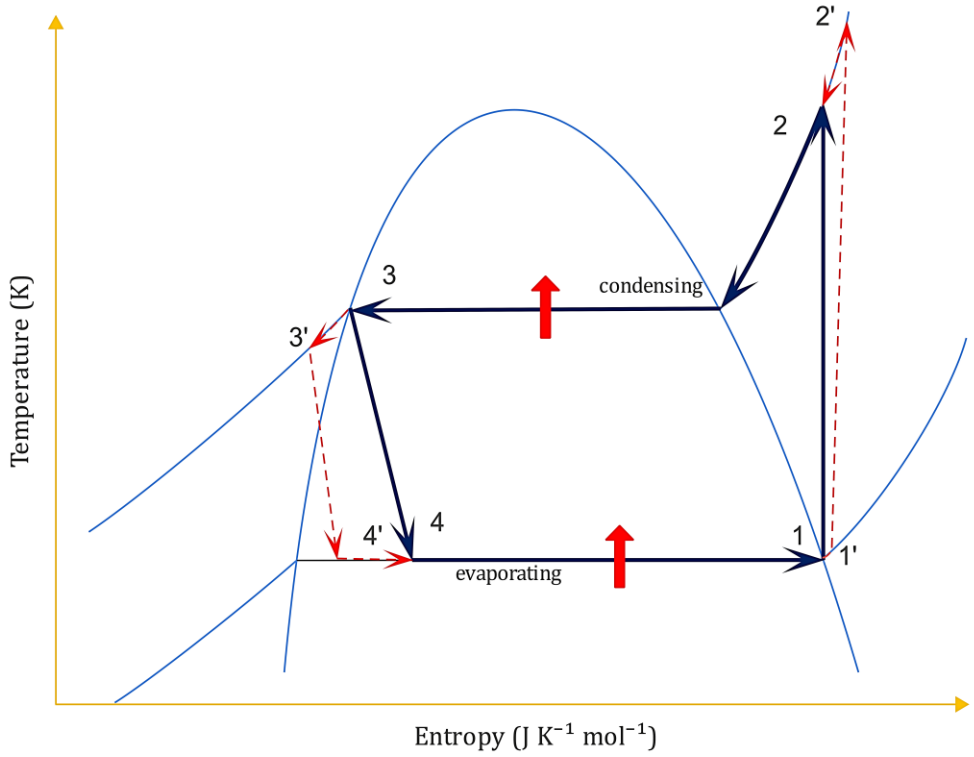

Figure 1.2 Ideal and non-ideal vapor compression cycle

Major entropy loss mechanisms are the source of irreversibility where potentially recoverable work is dissipated as entropy and non-isentropic compression; throttling losses in the expansion device [21], finite temperature differences in heat exchangers that perform the heat transferring process but with a price of entropy generation [23], deliberate superheat/subcooling for stability and control [21], and pressure drops in piping and components that alter operating pressures and degrade COP. All are elaborated for a heat pump in the following paragraphs.

- Compressor inefficiencies: Real-world compressors are not isentropic. Because of friction, eddy losses, heat transfer to the surroundings, and motor/electrical losses, the compression process generates entropy and requires more work than in the ideal process. Instead of following the vertical line of an ideal isentropic compression (process 1-2 in Fig. 1.2), the real compression route strayed rightward, increase in entropy, on a T-s diagram, as 1`-2` line depicted in Fig. 1.2. In practice, the isentropic efficiency of compressors is usually much lower than 100% (usually between 70 and 85% for many refrigerated compressors) because of these irreversible losses.

- Expansion (throttling) losses: This irreversible expansion process causes a noticeable rise in entropy when the liquid flashes into a mixture. The loss of enthalpy happens rather than converts into useful work, producing a cool combination of lower quality mixture. Efficiency is drastically decreased by this throttling loss as the energy that might have powered the cycle or reduced compressor work is lost as entropy increases. In other words, it is changed into kinetic energy and then thermal disorder and finally wasted.

- Heat exchanger temperature differences: The refrigerant and the heat-transfer fluid (air, water, etc.) in actual condensers and evaporators never stay at the same temperature throughout heat exchange; instead, a finite temperature differential, or *pinch* temperature, is always required to propel heat transfer. For instance, the refrigerant may evaporate at -5 °C while the air is at 0 °C, or it may condense at 40 °C while the cooling medium heats to 35 °C. Because heat flows with a temperature gradient, these limited temperature gaps result in entropy formation and make heat exchange less than completely reversible. In practice, designers must decide between larger exchanger surfaces and smaller temperature variations.

- Subcooling and superheating requirements: The majority of actual systems purposefully use some superheat (heating the vapour over saturation in the evaporator) and subcooling (cooling the refrigerant liquid below its saturation temperature in the condenser). By taking certain precautions, such as preventing liquid droplets from entering the compressor and guaranteeing complete liquid input to the expansion valve, stability and equipment protection are ensured. Subcooling and superheating are advantageous for safe operation, although they somewhat stray from the optimal cycle path. However, the evaporator is less efficient when there is excess superheat because some of the heat absorbed is sensible heat that raises the

vapour temperature without causing phase shift. About the condenser and subcooling, after a certain point, it just puts extra strain on the evaporator without increasing production. Since both processes take place with finite temperature differences and do not entirely contribute to beneficial heat transfer, both impacts add to the irreversibility. In Fig. 1.2 increasing entropy in these processes is shown.

- Pressure drops in piping and components: Frictional pressure losses occur as the refrigerant passes through pipes, valves, heat exchanger tubing, and filters. Because of these pressure dips, the condenser runs at a little higher pressure than the compressor discharge, or the evaporator runs at a little lower pressure than optimum. As a result, either the compressor has to work harder to maintain the necessary pressures, or the cycle has a less effective pressure/temperature lift than planned. Even while each pressure decrease may be small on its own, taken as a whole, they progressively diminish the cycle's efficiency.

Some strategies to enhance the vapour-compression cycle and lower these losses include the use of sophisticated compressors, improved heat exchanger designs, and optimised expansion devices. Careful heat pump design, such as lowering temperature differentials in the heat exchangers, increase efficiency and decreases entropy generation. As a result, in addition to source and sink temperatures, system design and component quality have a significant influence on a heat pump's performance. Despite these practical losses, heat pumps remain very efficient heating technology. Nevertheless, depending on the kind of heat pump and application environment, more cycle improvements could be added to ensure both efficiency and economic viability. The pressure drops of pipes and heat exchangers assumed zero in this thesis. Also, there are no super-heating and subcooling considered. But an isentropic efficiency of the compressors is added to the calculations.

The cycle that has been introduced in Fig. 1.1 is a single stage heat pump. The main problems of air-source heat pumps when using regular ASHP systems in cold climates during the winter are as follows:

1) Energy consumption increases, and COP decreases with decreasing ambient temperature [24].

2) When the outside temperature drops considerably, the compressor's discharge temperature in the ASHP system increases to the point where it is no longer functional as a result of the

increase in irreversibilities during the compression process, as well as the reduction in the mass flow rate [25].

Therefore, single-stage air source heat pumps are usually more suitable for applications with relatively small temperature lift (i.e., low heat production temperature, higher ambient air temperature, or both), e.g., underfloor heating.

Numerous approaches have been devised to tackle the problems mentioned, and they can be broadly divided into three main categories:

1) Recovering energy throughout the expansion process by using a power-producing device. To recover power from the expansion process, expanders have first been employed to replace the expansion valves. Numerous studies have shown that turbine expanders can recapture energy to lessen the irreversibility of the expansion process, but they are costly and mechanically complex. Energy recovery during the expansion phase has also been investigated for volumetric devices such as piston expanders, screws, scrolls, and rolling pistons.

2) Flash gas produced during expansion may enter the compressor and be recompressed in a single-stage system, causing waste and system heating. Employing a two-stage cycle to prevent flash gas from partially recompressing is suggested. Also, because it has two compressors, the pressure ratio between each stage is lower. A two-stage heat pump is shown in Fig. 1.3. In a two-stage compressed air source heat pump cycle with a flash tank positioned between stages for heating, the process begins as low-temperature, low-pressure refrigerant absorbs heat from the surrounding air in the evaporator and transforms the fluid into superheated vapor. This vapor is then compressed by the low-pressure compressor to an intermediate pressure. Afterward, a flash tank generates saturated vapor, which is mixed with the superheated refrigerant before entering the high-pressure compressor. The resulting high-pressure superheated vapor flows into the condenser, where it releases heat to the user side and condenses into a liquid. Before reaching the flash tank for cooling, the liquid refrigerant is throttled to a lower pressure. Once it exits the flash tank, it is further throttled to the evaporation pressure, allowing it to re-enter the evaporator and begin the cycle again by absorbing heat [26].

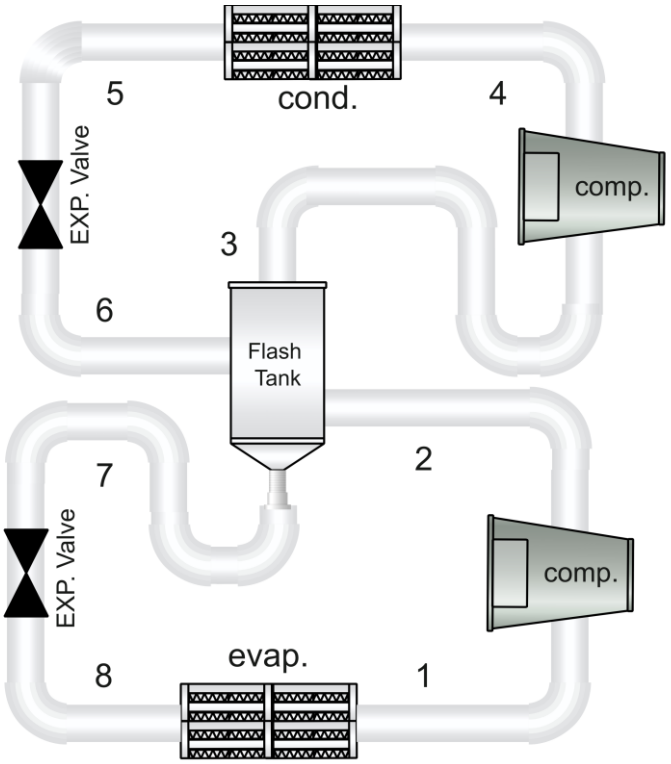

Figure 1.3 Schematic figure of a two-stage heat pump

It should be emphasised that the above-mentioned solutions add an additional mechanical component, either an expander or an additional compressor, to heat pumps, which increases complexity and expense.

3) Recovering some heat from the heated liquid refrigerant and saving in a storage tank and repurposing it as an auxiliary heat source. There is a concept called flexibility in heating/cooling systems which is possible by adding a storage tank to the system. Flexibility is defined as the ability to adjust the energy consumption of a cycle based on external signals such as outside temperature. The most common parameters that are focused on the flexibility of a system are the change in power consumption (*shaved electricity*) and shifted load (*shaved load*) [27]. For a cooling application in the summer season, for example, the city's electrical power grid is heavily loaded during peak hours to provide cooling. Conversely, during the night, there is a significant decrease in the requirement for cooling, which results in excess capacity that can be saved and used further [28]. Therefore, storage systems offer significant benefits in peak load reduction, energy supply and demand profile balancing, and lower cooling costs [29]. In section 1.2, the concept of using phase change material (PCM) tanks as a storage medium in a heat pump system is explained.

1.2 Phase Change Materials (PCMs) as a Superior TES Medium

The fundamental principle of PCM-based thermal energy storage is the material's ability to transition between different phases, often from solid to liquid and vice versa [30]. The significant feature of a PCM is the amount of energy that absorbs from its surroundings throughout the melting process without causing a discernible change in its own temperature. Energy that is absorbed or released without changing the temperature is known as latent heat [31]. However, after solidification, this stored latent heat is released back into the system. In the 18th century, British scientist Joseph Black provided the first explanation of latent heat.

While all materials may change their energy in certain circumstances, PCMs are used to do so reliably and effectively, storing or releasing large amounts of latent heat at a nearly constant temperature [32]. The great thermal energy storage capacity per unit volume of PCMs is a major benefit over traditional sensible heat storage medium, which stores energy by altering temperature rather than changing the material’s phase. This intrinsic characteristic means that far lower storage volumes are needed to get the same energy storage capabilities by a PCM [31].

If it is linked with a heat pump, PCMs' isothermal behavior allows them to prevent undesirable temperature fluctuations inside a system or room by maintaining a constant temperature, which will increase heat pump performance (because it reduces the required temperature lift/drop) and enhance occupant comfort. This contrasts sharply with sensible heat storage, where the temperature naturally changes during charging and discharging. The unique isothermal phase change feature of PCMs transforms thermal storage from a passive buffer into an active thermal regulator, lowering temperature variations during heat exchange and enabling more stable and efficient operation of heat pump systems. This enhances thermal comfort in the built environment and boosts system performance. Using PCM or any material to save some energy inside is known as Thermal Energy Storage (TES)[33].

TES efficiently shifts thermal loads by isolating energy output from consumption. TES may help minimise power demand by reducing energy consumption and the high costs of winter heating and summer cooling, and it can be used in both small and large residential buildings. TES is an essential part of both behavioural and economic demand response strategies when it is controlled well. When choosing the ideal TES system, factors including operating

conditions, system costs, practicality, and the quantity and duration of energy that has to be stored are taken into consideration. In addition, weather and building insulation affect the heat load. PCMs are widely used in TES because they are effective at heating and cooling through charge and discharge operations. By storing energy at times of low demand and utilising it during times of high demand, TES encourages cost savings and grid efficiency [34]. Thermal storage systems help address the challenges by shifting energy consumption from peak to off-peak periods. These systems can reduce costs and overall energy use by storing low-cost electricity as thermal energy in PCM tanks during off-peak hours and releasing it during peak periods [29].

Comprehending the basic concepts of PCMs is crucial to understanding their function in sophisticated thermal energy storage systems. PCMs are a perfect fit for flexible heat pumps because of their special thermophysical characteristics, which allow for effective and small energy control. Optimising operational and management tactics to maximise energy efficiency and cost-effectiveness while also feeding the building's load throughout the day is necessary to fully harvest these benefits [35]. In sub-section 1.2.1 the criteria of PCM selection is explained.

1.2.1 Criteria for PCM Selection in Heat Pump Applications

In order to efficiently meet building loads and maintain occupant comfort, choosing an appropriate PCM is a critical design challenge that is mostly determined by the required temperature range and the anticipated thermal energy storage capacity. Research indicates that storage units perform best when the PCM's melting point corresponds to the optimal comfort temperature of the hottest month for free cooling, and passive cooling is most effective when the PCM's melting point is between 20 and 22 °C [36]. Passive and active method of PCM integrating to the building/heating system of the building will be cleared out in section 1.2.2.

The thorough selection criteria include a suitable phase-transition range, high latent heat capacity, efficient heat transmission capabilities, stable phase equilibrium, high density, low vapour pressure to preserve containment integrity, and minimal volume change during phase transitions [32]. Selecting a PCM is a highly tailored technical venture rather than a generic one, as seen by the ongoing emphasis on bringing the PCM's melting point down to certain ambient or comfortable temperatures. If the PCM's phase change temperature is not properly matched with the heat pump's working temperature range and the building's thermal demand,

the system will not provide the maximum energy savings or comfort benefits. For example, in a hot area, a PCM will lose a considerable amount of its effectiveness if it does not fully solidified overnight [37]. This suggests that the *flexibility* of the heat pump system must extend to its PCM component in order to ensure both technical efficiency and financial return on investment, requiring careful consideration of application needs and geographic location. This highlights the need for sophisticated design methods and a deep understanding of local thermal properties. In addition of the material itself, the method of integrating is another key factor as well. In the next section, different PCM integrating configurations will be explained.

1.2.2 Various Configurations for Integrating PCM Tanks

Phase Change Materials can be incorporated directly into the building envelope or strategically into the heat pump machinery itself. The two main categories of integration techniques are named passive and active systems, respectively. The charging and discharging of passive storage, which usually uses PCM inside the building envelope, depends on changes in the surrounding temperature. In this setup, a heat exchanger is typically employed to couple the PCM-integrated building component (e.g., walls, ceilings) with the air handling unit (AHU) of the HVAC system. This allows the building structure itself to act as a thermal battery.This method makes use of the building's natural thermal mass [38]. Active storage designs, on the other hand, which frequently include distinct heat or cold stores, enable real-time control of the thermal energy storage process, which makes them far more successful for accomplishing demand management and grid flexibility goals [36]. In this configuration, the PCM is directly incorporated into key components of the heat pump's refrigeration cycle, such as the condenser or evaporator, or is coupled via a standalone storage tank.[9] This direct integration allows for highly efficient heat transfer with the refrigerant. In this study, the PCM is connected to the heating/cooling system, rather than the building, which means it is an active PCM storage system.

The effectiveness of PCM-integrated heat pumps in delivering demand response and energy savings is profoundly influenced by their active control and strategic placement within the HVAC system [36]. In the following sections 1.2.3 and 1.2.4, the concept of charging and discharging processes, or the operational cycles of a PCM tank in a heating and cooling systems will be explained, respectively.

1.2.3 Operational Cycles for Heating Applications (Charging and Discharging Processes)

The operational cycle for heating applications in a PCM-integrated heat pump system is designed to optimize energy use and leverage favorable energy pricing. Charging and discharging of a PCM in a heating system is elaborated as follows:

Charging Phase (Heating): During periods when electricity is inexpensive or renewable energy supply is abundant (e.g., nighttime, off-peak hours), the heat pump operates to generate thermal energy. This heat, typically sourced from the heat pump's condenser, is then transferred into the PCM modules within the storage tank. As PCM absorbs this heat, it undergoes a phase transition from solid to liquid, storing a large amount of latent heat without a significant increase in its own temperature. This stable temperature profile is ideal for controlled heating applications [31].

Discharging Phase (Heating): When there is a demand for heating (e.g., during daytime peak demand hours or when electricity prices are high), and the heat pump is either not actively running or operating at a reduced capacity, the PCM releases its stored thermal energy [30]. As the PCM solidifies, it provides a consistent and stable heat supply to the building [31]. This stored energy can then be utilized by the heat pump or directly by the building's heating system [30]. Crucially, the ability to store thermal energy means the heat pump does not need to be sized for the absolute peak thermal demand of the building. Instead, it can operate over a longer period at a lower, more efficient capacity to charge PCM, allowing for a longer recovery time and potentially reducing the capital expenditure on the heat pump by enabling the installation of a smaller, less expensive unit. PCM integration enables heat pump systems to strategically decouple thermal energy generation from immediate demand, allowing for optimized operation during off-peak electricity hours, leading to significant operational cost savings through time-of-use tariffs and potentially lower upfront capital expenditure due to reduced heat pump sizing requirements [39].

1.2.4 Operational Cycles for Cooling Applications (Charging and Discharging Processes)

The operational cycle for cooling applications similarly leverages the unique properties of PCMs to enhance efficiency and manage demand. Charging and discharging of a PCM in a cooling mode heat pump are as follows:

Charging Phase (Cooling): Similar to heating, the cooling cycle leverages off-peak hours (e.g., night-time) for charging. During this period, the heat pump operates to absorb heat from the PCM tank, effectively generating cold inside the PCM. This unwanted heat is then transferred to the outside, causing PCM to solidify and store the negative amount of heat as cold energy. A common PCM for cold storage has a phase change temperature of 10 °C [40].

Discharging Phase (Cooling): During periods of high cooling demand (e.g., hot daytime hours), the PCM releases the stored cold as it starts to be warm[41]. This allows the system to provide cooling to the building's circulation loop without the heat pump needing to run continuously or at full capacity, thereby shifting the cooling load away from peak electricity times [40].

This extends beyond mere energy shifting; it translates into a more stable and comfortable indoor environment and reduces the need for the heat pump to operate intensely during peak demand periods. This capability allows for more effective *peak shaving*, alleviating stress on the electrical grid during hot/cold weather for a cooling/heating system, respectively. All in all, PCM integration in heat pumps not only facilitates significant energy load shifting but also demonstrably enhances indoor thermal comfort by maintaining stable temperatures for extended periods, reducing the operational burden on the mechanical system during peak demand, contributing to both energy savings and a superior indoor environment, significantly enhancing energy efficiency, enabling sophisticated demand management, and contributing substantially to environmental sustainability.

1.3 Thesis Structure

In chapter 1, section 1.1, fundamentals of Vapour compression cycle of a heat pump, the definition of a heat pump, and its ideal and non-ideal forms in sub-section 1.1.1 have been explained. The advantage of a two-stage heat pump over single-stage is shown. What is a PCM tank and the reasons and advantages of inserting a PCM tank into heat pump system are explained in section 1.2. The selection criteria of PCM material for a system in sub-section 1.2.1, various configurations for Integrating PCM Tanks in sub-section 1.2.2 and Operational cycles of a PCM tank in both heating and cooling application have been shown in sub-sections 1.2.3 and 1.2.4, respectively.

In chapter 2, a review of the previously published papers has been summarized in four sections: In section 2.1, improvements in COP with using PCMs have been explained, which

in turn divided into three sub-sections to showcase different system's improvement by using PCM/storage tank: 2.1.1 Heating single-stage flexible system, 2.1.2 Heating two-stage flexible system, 2.1.3 Cooling flexible system. In section 2.2, the concept of demand side management and control strategies will be explained. It will be answered to the question: How will the system be controlled if a PCM tank is added to the system? What's the meaning of flexibility, demand side management and peak shaving in HVAC systems? What is the effect of adding a PCM tank to a heat pump? Section 2.3 refers to the previously published papers regarding techno-economic analysis and based on the information provided from the previously published papers, the research gap is revealed. In section 2.4 key objectives in this PhD thesis are mentioned. Chapter 3 explains the novel two-stage flexible system for heating, how to calculate the loads, how to run a flexible heat pump with a control strategy, which parameters are calculated as the results, etc. In chapter 3, a novel flexible two-stage heat pump has been studied and compared with a baseline two-stage heat pump, as well as the same flexible and baseline single-stage heat pump, in the same working conditions for heating application. A control strategy has been defined based on the heating duty, hour of the day, and storage tank status to run the system in different modes: 1- Normal operation, 2- Charging, 3- Discharging, and 4- Standby modes. The weather data of Glasgow and Birmingham cities, UK, for heating, have been used to acquire the variable hourly heating loads of a typical 4-story residential block via IESVE software. Also, to study the effect of heating load profile shape, a sinusoidal daily heating load profile has been created with the same maximum duty of variable load from IESVE.

Chapter 4 explains the same story but for cooling purposes. A PCM tank has been incorporated and connected to a flash tank via a separate fluid circuit rather than through a conventional PCM heat exchanger. A control strategy based on demand-side management (DSM) patterns for residential buildings has been implemented. The proposed system has been evaluated using real weather data and non-ideal, randomly varying cooling load profiles extracted from IESVE software for Rome and London. The key performance indicators include annual operational cost and seasonal COP, both of which are used to demonstrate the advantages of the proposed configuration (config. 1) over a baseline two-stage heat pump. This study aims to address the research gaps by proposing a new system that integrates a PCM tank at the intermediate stage of a two-stage heat pump, linked to the flash tank, and operating under real, variable load conditions. The central contribution of this work is the integration of system flexibility into a two-stage heat pump through a novel configuration. Research gaps and key objectives of this thesis will be elaborated in chapter 2. In addition, this thesis contributes to that effort by rigorously analysing both

thermodynamic performance and economic outcomes. Chapter 5, the second and third phase of this research will explain about designing of the heat exchangers and how to calculate the economic parameters. Knowing the heat transfer area is a crucial step to calculate the initial investment. Therefore, logically, first the system has been analysed via thermodynamic fundamental rules, then heat transfer analysis and heat exchangers' design have been performed and then economic parameters have been calculated.

Chapter 6 explains the final conclusions, while chapter 7 has a look at the future work that could be done based on this research.

Chapter 2 Literature Review

In this chapter the key research articles summerised and key information that required to perform this research has been introduced in three sections. The main focus of reviewing the previous works was to find out which correlations, methods, and economic parameters have been applied/calculated on which type of air-conditioning systems and how. Section 2.1 summarises improvements in COP with using PCMs for single-stage heating heat pumps (sub-section 2.1.1), heating two-stage systems (sub-section 2.1.2) and flexible cooling systems (sub-section 2.1.3), while section 2.2 refers to demand side management and control strategies, section 2.3 refers to techno-economic studies, and section 2.4 clarified the key objectives of this research.

2.1 Improvements in COP with using PCMs

PCM-based heat pump systems have demonstrated notable energy savings. One study reported a 4.6% electricity saving for cooling applications under forced convection compared to a heat pump without PCM [42]. This saving increased to 8.6% when natural convection was employed. However, energy-saving potential can vary with application; in a winter heating scenario, incorporating the same PCM under natural convection reduced energy savings by 1.4%, highlighting the context-dependent nature of benefits. Furthermore, PCM-enhanced systems exhibit an average of 17% higher energy storage capability during the charging phase compared to conventional sensible-only storage tanks [43]. More studies will be referred to in the following sub-sections, but the wide range of reported energy savings and COP improvements is not a contradiction but a critical observation regarding the complexity of these systems. It strongly suggests that the energy-saving potential is highly sensitive to specific design parameters (e.g., PCM type, melting temperature, integration configuration), operational strategies, and prevailing climatic conditions (e.g., summer vs. winter, specific regional climate). This implies that a *flexible* heat pump system requires meticulous engineering and optimization to achieve its full potential and to ensure optimal performance and maximize the return on investment, in a given application. In the next three sub-sections, improvement of a heat pump by PCM integration is explained for a single-stage heating heat pump (2.1.1), a two-stage heating heat pump (2.1.2), and cooling heat pump (2.1.3) have been elaborated.

2.1.1 Heating single-stage flexible system

Regarding single-stage heat pumps integrated with thermal storage systems, the following articles have been noticed*: Hutty et al.* [44] simulated an ASHP with two thermal storage- sensible and adsorption- in a 50-house neighbourhood with AnyLogic software, aimed to reduce the electricity peaks in demand. It has been shown that a 14% reduction is possible with either 0.25 m3 of adsorption thermal storage (ATS) or 5 m^3 of hot water storage in each residence. However, it has been concluded that considering the systems' increased expense and complexity, the appeal of ATS for a mere peak-shaving application becomes questionable*. Fernández et al.* [45] develops, builds, tests, and evaluates a water vapour compression chiller for experimentation that is coupled to a PCM TES tank, which serves as a substitute heat sink. They evaluated the transient model of the chiller-PCM system using experimental data. At last, the energy-saving values that the chiller-PCM system offers over a standard aerothermal chiller are determined by calculating the system's COP at various temperatures. The models revealed energy savings ranging from 5% to 15%. *Arteconi et al.* [46] analysed heat pumps with radiators or underfloor heating distribution systems coupled with TES in Northern Ireland, UK. The aim was to show how a heat pump system behaves and how it influences the building occupants' thermal comfort under a DSM strategy. The DSM control system designed to flatten the shape of the electricity consumption curve by switching off the heat pump during peak hours (16:00-19:00). It is proved that it's possible to achieve a good control of the indoor temperature, even if the heat pump was turned off for 3 hours, and to reduce the electricity bill up to £135, if a *time-of-use* tariff structure was adopted. A study by *Sultan et al.* [47] utilised an idealised method to analyse a novel heat pump (HP)-integrated TES system. At a phase change temperature of 30 °C for New York City and 20 °C for Houston and Birmingham, USA, the greatest reductions in power consumption, utility costs, and peak electric demand were attained. Peak heating load was shifted utilising a time-of-use utility schedule, which resulted in reductions of 47%, 53%, and 70% in peak energy usage in Houston, New York City, and Birmingham, respectively. However, the highest energy savings resulted is only 5.4%. When the TES capacity is matched with the daily building heating loads encountered during the most extreme ambient conditions, the maximum heating load shift from on-peak to off-peak hours is possible. In another research work, *Sultan et al.* [31] conducted a comprehensive analysis of PCM selection for heat pump-integrated TES across various system configurations. The authors compared PCMs with different melting temperatures and setups based on reported energy savings and demand reduction impacts and offered general guidance for designing efficient PCM-based TES systems in residential applications. It is identified that salt hydrate PCMs with melting

temperatures between 15–27 °C, integrated through the heat pump's air distribution system, offered the most favourable outcomes in terms of demand impact and energy savings. According to *Lin et al.*[48], an ASHP system that is combined with a latent heat thermal energy storage (LTES) unit, which is based on a condensing heat storage unit that is specially designed for heat exchange, can further enhance system performance in cold climates. This device's breakthrough is the direct heat transfer between the PCM and refrigerant, which drastically lowers heat loss. An experimental analysis of the system's thermal performance is conducted. Additionally, to study the charging and discharging properties of condensing heat storage units, a mathematical model is created and verified by experimental data. The average heat release power is 4.73 kW, and the heat storage capacity is 31.83 kWh, according to experimental data. Results from the simulation reveal that the PCM melting rate is accelerated by larger fin pitch and smaller tube diameter, but not significantly by variations in tube diameter. Increasing the water flow rate during the discharging time is necessary to sustain the heat-release power. As opposed to single-stage PCM, three-stage PCM enhances energy and performance. The entire energy efficiency is raised by 4.65%, and COP improvement may reach 4.01%. In order to increase its application in extremely low temperatures, the ASHP system, in conjunction with the LTES unit, is a viable strategy. *Bastani et al.* [49] proposed an innovative method for integrating PCM: the storage unit operates on the load side during charging in parallel with the condenser and replaces the external heat exchanger during discharging. The study explores two system configurations, series and parallel, and develops a detailed model to assess how different setups and building heating demands influence the charging process. Results indicate that PCM's low thermal conductivity is the primary factor limiting heat transfer to the storage unit. When there is no heating demand, charging does not significantly accelerate due to the heat pump's limited output and restricted heat flow within the refrigerant-PCM heat exchanger. While operating at reduced compressor speeds lowers the system's load, it also extends the charging duration. Moreover, during peak thermal demand, the system requires a heating capacity beyond its nominal rating to simultaneously meet building needs and charge the storage unit, increasing compressor workload and energy use during charging. *Hirschey et al.* [50] established the energy reduction and demand reduction potential of TES-integrated HPs with both analytical and numerical HP models. All possible temperature arrangements are considered for HP-TES systems with two fixed temperature bodies (application and TES) and one variable temperature (ambient). Results show that overall energy savings are most attainable when the TES temperature is near the application temperature, whereas a large temperature difference between the TES and the application leads to the highest peak demand reduction.

The potential for overall energy savings increases as the magnitude of ambient temperature fluctuations increases. *Xu et al.* [51] introduced three novel latent heat thermal energy storage (LHTES) integration layouts for heat pump systems, connecting the LHTES unit to the de-superheater (Case 2), the condenser of a cascaded booster cycle (Case 3), or both (Case 4). Using a quasi-steady-state model for a multi-family residence in Stockholm, these configurations were compared against a baseline system without storage (Case 0) and a conventional condenser-integrated layout (Case 1). Under an off-peak charging strategy (8 pm–6 am), Cases 2–4 achieved 22–26% higher heating performance factor (HPF) than Case 1 and reduced operational costs by 2–5% compared to Case 0. A daytime charging strategy (10 am–7 pm) was found to be more effective in lowering CO_2 emissions, achieving reductions of up to 14%. *Hu and Shen* [52] presents a novel PCM-based multifunctional heat pump system with integrated thermal storage. Testing revealed good performance in several modes, such as a COP of 2.1 for heating down to -15°C, a COP of 8.8 for space cooling and water heating combined, and a COP of more than 4.0 for water heating annually. The system's seasonal heating performance factor of 10.0 and cooling energy efficiency ratio of 18.0 demonstrate both operational flexibility and substantial energy savings potential. The integrated thermal storage allows load shifting and enhances the system's compatibility with variable renewable energy sources, making it an efficient way to decarbonise HVAC systems in cold and temperate climates. *Kelly, et al.* [53] evaluates the effects of load shifting on an ASHP in a detached home in the United Kingdom using a building energy simulation model. While simulating activities under the Economy 10 time-of-use tariff, they examined two thermal storage strategies: conventional hot water buffering and PCM-enhanced buffering. To fully shift heating operations to off-peak hours, 500 litres of PCM-enhanced storage or 1000 litres of standard hot water storage were required. However, the load shifting approach resulted in a 60% increase in overall power consumption, increased carbon emissions, and higher user fees due to subpar off-peak functioning. These findings suggest that PCM buffering can reduce the amount of storage needed, but the extensive and haphazard application of tariff-based shifting may worsen grid stability. Kumar, et al. [54] develops a comprehensive thermodynamic and control model of the device to evaluate an air-to-water reversible heat pump's versatility and potential for energy savings in an Italian office building. Systems with constant-speed and variable-speed compressors are evaluated by them using a control method based on heating curves. The model simulates startup and transitory conditions as well as dynamic and steady-state activity. According to the model, variable-speed compressors may see a 17%–50% boost in COP, especially when running at partial load. The issue of constant-speed units cycling a lot when there is minimal load,

which leads to inefficiencies, was also highlighted. These findings support the use of advanced controls and variable-speed technologies to increase flexibility and efficiency, allowing buildings to respond to grid signals effectively while maintaining indoor comfort. Inserting a PCM tank into a heat pump system is not only for residential areas. The COMHPTES project exemplifies ongoing efforts, aiming to develop innovative, cost-effective, compact, and modular heat pump (HP) and thermal energy storage (TES) technologies for industrial applications (ranging from 0.5 to 10 MW-t and 5 to 225°C) [42]. The results highlighted the expansion of PCM-integrated heat pump applications beyond residential buildings into the industrial sector, addressing significant thermal energy demands. The next sub-section explains the improvement of two-stage heat pumps by PCM integration, for heating applications.

2.1.2 Heating Two-stage Flexible Systems

Bertsch et al. [55] compared different heat pump cycles and concluded that the cascade cycle and the two-stage cycle with intercooling or economising outperform the conventional single-stage cycle when the ambient temperature becomes very low. *Roh et al.* [56] experimentally studied the effects of intermediate pressure on the heating performance of a vapour-injection heat pump system using R410A and indicated that a proper operating strategy was needed for the vapour-injection cycle. *Torrella et al.* [57] described a general method to analyse any configuration for two-stage vapour-compression refrigeration cycles. Two parameters are obtained: the degree of subcooling and the degree of desuperheating in the inter-stage configuration. Also, as inter-stage pressure plays a key role in the COP as well as the economy of two-stage refrigerating systems, the optimisation is performed. Although several methods for selecting the inter-stage pressure can be found in the related literature, the most famous one is the geometric mean of the condensing and evaporating pressures, which is only suitable for a perfect gas with the same temperature during suction of both stages. *Baakeem et al.* [58] performed the energy, exergy, and economic analysis of a multistage vapour-compression refrigeration system. An optimisation of the Conjugate Directions Method was carried out to maximise the COP by considering sub-cooling, de-superheating parameters, and evaporator and condenser temperatures as optimisation variables. Also, eight different working fluids are assumed to work inside the cycle: R717, R22, R134a, R1234yf, R1234, R410A, R404A, and R407C. The results showed that R717 is the best option among all refrigerants, while R407C will not be recommended. *Torrella et al.* [59] analysed a two-stage vapour-compression refrigeration system with direct liquid injection and a two-stage system with sub-cooler, experimentally in different evaporating

temperature ranges between 36 and 20 °C and in a condensing temperature range between 30 °C and 47 °C. The results show that the inter-stage working temperature/pressure achieved in the tests is not verified by the two common theoretical criteria or correlations: 1- the arithmetical mean of the condensing and evaporating temperatures, and 2- equal pressure ratios in the stages. *Deymi-Dashtebayaz et al.* [59] investigated the optimal mass flow rate of the injected refrigerant into a compressor in a two-stage compression cycle based on the operational data of a site in Mobarakeh Steel Company of Isfahan recorded over six working months, as a case study. To analyse, the first and second laws of thermodynamics, as well as environmental and economic analysis, are applied. The objective functions considered were the coefficient of performance, power consumption, exergy destruction, and efficiency. It is found that ambient temperature and the evaporator inlet chilled water temperature will have no effect on the optimal mass flow rate.Finally, the authors found that employing a two-stage compression refrigeration cycle leads to 16,600 GWh/year energy saving, 9700 ton/year CO2 reduction, and 1.9 million $/year cost saving in Iran's industrial sector. *Wang et al.* [60] proposed a novel method to inject the vapour inside flash tank and applied the extremum-seeking method as a real-time optimisation in a Modelica dynamic simulation to calculate the optimum pressure of inter-stage in a two-stage air-source heat pump. Controlling the intermediate pressure setpoint by the upper expansion valve eliminates the need to adjust the superheat for the injection loop. In other words, the injected medium remains saturated vapour, which retains the inherent merit of the flash-tank cycle concept. *Lugo-Méndez et al.* [61] derived an analytical expression to calculate the optimum interstage pressure of a multistage compressor with intercooling based on the minimum compression work. The optimal interstage pressures are calculated by considering different parameters, such as the geometric mean of the suction and discharge pressures, the geometric means of the pressure drops in the intercoolers, and the isentropic efficiencies of each compression stage. Finally, the obtained expression to achieve the optimal interstage pressures of a two-stage centrifugal compressor of natural gas provides a first approximation expression to calculate the optimal pressure. *Purohit et al.* [62] selected six common refrigerants (R134a, R22, and R143a as synthetic refrigerants and propane, carbon dioxide, and nitrous oxide) to study the effect of inter-stage pressure on the performance of a two-stage refrigeration cycle, based on thermodynamic analysis. In a range of -50 °C to -30 °C for evaporator temperature and 40 °C to 60 °C for condenser, the optimal inter-stage pressure is calculated with three classic correlations. Then, the values calculated via optimisation are compared to classic ones, which shows that for trans-critical cycles, the deviation of optimised inter-stage pressure from the classical ones is more considerable than that of sub-

critical cycles. This means COP will be less sensitive to interstage pressure in sub-critical cycles. Also, it is shown that COP goes higher with an increase in evaporator temperature.

When PCMs are taken into account in heat pumps and solar thermal energy storage, Kapsalis and Karamanis [63] draw the conclusion that more research and experimental work are needed to fully understand the impact of PCMs on building components and heat pump performance in various climates. *Kosan et al.* [64] present an experimental investigation of a novel latent heat storage unit integrated with the heat pump system condenser. Its novelty is that it added a phase-change material in a heat exchanger with the intention of storing the heat released from the heat pump condenser. The phase change material in the heat pump system is intended to be used for an efficient and sustainable heating system. Systems using solar-assisted heat pumps, as well as air-source heat pumps, have tested latent heat storage units designed for this use. A novel double-pass solar collector has also been designed for the solar-assisted heat pump. For air-source heat pump systems, the average coefficient of performance ranged from 2.19 to 2.34, while for solar-assisted heat pump systems, it ranged from 2.32 to 2.77. *Jin et al.* [65] provide a thorough analysis of the heat pump latent heat storage system for hot water supply to study storage medium matching and operation strategy evaluation. A case study for a subtropical home was created after a simulation platform was created to show the system's application possibilities. According to the findings, phase-change materials having melting points between 40 and 50 ◦C outperformed other materials in terms of cost and energy savings. In winter, the unit with a 75% storage medium that ran at a setpoint of 57.5–60 ◦C significantly moved the loads to off-peak hours. A comparison was made between the system's energy and economic performance under various operating techniques. *Woods et al.* [66] developed a numerical method to simulate a cascaded two-stage vapour compression heat pump with an integrated PCM heat exchanger in the middle of the cycle to connect the upper and lower cycles. The aim was to control the system with and without a pick shaving strategy to compare the results. The system stored thermal energy during a cold morning and charged it in the relatively warm afternoon while still providing space heating. The results were shown for only one day, which is reasonable, as the load profiles of the days are the same sinusoidal curve, although, in everyday life, the heating profile is not ideal for a flexible system. Due to the sinusoidal shape of the loads, the charge and discharge hours are predefined and fixed. In the range of the summit of the curve at (3:00 – 9:00), discharge will happen, while near the valleys (14:00 – 20:40), charging is the working mode. The results reveal that in discharge mode, electricity usage is 4.5 kWh, while in charging mode, it will be 3.9 kWh, which means, all in all. 0.8 kWh energy (1.2%) has been saved in one day for an ideal sinusoidal load.

However, it is claimed that flexibility decreases the peak electricity by 23%. It should be noted that this 23% is only within the discharging time section, not on a yearly timetable. Showing that in the discharging mode, the electricity will be lower, hides the fact that in the charging mode, there will be some electricity usage that does not exist in normal working. In a fair method to calculate how much electricity usage and price will decrease, yearly data at an hourly pace is common in the literature. *Bahman, et al.* [67] performed a multi-objective simulation-based optimisation of a two-stage vapor-injected heat pump designed for usage in severely cold areas, like Minneapolis, USA. Using NSGA-II, a multi-objective genetic algorithm, the model assesses five refrigerants (R-32, R-290, R-410A, R-454A, and R-452B) in order to maximise both cost and performance. The results showed that R-32 had the lowest destruction cost and the best energy performance, whereas R-290 had the lowest heat cost but the highest overall investment and destruction cost. The system achieved a minimum unit cost of heating (UCH) of $0.19/kWh and a heating COP of up to 5.2. *Minglu et al.* [68] used reverse cycle defrosting based on TES to overcome defrosting problems in a cascade air source heat pump. TES-based defrosting cycles cause multi-mode heat discharge in the phase change material because of the different circumstances in the high-temperature cycle and the low-temperature cycle. Having the goal of optimising control techniques for the TES-based defrosting cycle, their work discussed parameters impacting heat transfer and analysed heat coupling between high and low cycles across five scenarios with varying outside circumstances. However, it has not been referred to as reducing power consumption through peak shaving or the annual running price. *Huang et al.* [69] developed a numerical model for a cascaded vapour compression heat pump system integrated with a PCM TES device. This innovative system allows for independent control of TES charging and discharging, separate from the building's thermal load, enabling more efficient management of electricity use. The model was used to evaluate the system's performance under peak shaving and no-shaving scenarios, as well as the impact of different PCM transition temperatures. Results showed that peak shaving effectively reduces peak electricity demand, with a 23.5% reduction achieved using a PCM transition temperature of 10 °C. Although charging the TES requires additional energy, the net savings during the discharge window amounted to 0.8 kWh. Higher transition temperatures enhanced both peak reduction (17% to 28%) and energy savings (12% to 24%). When compared to a conventional air-source heat pump with electric resistance heating, the system with PCM at 10 °C and peak shaving delivered the highest overall energy savings of 45.5%.

All in all, researchers found that peak demand reduction, cost, and energy savings varied significantly based on the PCM phase change temperature, total TES storage capacity,

system configuration, and the building's location and environment. The next sub-section elaborated the improvement of cooling systems by PCM integrating.

2.1.3 Cooling Flexible Systems

Farid et al. [70] studied how PCMs can balance supply and demand and store excess energy in buildings to increase energy efficiency. One experimental set was used as a control, and the other was equipped with PCM storage devices. To lower heating and cooling loads, the PCMs conserved solar energy in the winter and cool night air in the summer. The findings revealed notable energy savings: 10% in January, 10.3% in June/July, 30% in March/April for cooling, and 40% for heating in May. The results demonstrate how PCMs can lower energy use all year long. In order to lower Adelaide, Australia's high summer power demand for cooling, *Farah et al.* [71] combined an ASHP with a phase change thermal energy storage unit. The system with a PCM unit stores energy during low temperatures and releases it during periods of high demand, allowing the system to function in four modes. According to simulations, a system with a PCM unit uses 6–11% less electricity and supplies 13–25% of cooling energy. Cost savings vary by modality, ranging from 7 to 14%. *Chaiyat et al.* [72] explore using PCM to enhance air conditioner efficiency in Thailand's climate. Rubitherm20 (RT-20) PCM balls were used to lower the temperature of air entering the evaporator coil. The PCM bed without bypass tubes was chosen to improve cooling efficiency. Results showed a 3.09 kWh/day reduction in electricity consumption, leading to a 9.10% annual cost saving and a payback period of 4.15 years. The energy performance of charging a PCM storage tank using an air-source heat pump is investigated by *Li et al.* [73]. A simulation platform developed with TRNSYS and MATLAB was validated with experimental data. The study looked at how different water mass flow rates affected inlet/outlet temperatures, charging time, and overall energy use. The study describes a strategy for optimising the combination of air-source heat pumps and PCM storage tanks. The results showed that increasing water flow rates reduced charging time but increased inlet temperature while decreasing outlet temperature. *Sánchez et al.* [74] discuss the use of Phase Change Material (PCM) storage tanks in the Solar Decathlon HVAC system. The PCM storage tanks keep the system's COP steady and independent of external temperature changes. According to simulations, employing the warm PCM tank as a dissipation reservoir can result in an energy savings of 18.97%. *Shafii et al.* [75] have examined a single-stage vapour-compression cooling system in Tehran, Iran, which is connected to a PCM through its condenser. The system's load profile and temperature are shaped as an example of the warmest day of the year. The outcomes demonstrated that PCM lowers power usage at peak load times. On the warmest

day of the year, the PCM volume of 154 L has a 2.9% reduction in daily energy usage and a 0.9% reduction in electrical peak load. Based on the power usage price, economic research indicated that integrating PCM storage can result in peak shavings of up to 69%, making it extremely beneficial from an economic viewpoint. To reduce the amount of energy used by an air conditioning system, *Sanaye et al.* [76] investigated the use of Ice Thermal Energy Storage (ITES) devices. Partial load (POM) and full load (FOM) are the two operating modes for ITES systems. It has been shown that POM's power consumption dropped by 10.23% and FOM's by 11.83% when ITES systems were used. Furthermore, there was a considerable drop in power costs, 32.65% for FOM and 13.45% for POM, when energy usage was switched from peak to off-peak hours. A novel ice energy storage system is being created and coupled to an air-conditioning system by *Zhang et al.* [28]. The SIMULINK model dynamically simulates the amount of energy used and the costs for cooling an average home by considering hourly temperature and peak/off-peak power pricing data. For two US cities, the model predicts that during the six months of the cooling season, significant energy cost reductions (up to 3 times) can be realised in areas with high peak electricity prices. *Hosseini Rahdar et al.* [77] examined a vapour compression air conditioning system that utilises two hybrid strategies: one that employs a PCM tank for complete storage and an ITES system to transfer power consumption from peak to off-peak hours. Compared to traditional systems, power utilisation is 7.58% lower with the PCM tank and 4.59% lower with the ITES system. CO2 emissions for ITES and PCM systems are also 17.8% and 27.2% lower, respectively, than for the traditional system. *Gado et al.* [30] simulated an integrated PCM storage tank and heat pump with MATLAB-SIMULINK all year round in Egypt. During the summer, the HP cooling load is decreased during the day by using the cooling energy that was stored during the night inside the hot room. Nevertheless, in the winter, the HP heating demand at night is lessened by the hot storage energy that the PCM stores during the day. Building spaces are equipped with phase change temperature sensors (RT 18 HC) set to 17–19 ◦C for summer and winter, respectively. MATLAB-Simulink is used to construct the mathematical modelling of the PCM-based HP system, which is then verified by published research. Results show that, when forced convection is used, PCM-based HP considerably achieves 4.6% electricity savings over HP without PCM during the summer. The average cooling capacity and COP decrease from 2.8 kW and 12 to 2.6 kW and 8, respectively, when the external temperature rises from 35 to 40 ◦C. When choosing natural convection over forced convection counterparts for PCM platers, there is a noticeable difference that highlights an 8.6% electricity savings at an ambient temperature of 35 ◦C. *Erdemir et al.* [78] provided a feasibility analysis on the utilisation of thermal energy storage to move heating and cooling

loads to off-peak times to balance the supply and demand for electricity. The study's conclusion notes that thermal energy storage has a significant potential to move the peak load of electricity to off-peak hours based on the cooling and heating loads. By moving heating and cooling loads to off-peak hours and implementing storage, the peak electricity loads can be decreased by 25% and 45% for heating and cooling, respectively. Moreover, thermal energy storage devices can assist in lowering household heating and cooling expenses in Canada by 18% and 20%, respectively. However, in the study, an average daily sinus-shaped cooling profile was considered.

A summary of some papers referred to in this section is shown in Table 1.1. The aim of reviewing the previous articles is to find out the effect of inserting PCM in the system, the type of the system, concept of the flexibility in these systems, method of simulation, type of PCM and amount of melting temperature, types of the results were important to notice and consider in the research. As seen from the table, the energy savings are variable from case to case, no dynamic analysis has been done sometimes, no SCOP calculated, no proper load for demands has been considered. In section 2.4, it will be referred to the research gaps and key objectives of this research and how the author tried to cover the research gaps. In the following section, the concept of demand side management and control strategies will be explained.

Table 2.1 Summary of the references studied cooling systems with storage tank - dynamic simulation approach.

Authors	Title/content	System or Heat pump	COP included	Ambient temperature	Any results
Farid *et al.* [70]	Experimental active PCM storage system in a building for heating/cooling	GREE heat pump, Model GWH09MBK3DNA4H/O	No dynamic COP variation is shown/NO SCOP is calculated.	weather conditions in the city of Auckland, New Zealand, from LabVIEW software	energy savings: 10% in January, 10.3%
Farah *et al.* [71]	Numerical investigation of phase change material thermal storage for space cooling	Single-stage HP	No dynamic COP variation is shown/NO SCOP is calculated.	Meteorological Year Climate File 2016 for the City of Adelaide	6–11% less electricity and supplies, 13–25% of cooling energy
Chaiyat *et al.* [72]	(PCM) to enhance air conditioner efficiency in Thailand's climate	Single-stage HP	No dynamic COP variation is shown/NO SCOP is calculated.	-	3.09 kWh/day reduction in electricity consumption, leading to a 9.10% annual cost saving
Li *et al.* [73]	a comprehensive study with TRANSYS to	Single-stage HP	No dynamic COP variation is shown	Transys weather data	No reduction in energy saving was discussed

	provide an optimisation guideline				
Sánchez *et al.* [74]	Experimental Improvement of a heat pump-based HVAC system with PCM thermal storage	Terra 7 S/W from the Austrian company IDM	COP hourly calculated. No price has been calculated.	Variable real data	Energy savings of 18.97%
Shafii *et al.* [75]	a vapour-compression cooling system utilising a PCM heat exchanger	Single-stage HP	COP hourly calculated	Dom-shaped load for only one day	2.9% reduction in daily energy usage and a 0.9% reduction in electrical peak load
Sanaye *et al.* [76]	(ITES) for air-conditioning applications in full and partial load operating modes	Single-stage HP	COP only at the optimum point	Dom-shaped load, repetitive for the whole year	power consumption dropped by 10.23%-11.83%
Zhang *et al.* [28]	Modelling using Simulink A building cooling system integrating with a novel ice-based storage tank	Home cooling system with supercooling energy storage	COP hourly calculated	Variable load for 200 days	reduction in energy cost (up to 3X)
Erdemir *et al.* [78]	A case study for Canada	normal heating and cooling system with multi-way valves	No COP/SCOP calculation	Sinus shape for 1 day	18% and 20% for heating and cooling

In section 2.1, the improvement of heat pump/air-conditioning systems has been checked, mostly to understand configuration, and methods of simulations, and the results that should be expected from a flexible system. In the next section, a key part of a flexible system, its brain, is explained clearly.

2.2 Demand side management and control strategies

PCM-based TES is a widely recognized an effective solution for shifting peak energy demand in buildings, thereby contributing significantly to grid stability [36]. By storing or releasing latent heat at almost consistent temperatures, the PCM tank functions as a thermal battery. This decouples thermal demand from power demand by enabling the heat pump to run during off-peak hours. This feature is essential for load shifting, lowering peak energy use, and boosting grid stability in flexible heat pump systems. Without immediately turning on the compressor, the heat pump may be programmed to charge the PCM tank when energy

is most affordable or clean and to discharge it when heating or cooling is required. PCMs facilitate the temporal shifting of heating and cooling loads: thermal energy can be stored during periods of high renewable energy supply or low demand and subsequently released when demand is high or renewable supply is low, in a heating system. This capability is fundamental to enabling demand response programs [43].

But in practice, the flexible system needs a brain, a control strategy, a set of commands to follow, ordering the system open/close valves and making the system run in different working modes, and charge/discharge the PCM tank when it is required.

There are different HVAC control methods: bang-bang control, Proportional-Integral-Derivative (PID) control, RBC (Rule-based control), and Model Predictive Control (MPC). The latest one offers significant advancements. Bang-bang control, the simplest form of feedback regulation, frequently causes temperature overshoots and energy inefficiencies due to its binary on/off switching based on deviation from a set-point. PID controllers improve temperature tracking by applying proportional, integral, and derivative adjustments; however, they are often difficult to tune and still lack optimal energy efficiency [79]. RBC, while more advanced, employs designer-defined rules to adjust set-points based on situational factors. However, suitable for managing complex systems, it remains non-optimised and highly dependent on expert knowledge. RBC control typically begins with heuristic logic following the structure: *if (condition is met), then (action is triggered)*. These systems generally rely on monitoring a specific *trigger* parameter, such as room temperature, with a predefined threshold. When the threshold is reached, the heat pump operates according to the programmed control strategy [80]. In contrast, MPC control solves an optimisation issue at each time step and predicts future behaviour using a mathematical model of the HVAC system. It seeks to reduce a cost function, while adhering to system limitations, usually balancing comfort and energy consumption. MPC constantly predicts performance over a predetermined future time while operating at a high degree of supervisory control. Modelling the building's HVAC dynamics, including room temperature, system reactions, and outside effects, is the first step in the process. The model forecasts future circumstances at each stage and determines the optimal control action (such as modifying fan speed), implementing just the initial action before resuming with fresh data. Although this technique requires accurate models and a large amount of processing power, it enables anticipatory, constraint-aware management that enhances comfort and energy efficiency [81].

There will be more flexibility, responsiveness, and energy efficiency if the heat pump is paired with demand side management (DSM) and advanced control systems. Another question just raised up. What is demand side management or DSM strategy?

DSM is all strategies intended to affect the consumer's energy consumption via the control method of the heating/cooling systems. These strategies concentrate on improving the heating/cooling load's shape, which helps to optimise the whole power system, from generation to distribution to final usage [82]. Fig. 2.1 shows different methods of DSM. In this study, peak clipping or load shifting have been desired. Any electricity or load usage/providing decreased at peak hours in a system is considered peak shaving. When designing a heat pump system integrated with TES, it is essential to consider control strategies coupled with demand-side management within the smart grid framework [83].

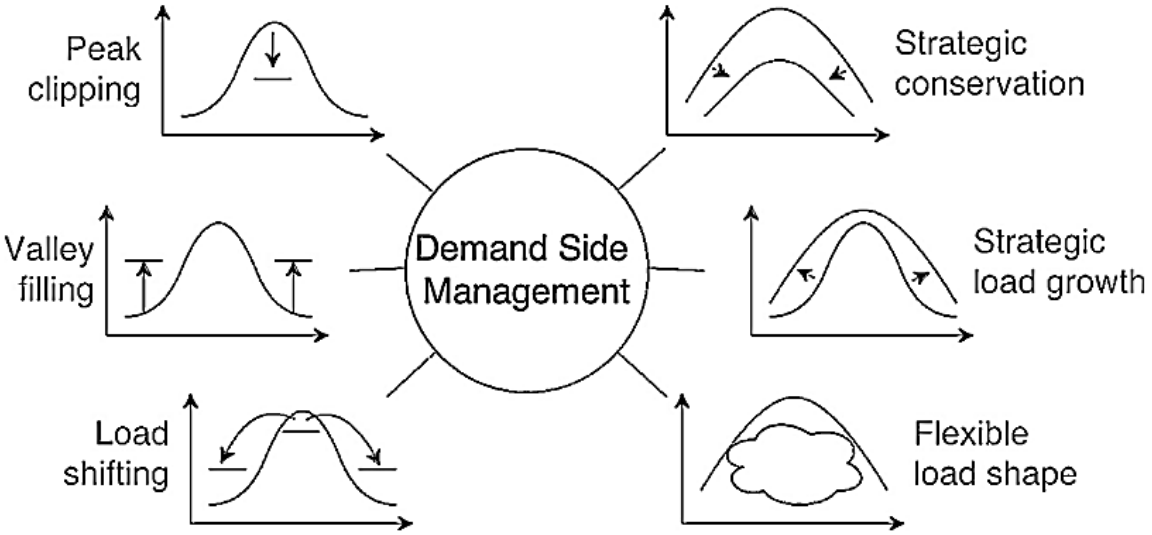

Figure 2.1 Control strategies as demand side management (DSM) [84]

DSM initiatives are generally categorised into three main types: energy reduction programs, load growth and conservation programs, and load management programs [85]. Energy reduction programs focus on minimising energy use by adopting energy-efficient technologies and practices without compromising user comfort. Load growth and conservation programs require careful planning for infrastructure expansion and procuring new equipment. On the other hand, load management often employs pricing mechanisms, such as time-of-use tariffs, that incentivise consumers, particularly in the commercial and industrial sectors, to shift energy usage to off-peak periods when electricity prices are lower. Key barriers to the effective implementation of DSM include challenges related to accountability, political independence, and the lack of robust monitoring and evaluation

frameworks [86]. In the following paragraphs, some previously published research articles about control startegies and DSM schems in heat pumps have been summerised. The aim of reviewing them was to understand the common control strategies of a flexible heat pump, how to start/stop charging and discharging in a flexible system and to answer this question: what kind of demand side management have been applied in the published studies?

In order to find out how house heat pumps may help demand-side response (DSR) in the UK energy system, 76 properties with air-source heat pumps, 31 of which had a special control system, were employed in a field trial by *Sweetnam et al*. [87]. The objective was to ascertain if automated controls might optimise heat pump operation to match time-varying electricity prices without the need for human intervention. Rather than focusing on thermal storage, the testing focused on devices that took use of the thermal inertia of buildings. The results showed that the controller effectively reduced the peak evening power usage by shifting loads to other periods. Some inhabitants, however, found the increased inside temperatures during the day and at night to be unpleasant. Interviews with participants exposed issues such a lack of zoning, noise disturbances, and trouble using the control interface. Although DSR is theoretically feasible and beneficial for short-term peak reduction, the study's conclusions suggest that clever control of DSR may compromise occupant comfort over long periods of time. Future improvements might include thermal covers, better zoning, or dedicated storage to boost user satisfaction while preserving flexibility. *Rapucha, et al.* [88] examine how intelligently regulated heat pumps may aid in balancing the electricity needs of the home. Using TRNSYS simulations, the study investigated the performance of air source and ground source heat pumps under smart control systems that respond to grid signals and rooftop solar generation in typical South Australian homes. The findings demonstrated the great potential of load shifting, which involves adjusting energy consumption from periods of high demand to periods of ample renewable energy. Additionally, advanced controls improved solar power self-consumption and reduced total emissions. The solutions were particularly effective in reducing the stress on energy infrastructure and enhancing grid stability. By encouraging a more thorough integration of smart HVAC systems in residential buildings, the findings aid in the expansion of renewable energy sources. Kumar, et al. [54] constructs a linked thermodynamic and control model of an air-to-water heat pump system to optimise dynamic behaviour and energy efficiency in home heating applications. In addition to simulating control strategies that adjust to shifting thermal loads and ambient conditions while preserving a pleasant interior temperature, the model incorporates important system components such as compressor dynamics, expansion valves, and heat exchangers. Simulations validated the model's accuracy and demonstrated

that advanced control techniques, such predictive and adaptive control, may significantly improve system COP, reduce cycle losses, and consume less energy. The integrated modelling framework allows control engineers and heat pump designers to work together to improve system performance and design. Using both modelling and experimental, *Wei, et al.* [89] investigates a quasi-two stage compression air source heat pump (QTASHP) in Harbin, China, that runs at extremely low temperatures. To maintain consistent performance down to −27.5°C and lower high discharge temperatures, a novel segmented control strategy was developed. The device could operate securely at a maximum discharge temperature of 112°C, according to test rig trials. Using the DeST modelling platform, the SCOP was found to be 2.35 and the primary energy efficiency to be 0.88. When compared to conventional central heating, the QTASHP reduced CO_2 emissions by 14.76% and achieved a dynamic payback period of 9.86 years in energy-efficient buildings. The results demonstrate that the system is suitable for extremely cold climates when enhanced with advanced management strategies. *Crawley, et al.* [90] performed an empirical study, describing the real implementation of three demand response (DR) strategies for heat pumps in UK households, with a focus on reducing power consumption during the peak hours of 4-7 p.m. Each family employed a variety of strategies, including lowering air temperature setpoints, lowering flow temperature, and shutting down the compressor entirely. The data was collected using in situ monitoring devices and smart meters. According to the study, electricity savings during peak periods ranged from 56% to 90%, depending on the technique and compatibility with heating systems. However, unanticipated outcomes were seen, including post-event overcompensation and decreased thermal comfort, especially when controls conflicted with the integrated heat pump's logic. The study concludes that effective DR strategies must be integrated into the overall design of the heating system and control logic to minimise rebound effects and ensure occupant comfort. In order to conduct an empirical research, *Hanmer, et al.* [91] gathered information from 71 homes in the UK that had implemented a hybrid heat pump experiment, which involved replacing gas boilers with combination boilers and smart heating controls. The study examined the effects of pre-heating and the continuous low-power operation of heat pumps on daily heating trends. It also includes interviews with eleven households to get information on comfort preferences. Setpoint temperature data showed that many homeowners increased their evening settings, suggesting that their comfort requirements were not fully met by the flattened thermal profile from preheating. Despite efforts to shift heating operations away from times of excessive power consumption, manual overrides and behavioural adjustments revealed a gap between control algorithms and user needs. The findings demonstrate the importance of adaptive control systems that

adjust heat distribution to patterns of occupancy and household activities. Using Simscape (MATLAB), Singh and Sørensen [92] developed a comprehensive dynamic model of a home vapor-compression ASHP heating system. The expansion valve, controller, compressor, condenser, evaporator, and building space are the key components of the model, which employs R-407c as the refrigerant. It simulates system activity in a range of environmental conditions to assess thermal performance and dynamic responsiveness. The model's ability to maintain interior comfort setpoints and accurately replicate transitory reactions - like warming up after a drop in outside temperature - was confirmed. Even in the absence of specific COP values, the simulation showed that such a model could predict system efficiency, assess control strategies, and optimise operations in response to changing loads. This tool may be used to evaluate the viability of heat pumps in real-world situations and plan the integration of decentralised heat pumps into district heating systems. MPC-based DSM tactics, which usually adhere to an intricate two-step optimisation framework, provide creative solutions for effective DSM. MPC techniques for heat pump heat storage and heating have been explicitly studied in research articles, looking at how various control settings and storage tank sizes affect system load duration and user costs [39]. Advanced control techniques like MPC are the *brains* that really unlock the *energy flexibility* and financial advantages, even if PCMs offer the physical medium for energy storage. Having a PCM tank alone is not enough; smart algorithms are needed to make decisions on the go. when to charge (for example, in response to grid signals, renewable energy availability, or current electricity pricing) and when to discharge (for example, during periods of high power-costs or peak demand). It is this dynamic management that makes l*oad shifting* possible [43], *reducing user cost* [39], and *alleviating congestion in electricity grid* [93]. Demand response and grid integration are still largely unfulfilled without such intelligent controls. For PCM-integrated heat pump systems to maximise their economic and grid-level benefits, new control strategies, in particular, Model Predictive Control, must be incorporated. These sophisticated controls dynamically manage energy storage and release based on economic signals, predictive models, and real-time situations, allowing for optimal load shifting, cost savings, and improved grid stability.

In this study, two demand side management have been applied: First, this study applies time-of-use tariffs to calculate the exact amount of the customer's payments. Elevated tarriffs push the costumers use less electricity at rush hours, as the unit cost of electricity is higher at the peak hours compared to the other times of the day. Second, the system is off at nights, which sometimes named as nigh-loads shaving.

In the next section, it has been looked at the research papers that worked on techno-economic analysis of conventional/flexible heat pumps.

2.3 Techno-economic analysis of flexible /conventional air-source heat pumps

Economic viability is a crucial component of retrofitting or designing new systems, and any substitution of the traditional systems must be competitively priced in order to be an effective rival to replace the established ones. The assessment of these new systems' economic feasibility has been the subject of a few publications published in the literature in recent years. The following paragraphs show the gist of the studies that have been performed so far with regard to techno-economic and feasibility analysis of heating/cooling systems or air-source heat pumps.

To assess the economic viability of a novel frost-free ASHP system, *Wang et al.* [94] studied three Chinese cities, Xi'an, Shenyang, and Hefei. With operational cost reductions ranging from 23.2% to 29.0% across the three locations, the analysis showed significant cost gains. As a result, at 4.2 years in Xi'an, 3.3 years in Shenyang, and 4.03 years in Hefei, the initial investment of 23-26% dropped dramatically to just 4-6% over the course of a 20-year operation period. The feasibility of retrofitting Canadian homes with air-to-water heat pumps (AWHPs) to create net/near-zero energy buildings is assessed in a study by *Asaee et al.* [95]. To evaluate energy savings, emissions reductions, and economic viability, researchers examined over 17,000 distinct homes. According to the study, 71% of Canadian households, or over 6.3 million residences, qualify for AWHP retrofits, which could result in 36% lower energy use (520.8 petajoules) and 23% lower greenhouse gas emissions (15.16 million tons). To study via energy, energy efficiency, economics, and environmental viewpoints, *Navidbakhsh et al.* [96] studied a hybrid ITES system with PCM for air conditioning applications. Through multi-objective optimisation, it is shown that the hybrid system showed notable gains in energy efficiency and environmental effect: It was able to reduce CO2 emissions by up to 17.5% and electricity consumption by up to 17.1%, despite having a slightly longer payback period (3.97 years) than the basic ITES system (3.39 years). By contrasting ASHPs with more traditional heating techniques, including direct electric heating, gas boilers, and coal-fired boilers, *Zhang et al.* [97] assessed the viability of low-temperature air source heating heat pumps for the colder regions of northern China. The analysis showed that despite requiring a higher initial investment, the heat pump system was more cost-effective in the long run due to its dual heating and cooling capabilities and lower

operating expenses. *Nolting et al.* [98] examined time-of-use and market price-based control strategies to examine heat pump flexibility in the German energy system using validated MODELICA simulations. Time-of-use control with current tariffs showed efficiency losses of up to 16 percent and increased annual operating costs by about €40. Using the techno-economic analysis, *Alshehri et al.* [99] present a comparison of Ground Source Heat Pump (GSHP) and ASHP systems in hot, dry climates, using Saudi Arabia as a case study. The analysis revealed that GSHPs can achieve substantial energy consumption reductions and CO2 emissions savings compared to ASHPs but require a lengthy payback period of 10-20 years, depending on system configuration and local conditions. To assess the techno-economic performance of cascade air-to-water heat pumps (CAWHP) in residential building retrofits, *Le et al.* [100] used experimentally validated TRNSYS models, including scenarios with TES. It has been shown that although the CAWHP systems were more cost-effective than low-efficiency gas boilers, they are still unable to compete economically with gas boilers and high-efficiency gas boilers (90%) despite showing notable CO2 reductions (14-57%). By applying the economic analysis method on thermally integrated pumped-thermal energy storage (TI-PTES) systems, *Iqbal et al.*[101] examined two types: *cold TI-PTES* that used vapour compression refrigeration and *hot TI-PTES* that used a high-temperature vapour compression heat pump. The results of the economic analysis showed that, at a 0.5 MW scale, cold TI-PTES needed $3.21M with a Levelized Cost Of Storage (LCOS) of $0.31/kWh, whereas hot TI-PTES required $ 4.31 M. Better economic performance at bigger sizes might be demonstrated by the LCOS dropping to $0.25/kWh for hot TI-PTES and $0.23/kWh for cold TI-PTES for larger scale applications (5 MW, 8-hour storage). The viability of using TES-based air source heat pumps rather than traditional reverse cycle defrosting (RCD) systems is examined by *Li et al.* [102], including financial analysis. According to key findings, TES-based ASHPs can perform better than conventional systems in some situations. At ambient temperatures between -2°C and 2°C, they exhibit efficiency gains of 3.0-19.5%. The study highlights that appropriate system design and control are necessary for a successful deployment. To assess a novel air conditioning system that integrates latent heat thermal storage (LHTS) with a refrigeration system, *Mosaffa et al.* [103] studied three separate phase change materials (PCMs) with different slab configurations, RT27, S27, and SP25, which were analysed in order. Testing showed that with a cooling load of 11.8 kW, SP25 (Case 3) had the highest Coefficient of Performance (COP) at 3.434. RT27 (Case 1) had the best exergy efficiency at 2.93% and the highest product exergy rate of 0.084 kW. S27 (Case 2) was the most cost-effective, with the lowest total cost rate of $4,094 $/year and the lowest CO2 emissions. A mathematical model for assessing the

potential of three ecological refrigerants (R290, R600a, and R1234yf) in vapour compression systems is presented by *Paula et al.* [104]. The analysis took into account a number of variables, such as the overall plant cost rate, COP, exergy efficiency, and environmental effect (TEWI, or total equivalent warming impact). A thorough cost analysis showed that while environmental penalty costs from CO2 emissions were negligible at less than 2.60%, operational costs accounted for almost 73% of overall expenses. In this study, the environmental costs have been neglected, given that most of the costs would be the capital cost of the components. In order to optimise design factors for both performance and cost-effectiveness, *Mansuriya et al.* [105] examined a hybrid cooling system that combined vapour compression refrigeration with liquid desiccant dehumidification. With the hybrid system obtaining a COP range of 5.7-6.4 (compared to 3.8 for conventional systems) and a 68.4% increase in efficiency, the results showed significant gains over traditional systems. With a 1.54-year payback period, the technology demonstrated economic viability and greatly decreased electricity consumption.

2.4 Research Gaps and Key Objectives in this PhD Study

some studies have been performed so far to investigate the flexibility of air-conditioning systems, especially heat pumps with storage tanks. Two crucial aspects have been raised in these studies. First, in some cases, electricity usage reduction, cost, and energy savings were studied, but the results varied significantly based on the PCM phase change temperature, total TES storage capacity, system configuration, control strategy, and the building's location and environment.

Given the reviewing of the previous works, it is noticed that dynamic-numerical time-paced analysis, SCOP calculation to compare different systems, assuming proper realistic loads, considering a smart Control Strategy, Comprehensive Benchmarking, and economic analysis have been overlooked in most cases.

First, one of the primary challenges associated with adopting flexible systems is demonstrating their economic feasibility. In some research, the annual operational cost of systems has often been overlooked, while some research has examined reductions in electricity usage, cost savings, and energy efficiency. However, the findings vary significantly depending on several factors, including the PCM phase change temperature, total TES capacity, system configuration, control strategy, and the building’s geographic and climatic context. Second, some studies have neglected to consider the seasonal system's

COP. Third, many of these studies rely on representative or idealised daily load profiles, typically semi-sinusoidal patterns over a single day (e.g. riahi, et al. [75], Erdemir and Dincer [78]), which do not reflect realistic seasonal variability and may lead to overly optimistic results. This study has considered a whole season, with randomly variable loads extracted from IESVE software. Second, in some cases in the literature review, DSM or peak-shaving expressions are referred to in their manuscripts.

While single-stage systems with PCM tanks have been studied to some extent, flexible two-stage systems incorporating PCM storage require more studies. To the best of the authors' knowledge, the specific configuration presented in this thesis, featuring a PCM tank with salt hydrate connected via a fluidic loop, has not previously been investigated or compared with other systems.

On the other hand, economic viability is a crucial component of retrofitting or designing new systems, and any substitution of the traditional systems must be competitively priced in order to be an effective rival to replace the established ones. The assessment of these new systems' economic feasibility has been the subject of a few publications published in the literature in recent years. The objective of this research was to improve the heating/cooling systems by introducing a novel system and filling in the mentioned research gaps. The technical challenges to perform as such were mostly adding the details of the control strategy, and calculate the loads based on the real data for a case residential block which required learning a new software (IESVE). The details of control strategy, how to define charging and discharging in heating and cooling modes require high punctuality. Key objectives will be elaborated in the following paragraphs:

2.4.1. A novel two-stage flexible heat pump, with a PCM tank fluidly connected to the flash tank, has been proposed.

2.4.2. Three-phase analysis has been applied to the proposed system: Thermodynamics, heat transfer analysis (Heat exchanger design), and techno-economic analysis (TEA).

2.4.3. A control strategy based on the heating/cooling load, time of the day, and PCM tank status has been proposed to run the system in different operating modes hourly.

2.4.4. Four valves have been inserted in the cycle and manipulating them will lead to running the system in different modes: charging, discharging, normal, and standby modes.

2.4.5. To study the effect of weather conditions on flexibility, the weather data of four different cities have been studied: Glasgow and Birmingham, UK, for heating and Rome and London for cooling purposes.

2.4.6. To study the effect of heating load profile shape, two types of loads have been created and used to run the heat pump with: a) Variable loads exported from IESVE software for a residential block, and a sinusoidal load with the same maximum peak load.

2.4.7. The results of the novel flexible two-stage system will be compared to those of the baseline system (a two-stage heat pump without PCM), as well as with a baseline and flexible single-stage heat pump.

2.4.8. To study the effect of the configuration of the flexible system in heating in both single and two-stage forms, the results will be compared with another flexible system, common in literature, in which the PCM is placed after the condenser as a sub-cooler.

2.4.9. For cooling, the results of the novel flexible two-stage cooling will be compared to those of the baseline system, a baseline and flexible single-stage heat pump, and a second configuration of a flexible two-stage heat pump in the same weather data and control strategy and working conditions, except the charging/discharging trigger.

2.4.10. The TEA is performed by calculating the economic parameters - PP, IRR, NPV, MOIC. - to study the viability of the mentioned flexible two-stage system heat pump by applying a techno-economic viewpoint.

Chapter 3

Peak-shaving investigation of a novel flexible two-stage heat pump for heating

3.1 Introduction

In this study, a new system has been proposed to address the research gap using a two-stage heat pump with a PCM tank in the middle stage connected to the flash tank, working with real variable loads.

The specific objectives to investigate in this work include: 1. A novel two-stage flexible heat pump, with a PCM tank fluidly connected to the flash tank, has been proposed. 2. A control strategy based on the heating load, time of the day, and PCM tank status has been proposed to run the system in different operating modes, hourly. 3. Four valves have been inserted in the cycle and manipulating them will lead to running the system in different modes: charging, discharging, normal, and off modes. 4. To study the effect of weather conditions on flexibility, the weather data of two different cities has been studied: Glasgow and Birmingham, UK. 5. To study the effect of heating load profile shape, two types of loads have been created and used to run the heat pump with: a) Variable loads exported from IESVE software for a residential block, and a sinusoidal load with the same maximum peak load. 6. To study the effect of the configuration of the flexible system, the results will be compared with another flexible system in which the PCM is placed after the condenser as the sub-cooler. 7. The results of the novel flexible two-stage system will be compared to those of the baseline system (a two-stage heat pump without PCM), as well as with a baseline and flexible single-stage heat pump.

3.2 Methodology

The method of simulations has been elaborated in this section, which includes the following subsections: 3.3.1- System description 3.3.2- Operating modes of the flexible two-stage heat pump 3.3.3- Flexible two-stage heat pump versus the other flexible systems., 3.3.4- Basic assumptions of simulations, 3.3.5- Loads of IESVE and simulation logic, 3.3.6- Mathematical governing equations, 3.3.7- Annual price calculations.

3.2.1 System description

A novel flexible two-stage heat pump has been studied and compared with the baseline two-stage heat pump in heating applications. As an air-source heat pump, it uses the ambient air as its heat source and includes a compressor and expansion valve at each stage. The upper stage has the condenser, and the lower one has the evaporator, and both are connected to a flash tank. A fluidic circuit connects a PCM tank to the flash tank. Four valves are inserted before both compressors and expansion valves, which control the system's operation modes. The ambient air is the hot stream of the evaporator. It will heat the cold stream of the working fluid in the evaporator and turn the working fluid into a saturated vapour state. The compressor at the lower stage compressed the saturated vapour at the outlet of the evaporator and turned it into superheated vapour. To avoid having flash gas throttled to the evaporation pressure and the requirement for further recompression, which would require more compression power, a flash tank is provided to evacuate the flash gas at the intermediate pressure. Compressor I's (the lower stage compressor) vapour is further intercooled by the flash tank, which lowers the amount of compression power needed by Compressor II, the high-pressure stage compressor. Because of this, compared to a single-stage running at the same temperature lift, the system's COP is substantially higher.

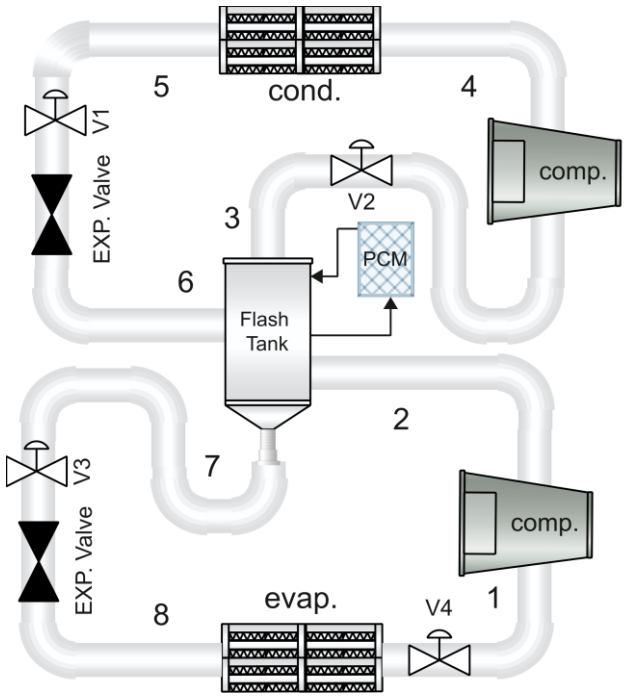

(a)

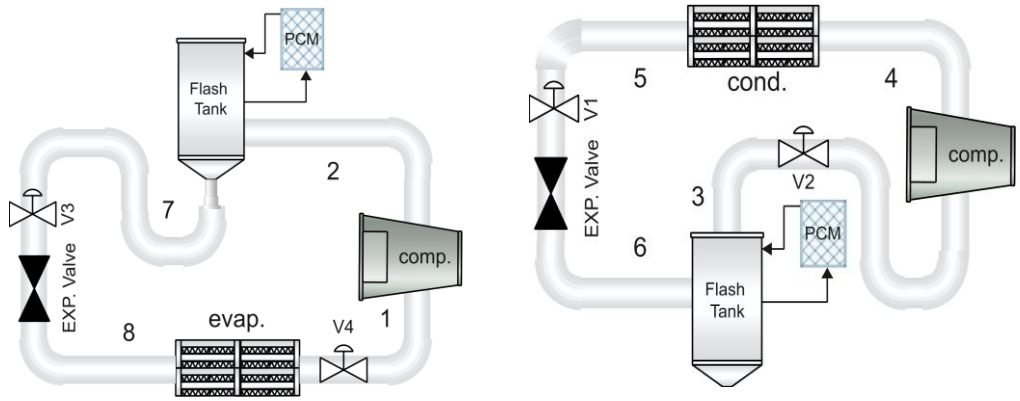

(b) (c)

Figure 0.1 Schematic figure of the proposed flexible two-stage heat pump (a), charging (b), discharging (c).

R134a, as the working fluid, will enter a flash tank, where the main entering stream will be divided into two outlets: A stream of saturated liquid and a saturated vapour one. The liquid stream will enter the lower stage expansion valve to decrease the pressure of the working fluid and then go through the evaporator, while the vapour stream will enter the upper compressor and turn into superheated vapour and then go through the condenser. The air stream at the condenser is the room airflow, which will be heated by the energy transferred through the condenser from its hot stream to the cold stream. The working fluid, which was the hot stream, will expand in an expansion valve within an enthalpy-constant process after being a saturated liquid in the condenser. Then, the two-phase working fluid exits from the expansion valve and enters the flash tank.

3.2.2 Operating modes of the flexible heat pump, configurations, and calculation methods

To operate the system in different modes, a suitable control strategy is required.

The novel flexible two-stage heat pump will work in four modes by manipulating the four inserted valves, as Fig. 3.1 (a), (b) and (c) and Table 3.1 show: Mode 1: Normal heating with a two-stage heat pump when four vales are open, shown in Fig. 3.1 (a), Mode 2: Charging - when valves 3 and 4 are open and the rest are closed, shown in Fig. 3.1 (b). Mode 3: Discharging - when valves 1 and 2 are open, and the rest are closed, shown in Fig. 3.1 (c). In the charging mode of the heating application, the PCM will be charged with the thermal energy of the hot stream 2-3. Therefore, the interstage temperature is defined as the approach temperature added to the PCM temperature, while for the discharging mode, the interstage needs to be lower than the PCM melting temperature, as the PCM has been cooled until being fully discharged via transferring the thermal energy to stream 3-6. The meaning of a fully charged/discharged PCM tank will be defined later in the methods section. Table 3.1

shows the operation modes and valve status in the proposed flexible two-stage heat pump. Fig. 3.2 (a), (b), and (c) show the T-s diagrams of the normal operation mode, charging, and discharging modes of the two-stage flexible heat pump. In the next section, 3.3.4, the details of the control strategy will be elaborated. Thermophysical properties have been calculated in the code via linking MATLAB [106] to NIST23-REFPROP V10 [107].

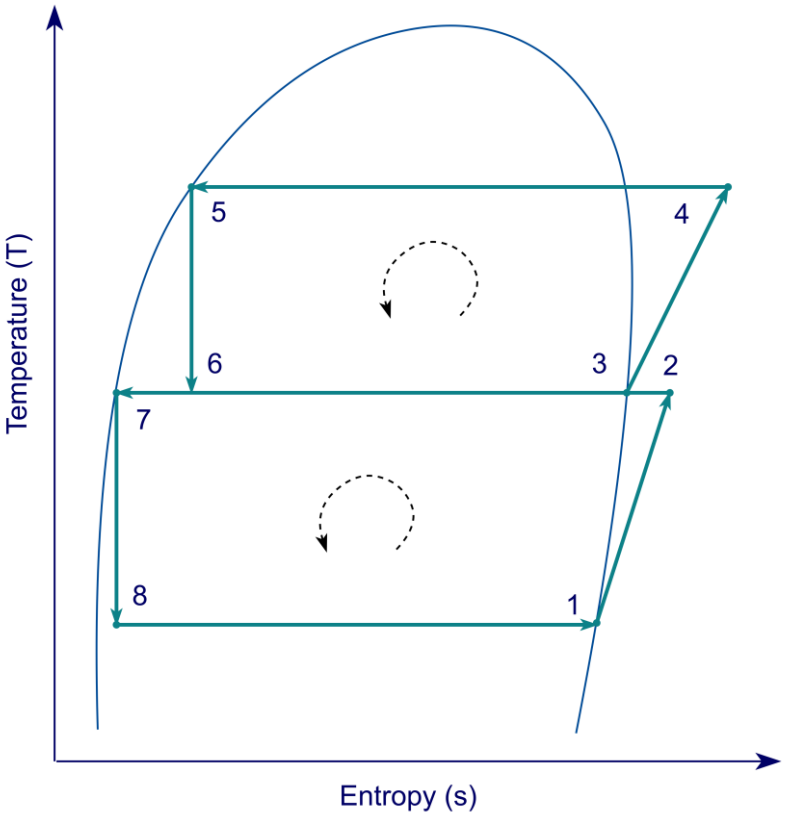

(a)

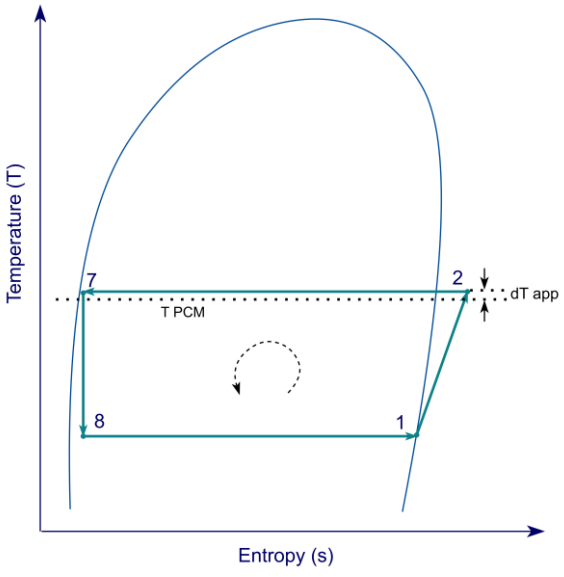

(b)

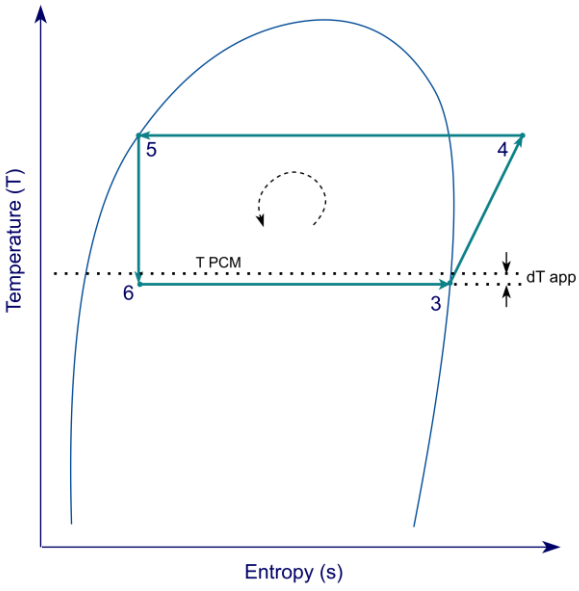

(c)

Figure 0.2 T-s diagram of the proposed flexible two-stage heat pump in (a) normal working, (b) charging and (c) discharging modes.

Table 0.1 Four operational modes of the proposed flexible heat pump system.

Mode	Comp. I	Comp. II	Pump	V1	V2	V3	V4
1 Normal	on	on	standby	on	on	on	on
2 Charging	standby	on	on	standby	standby	on	on
3 Discharging	on	standby	on	on	on	standby	standby

3.2.3 Basic assumptions and control strategy of simulation

Table 3.2 represents the required assumptions to start the simulation of the systems for the heating application, except the heating load and ambient temperature, which are variable throughout the year and will be exported from IESVE software [108]. For the heating application, the evaporator temperature varies based on the ambient temperature, and it is assumed to be 10 degrees lower than the outside temperature. The condenser temperature is considered 45 degrees. The melting temperature is assumed to be 20 degrees. Compressor second law efficiency, or the isentropic efficiency and approach temperature of the streams passing through the PCM storage tank, are assumed to be equal to 80% and 3 degrees, respectively. Working fluid has been considered R134a [75].

Table 0.2 Simulation assumptions for heating application.

Parameters	Value	Unit
Condenser Temperature [109]	45	℃
Evaporator Temperature	$T_{atm} - 10$	℃
PCM Melting Temperature [49]	20	℃
Weather Data	Glasgow and Birmingham, UK	-
η_{comp} [110]	80%	-
Approach Temperature difference	3	-

Table 0.3 Salt hydrate PCM properties coupled to the flexible heat pumps.

Parameters	Value	Unit
Initial PCM temperature	15	℃
Mass of PCM	1000	kg
$C_{p,PCM}$	2	$kJ.kg^{-1}.K^{-1}$
L_{fus} [49]	195	$kJ.kg^{-1}$
$Q_{Max\ th,PCM}$	205	MJ

Table 3.3 shows the PCM properties such as mass, initial temperature, Specific Heat at constant pressure, and heat of fusion (required energy for melting), and based on that information, the maximum energy capacity of PCM has been calculated and added to the Table. The PCM thermal capacity and related correlation will be written in section 3.3.6,

Mathematical governing equations. The assumptions are written in Tables 3.2 and 3.3. The following rules have been applied while simulating:

- Heat transfer takes place under isothermal conditions in all heat exchangers.

- Specific Heat at constant pressure is considered constant to simplify the simulation.

- No heat and pressure losses have been considered for the working fluid passing through pipes and heat exchangers.

- In the normal two-stage heat pump, the interstage temperature is a sensitive parameter that is normally optimised. To simplify, in this study, it has been assumed that the interstage temperature equals the interstage temperature in the flexible system. The interstage temperature of the proposed flexible system is equal to the summation of the approach temperature and the melting PCM temperature. To have a fair comparison, in the baseline two-stage systems without PCM tanks, the interstage temperature will be a flexible system's interstage temperature. In the second flexible configuration, the interstage temperature cannot be the summation of the approach temperature and the melting PCM temperature, as it needs to be less than the melting temperature plus the approach temperature difference. It has been assumed that it is 10 degrees less than the summation of the melting temperature and the approach temperature difference.

- The systems are working from 7 a.m. until 11 p.m. except for the flexible systems at nighttime (11 p.m. to 7 a.m.), in which charging mode is possible if the duty is low enough. This strategy is called night load shaving, and it's a type of demand-side strategy (DSM). In this study, triggering of charging and discharging is based on the amount of heating duty. If the duty is less than 15% of the maximum heating load (=20 kW of 134 kW of maximum heating duty), the charging will start with no regard to the time. While discharging will start when the heating load is higher than 20kW. However, for Birmingham weather, the trigger assumed the same 20 kW.

- After importing ambient temperature and variable heating load from IESVE, the control strategy in this simulation will decide if the system will operate in charging, discharging, normal operation, or standby mode. Table 3.6 shows the system's operation modes logically on different occasions, based on the duty, time of the day,

and status of the PCM tank. Based on the control strategy, the provided heat will be varied in different modes, as the aim is different in each mode. As in charging, the aim is to charge the PCM; the heating load of the charging mode equals the energy rate transferred to the PCM tank during charging. While in discharging and normal modes, the aim is to provide the heating load of the residential block, and the provided load will be the same heating loads extracted from the IESVE model shown in Fig. 3.8.

- For the heating application, the system has been analysed from October to March, and the rest of the year has been assumed off.

- In addition, as it will be explained later, a sinusoidal load has been created with the same maximum heating load as that of the IESVE exported loads. The aim is to compare the results to see if there is any difference with different heating load profiles.

First, the state points of a flexible two-stage heat pump in heating application in normal working mode will be calculated based on the following steps, based on the state points of in Fig. 3.1 (a), (b) and (c). To calculate the thermodynamic properties of each state point two independent properties are required. Thermodynamic properties include pressure (P), Temperature (T), Enthalpy (h), quality (Q), and Entropy (s). In each state point, calculations started with independent properties lead to (presented with → symbol) the third calculated property, as shown below. $\dot{m}$ refers to mass flow rate in kg. s^{-1} and η_{comp} is isentropic efficiency of the compressors.

- State point 1: evaporator outlet, evaporator temperature, saturated vapour state.

$$\begin{cases} T_1 = T_{eva}, T_{eva} = T_{atm} - \Delta T_{app} \\ Q_1 = 1, \text{saturated vapour} \end{cases} \rightarrow h_1 \qquad \textbf{Equation 0-1}$$

- State point 2: compressor outlet (isentropic efficiency 80% [110]), and pressure of state point 6.

$$\begin{cases} P_2 = P_6 \\ \eta_{comp} = \dfrac{h_{2s} - h_1}{h_2 - h_1} \rightarrow h_2 \end{cases} \qquad \textbf{Equation 0-2}$$

- State point 3: flash chamber outlet, saturated vapour, pressure of state point 6.

$$\begin{cases} P_3 = P_6 \\ Q_3 = 1, \text{saturated vapour} \end{cases} \rightarrow h_3$$ **Equation 0-3**

- State point 4: compressor outlet (isentropic efficiency 80% [110]), pressure of the condenser.

$$\begin{cases} P_4 = P_5 \\ \eta_{comp} = \dfrac{h_{4s} - h_3}{h_4 - h_3} \end{cases} \rightarrow h_4$$ **Equation 0-4**

- State point 5: condenser outlet (fixed temperature), saturated liquid.

$$\begin{cases} T_5 = T_{cond}, T_{cond} = cte \\ Q_5 = 0, \text{saturated vapour} \end{cases} \rightarrow h_5$$ **Equation 0-5**

- State point 6: interstage temperature (melting PCM temperature $T_{melting}$ plus approach temperature ΔT_{app}). The interstage temperature of normal working has been defined in the same way as the charging mode. Also, the conventional system's interstage has been defined the same as the flexible system's interstage, to prevent having any difference due to different interstage pressure or temperature.

$$\begin{cases} T_6 = T_{interstage}, T_{interstage} = T_{melting} + \Delta T_{app} \\ h_6 = h_5 \end{cases} \rightarrow P_6$$ **Equation 0-6**

- State point 7: saturated liquid, interstage pressure.

$$\begin{cases} P_7 = P_6 \\ Q_7 = 0, \text{saturated liquid} \end{cases} \rightarrow h_7$$ **Equation 0-7**

- State point 8: enthalpy of state point 6, pressure of the evaporator

$$\begin{cases} h_8 = h_7 \\ P_8 = P_1 \end{cases}$$ **Equation 0-8**

The mass flow rates come from Eq. 3-9, and duty refers to the heating load extracted from IESVE or the sinus-shaped loads:

$$\begin{cases} \dot{m}_2 = \dfrac{\text{duty}}{h_4 - h_5} \\ \dot{m}_1 = \dot{m}_2 . \dfrac{h_3 - h_6}{h_2 - h_7} \end{cases}$$ **Equation 0-9**

Second, in the charging mode, we'll have the PCM as a condenser. The state points and mass flow rate of the charging mode will be calculated based on the following steps:

$$\dot{m}_c = 0.06, \text{constant.}$$ **Equation 0-10**

- State point 7: saturated liquid, Temperature of charging, which is PCM melting temperature, is added to the approach temperature. This temperature definition will charge the PCM over time.

$$\begin{cases} T_{7c} = T_{melting} + \Delta T_{app} \\ Q_{7c} = 0, \text{saturated liquid} \end{cases} \rightarrow h_{7c}$$ **Equation 0-11**

- State point 8: enthalpy of state point 6, pressure of the evaporator.

$$\begin{cases} h_{8c} = h_{7c} \\ P_{8c} = P_1 \end{cases}$$ **Equation 0-12**

Finally, the discharging mode will have the state points based on the following steps:

$$\dot{m}_d = \frac{\text{duty}}{h_{4d} - h_5}$$ **Equation 0-13**

- State point 3: The pressure of interstage in discharging, saturated vapour.

$$\begin{cases} P_{3d} = P_{6d} \\ Q_3 = 1, \text{saturated vapour} \end{cases} \rightarrow h_{3d}$$ **Equation 0-14**

- State point 4: compressor outlet, pressure of interstage.

$$\begin{cases} P_{4d} = P_5 \\ \eta_{comp} = \dfrac{h_{4sd} - h_{3d}}{h_{4d} - h_{3d}} \rightarrow h_{4d} \end{cases}$$ **Equation 0-15**

- State point 6: interstage temperature (melting PCM temperature minus approach temperature), enthalpy of condenser outlet.

$$\begin{cases} T_{6d} = T_{melting} - \Delta T_{app} \rightarrow P_{6d} \\ h_{6d} = h_5 \end{cases}$$ **Equation 0-16**

On the other hand, to compare the results with a common flexible heat pump in the literature, a similar single-stage flexible heat pump, and another configuration of flexible heat pump in single and two-stage models have been studied and simulated based on the energy storage concept, which will be elaborated in the following paragraphs.

In Fig. 3.3 (a), a single-stage heat pump that is connected to a PCM storage tank has been shown. The two valves control the fluid streams into/out of the PCM tank. With the closed valves, the system will work in normal heating mode while charging will happen when valve 2 is closed, and the PCM will play the role of the condenser. The working fluid after the condenser will be saturated liquid, which means it will transfer its energy to the PCM, and the PCM will be charged. While in the discharging mode, valve 1 is closed, and the PCM tank is the evaporator, which will lose its energy to vaporise the working fluid during the evaporation process. Fig. 3.3 (a), (b), and (c) represent the schematic figures of normal heating, charging, and discharging modes of a single stage heat pump, respectively. Fig. 3.4 shows the T-s diagrams of the mentioned modes of a single-stage flexible heat pump in this specific configuration. As it is represented, the evaporator and condenser temperatures would be adjusted based on the PCM temperature in charging and discharging modes, as the PCM tank plays the role of an evaporator and condenser in different modes, as explained previously.

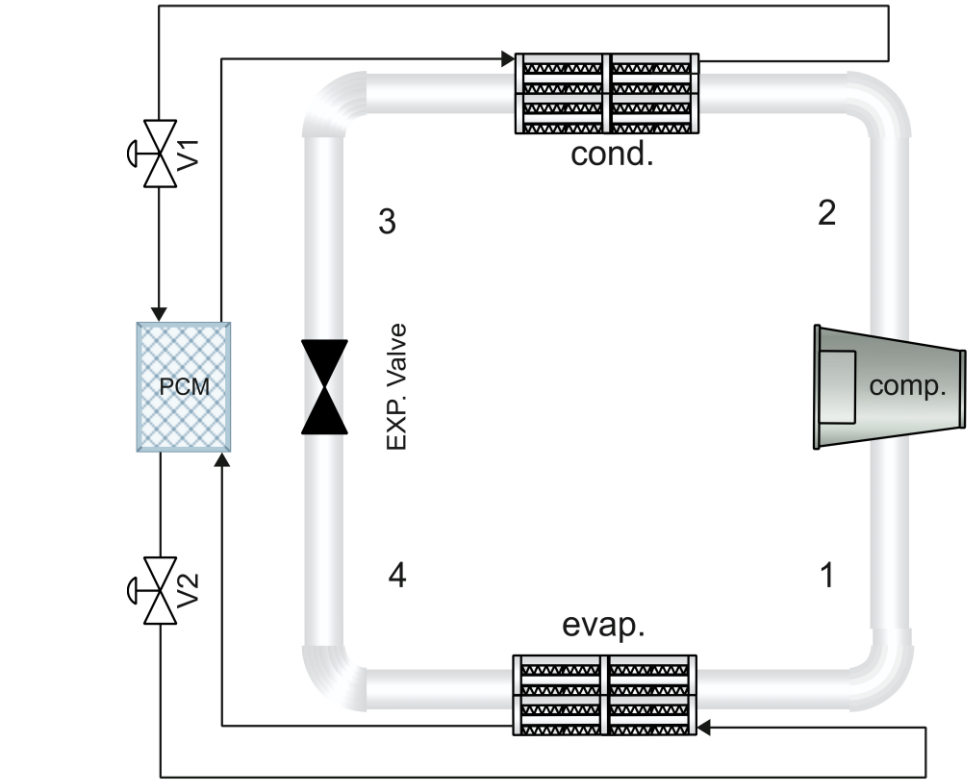

(a)

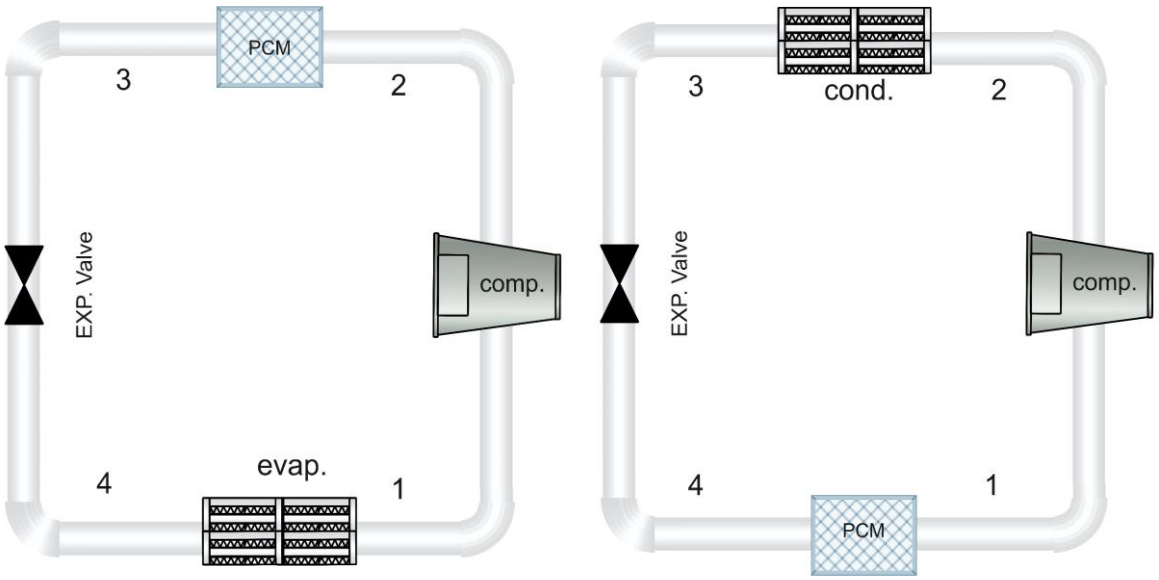

(b) (c)

Figure 0.3 Flexible single-stage heat pump, normal operation with closed valves (a), charging mode (b), and discharging mode (c).

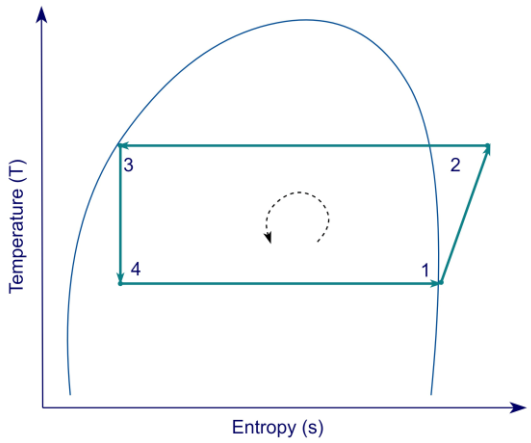

(a)

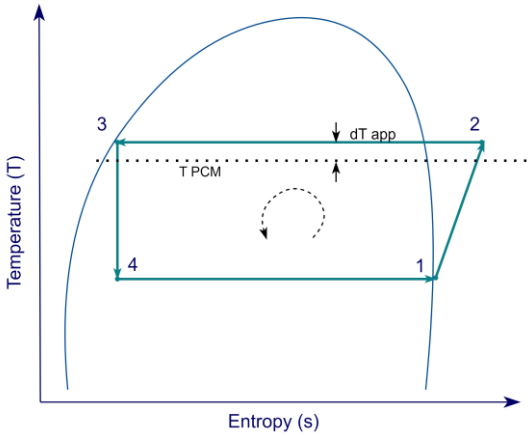

(b)

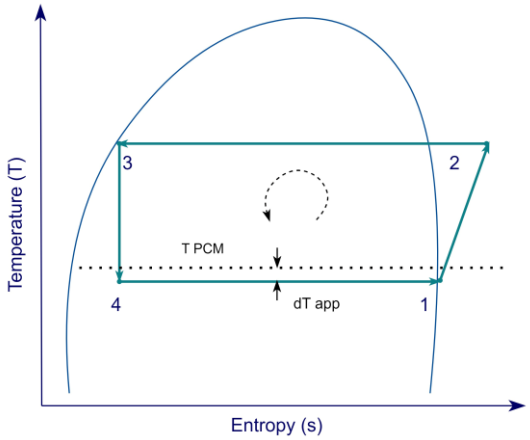

(c)

Figure 0.4 T-s diagrams of (a) Normal operation, (b) charging, and (c) discharging process of a flexible single-stage heat pump in the heating application.

Based on the schematic figure of the flexible heat pump in Fig. 3.3, step-by-step will be explained in the following paragraphs how the properties of state points have been calculated for the flexible configuration of the single-stage heat pump.

In normal working mode:

- State point 1: The evaporator outlet will have a saturated vapour state, and a fixed temperature of 10 degrees lower than the weather temperature.

$$\begin{cases} T_1 = T_{eva}, T_{eva} = T_{atm} - \Delta T_{app} \\ Q_1 = 1, \text{saturated vapour} \end{cases} \rightarrow h_1$$

Equation 0-17

- State point 2: outlet of the compressor, pressure of outlet of the condenser (state point 3).

$$\begin{cases} P_2 = P_3 \\ \eta_{comp} = \dfrac{h_{2s} - h_1}{h_2 - h_1} \rightarrow h_2 \end{cases}$$ **Equation 0-18**

- State point 3: condenser outlet, fixed temperature of condenser, saturated liquid.

$$\begin{cases} T_3 = T_{cond}, T_{cond} = cte \\ Q_3 = 0, \text{saturated vapour} \end{cases} \rightarrow h_3$$ **Equation 0-19**

- State point 4: outlet of the expansion valve, evaporator pressure, enthalpy of the condenser outlet, and enthalpy.

$$\begin{cases} h_4 = h_3 \\ P_4 = P_1 \end{cases}$$ **Equation 0-20**

For the charging mode, the PCM will be connected to the condenser, and rather than providing duty for the residential block, the system will charge the PCM:

$$\dot{m}_c = 0.06\ kg.s^{-1}, \text{constant.}$$ **Equation 0-21**

- State point 2: Outlet of the compressor: the same as normal working.

$$\begin{cases} P_{2c} = P_{3c} \\ \eta_{comp} = \dfrac{h_{2sc} - h_1}{h_{2c} - h_1} \rightarrow h_{2c} \end{cases}$$ **Equation 0-22**

- State point 3: Outlet of the PCM tank as the condenser, its temperature will be higher than the melting temperature and in a liquid state. The temperature difference of the state point with the malting temperature will be the approach temperature difference.

$$\begin{cases} T_{3c} = T_{melting} + \Delta T_{app} \\ Q_{3c} = 0, \text{saturated vapour} \end{cases} \rightarrow h_{3c}, P_{3c}$$ **Equation 0-23**

- State point 4: Outlet of the expansion valve: Pressure is as much as the evaporator pressure, and enthalpy is equal to the enthalpy of state point 3 in charging mode.

$$\begin{cases} h_{4c} = h_{3c} \\ P_{4c} = P_1 \end{cases}$$ **Equation 0-24**

In the discharging mode, we will have the PCM in an evaporator role. The state points in a discharging mode will be as follows:

$$\dot{m}_d = \frac{\text{duty}}{h_{2d} - h_3} \quad \textbf{Equation 0-25}$$

- State Point 1: PCM outlet, melting temperature minus approach temperature difference, saturated vapour.

$$\begin{cases} T_{1d} = T_{melting} - \Delta T_{app} \\ Q_{1d} = 1, \quad \text{saturated vapour} \end{cases} \rightarrow P_{1d}, h_{1d} \quad \textbf{Equation 0-26}$$

- State point 2: Compressor outlet, pressure of the condenser.

$$\begin{cases} P_{2d} = P_3 \\ \eta_{comp} = \frac{h_{2sd} - h_{1d}}{h_{2d} - h_{1d}} \rightarrow h_{2d} \end{cases} \quad \textbf{Equation 0-27}$$

- State point 4: Expansion valve outlet, pressure of the PCM outlet, and enthalpy of the condenser outlet.

$$\begin{cases} h_{4d} = h_3 \\ P_{4d} = P_{1d} \end{cases} \quad \textbf{Equation 0-28}$$

3.2.4 Comparing the results with Other flexible configurations of single and two-stage Heat pumps

To study other configurations of flexible heat pumps and compare them to the novel proposed configuration, the PCM tank has been added to the system as a sub-cooler. This is not a novel configuration, at least in the single-stage model. In this configuration, the main components are the same. The system can operate in different modes, similar to any flexible heat pump. In this type of configuration, in the charging mode, the working fluid exiting the condenser will enter the PCM tank, which will decrease its energy even more and increase the thermal energy of the PCM tank. This means that the PCM tank, as a sub-cooler, will be charged with thermal energy. The schematic figures of normal operation mode, charging, and discharging have been shown in Figs 3.5 and 3.6 for two-stage and single-stage, respectively.

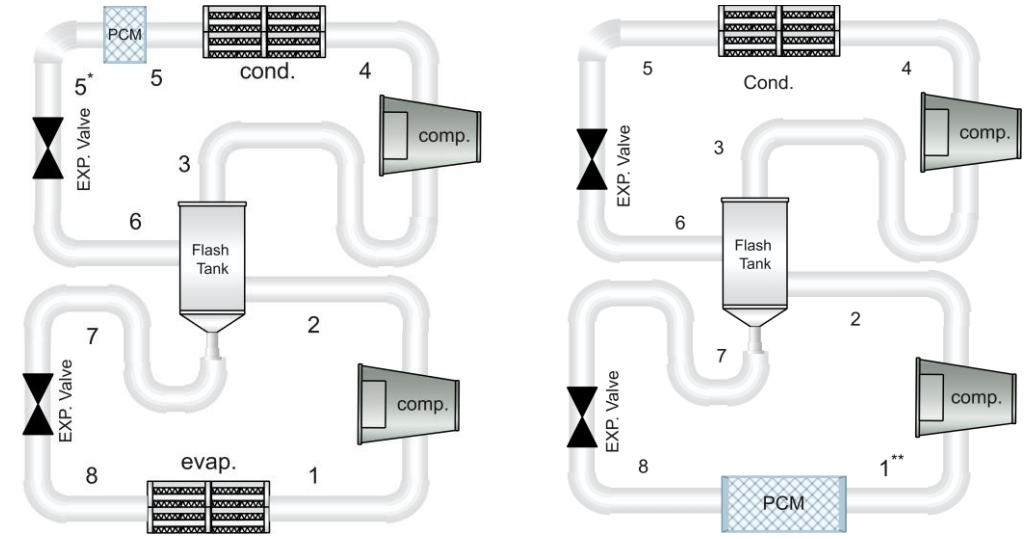

(a) (b)

Figure 0.5 Second configuration of flexible two-stage heat pump charging mode (a) and discharging mode (b).

The state points properties of config. 2 of the two-stage heat pump shown in Fig. 3.5 are elaborated as follows:

$$\begin{cases} \dot{m}_2 = \dfrac{\text{duty}}{h_4 - h_5} & (a) \\ \dot{m}_1 = \dot{m}_2 . \dfrac{h_3 - h_6}{h_2 - h_7} & (b) \end{cases}$$ **Equation 0-29**

- State point 1: evaporator outlet, evaporator temperature, saturated vapour state.

$$\begin{cases} T_1 = T_{eva}, T_{eva} = T_{atm} - \Delta T_{app} \\ Q_1 = 1, \text{saturated vapour} \end{cases} \rightarrow h_1$$ **Equation 0-30**

- State point 2: compressor outlet (isentropic efficiency 80% [110]), and pressure of state point 6.

$$\begin{cases} P_2 = P_6 \\ \eta_{comp} = \dfrac{h_{2s} - h_1}{h_2 - h_1} \rightarrow h_2 \end{cases}$$ **Equation 0-31**

- State point 3: flash chamber outlet, saturated vapour, pressure of state point 6.

$$\begin{cases} P_3 = P_6 \\ Q_3 = 1, \text{saturated vapour} \end{cases} \rightarrow h_3$$ **Equation 0-32**

- State point 4: compressor outlet (isentropic efficiency 80% [110]), pressure of the condenser.

$$\begin{cases} P_4 = P_5 \\ \eta_{comp} = \dfrac{h_{4s} - h_3}{h_4 - h_3} \rightarrow h_4 \end{cases}$$ **Equation 0-33**

- State point 5: condenser outlet (fixed temperature), saturated liquid.

$$\begin{cases} T_5 = T_{cond}, T_{cond} = cte \\ Q_5 = 0, \text{saturated vapour} \end{cases} \rightarrow h_5$$ **Equation 0-34**

- State point 6: interstage temperature (melting PCM temperature plus approach temperature). The interstage temperature, in this case, cannot be $T_{melting} + \Delta T_{app}$. Therefore, it has decreased 10 degrees.

$$\begin{cases} T_6 = T_{interstage}, T_{interstage} = T_{melting} + \Delta T_{app} - 10 \\ h_6 = h_5 \end{cases} \rightarrow P_6$$ **Equation 0-35**

- State point 7: saturated liquid, interstage pressure.

$$\begin{cases} P_7 = P_6 \\ Q_7 = 0, \text{saturated liquid} \end{cases} \rightarrow h_7$$ **Equation 0-36**

- State point 8: enthalpy of state point 6, pressure of the evaporator.

$$\begin{cases} h_8 = h_7 \\ P_8 = P_1 \end{cases}$$ **Equation 0-37**

Second, in a charging mode, we'll have the PCM as a condenser. The state points of a charging mode will be calculated based on the following steps:

$$\dot{m}_c = 0.06\ kg.s^{-1}, \text{constant.}$$ **Equation 0-38**

- State point 5`: PCM outlet temperature in charging mode,

$$\begin{cases} T_5 = T_{melting} + \Delta T_{app} \\ P_{5*} = P_5 \end{cases} \rightarrow h_{5*}$$ **Equation 0-39**

- State point 6c: enthalpy of state point 5*

$$\begin{cases} h_{6c} = h_{5*} \\ P_{6c} = P_6 \end{cases}$$ **Equation 0-40**

- State point 7c: saturated liquid

$$\begin{cases} P_{7c} = P_{6c} \\ Q_{7c} = 0, \text{saturated liquid} \end{cases} \rightarrow h_{7c}$$ **Equation 0-41**

- State point 8: enthalpy of state point 7c, pressure of the evaporator.

$$\begin{cases} h_{8c} = h_{7c} \\ P_{8c} = P_1 \end{cases}$$ **Equation 0-42**

- State point 3c: flash chamber outlet, saturated vapour, the pressure of state point 6.

$$\begin{cases} P_{3c} = P_{6c} \\ Q_3 = 1, \text{saturated vapour} \end{cases} \rightarrow h_{3c}$$ **Equation 0-43**

- State point 4c: compressor outlet (isentropic efficiency 80% [110]), pressure of the condenser.

$$\begin{cases} P_{4c} = P_5 \\ \eta_{comp} = \dfrac{h_{4sc} - h_{3c}}{h_{4c} - h_{3c}} \end{cases} \rightarrow h_{4c}$$ **Equation 0-44**

Finally, the discharging mode will have the state points based on the following steps:

- State point 1**:

$$\begin{cases} T_{1**} = T_{melting} - \Delta T_{app} \\ Q_{1**} = 1 \end{cases} \rightarrow h_{1**}$$ **Equation 0-45**

- State point 2d: compressor outlet (isentropic efficiency 80% [110]), and pressure of state point 3.

$$\begin{cases} P_{2d} = P_3 \\ \eta_{comp} = \dfrac{h_{2sd} - h_{1**}}{h_{2d} - h_{1**}} \end{cases} \rightarrow h_{2d}$$ **Equation 0-46**

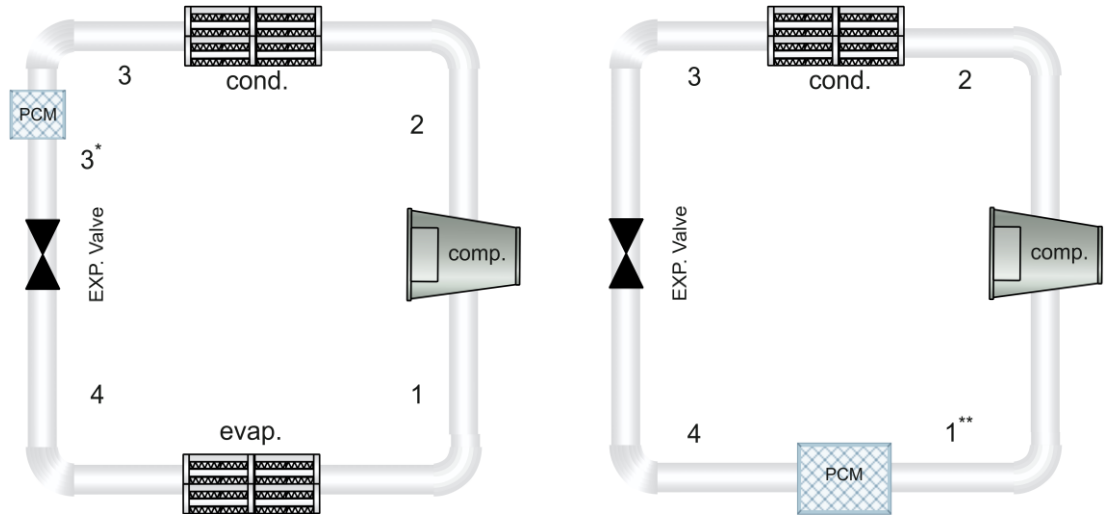

(a) (b)

Figure 0.6 Second configuration of flexible single-stage heat pump charging mode (a) and discharging mode (b).

In the normal working mode of config. 2 of the single-stage heat pump, we will have state points as follows:

- State point 1: The evaporator outlet will have a saturated vapour state, and a fixed temperature of 10 degrees lower than the weather temperature.

$$\begin{cases} T_1 = T_{eva}, T_{eva} = T_{atm} - \Delta T_{app} \\ Q_1 = 1, \text{saturated vapour} \end{cases} \rightarrow h_1 \quad \textbf{Equation 0-47}$$

- State point 2: outlet of the compressor, pressure of outlet of the condenser

$$\begin{cases} P_2 = P_3 \\ \eta_{comp} = \dfrac{h_{2s} - h_1}{h_2 - h_1} \rightarrow h_2 \end{cases} \quad \textbf{Equation 0-48}$$

- State point 3: condenser outlet, fixed temperature, saturated liquid.

$$\begin{cases} T_3 = T_{cond} \\ Q_3 = 1, \text{saturated vapour} \end{cases} \rightarrow h_3, P_3 \quad \textbf{Equation 0-49}$$

- State point 4:

$$\begin{cases} P_4 = P_1 \\ \eta_{comp} = \dfrac{h_{4sd} - h_{3d}}{h_{4d} - h_{3d}} \rightarrow h_{4d} \end{cases}$$ **Equation 0-50**

In the charging mode of config. 2 of the single-stage heat pump, we will have state points as follows:

$$\dot{m}_c = 0.06\ kg.s^{-1}, \text{constant.}$$ **Equation 0-51**

- State point 3*:

$$\begin{cases} T_{3*} = T_{melting} + \Delta T_{app} \\ P_{3*} = P_3 \end{cases} \rightarrow h_{3*}$$ **Equation 0-52**

- State point 4c:

$$\begin{cases} P_{4c} = P_1 \\ \eta_{comp} = \dfrac{h_{4sc} - h_{3*}}{h_{4c} - h_{3*}} \rightarrow h_{4c} \end{cases}$$ **Equation 0-53**

In the discharging mode, we will have the PCM in an evaporator role. The state points in a discharging mode will be as follows:

- State point 1**:

$$\begin{cases} T_{1**} = T_{melting} - \Delta T_{app} \\ Q_{1**} = 1, \quad \text{saturated vapour} \end{cases} \rightarrow h_{1**}$$ **Equation 0-54**

- State point 2d:

$$\begin{cases} P_{2d} = P_3 \\ \eta_{comp} = \dfrac{h_{2sd} - h_{1**}}{h_{2d} - h_{1**}} \rightarrow h_{2d} \end{cases}$$ **Equation 0-55**

- State point 4d:

$$\begin{cases} P_{4d} = P_{1**} \\ h_{4d} = h_3 \end{cases}$$ **Equation 0-56**

3.2.5 Loads of IESVE and simulation logic:

To calculate the required variable heating loads for Glasgow and Birmingham, UK, a four-story residential building was created based on a predefined geometry in IESVE, as shown in Fig. 3.7. To calculate the loads of heating/cooling, a geometry is required to be created in IESVE. There are three ways to create a geometry, (a) create from scratch, (b) Import from Revit, (c) use predefined geometries. As the loads are the aim, not the geometry itself, a predefined residential geometry is selected from the predefined geometry options in IESVE.

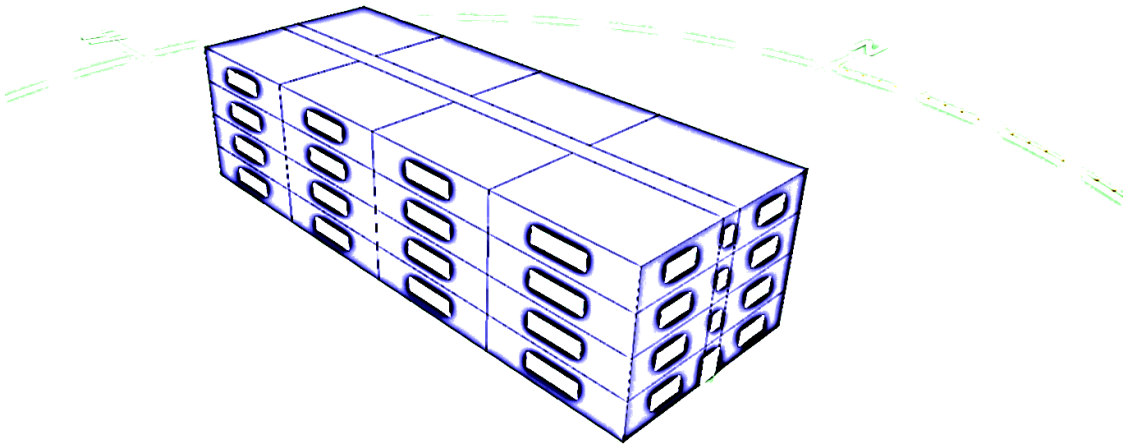

Figure 0.7 Geometry of the predefined residential block from IESVE.

The assumptions used to create the energy model of the residential block in IESVE are shown in Table 3.4, while the U values of the building's components are written in Table 3.5. However, the U values are automatically defined in the building geometry.

Table 0.4 Residential Block's geometry and energy Model Parameters in IESVE software.

Parameters	Value	Unit
Area	3,134.92	m^2
External wall area	1,542.19	m^2
External Opening Area	231.38	m^2
Room set point	19	$℃$
DHW consumption	0	$l.h^{-1}$
Internal Gains		
Occupancy	25	$m^2\ per\ person$
People's Max sensible gain	64	$w\ per\ person$
latent	70	$w\ per\ person$
Lighting Max sensible gain	6.5	$w\ per\ m^2$
Equipment sensible gain	2.4	$w\ per\ m^2$
Equipment Max power consumption	4.8	$w\ per\ m^2$
Infiltration (Air Leakage)	0.6	Ach (air changes per hour)

Natural ventilation (Air change)	0.3	Ach (air changes per hour)

Table 0.5 Default U values of the walls, Roof, Floor, windows, doors, etc, from predefined geometry in IESVE.

Components	U values ($w/m^2.K$)	Thickness (mm)
Internal ceiling/Floor	1.0866	282.5
External window	1.6	24.0
Exposed Floor	0.22	268.0
Internal Partition	1.7888	75.0
Roof	0.18	317.0
External wall	0.2599	208.0

Fig. 3.8 (a)-(d) shows the ambient temperature and heating loads of two Uk cities extracted from IESVE software: Glasgow and Birmingham, as a sample of cooler and warmer cities in UK. Also, to compare with variable loads from IESVE, a sinousoidal load has been created based on maximum load of Glaswiegen heating load came from IESVE, which is shown in Fig. 3.9. Sinousoidal load was one of the common assumption to be found is a sinous-shaped load for one day, or extended for the whole year.

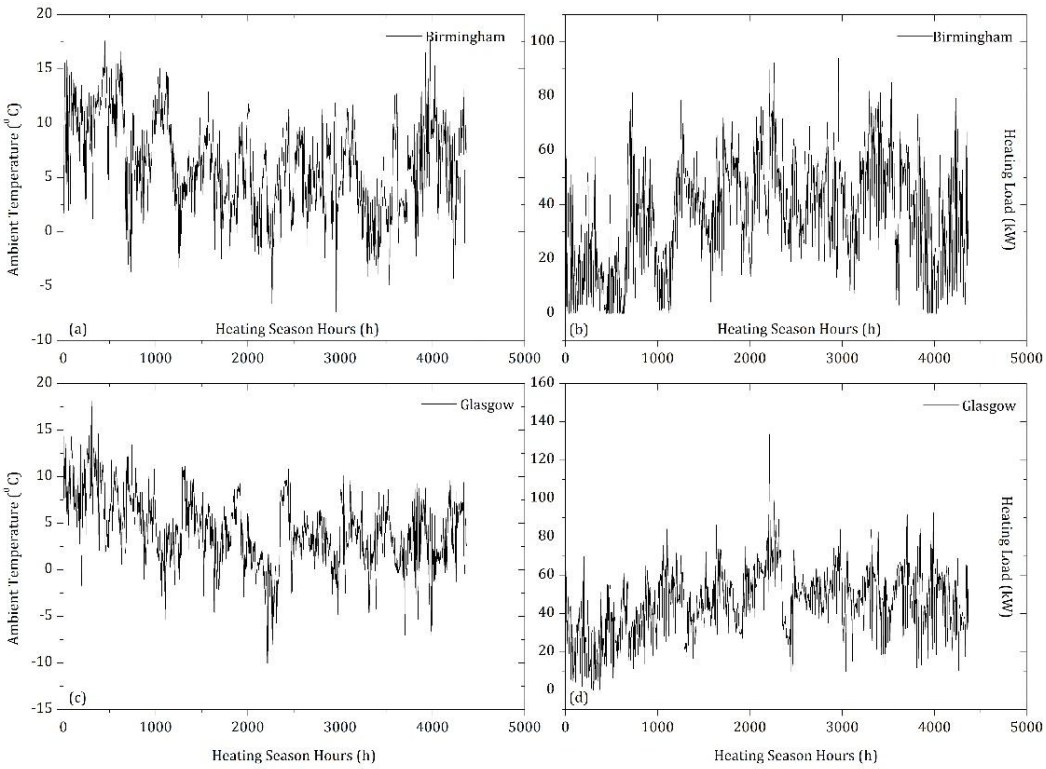

Figure 0.8 Ambient temperature and heating loads input for Birmingham (a) - (b), and Glasgow, Scotland, UK, (c)-(d).

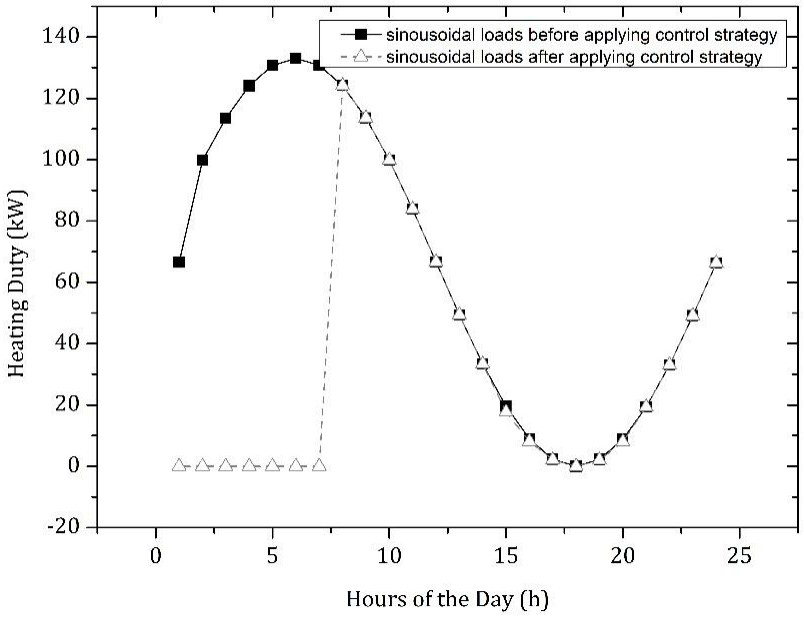

Figure 0.9 A sinusoidal load profile per day as input (repeated for the whole season).

Table 3.6 shows the working status of the baseline and flexible systems based on the indicator parameters, heating load or duty from IESVE, time of the day, and stored thermal energy of the PCM tank. At each hour, the heating duty will be checked. If it is lower than 20 kW, no matter what the time is, the charging will start until the PCM tank is fully charged. After having a fully charged PCM tank, even if the charging triggers are ready to activate the charging, that will not happen, as the PCM tank has reached its maximum capacity. To define mathematically what the fully charged state is, a parameter named SOC (State of Charging) has been defined and calculated. SOC is the amount of thermal energy inside the PCM tank's divided by the theoretically PCM tank maximum storage capacity, or it is defined as the ratio of the available capacity at the i-th hour of the day, $Q_{PCM}(i)$, compared to the maximum possible charge that can be stored in a storage tank or battery, i.e., the maximum nominal capacity of PCM $Q_{Max\ th,PCM}$.

$$\mathrm{SOC(i)} = \frac{\mathrm{Q_{PCM}(i)}}{\mathrm{Q_{Max\ th,PCM}}}$$

Equation 0-57

A fully charged battery/storage tank has an SOC of 1 or 100%, while a fully discharged battery has an SOC of 0 or 0% [111]. In this study, it is considered that if the amount of SOC is higher than 96%, it is assumed that the PCM tank is fully charged, and if it is less than 4%, it is said that the PCM tank is fully discharged. SOC is defined and has been used many times previously in some published research articles, such as *Huang, et al.* [69].

Table 0.6 Working status of the normal and flexible two-stage heat pump in heating application.

Time	duty	PCM state	Baseline	Flexible
0-7	Duty<20 kW	QPCM Max	-	
		QPCM not 0		Charging
		QPCM=0		
	Duty>20 kW	QPCM Max	-	
		QPCM not 0		
		QPCM=0		
7-23	Duty<20 kW	QPCM Max	-	
		QPCM not 0	Normal	Charging
		QPCM=0		
	Duty>20 kW	QPCM Max	-	Discharging
		QPCM not 0	Normal	
		QPCM=0		Normal

The flowchart of the system's logic, matched with Table 3.6, has been shown for heating in Fig. 3.10. As shown, starting with inputs including the assumptions and data extracted from IESVE, first, the heating load mentioned as duty will be checked. If it is higher than 20 kW, the PCM status will be checked. If it is not fully charged, the system will go to charging mode until it gets a fully charged PCM tank. The meaning of fully charged has been explained in this section. In a fully charged state, the system will be switched to normal working mode.

If the duty is lower than 20 kW, and it is between 7 a.m. and 11 p.m., the PCM status will be checked again. If there is any energy saved in the PCM tank, the system will be switched to discharging mode until the tank is fully discharged, if nothing is changed. However, at nighttime, the system will be in standby mode (off).

Figure 0.10 Flowchart of the simulation for heating in this study.

3.2.6 Mathematical governing equations:

To analyse the systems based on thermodynamic fundamentals in MATLAB, the first and second laws of thermodynamics have been applied, and each component is assumed to be a control volume. Based on the 1st and 2nd laws of thermodynamics, the corresponding mass and energy balances of each component are given in Eqs. 3-58 and 3-59.

$$\sum \dot{m}_{in} = \sum \dot{m}_{out} \quad \textbf{Equation 0-58}$$

$$\sum \dot{m}_{in} h_{in} + \dot{Q} = \sum \dot{m}_{out} h_{out} + \dot{W} \quad \textbf{Equation 0-59}$$

$\dot{m}$ shows the mass flow rate ($kg.s^{-1}$), while h refers to enthalpy (kJ.kg^{-1}.K^{-1}). $\dot{Q}$ is the heat transfer via that control volume component, while $\dot{W}$ is the work production or consumption. The work consumption for all components is assumed to be zero except for compressors, while heat transfer is zero for those compressors. If there is any index in the correlations, it is based on the schematic figures shown in Figs. 3.1 – 3.6 in this chapter.

To elaborate more, the mass flow rates of upper and lower cycles in a two-stage heat pump will be calculated as Eq. 3-60 and 3-61. $duty(i)$ is the heating duty coming from Fig. 3.8 (b) and (d). T refers to the temperature in K for Birmingham and Glasgow, respectively. ΔT_{app} is the approach temperature difference defined to calculate the interstage temperature regarding the PCM melting temperature in different modes.

$$\dot{m}_2(i) = \frac{\text{duty(i)}}{h_4 - h5} \quad \textbf{Equation 0-60}$$

$$\dot{m}_1(i) = \dot{m}_2(i) \times \frac{h_3 - h_6}{h_2 - h_7} \quad \textbf{Equation 0-61}$$

$$T_{7,c} = T_{PCM} + \Delta T_{app} \quad \textbf{Equation 0-62}$$

The thermal energy rate of charging $\dot{Q}_c(i)$, which is responsible for charging the PCM tank, will be calculated as follows in Eq. 3-64. $\dot{m}_c$ is the mass flow rate of the charging mode $\dot{m}_c(i)$, which will be constant as in Eq. 3-63 in all cycles.

$$\dot{m}_c(i) = 0.06\ kg.s^{-1} \quad \textbf{Equation 0-63}$$

$$\dot{Q}_c(i) = \dot{m}_c(i) \times (h_{2,c} - h_{7,c}) \quad \textbf{Equation 0-64}$$

The work consumption of the compressor in charging mode is written as:

$$\dot{w}_c(i) = \dot{m}_c(i) \times (h_{o,c} - h_{i,c})$$ **Equation 0-65**

The PCM tank will be charged at a rate that comes from correlation (3.8) at each hour of charging. To convert the energy rate to the amount of energy stored in the PCM in Joules, the rate should be multiplied by the number of seconds per hour. This will convert kW to Joules, as shown in Eq. 3-66:

$$Q_{PCM}(i) = \dot{Q}_c(i) \times 3600$$ **Equation 0-66**

PCM tank energy in (i-1)-th time pace will be calculated from Eq. 3-67 by substituting i-1 with i (Q(i-1)), and will be added to the energy of the i-th time pace, which leads to calculating the total PCM energy amount stored at the i-th time pace:

$$Q_{PCM}(i) = Q_{PCM}(i-1) + \dot{Q}_c(i) \times 3600$$ **Equation 0-67**

In discharging mode, the temperature of the state point 6 in Fig. 3.2 (b) is lower than the PCM tank temperature:

$$T_{6,d} = T_{PCM} - \Delta T_{app}$$ **Equation 0-68**

The discharging thermal energy rate at the i-th time step, if it is in the discharging mode, will be calculated as:

$$\dot{Q}_d(i) = \dot{m}_d(i) \times (h_{3,d} - h_{6,d})$$ **Equation 0-69**

The PCM thermal energy amount at each time step in discharging mode will be expressed as:

$$Q_{PCM}(i) = Q_{PCM}(i-1) - \dot{Q}_d(i) \times 3600$$ **Equation 0-70**

As previously explained, to stop charging and discharging, a parameter named SOC (status of charging) has been defined.

$$SOC(i) = \frac{Q_{PCM}(i)}{Q_{Max,PCM,th}}$$ **Equation 0-71**

$Q_{PCM}(i)$ comes from Eq. 3-70, while $Q_{PCM,th}$ is the maximum PCM tank capacity. It is assumed that 1000 kg PCM is stored in the PCM tank with the maximum capacity, shown in Eq. 3-72:

$$Q_{Max,PCM,th} = m_{PCM}.C_{P,PCM}.|(T_{Melt,PCM} - T_{PCM.ini})| + m_{PCM}.L_{fus}$$ **Equation 0-72**

The hourly COP of the system at each hour can be written as the following correlation:

$$COP(i) = \frac{\dot{Q}_H(i)}{\dot{w}_{tot}}$$ **Equation 0-73**

However, to compare a flexible two-stage heat pump with the baseline one, the seasonal coefficient of performance is computed as COP in every hour of the year, which is not a proper parameter to compare two systems fairly to find out which system is working more efficiently. It is not reasonable to compare a set of COPs for both systems one by one during the whole heating/cooling season. Therefore, SCOP or seasonal coefficient of performance is defined as the accumulated heating demand divided by accumulated electricity usage during a specific time duration [112].

$$SCOP = \frac{\sum Q_H}{\sum W_{comp}}$$ **Equation 0-74**

However, the above-mentioned correlation is in its general form, and it could be written as Eq. 3-74. As the flexible system works in different modes at a specific duration for each mode, SCOP should be calculated as a weighted summation at each mode's duration. Therefore, SCOP would be elaborated as follows:

$$SCOP = \frac{\sum_{i=1}^{j} \dot{Q}_H(i) \times t_{mode}(i)}{\sum_{i=1}^{j} \dot{W}_{comp}(i) \times t_{mode}(i)}$$ **Equation 0-75**

j is the number of the he modes. $t_{mode}(i)$ is the duration of mode in that time pace. $\dot{Q}_H(i)$ is the provided heating load that varies based on Eq. 3-77. If the duration of each mode is one hour for all modes, then it would be simplified as the following correlation:

$$SCOP = \frac{\dot{Q}_{H,c} + \dot{Q}_{H,d} + \dot{Q}_{H,Norm}}{\dot{W}_c + \dot{W}_d + \dot{W}_{Norm}}$$ **Equation 0-76**

$\dot{Q}_H$ in Eq. 3-74 – Eq. 3-76 will vary in different operation modes, as in different modes the system's demand or duty will be varied, as explained before. In charging, the objective is to charge the PCM tank, therefore the numerator of the COP definition would be the heat transfer rate of entering to the PCM tank ($\dot{Q}_c$). While in discharging and normal working mode, the objective is to provide the heating load to the building (Building $\dot{Q}_H$). Eq. 3-77 shows the general form of the provided heat in each mode:

$$\begin{cases} \dot{Q}_H = \dot{Q}_c, \text{ in charging mode} & \text{(a)} \\ \dot{Q}_H = \text{Building } \dot{Q}_H, \text{ in discharging mode.} & \text{(b)} \\ \dot{Q}_H = \text{Building } \dot{Q}_H, \text{ in normal working mode.} & \text{(c)} \end{cases}$$

Equation 0-77

In the following Table, the provided heating load and work consumption of each mode have been shown to clarify the hourly calculation method, for config. 1 and config. 2 of the two-stage heat pump:

Table 0.7 Correlations of hourly numerical calculations for the flexible two-stage heat pumps.

Operational mode	Mass flow rates (kg. S^{-1})	Provided heating load	Work consumption
Config. 1 - Proposed configuration of two-stage flexible ehat pump (Fig. 3.1)			
Normal	$\dot{m}_2 = \frac{dutyh}{h_4 - h_5}$ $\dot{m}_1 = \dot{m}_2(\frac{h_3 - h_6}{h_2 - h_7})$	$\dot{Q}_N = duty = \dot{m}_1(h_4 - h_5)$	$\dot{w}_N = \dot{w}_1 + \dot{w}_2$ $\dot{w}_1 = \dot{m}_1(h_2 - h_1)$ $\dot{w}_2 = \dot{m}_2(h_2 - h_1)$
Charging mode	$\dot{m}_c = 0.06\ kg.s^{-1}$	$\dot{Q}_c = \dot{m}_c(h_{2c} - h_{7c})$	$\dot{w}_c = \dot{m}_c(h_{2c} - h_{1c})$
Discharging mode	$\dot{m}_d = \frac{dutyh}{h_{4d} - h_{5d}}$	$\dot{Q}_d = duty = \dot{m}_d(h_{4d} - h_{5d})$	$\dot{w}_d = \dot{m}_d(h_{3d} - h_{4d})$
Config. 2 - Second configuration (Fig. 3.5)			
Normal	$\dot{m}_2 = \frac{dutyh}{h_4 - h_5}$ $\dot{m}_1 = \dot{m}_2(\frac{h_3 - h_6}{h_2 - h_7})$	$\dot{Q}_N = duty = \dot{m}_1(h_4 - h_5)$	$\dot{w}_N = \dot{w}_1 + \dot{w}_2$ $\dot{w}_1 = \dot{m}_1(h_2 - h_1)$ $\dot{w}_2 = \dot{m}_2(h_2 - h_1)$
Charging mode	$\dot{m}_c = 0.06$	$\dot{Q}_c = \dot{m}_c(h_5 - h_*)$	$\dot{w}_c = \dot{m}_c(h_{4c} - h_{3c})$
Discharging mode	$\dot{m}_d = \dot{m}_2(\frac{h_3 - h_6}{h_{2d} - h_7})$	$\dot{Q}_d = duty = \dot{m}_d(h_{**} - h_8)$	$\dot{w}_d = \dot{m}_d(h_{2d} - h_{**})$

3.2.7 Annual price calculations:

In the end, the price of electricity usage has been calculated for the mentioned systems. The most important aspect of the flexible systems is utilising off-peak electricity price cuts. To calculate the variable price of the electricity, and compare the systems from an economic viewpoint, *cosy octopus* tariff package is used from Octopus Energy [113], specifically defined for heat pump users, which is as follows: 1- (4-7 p.m.) 48.36 p/kWh, 2- (4-7 a.m.) 18.13 p/kWh, 3- (1-4 p.m.) 18.13 p/kWh, 4- (the other times) 30.22 p/kWh [113]. Therefore, the total price of used electricity in Pounds Sterling (£) would be as follows:

$$Price = \sum_{i=1}^{n} \dot{w}_{tot}(i) \times c(i)$$

Equation 0-78

c(i) is the hourly unit cost of the electricity, while $\dot{w}_{tot}(i)$ is the hourly work consumption of the compressors, which varies based on different modes.

3.3 Results and discussion

In this section, the results will be discussed in two sections: First, in section 3.4, the results of a two-stage flexible system (Fig. 3.1) will be compared with a single-stage (Fig. 3.3) as well as the second flexible configuration in two- and single-stage forms (Figs. 3.5 and 3.6). Second, in sec. 3.4.2. the validation has been performed and explained.

3.3.1 Flexible two-stage heat pump versus the other flexible systems:

In this study, a novel flexible two-stage heat pump is introduced, simulated, and finally compared with a baseline two-stage system, as well as a flexible single-stage heat pump in baseline and flexible types. Also, a second configuration has been studied and compared with the mentioned systems. The aim is to study the feasibility of peak-shaving and price reduction of the novel flexible two-stage heat pump and compare the results with those of the mentioned flexible systems. The schematic figures of the flexible systems have been shown in Figs. 3.1, 3.3, 3.5 and 3.6. In all cases, the energy stored in PCM will be used for home heating duties (config. 1), or subcooling (in the second type of flexibility configuration- config. 2), and not for defrosting or other aims. Heating loads have been calculated with IESVE software for Glasgow and Birmingham in the UK for heating, which have been shown in Fig. 3.8 (d) for Glasgow.

The parameters needed or assumed to calculate the loads with IESVE software are shown in Tables 3.4 and 3.5. The rest of the assumptions that are needed to perform the analysis are written in Tables 3.2-3.3. A PCM tank has been connected to the flash tank to store the energy when there is no required duty, and that stored energy will be used at the proper time. A control strategy has been devised to run the system in different modes in different situations based on the expected duty, PCM charging status, and time of that day. To compare the studied cases together, SCOP has been calculated for all, as SCOP shows the coefficient of performance of the whole heating season.

In Table 3.8, SCOPs of the proposed two-stage compared to other flexible heat pumps have been shown. The three parameters that have been investigated as the key results for heating application have been shown in the Table: SCOP: seasonal coefficients of performance, the annual price of electricity consumption, and the work consumption itself. As shown in the Table, the SCOP of the proposed flexible system in any case is higher than that of the baseline cases, because the proposed flexible systems will consume less electricity.

As the thermal energy saved in the PCM has been released after the discharging trigger kicked in (more than 20 kW heating loads), the lower compressor will be off in the discharging mode. On the other hand, in charging mode, the baseline system is off, while the flexible system is charging the PCM tank under the same conditions. However, as it is providing some heating load to save in the PCM tank, it will add the whole annual heating load. Therefore, in both cases, it will increase the SCOP.

On the other hand, due to less electricity usage, the annual price of electricity usage will be lower. In the heating system, flexibility helped to increase the SCOP by 1.67%, while the price has been reduced by £163 with a variable load from IESVE. The work consumption and Price are 1.74% and 1.68% lower, respectively, in a two-stage flexible system. In a similar single-stage, the SCOP is 0.78% higher, and work consumption and price are 0.8% and 0.88% lower.

In addition, the two-stage of the second configuration (config. 2 in Fig. 3.5) flexible heat pump shows less favourable results compared to config. 1 (Fig. 3.1). The reason is that in defining the details in the simulation for this configuration, the PCM is added only as the sub-cooler after the condenser, not as the load provider, which means less energy will be stored in the PCM tank of this type compared to config.1. It is the same for single-stage heat pumps that have been studied in this work. The second configuration type shows lower SCOP, lower price, and work consumption, compared to those of the baseline type.

On the other hand, Table 3.8 shows the results of the sinusoidal heating load, which presented a better result compared to the variable loads from IESVE. With a sinusoidal load, the price of the two-stage system will be reduced by £174 annually, compared to the baseline system. The SCOP will be increased by 5.31% with the proposed flexible system, while work consumption and price will be decreased by 2.1% and 3.2%.

The annual price difference is £1299 between a two-stage heat pump working in real weather compared to one with sinusoidal loads. On the other hand, a single-stage system with sinusoidal loads shows 4.8% better SCOP, 1.54% lower price, and 2.65% lower work consumption, as a sinus profile will provide the chance of charging and discharging every day and at a specific hour of the day. While in real conditions, a system wouldn’t be that lucky to have that favourable load profile every day. Therefore, although a better result has been shown with a sinus load profile, it couldn’t be used to justify using the flexible two-stage system. It is only added to show that, despite different claims in the literature,

flexibility relates to many parameters, and the most important one is the load profile shape. Also, the claims of superiority of the flexible systems with calculated results for one day couldn't be reliable, as the heating/cooling systems will be working for the whole season, not for one day, and that's the reason SCOP is calculated here to compare the systems.

Table 0.8 Heating results for Glasgow/ UK/ Single and two-stage cycles/two different loads profile.

Cycle type	Model/Load	SCOP (-)	Price (£)	$\dot{W}_{comp}$(kW)
Variable load				
Two-stage	baseline	4.4654	9,668	30,314
	flexible config. 1 (proposed)	4.5403	9,505	29,784
	flexible config. 2	4.3950	9,629	30,190
Single-stage	baseline	4.0787	10,585	33,189
	flexible config. 1	4.1108	10,500	32,896
	flexible config. 2	4.0114	10,550	33,077
Sinusoidal Load				
Two-stage	baseline	4.5276	8,369	29,487
	flexible config. 1 (proposed)	4.7679	8,195	28,547
Single-stage	baseline	4.1376	9,159	32,267
	flexible config. 1	4.3333	9,018	31,410

Table 3.9 shows the capacities of the system's components for the proposed two-stage heat pump; however, it doesn't mean that all should be provided by one heat pump. A residential area will normally be designed to have a heat pump per flat.

Tale 0.9 Component heat transfer /work consumptions in the proposed flexible and similar baseline system/ Glasgow weather.

Components		
total work of Compressor I	16,606 kW (max hourly: 18.98 kW)	20,302 kW
total work of Compressor II	12,826 kW (max hourly: 10.31 kW)	10,012 kW
heat transfer of evaporator	104,510 kW (max hourly: 76.96 kW)	105,050 kW
heat transfer of Condenser	135,230 kW (max hourly: 10.63)	135,370 kW

To study the effects of the weather, the same method has been applied to Birmingham weather conditions, and results have been shown in Table 3.10. As shown, the milder weather will help the higher SCOP of a system, compared to the SCOP of the same system working in Glasgow. Also, SCOP improvement of a flexible system is higher in Birmingham, compared to Glasgow. The reason is that the heating loads in Birmingham are lower compared to those of Glasgow. On the other hand, during the load sacrificing, as the charging/discharging trigger, it has been selected to use 15% of the maximum load for Glasgow (20 kW), while for Birmingham, the same trigger has been used. Therefore, flexibility shows higher results, while if a lower trigger had been used, the results possibly wouldn't be better, compared to those of Glasgow.

Table 0.10 Heating results of proposed flexible heat pump for Birmingham, UK/ Single and two-stage cycle.

Cycle type	model	SCOP	Price (£)	$\dot{W}_{comp}$ (kW)
Two-stage	baseline	4.5835	7,241	22,734
	Flexible config. 1 (proposed)	4.7278	7,112	22,396
Single-stage	baseline	4.190	7,920	24,866
	Flexible config. 1	4.2890	7,841	24,687

Fig. 3.11 (a)-(o) presents the daily work consumption and required duty in 24 hours of the randomly selected days of 7th to 31st of October, for the proposed two-stage flexible heat pump, working in Glaswegian weather conditions. Fig. (a) is shown here, and the rest are added to Appendix B. The short, dashed lines show the baseline two-stage heat pump, while the longer dashed lines are for the proposed flexible heat pumps. On the other hand, the solid line presents the heating loads that have been extracted from IESVE for Glasgow, UK. The reason that the days have not been selected based on a specific pattern is that the loads extracted from IESVE are quite varying without a pattern, as seen in Fig. 3.8 (d). In Fig. 3.11, the baseline work consumption can be compared with that of the flexible two-stage ASHP hourly. It could be seen in the figures that when the duty is lower than 20 kW, charging has happened, which leads to lower work consumption, as only one of the compressors will be working. On the other hand, in the next hours after the charging, if the charging state is higher than 4%, it means discharging could happen if the time is between 7 a.m. and 11 p.m. For example, for the 7th of October, it is shown that despite the heating duty, the heating system is off, as a scheme of night load shaving until 7 a.m. As shown, the work consumption until 7 a.m. is zero, as the system is off in both baseline and flexible systems. After that, until around 1 p.m., as there was no energy in the PCM tank, the system had to work in normal operation mode, which led to a work consumption equal to the baseline system's work. Then, the load is going to be decreased to 8 kW. It means that in the range of lower than 20 kW, the system will start to charge, and it is the reason for the lower work consumption around the range of 1-5 p.m. After that, the loads gradually go higher than 20 kW, which means that it is possible to jump to discharging mode, as there is some amount of energy in the PCM. From 6-8 p.m. in the figure, the work consumption is lower than the similar baseline system, as the flexible one is working in the discharging mode, which uses only one of the compressors and leads to consuming less compressor power compared to the work of the baseline compressors. After finishing the PCM tank energy, the system will be back to normal operation mode after 8 p.m.

As it is presented, the shape of the heating load and work consumption is the same on a day, as work consumption has been calculated with the mass flow rate, which comes from the

heating load. Also, no two days are exactly similar to each other, as the loads are randomly changing from day to day.

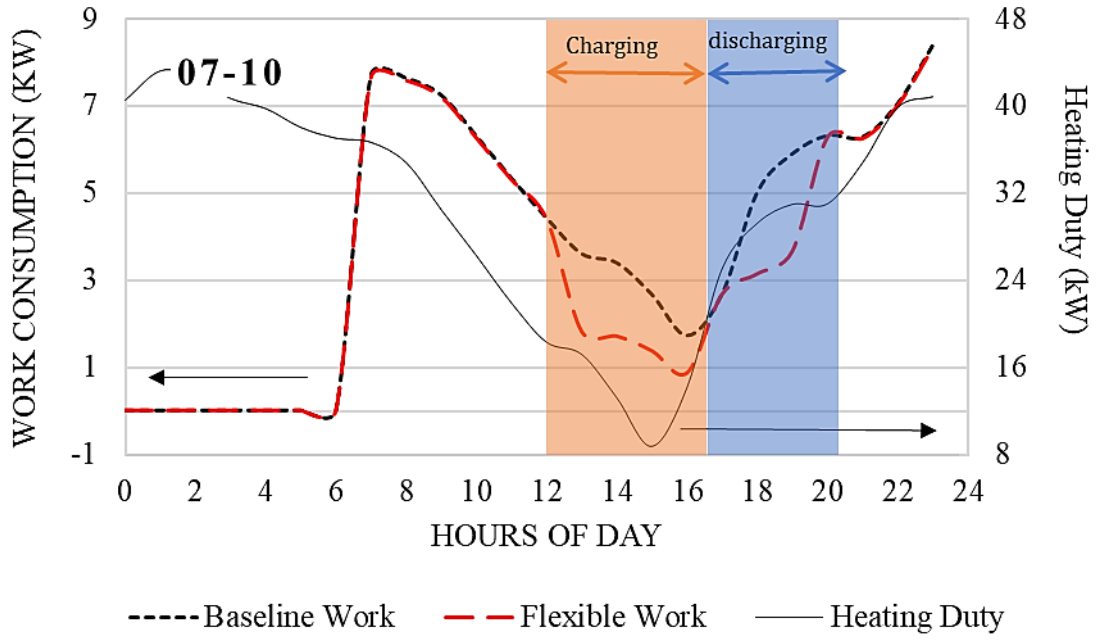

(a)

Figure 3.11 (a) Variation of daily work consumption of baseline and flexible two-stage system in heating versus heating duty extracted from IESVE during 24 hours of the day for randomly selected days of the heating season in October (The rest of the figures are in Appendix B (b)-(o)).

3.3.2 Validations

An ice-storage tank connected to a single-stage heat pump has been simulated in its full load operating mode, based on the original study of *Sanaye et al.* [76]. However, there are some differences in the assumptions and control strategy of the selected paper to validate this study. Sanaye's work has some similarities, such as hourly calculation, variable loads, configuration, etc. The biggest difference was that Sanaye's work was designed for cooling applications, which does not affect the validation aim, as the method is the same for both applications. The ice storage has been used as the evaporator in charging mode, while during discharging, it will be connected to the air-cooling loop of the building to provide the cooling load. The cooling load is digitised from Fig. 4 of *Sanaye and Hekmatian* [76], and optimal working conditions provided in Table 5 of *Sanaye and Hekmatian* [76] (optimum values) have been used as assumptions to validate this study. Based on that Table, the evaporator and condenser temperatures are -5.12 and 38.46 ℃, respectively. The storage tank capacity would be large enough to charge the tank for 8 hours at a constant rate. The system will be run in charging mode during the night from 7 p.m. to 7 a.m., and discharging from 7 a.m. to

7 p.m. and will be in standby mode from 7 p.m. to 11 p.m. The results, shown in Table 3.11, compared to the results of the reference, show a great level of compatibility when $\eta_{is,comp}$ equals 97%:

Table 0.11 Validation results based *on Sanaye and Hekmatian* [76]

Hourly results' parameters in charging	Values	Reference's results (Unknown $\boldsymbol{\eta_{is,comp}}$)	Difference percentage
Evaporator heat transfer rate	1596 kW	1596 kW	0%
mass flow rate	11.28 kg.s^{-1}	11.15 kg.s^{-1}	1.17%
compressor work usage ($\eta_{is,comp} = 85\%$)	384.78 kW	335.73 kW	14.6%
compressor work usage ($\eta_{is,comp} = 97\%$)	337.18		0.43%
condenser heat transfer ($\eta_{is,comp} = 85\%$)	1981.28 kW	1932	2.55%
condenser heat transfer ($\eta_{is,comp} = 97\%$)	1933.68		0.087%
COP ($\eta_{is,comp} = 85\%$)	4.14	4.7543	-14.84%
COP ($\eta_{is,comp} = 97\%$)	4.7348		-0.41%

3.4 Summary of the chapter

In this chapter, a thermal energy storage system is introduced to a two-stage heat pump system in a novel configuration for heating. The novel flexible two-stage heat pump has been studied and compared with a baseline two-stage heat pump, as well as the same flexible and baseline single-stage heat pump, in the same working conditions. A control strategy has been defined based on the heating duty, hour of the day, and storage tank status to run the system in different modes: 1- Normal operation, 2- Charging, 3- Discharging, and 4- Standby (off) modes. The weather data of Glasgow and Birmingham cities, UK, have been used to acquire the variable hourly heating loads of a typical 4-story residential block via IESVE software. Also, to study the effect of heating load profile shape, a sinusoidal daily heating load profile has been created with the same maximum duty of variable load from IESVE. The results show that a flexible two-stage system shows 1.67% and 5.31% higher seasonal COP (seasonal coefficient of performance) with real variable loads and sinusoidal loads, respectively. While the maximum 2.1% cut price has been shown with sinusoidal loads, the price cut for the real variable loads is less than that.

Chapter 4 Investigation on the peak shaving potential of a new flexible two-stage heat pump for Cooling

4.1 Introduction

One of the primary barriers to adopting flexible cooling energy systems remains their economic feasibility. In addition, previous studies often neglected to evaluate COP, and many of them used simplified sinusoidal daily load profiles, which may overestimate the performance of the flexible systems. This chapter proposes a two-stage heat pump integrated with a PCM tank connected to the flash tank via a fluid circuit for a cooling heat air-source heat pump. The addition of PCM makes the system flexible in storing energy and controlling cooling capacity, which is the reason why the system is named 'flexible'. This system is investigated with real-world weather data and two key parameters, annual price and seasonal COP (SCOP), to demonstrate its advantages over a conventional two-stage heat pump. Furthermore, a demand-side management (DSM)-based control strategy for residential buildings is implemented in this study.

Key objectives and innovations of this chapter are summarised as follows:

4.1.1. A novel two-stage flexible heat pump integrated with a PCM tank fluidly connected to the flash tank for cooling application has been proposed.

4.1.2. A control strategy based on the cooling load, time of the day, and PCM tank status for a residential block has been proposed to run the system in different operating modes.

4.1.3. Two conventional heat pumps (a single-stage system and a two-stage system), serve as the baseline systems, have been enhanced with additional valves to operate in different modes: charging, discharging, normal operation, and standby modes.

4.1.4. The effect of real-world weather conditions on the flexibility of the heat pump systems is investigated using the weather data of Rome and London.

4.1.5. Two configurations are applied to the flexible two-stage and single-stage system for cooling: config. 1 is newly proposed in this study, and the second configuration is a common

configuration in literature. The performance of the novel configuration is compared to that of the other four systems: a conventional two-stage heat pump, a conventional single-stage heat pump, as two baseline systems, a flexible single-stage heat pump and a second configuration (config. 2) of a flexible two-stage system. All used the same weather data and control strategy and working conditions, except the charging/discharging trigger, which will be explained in the next section.

The difference between this chapter and previous chapter is the difference between heating and cooling system: 1- the definition of SCOP/COP for heating/cooling systems are different, as in heating system the aim is to pass the heat from the outsidle of the building to inside of the room, while a cooling system is taking out the heat from inside of the room to the outside of the building. The numerator of COP definition is the aimed thermal energy (taken in for heating and taken out for cooling) 2- The PCM tank in heating will gain energy and its temperature will be increased, or can be melted, but in cooling it's the opposite. The PCM in cooling system will lose energy and could be solidified. The reason is that in discharging mode of heating, it is expected the thermal energy extracted from the PCM tank and increase the temperature of the residential/heated spaces of the building, while in discharging of cooling system, the PCM tank will absorb the heat pf the cooled spaced in the building and gain energy. The rest of the details are the same, including the logic, the general equations, etc. A part of the difference of the heating and cooling systems is cleared in the flow-chat of the systems, Fig. 3.10 in chapter 3 and Fig. 4.7 in this chapter.

4.2 Methodologies

Section 4.2.1 introduces all systems, including the proposed novel two-stage flexible heat pump (config. 1), a conventional two-stage heat pump, a conventional single-stage heat pump, a flexible single-stage heat pump and a second configuration (config. 2) flexible two-stage heat pump. Load calculations have been explained in section 4.2.2. The control strategy, which defines the working of the system based on operating modes, has been explained in section 4.2.3. Mathematical governing equations have been elaborated in section 4.2.4. Finally, the annual price calculation is referred to in section 4.2.5 and validation in section 4.2.6.

4.2.1 System description

A new flexible two-stage heat pump has been investigated for cooling applications, and results have been compared with the baseline/standard two-stage cooling heat pump. In the new flexible two-stage heat pump, each stage consists of an expansion valve, a compressor, and an interior heat exchanger to absorb heat from the environment (indoor air in cooling mode). Both stages are connected to a shared flash tank. A fluid circuit connects a PCM tank to the flash tank, which makes the heat pump 'flexible'. Four control valves, positioned upstream of the expansion valves and compressors, enable the system to switch between operational modes: charging, discharging, normal operation, and standby modes.

For the two-stage baseline system in cooling mode, the evaporator absorbs heat from the indoor air and heats the cold refrigerant to vaporise. As the indoor air passes through the evaporator, its temperature is reduced due to the heat transfer from the indoor air to the refrigerant. Next, the vaporised refrigerant is compressed to high-temperature vapour by the compressor, and then enters the condenser, where the refrigerant vapour releases heat to the outdoor air and turns back to a liquid phase. The liquid refrigerant flow from the condenser undergoes a constant-enthalpy expansion process through the expansion valve, reducing its temperature and pressure and becoming a mixture of liquid and vapour. Subsequently, the two-phase refrigerant R134a flows into the flash tank and is split into two streams: a saturated liquid and saturated vapour. The liquid stream enters the lower-stage expansion valve, further reducing pressure before entering the evaporator, whilst the vapour stream flows through the top compressor and becomes superheated vapour before entering the condenser. This completes the cycle, which repeats continuously.

Fig. 4.1(a) is the schematic diagram of the proposed novel two-stage flexible heat pump. Fig. 4.1 (b) and (c) show the charging and discharging modes, respectively. The PCM plays multiple roles in different modes. It is the evaporator in charging mode, but it becomes a condenser during discharging. The PCM tank is disconnected in normal operation mode. In Fig. 4.1 (b) (charging mode), the exterior heat exchanger (condenser) transfers the heat from the ambient to the working fluid in streamline 4-5. PCM acts as an evaporator and releases heat to the working fluid in the streamline 6-3, and therefore, the temperature in the PCM tank drops. Fig. 4.1 (c) (discharging mode), PCM acts as a condenser. It absorbs heat from the working fluid in streamline 2-7 and thus experiences a rise in its own temperature. Fig. 4.2 shows the T-s diagrams of the three modes (normal working, charging and discharging) in Fig. 4.1. Here, an approach temperature is assumed as a constant to indicate the interstage

temperature in the novel two-stage HP and its different operational modes. In the charging mode, as shown in Fig. 4.2(b), the PCM is supposed to be charged by transferring heat to the cold working fluid in streamline 3-6, until being fully charged. Therefore, the interstage temperature is defined as the PCM temperature minus the approach temperature. For the discharging mode as shown in Fig. 4.2(c), the interstage temperature is required to be higher than the PCM melting temperature, as the PCM has been heated by the hot working fluid from the streamline 2-7 to the PCM until being fully discharged. The criteria for 'fully charged' and 'fully discharged' status will be mathematically defined in subsequent sections.

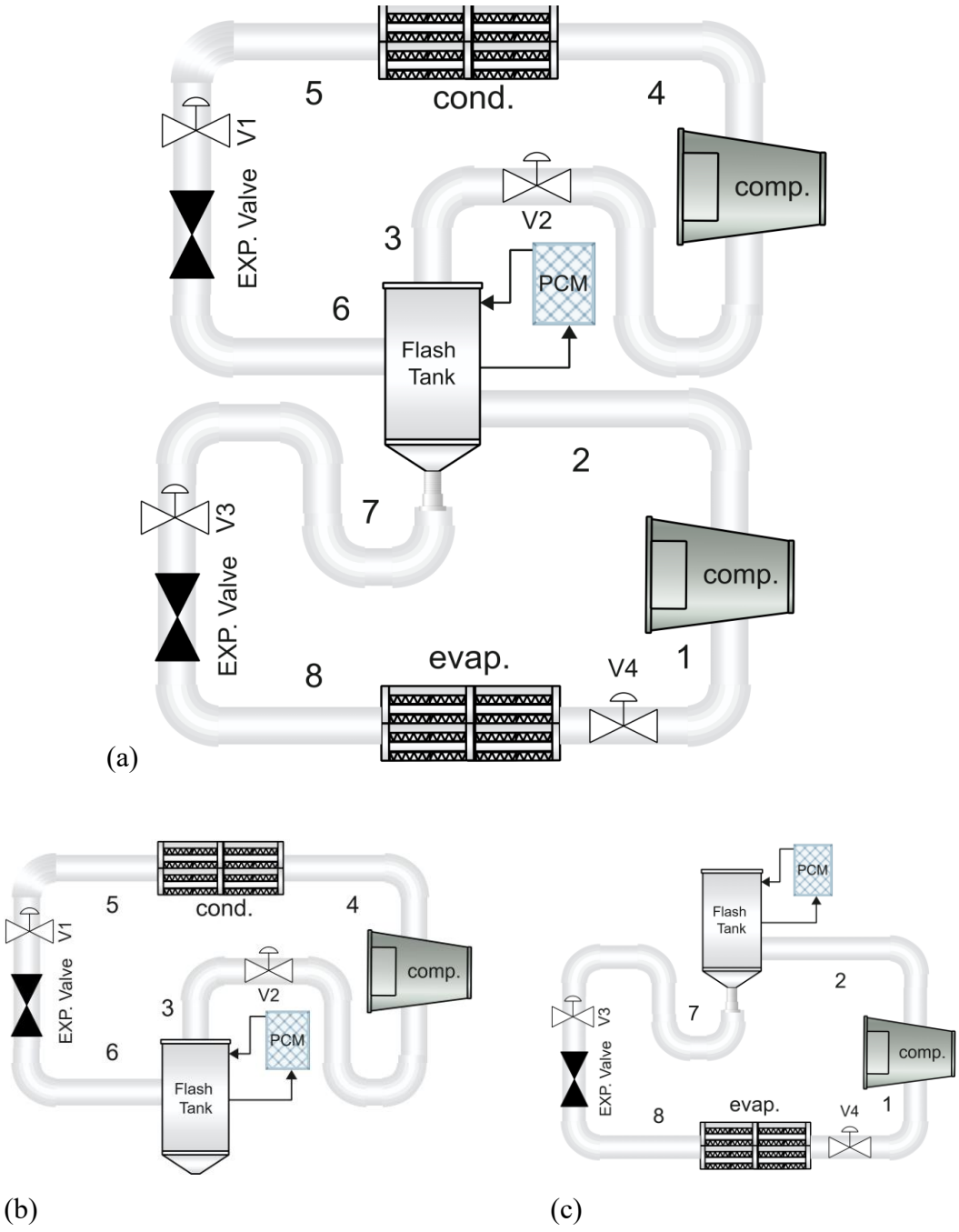

Figure 4.1 Schematic figure of a flexible two-stage heat pump (config. 1) during (a) normal working mode (b) charging mode, (c) discharging mode in cooling application.

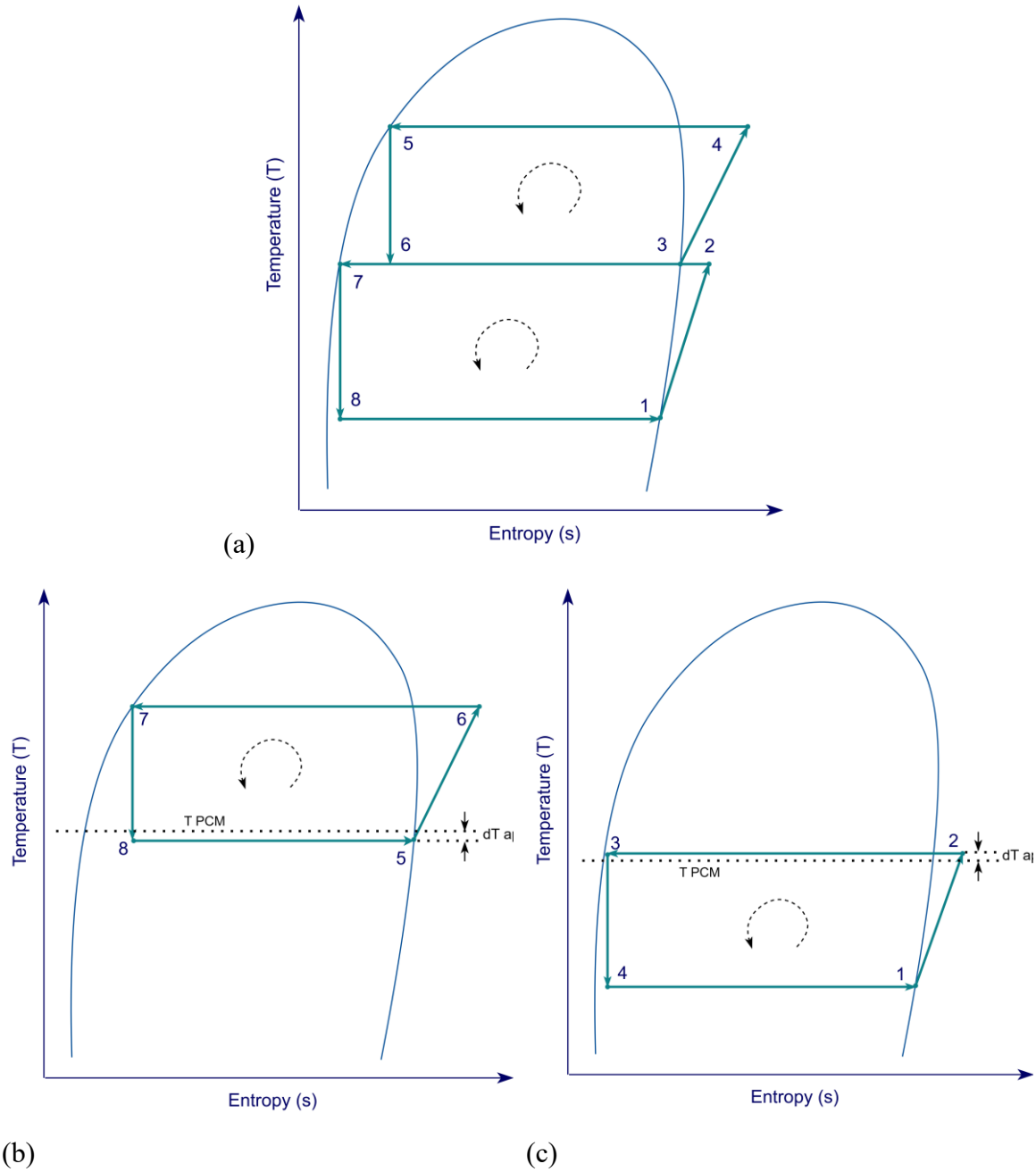

Figure 4.2 T-s diagrams of a flexible two-stage heat pump during (a) normal working mode (b) charging mode, (c) discharging mode in cooling application.

Table 4.1 Four operational modes of the proposed flexible heat pump system.

Mode	Comp. I	Comp. II	Pump	V1	V2	V3	V4
1 Normal	on	on	standby	on	on	on	on
2 Charging	on	standby	on	on	on	standby	standby
3 Discharging	standby	on	on	standby	standby	on	on

Table 4.1 shows the operational modes and valve status in the proposed flexible two-stage heat pump (config. 1). Upper cycle valves and one compressor (V1, V2 and upper Comp.) are working in charging mode, while, in discharging mode, the lower cycle's valves and the other compressor (V3, V4 and lower Comp.) are switched on. A flexible single-stage heat

pump is also analysed as the additional flexible system (config. 2) represented in Fig. 4.3, where the PCM is added to the cycle with manipulating valves. The PCM plays the same role as it does in the proposed flexible two-stage heat pump.

For the cooling application, the concept and method are the same as for heating system, except that the PCM would be located in its right place to support the charging and discharging process. In a charging mode at cooling application, PCM would have an evaporator role, while in cooling/discharging, the PCM is inserted in the cycle as the condenser.

All systems are modelled in MATLAB, utilising the thermophysical properties extracted from REFPROP (NIST-23). All assumptions and input parameters are summarised in Table 4.2. The evaporator has a fixed temperature, while the condenser, which is in contact with the ambient air, has variable hourly values. Therefore, it is assumed that the condenser temperature is 15 ℃ higher than the ambient temperature.

The cooling loads of the system are required to be calculated hourly, which will be elaborated in section 4.3.2. The loads are acquired for a 4-story residential building from IESVE software. A control strategy is introduced to the system in section 4.3.3 to operate it hourly based on time, PCM status, and cooling load. Mass and energy balance equations are applied to the components of the systems in each hour, which are mentioned in section 4.3.4.

Table 4.2 Simulation assumptions for cooling application.

Parameters	Value	Unit
evaporator Temperature [114]	-5	℃
condenser Temperature	$T_{atm} + 15$	℃
PCM Melting Temperature [49]	20	℃
Weather Data	London, UK / Rome, Italy	-
η_{comp} [110]	80%	-
Approach Temperature	3	℃

The properties of state points in the normal working mode of the cooling application will be calculated based on the following steps. The equations might look the same, but there are subtle differences between the equations in this section and those in the previous chapter, as these ones are written for cooling applications. The outlet air is connected to the condenser rather than to the evaporator. Charging the PCM tank means decreasing its temperature rather than increasing it.

- State point 1: evaporator outlet, fixed evaporator temperature, saturated vapour.

$$\begin{cases} T_1 = T_{eva}, T_{eva} = cte. \\ Q_1 = 1, \text{saturated vapour} \end{cases} \rightarrow h_1$$ **Equation 4-1**

- State point 2: compressor outlet (isentropic efficiency 80% [110]), pressure of state point 6.

$$\begin{cases} P_2 = P_6 \\ \eta_{comp} = \dfrac{h_{2s} - h_1}{h_2 - h_1} \end{cases} \rightarrow h_2$$ **Equation 4-2**

- State point 3: flash chamber outlet, saturated vapour, temperature of state point 6.

$$\begin{cases} P_3 = P_6 \\ Q_3 = 1, \text{saturated vapour} \end{cases} \rightarrow h_3$$ **Equation 4-3**

- State point 4: compressor outlet (isentropic efficiency 80% [110]), pressure of the condenser.

$$\begin{cases} P_4 = P_5 \\ \eta_{comp} = \dfrac{h_{4s} - h_3}{h_4 - h_3} \end{cases} \rightarrow h_4$$ **Equation 4-4**

- State point 5: Condenser outlet (which is 15 degrees higher than ambient temperature), saturated liquid.

$$\begin{cases} T_5 = T_{cond}, T_{cond} = T_{melting} + 15 \\ Q_5 = 0, \text{saturated vapour} \end{cases} \rightarrow h_5$$ **Equation 4-5**

- State point 6: interstage temperature (melting PCM temperature minus approach temperature), enthalpy of condenser outlet.

$$\begin{cases} T_6 = T_{interstage}, T_{interstage} = T_{melting} - \Delta T_{app} \\ h_6 = h_5 \end{cases} \rightarrow P_6$$ **Equation 4-6**

- State point 7: saturated liquid, interstage pressure.

$$\begin{cases} P_7 = P_6 \\ Q_7 = 0, \text{saturated liquid} \end{cases} \rightarrow h_7$$ **Equation 4-7**

- State point 8: enthalpy of state point 6, pressure of the evaporator.

$$\begin{cases} h_8 = h_7 \\ P_8 = P_1 \end{cases}$$ **Equation 4-8**

The mass flow rates come from:

$$\begin{cases} \dot{m}_1 = \dfrac{\text{duty}}{h_1 - h_8} \\ \dot{m}_2 = \dot{m}_1 . \dfrac{h_2 - h_7}{h_3 - h_6} \end{cases}$$ **Equation 4-9**

The properties of state points in the charging process at cooling application will be as follows:

$$\dot{m}_c = 0.02 \text{ kg}. s^{-1}, \text{constant}.$$ **Equation 4-10**

- State point 3c: Temperature, saturated vapour.

$$\begin{cases} T_{3c} = T_{melting} - \Delta T_{app} \\ Q_{3c} = 1, \text{saturated vapour} \end{cases} \rightarrow h_3$$ **Equation 4-11**

- State point 4c: compressor outlet, pressure of interstage.

$$\begin{cases} P_{4c} = P_6 \\ \eta_{comp} = \dfrac{h_{4s} - h_{3c}}{h_4 - h_{3c}} \rightarrow h_{4c} \end{cases}$$ **Equation 4-12**

- State point 6: interstage temperature (melting PCM temperature minus approach temperature), enthalpy of condenser outlet.

$$\begin{cases} T_{6c} = T_{melting} - \Delta T_{app} \rightarrow P \ \& x \\ h_{6c} = h_5 \end{cases}$$ **Equation 4-13**

While in the discharging mode, the properties are calculated based on the following steps:

- State point 2: compressor outlet, pressure of state point 7d (interstage pressure).

$$\begin{cases} P_{2d} = P_{7d} \\ \eta_{comp} = \dfrac{h_{2sd} - h_1}{h_{2d} - h_1} \rightarrow h_{2d} \end{cases}$$ **Equation 4-14**

- State point 7: saturated liquid, interstage pressure.

$$\begin{cases} T_{7d} = T_{melting} + \Delta T_{app} \\ Q_{7d} = 0, \quad \text{saturated liquid} \end{cases} \rightarrow h_{7d}$$ **Equation 4-15**

- State point 8: enthalpy of state point 6, pressure of the evaporator.

$$\begin{cases} h_{8d} = h_{7d} \\ P_{8d} = P_1 \end{cases}$$ **Equation 4-16**

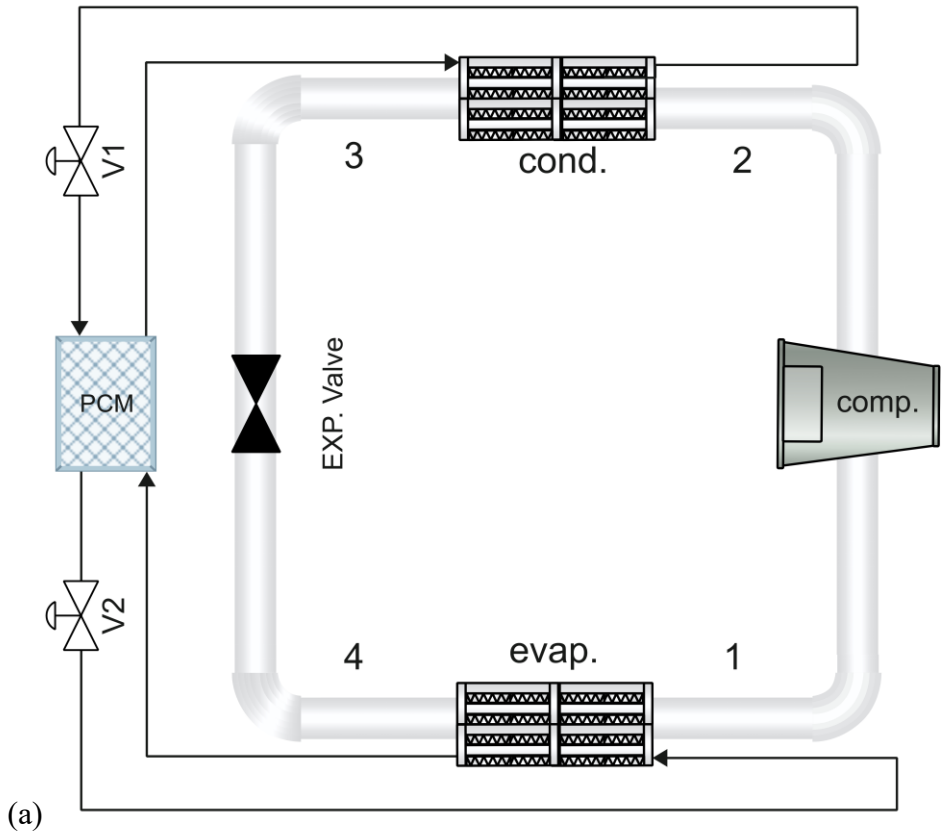

(a)

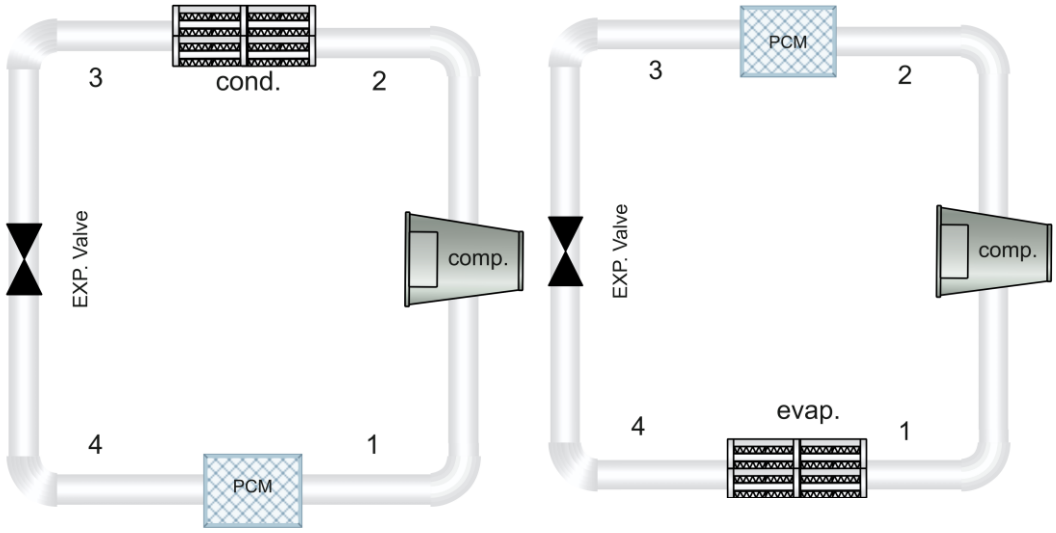

(b) (c)

Figure 4.3 Schematic figures of a flexible single-stage heat pump in the normal operating mode (a) charging and (b) discharging operational modes (c) for cooling application.

The properties of state points in the other configurations of cooling application will be calculated based on the following steps.

- State point 1: evaporator outlet, fixed evaporator temperature, saturated vapour.

$$\begin{cases} T_1 = T_{eva}, T_{eva} = cte. \\ Q_1 = 1, \text{saturated vapour} \end{cases} \rightarrow h_1$$ **Equation 4-17**

- State point 2: compressor outlet (isentropic efficiency 80% [110]), pressure of state point 6.

$$\begin{cases} P_2 = P_3 = P_{cond} \\ \eta_{comp} = \dfrac{h_{2s} - h_1}{h_2 - h_1} \rightarrow h_2 \end{cases}$$ **Equation 4-18**

- State point 3: condenser outlet, saturated liquid.

$$\begin{cases} T_3 = T_{cond} = T_{atm} + 15 \\ Q_3 = 0, \text{saturated liquid} \end{cases} \rightarrow h_3, P_{cond}$$ **Equation 4-19**

- State point 4: compressor outlet (isentropic efficiency 80% [110]), pressure of the condenser.

$$\begin{cases} P_4 = P_1 \\ \eta_{comp} = \dfrac{h_{4s} - h_3}{h_4 - h_3} \rightarrow h_4 \end{cases}$$ **Equation 4-20**

The mass flow rates come from:

$$\dot{m}_1 = \frac{duty}{h_1 - h_4}$$ **Equation 4-21**

The properties of state points in the charging process at cooling application will be as follows:

$$\dot{m}_c = 0.02\ kg.s^{-1}, \text{constant.}$$ **Equation 4-22**

- State point 1c: Temperature, saturated vapour.

$$\begin{cases} T_{1c} = T_{melting} - \Delta T_{app} \\ Q_1 = 1, \text{saturated vapour} \end{cases} \rightarrow h_{1c}, s_{1c}$$ **Equation 4-23**

- State point 2: compressor outlet (isentropic efficiency 80% [110]), pressure of state point 6.

$$\begin{cases} P_2 = P_3 = P_{cond} \\ \eta_{comp} = \dfrac{h_{2sc} - h_{1c}}{h_{2c} - h_{1c}} \rightarrow h_{2c} \end{cases}$$ **Equation 4-24**

While in the discharging mode, the properties are calculated based on the following steps:

- State point 1d: evaporator outlet, evaporator temperature, which is 10 degrees lower than ambient temperature, saturated vapour.

$$\begin{cases} T_{1d} = T_{melting} + \Delta T_{app} \\ Q_{1d} = 0, \text{saturated liquid} \end{cases} \rightarrow h_{1d}, s_{1d}$$ **Equation 4-25**

- State point 2: compressor outlet, pressure of state point 3d.

$$\begin{cases} P_{2d} = P_{3d} \\ \eta_{comp} = \dfrac{h_{2sd} - h_{1d}}{h_{2d} - h_{1d}} \rightarrow h_{2d} \end{cases}$$ **Equation 4-26**

- State point 4: enthalpy of state point 6, pressure of the evaporator.

$$\begin{cases} h_{4d} = h_{3d} \\ P_{4d} = P_{1d} \end{cases}$$ **Equation 4-27**

Furthermore, the new flexible two-stage heat pump (config. 1) is also compared with a second configuration (config. 2) where the PCM storage tank is only used for superheating the working fluid after the evaporator, shown in Figs 4.3. and 4.4 for single-stage and two-stage air-source heat pumps. It means that both stages are working in all modes. In contrast, in the originally proposed configuration (config. 1) for the flexible two-stage heat pump, only one of the compressors is working during charging and discharging. The following figure represents the schematic figure of the second configuration (config. 2) of the flexible two-stage heat pump.

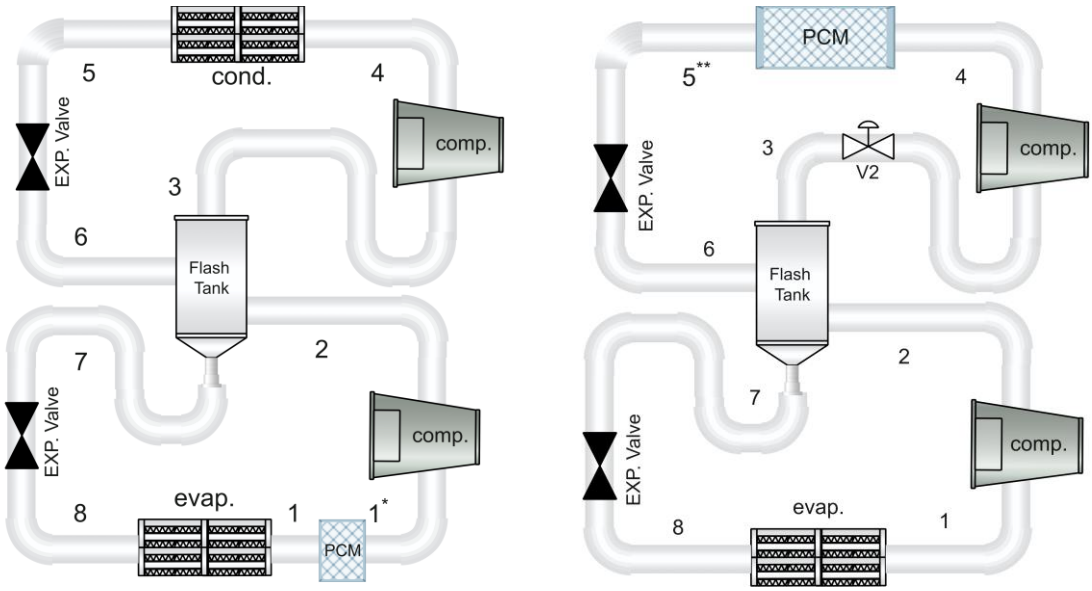

(a) (b)

Figure 4.4 Schematic figures of the second configuration (V2) of flexible two-stage heat pump (a) charging and (b) discharging operational modes, for cooling application.

The properties of state points in the normal working mode of the cooling application will be calculated based on the following steps.

- State point 1: evaporator outlet, fixed evaporator temperature, saturated vapour.

$$\begin{cases} T_1 = T_{eva}, T_{eva} = cte. \\ Q_1 = 1, \text{saturated vapour} \end{cases} \rightarrow h_1$$ **Equation 4-28**

- State point 2: compressor outlet (isentropic efficiency 80% [110]), pressure of state point 6.

$$\begin{cases} P_2 = P_7 \\ \eta_{comp} = \dfrac{h_{2s} - h_1}{h_2 - h_1} \rightarrow h_2 \end{cases}$$ **Equation 4-29**

- State point 3: flash chamber outlet, saturated vapour, temperature of state point 6.

$$\begin{cases} T_3 = T_{interstage} \\ Q_3 = 1, \text{saturated vapour} \end{cases} \rightarrow h_3$$ **Equation 4-30**

- State point 4: compressor outlet (isentropic efficiency 80% [110]), pressure of the condenser.

$$\begin{cases} P_4 = P_5 \\ \eta_{comp} = \dfrac{h_{4s} - h_3}{h_4 - h_3} \rightarrow h_4 \end{cases}$$ **Equation 4-31**

- State point 5: Condenser outlet (which is 15 degrees higher than ambient temperature), saturated liquid.

$$\begin{cases} T_5 = T_{cond}, T_{cond} = T_{melting} + 15 \\ Q_5 = 0, \quad \text{saturated vapour} \end{cases} \rightarrow h_5$$ **Equation 4-32**

- State point 6: interstage temperature (as PCM outlet temperature is melting PCM temperature minus approach temperature, interstage T needs to be lower, as it is expansion valve outlet temperature.), and its enthalpy is the enthalpy of the condenser outlet.

$$\begin{cases} T_6 = T_{interstage}, T_{interstage} = T_{melting} - \Delta T_{app} - 10 \\ h_6 = h_5 \end{cases} \rightarrow P_6$$ **Equation 4-33**

- State point 7: saturated liquid, interstage pressure.

$$\begin{cases} P_7 = P_6 \\ Q_7 = 0, \quad \text{saturated liquid} \end{cases} \rightarrow h_7$$ **Equation 4-34**

- State point 8: enthalpy of state point 6, pressure of the evaporator

$$\begin{cases} h_8 = h_7 \\ P_8 = P_1 \end{cases}$$ **Equation 4-35**

The mass flow rates come from

$$\begin{cases} \dot{m}_1 = \dfrac{\text{duty}}{h_1 - h_8} \\ \dot{m}_2 = \dot{m}_1 . \dfrac{h_2 - h_7}{h_3 - h_6} \end{cases}$$ **Equation 4-36**

The properties of state points in the charging process at cooling application will be as follows:

$$\dot{m}_c = 0.02 \text{ kg}. s^{-1}, \text{constant}.$$ **Equation 4-37**

- State point 1*:

$$\begin{cases} T_{1*} = T_{melting} - \Delta T_{app} \\ P_{1*} = P_1 \end{cases} \rightarrow h_{1*}$$ **Equation 4-38**

While in the discharging mode, the properties are calculated based on the following steps:

- State point 5**:

$$\begin{cases} \mathbf{T_{5**} = T_{melting} + \Delta T_{app}} \\ \boldsymbol{P_{5**} = P_5} \end{cases} \rightarrow \mathbf{h_{5**}}$$ **Equation 4-39**

- State point 6d:

$$h_{6d} = h_{5**}$$ **Equation 4-40**

$$\dot{m}_d = \dot{m}_1 . \frac{h_2 - h_7}{h_3 - h_{6d}}$$ **Equation 4-41**

4.2.2 Loads of IESVE and simulation logic:

To calculate the required variable cooling loads for London, UK, and Rome, Italy, a four-story residential building is created based on a predefined geometry in IESVE software, as shown in Fig. 3.7 of Chapter 3.

Table 4.3 shows all parameters of the residential block's energy model in IESVE, and Table 4.4 lists the U values of the building components. The U values of other components are automatically specified as default values by IESVE. Finally, the cooling loads are shown in Fig. 4.5 for Rome, Italy, and Fig. 4.6 for London, UK.

Table 4.3 Residential Block's geometry and energy Model Parameters in IESVE software.

Parameters	Value	Unit
Area	3,134.92	m^2
External wall area	1,542.19	m^2
External Opening area	231.38	m^2
Room set point	19	$℃$
DHW consumption	0	$l.h^{-1}$
Internal Gains		
Occupancy	25	$m^2\ per\ person$
Max sensible gain	64	$w\ per\ person$
latent	70	$w\ per\ person$
Equipment sensible gain	2.4	$w\ per\ m^2$
Equipment Max power consumption	4.8	$w\ per\ m^2$
Infiltration (Air Leakage)	0.6	Ach (air changes per hour)
Natural ventilation (Air change)	0.3	Ach (air changes per hour)

Table 4.4 Default U values of the walls, Roof, Floor, windows, doors, etc., from predefined geometry in IESVE.

Components	U values ($\boldsymbol{w/m^2.K}$)	Thickness (mm)
Internal ceiling/Floor	1.0866	282.5
External window	1.6	24.0
Exposed Floor	0.22	268.0
Internal Partition	1.7888	75.0
Roof	0.18	317.0
External wall	0.2599	208.0

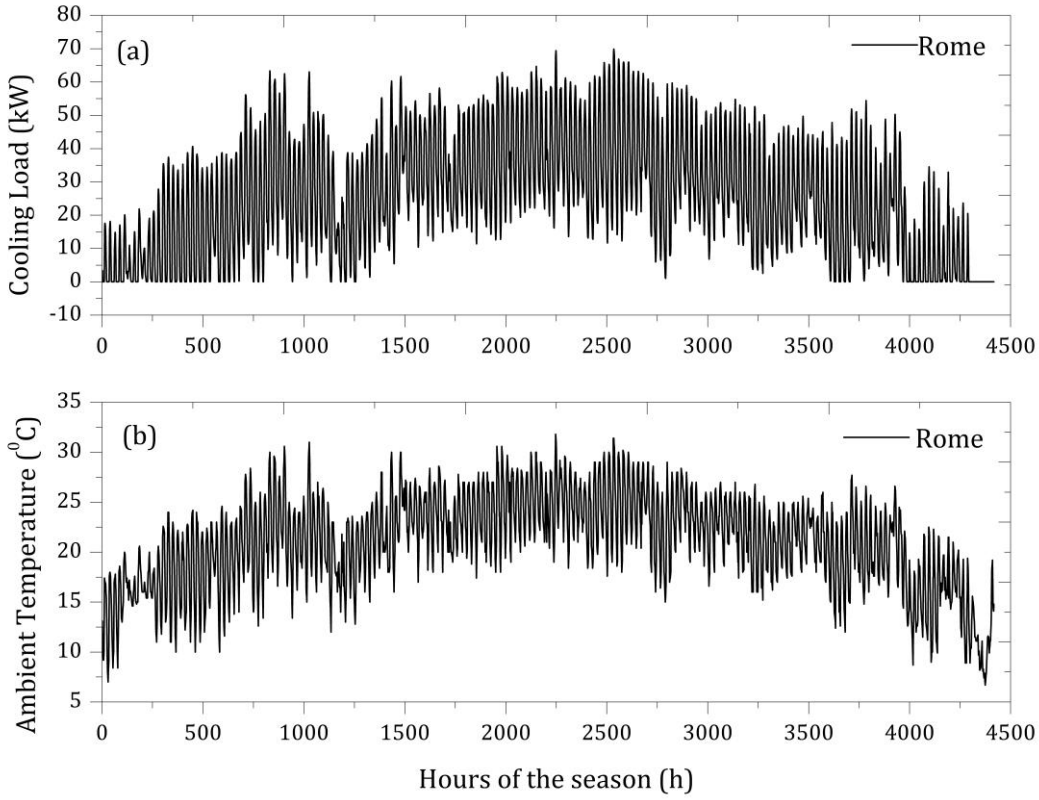

Figure 4.5 Cooling loads for (a) and ambient temperature (b) of the residential building in Rome/ Italy.

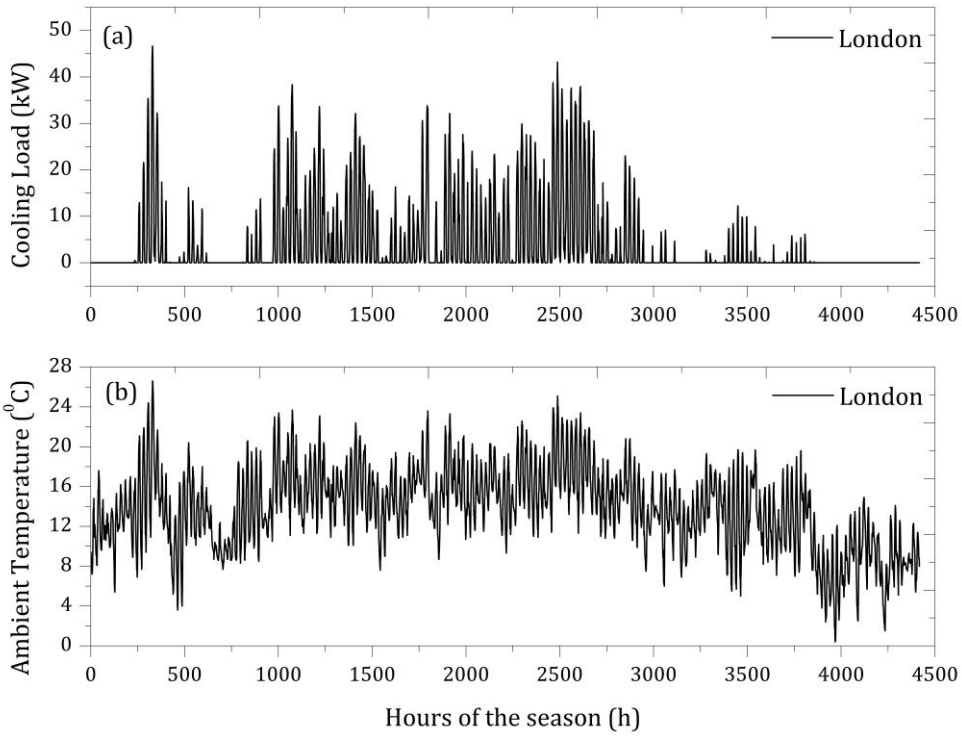

Figure 4.6 Cooling loads (a) and ambient temperature (b) of the residential building in London/UK.

4.2.3 Control Strategy

The MATLAB simulation of the flexible heat pumps is conducted using the following rules:

- There is no heat or pressure loss in the working fluid when running through the system via pipes and heat exchangers.

- The system is running from May to October for cooling applications only, and the rest of the year is switched off.

- To simplify the engineering simulation, for the conventional two-stage heat pump, the interstage temperature is assumed to be the same as the interstage temperature in the flexible system. However, generally, optimisation is required to calculate the optimum interstage temperature. It is assumed that the flexible system's interstage temperature equals the approach temperature minus the PCM's melting point (i.e., the interstage temperature during charging). To ensure a fair comparison, the interstage temperature in the conventional two-stage baseline heat pump system, which has no PCM tanks, is assumed identical to the interstage temperature of the flexible two-stage heat pump.

- All systems operate from 7 a.m. to 11 p.m. to heat the residential building, whilst the flexible systems operate from 11 p.m. to 7 a.m., when it is possible to enter the charging mode if the load is low enough. This method, known as *night load shaving*, belongs to the category of Demand-Side Management (DSMs). The cooling load in this study determines when to charge or discharge the PCM tank. Regardless of time, charging will begin if the load is less than a trigger. The trigger here means 15% of the maximum cooling load under a specific weather condition. When the cooling load exceeds the trigger amount, discharging will begin. The triggers for Rome and London are 10 kW and 7 kW, respectively. However, since the average cooling load in London is lower than that of Rome, an additional 3 kW trigger is added to simulations for London.

- The control strategy in this simulation determines whether the system operates in charging, discharging, normal operation, or standby mode after importing the data of ambient temperature and variable cooling load from IESVE. The system's operational modes depend on the load, time of day, and PCM tank status (fully

charged, partially charged or fully discharged), as shown in Table 4.5. In charging mode the cooling load in the charging mode is equal to the heat being transferred to the PCM tank, while in discharging and normal operation modes, the aim is to provide the cooling load of the residential block, and the provided load will be the same cooling loads imported from the IESVE model shown in Fig. 4.5 and 4.6 for Rome, Italy and London, UK.

- A parameter named Status of Charge (SOC) is used to indicate the charging and discharging modes. If SOC is more than or equal to 0.96, the storage tank is assumed to be fully charged, and the charging should be stopped, followed by the normal operation or discharging depending on other parameters. If SOC is lower than 0.04, it means the tank is fully emptied or discharged. This method of starting and stopping charging and discharging helps to simplify the simulation. Fig. 4.7 shows the logic of the control strategy and the role of SOC in calculations. Based on the time of day, cooling load, and PCM status, the algorithm of the control strategy will distinguish between different operational modes of the flexible systems. Table 4.5 shows the logic of the control strategy. The load is regularly checked. If it is lower than the trigger, the PCM status will be checked regardless of time. If the PCM is not fully charged, the system will switch to charging mode. If it is daytime and the PCM is not empty, discharge will be triggered to provide the cooling loads of the building.

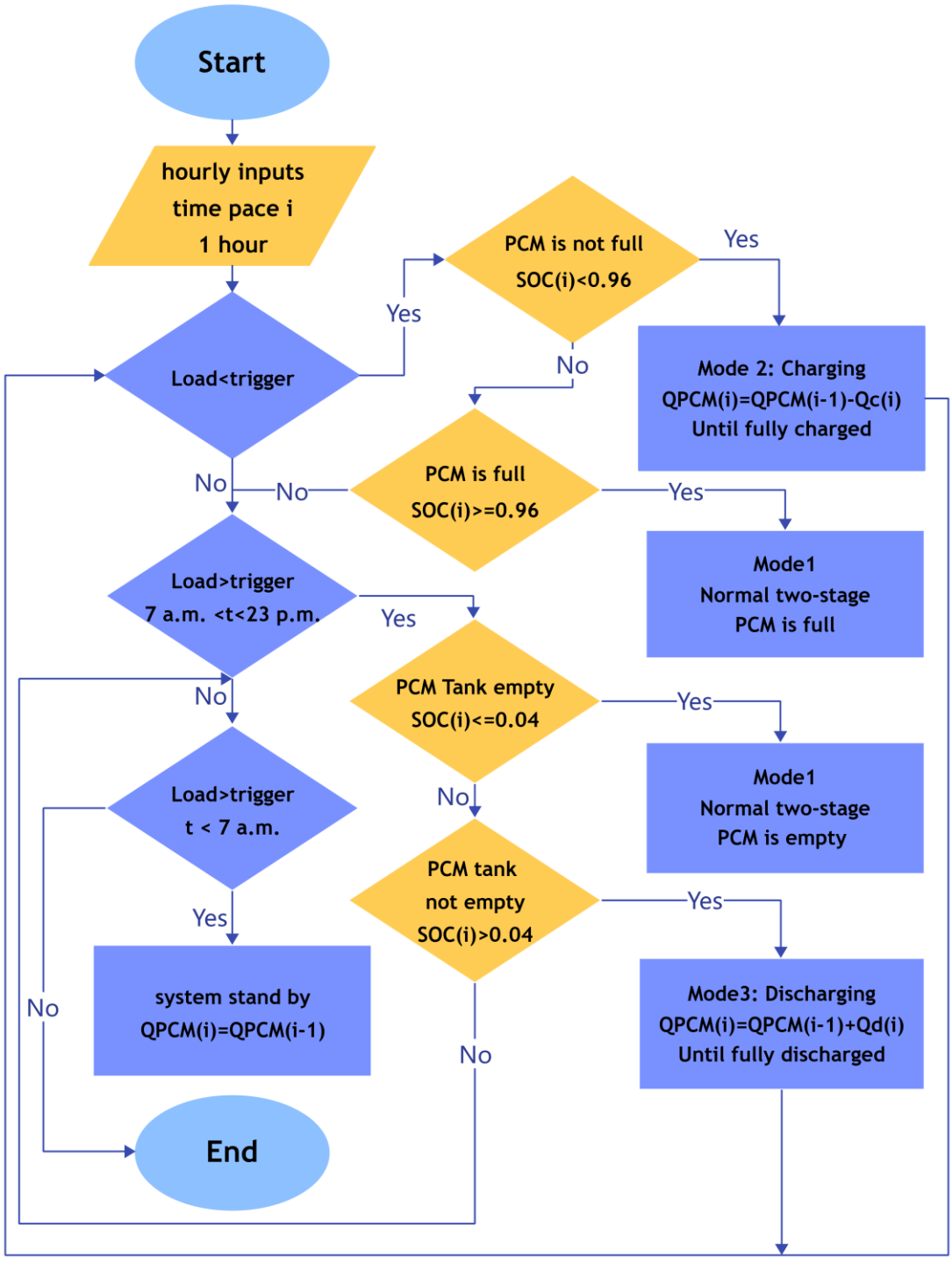

Figure 4.7 Flowchart of the simulation for a flexible two-stage heat pump: Cooling application.

Table 4.5 Working status of the normal and flexible two-stage heat pump in cooling application.

Time	duty	PCM state	Baseline	Flexible
0-7	Duty<trigger	QPCM Max	-	
		QPCM not 0		Charging
		QPCM=0		
	Duty>trigger	QPCM Max	-	
		QPCM not 0		
		QPCM=0		
7-23	Duty<trigger	QPCM Max	-	
		QPCM not 0	Normal	Charging
		QPCM=0		
	Duty>trigger	QPCM Max	-	Discharging
		QPCM not 0	Normal	
		QPCM=0		Normal

4.2.4 Mathematical governing equations

The first and second laws of thermodynamics are applied to each component of the system as a control volume. Eqs. 4-42 and 4-43 are the continuity and energy equations for each component, respectively.

$$\sum \dot{m}_{in}(i) = \sum \dot{m}_{out}(i) \qquad \textbf{Equation 4-42}$$

$$\sum \dot{m}_{in}(i) h_{in}(i) + \dot{Q}(i) = \sum \dot{m}_{out}(i)\, h_{out}(i) + \dot{W}(i) \qquad \textbf{Equation 4-43}$$

$\dot{m}$ is the mass flow rate ($kg.s^{-1}$), while h refers to enthalpy (kJ.kg^{-1}.K^{-1}). $\dot{Q}$ is the heat transfer rate through the component, i is the number of the time step (hour), and $\dot{W}$ is the power rate. Heat transfer via compressors and expansion valves, as well as work production/usage of heat exchangers, are considered zero.

For the baseline two-stage heat pump, its hourly mass flow rates of upper and lower cycles at each time step are calculated by Eqs. 4-44 and 4-45. $\dot{Q}_L(i)$ shows the hourly cooling load for the i -th hour of the season from Fig. 4.5 and Fig. 4.6. It should be noted that the mass flow rate in Eq. 4-44 would be zero if the cooling load rate is zero, which means the system is switched to the charging mode, the mass flow rate would be zero, and the system won't work at all in charging mode if the duty is zero. To prevent zero values for charging mass flow rate, the mass flow rate of the charging is set constant at 0.02 $kg.s^{-1}$. All in all, the initial flow rates of upper and lower cycles are also set to 0.02 $kg.s^{-1}$ to avoid errors.

$$\dot{m}_2(i) = \frac{\dot{Q}_L(i)}{h_4 - h5}$$ **Equation 4-44**

$$\dot{m}_1(i) = \dot{m}_2(i) \times \frac{h_3 - h_6}{h_2 - h_7}$$ **Equation 4-45**

$$T_{3\&6\,,c} = T_{PCM} - \Delta T_{app}$$ **Equation 4-46**

T_{PCM} is the melting point of PCM (K). $T_{3\&6\,,c}$ shows the temperature of state points 3 and 6 during charging. ΔT_{app} is the approach temperature difference, as shown in Eq. 4-46. The heat transfer rate of charging the PCM tank is calculated in Eq. 4-48. $\dot{m}_c$ is the mass flow rate of the charging mode cycle shown in Eq. 4-47. In charging mode, there is no cooling load for the building. The heat transfer rate of charging $\dot{Q}_c(i)$ will be calculated as shown in Eq. 4-48, which is also known as the charge rate of the PCM. The heat transfer between the PCM tank and the ambient air is assumed to be zero.

$$\dot{m}_c(i) = \ 0.02\ kg.s^{-1}$$ **Equation 4-47**

$$\dot{Q}_c(i) = \dot{m}_c(i) \times (h_{3c} - h_{6c})$$ **Equation 4-48**

The work consumption rate of the compressor in charging mode is written as:

$$\dot{w}_c(i) = \dot{m}_c(i) \times (h_{4c} - h_{3c})$$ **Equation 4-49**

To convert the heat transfer and power consumption rates to the amount of energy in kJ, the rate (kJ. s^{-1}) should be multiplied by the seconds in an hour. This will convert kW to Joules. With the heat transfer rate and power rate, the charged PCM energy at each time $Q_{PCM}(i)$ of PCM and power consumption of the charging can be calculated using Eq. 4-50 and 4-51, respectively.

$$Q_{PCM}(i) = \dot{Q}_c(i) \times 3600$$ **Equation 4-50**

$$W(i) = \dot{w}_c(i) \times 3600$$ **Equation 4-51**

The PCM energy at the (i-1)-th time step is calculated by substituting i-1 with i in Eq. 4-50. The relation between the PCM energy at the i-th time step and at the (i-1)-th time step is shown in Eq. 4-52. The PCM energy is checked hourly to calculate the state of charge (SOC) of the tank using Eq. 4-56.

$$Q_{PCM}(i) = Q_{PCM}(i-1) - \dot{Q}_c(i) \times 3600$$ **Equation 4-52**

In discharging mode, the temperature of the state points 2 and 7 is lower than the PCM tank temperature:

$$T_{2\&7,d} = T_{PCM} - \Delta T_{app}$$ **Equation 4-53**

The discharging heat transfer rate at each time step is calculated as:

$$\dot{Q}_d(i) = \dot{m}_d(i) \times (h_{2d} - h_{7d})$$ **Equation 4-54**

The PCM energy at each time step in discharging mode is obtained using Eq. 4-55.

$$Q_{PCM}(i) = Q_{PCM}(i-1) + \dot{Q}_d(i) \times 3600$$ **Equation 4-55**

As mentioned previously, the SOC is defined as an indicator to stop charging and discharging, which is calculated by:

$$SOC(i) = \frac{Q_{PCM}(i)}{Q_{Max,PCM,th}}$$ **Equation 4-56**

$Q_{PCM,th}$ is the theoretical maximum capacity of the PCM tank. It is assumed that it is equal to the capacity of 1000 kg of PCM stored in the PCM tank, shown in Eq. 4-57:

$$Q_{Max,PCM,th} = m_{PCM}.C_{P,PCM}.|(T_{Melt,PCM} - T_{PCM.ini})| + m_{PCM}.L_{fus}$$ **Equation 4-57**

$C_{P,PCM}$ is the specific heat capacity at constant pressure of the PCM and L_{fus} is the enthalpy of fusion of PCM. $T_{Melt,PCM} - T_{PCM.ini}$ is the temperature difference of the PCM from the beginning of working until it melts completely.

The hourly COP of the system at each hour can be calculated as:

$$COP(i) = \frac{\dot{Q}_L(i)}{\dot{w}_{tot}}$$ **Equation 4-58**

However, in order to compare the flexible two-stage heat pump (config. 1) to the baseline two-stage heat pump, the seasonal coefficient of performance is calculated. Because COP per hour of the year is not a valid criterion for fairly comparing two systems to determine which one is operating more efficiently. It is not fair to compare a series of COPs for both systems, one at a time, throughout the cooling season. The SCOP, or the seasonal coefficient of performance, is defined as the accumulated cooling load divided by the accumulated electricity usage during a certain period [112].

$$SCOP = \frac{\sum Q_L}{\sum W_{comp}}$$ **Equation 4-59**

Since the heat pump systems work in multiple modes, the duration of each mode should be accounted for when calculating the SCOP. In this research, the time step of each mode is an hour, and the control strategy will decide whether to switch operational mode at the end of each hour. Therefore, we only need to calculate $\sum Q_L$ and $\sum W_{comp}$ by making the sums of the $\dot{Q}_L(i)$ and $\dot{W}_{comp}(i)$ at all time steps respectively, so Eq. 4-60 becomes:

$$SCOP = \frac{\sum_{i=1}^{j} \dot{Q}_L(i)}{\sum_{i=1}^{j} \dot{W}_{comp}(i)}$$ **Equation 4-60**

Where j is the number of hours of the cooling season. $\dot{Q}_L$ varies in different operational modes due to the variable demands. Its value could be specified according to Eq. 4-61. As shown, in three different modes, the aim cooling load is different. In a cooling flexible system, the goal of running system in charging mode is to charge the PCM tank, while in discharging and normal working mode, the goal will be providing the cooling load to the building.

$$\begin{aligned} &\dot{Q}_L = \dot{Q}_c, \text{ in charging mode} && \text{(a)} \\ &\dot{Q}_L = \text{Building cooling loads, in discharging mode} && \text{(b)} \\ &\dot{Q}_L = \text{Building cooling loads, in normal operational mode} && \text{(c)} \end{aligned}$$ **Equation 4-61**

4.2.5 Annual price calculations

Finally, the cost of electricity usage for the aforementioned systems has been computed. The most significant feature of flexible systems is utilising off-peak electricity price reductions. To find the variable electricity price and analyse the systems from an economic perspective, the authors chose the *cosy octopus* tariff package from Octopus Energy, which is particularly designed for heat pump users. Its prices are: 1- (4 p.m. - 7 p.m.) 48.36 p/kWh, 2- (4 a.m. - 7 a.m.) 18.13 p/kWh, 3- (1 p.m. - 4 p.m.) 18.13 p/kWh, and 4 - (other hours) 30.22 p/kWh [113]. This tariff package is applied to both cities to have a fair comparison. Therefore, the total cost for using electricity in Pounds Sterling is as follows:

$$Price = \sum_{i=1}^{n} \dot{w}_{tot}(i) \times c(i)$$ **Equation 4-62**

c(i) is the hourly unit cost of electricity, while $\dot{w}_{tot}(i)$ is the hourly work consumption of the compressors, which varies based on different modes.

4.2.6 Validations

An ice-storage tank connected to a single-stage heat pump is simulated in its full-load mode against the results of *Sanaye et al.*'s study [76]. There are some differences in the assumptions and control technique between Sanaye's work and this paper such as similar daily cooling load for the whole season, details in configuration which could be ignored, fixed charging and discharging hours per day, however *Sanaye*[76] 's work shares certain cases, such as hourly computation, variable loads, and general system configuration which is matched with a single-stage heat pump in this study. In charging mode, the ice storage serves as the evaporator, while in discharging, it is connected to the building's air-conditioning loop to provide the cooling load. The cooling load is obtained from Fig. 4 of Sanaye and Hekmatian [76], and the optimal operating conditions are supplied in Table 5 of the reference *Sanaye and Hekmatian* [76] (optimum values), which are utilised as assumptions to validate this research. Sanaye[76]'s work calculated storage efficiency via heat transfer analysis. To simplify, the storage efficiency is assumed to be 85%.

The Table in the reference *Sanaye and Hekmatian* [76] shows that the evaporator and condenser temperatures are -3.11 and 38.46 ℃, respectively. The storage tank capacity is sufficient to charge the tank at a constant rate for 8 hours. The system will charge from 12 a.m. to 7 a.m., discharge from 8 a.m. to 6 p.m., and standby from 7 p.m. to 11 p.m. The results, displayed in Table 4.6, suggest that the simulated results show good agreement compared with those from the references.

Table 4.6 Validation results based on *Sanaye et al.* [76]

Hourly results' parameters in charging	Values calculated	Reference's values	Difference percentage
Evaporator heat transfer rate	1580.25 kW	1596 kW	-0.98%
mass flow rate	11.07 $kg.s^{-1}$	11.15 $kg.s^{-1}$	-0.72%
compressor work usage	357.01 kW	335.73 kW	6.34%
condenser heat transfer	1937.35 kW	1932 kW	0.28%
COP	4.4252	4.7543	-6.92%

4.3 Results and discussion

A new configuration (config. 1) of a two-stage flexible heat pump for cooling applications is proposed and compared with 1- a conventional two-stage heat pump 2- flexible single-stage 3- conventional single-stage and 4- another configuration of flexible two-stage heat pump (config. 2). Hourly weather data and cooling loads of a residential block in two cities, London UK, and Rome/Italy are imported into the simulation. The aim is to acquire SCOP, annual economic cost, and power consumption (electricity usage) of the mentioned heat pumps and find out if the flexibility is effective in reducing electricity consumption.

Fig. 4.8 (a) represents the hourly stored energy by the PCM during a hot season in Rome, which indicates that the PCM is charged at lower loads shown in Fig. 4.5 (b). Compared to the cooling load of Rome shown in Fig. 4.5 (b), when the loads are lower, PCM will be charged. Fig. 4.8 (b) shows that the power consumption is higher in the middle of the season due to the higher temperature of the ambient air shown in Fig. 4.5 (b), although the PCM is empty at this moment, as illustrated in Fig. 4.8 (c). Due to the control strategy designed in this study, PCM stored energy is not being used at the peak of the season. However, during the day and the loads are higher than the trigger (10 kW assumed for Rome), the tank will be discharged if it has energy (SOC>0.04). The reason for this strategy is that it is difficult to save energy for the peaks of seasonal consumption, but easier to use it at the first chance.

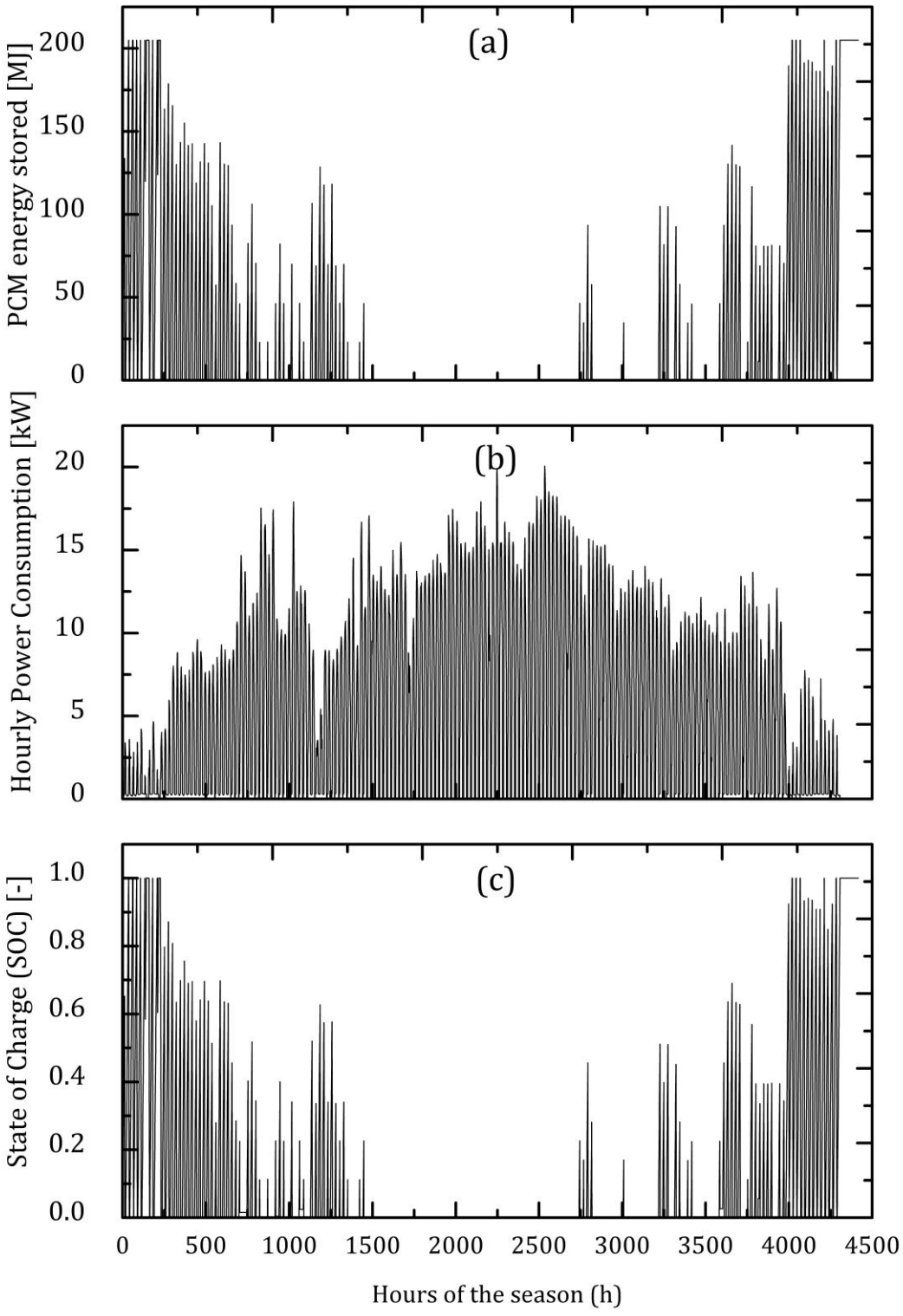

Figure 4.8 PCM stored energy (a), Hourly power consumption (electricity usage) (b), and SOC of the proposed system in Rome weather conditions.

Fig. 4.9 shows the electricity usage of the baseline two-stage pump and flexible two-stage heat pump for cooling in four days in May. Firstly, the curve shapes of the cooling loads and electricity usage are the same, since the electricity usage means the work done by compressors, and the electricity usage divided by the cooling load is the seasonal COP

according to Eq. 4-58, 4-59. In addition, the hours during electricity usage have been decreased by the flexible two-stage heat pump, compared to the baseline system, as shown in Fig. 4.9. The PCM tank is charged during the hours when cooling loads are lower than the trigger (7 kw in Fig. 4.9). Whenever it is required to provide the loads in cases of higher than trigger loads, the status of the PCM tank is checked. If there is enough energy inside the tank, it will start to discharge. At those discharging hours, there is less electricity consumption compared to the baseline system, because there is no PCM tank in the baseline system to release its energy, and all loads are provided by electricity to run compressors in both higher and lower cycles. In contrast, in the discharging mode of the flexible two-stage system, only the lower compressor works. Moreover, in charging mode, the electricity usage would be less than the baseline one, as only one compressor works during charging if the charging takes place during the day. However, charging at night would increase energy consumption by the flexible two-stage system compared to the baseline system, as the baseline system is completely off during the nighttime. For instance, there was no cooling load until 10 a.m. on the 5th of May, as shown in Fig. 4.9 (a). However, due to the predefined charging mass flow rate of the working fluid, some work was done by the compressors in charging mode in the hours before 10 due to lower loads compared to the trigger. Then the load increased as the outside temperature went higher, until around 16 p.m.. Before 10 a.m., the cooling load was lower than 7 kW (the charging/discharging trigger), and the system was working in its charging operation mode.. After 12 at noon, the load went higher than 7 kW, which was the trigger to start discharging mode, where only one of the compressors was working in the two-stage cycle, and the power consumption by the flexible system was lower than the baseline system. Discharging continued until the tank was emptied by 16 p.m. Between 16 p.m. and 20 p.m., the load was higher than 7 kW, but the flexible system worked as the baseline system since the PCM tank had already been emptied. Consequently, the power consumption by the flexible and baseline systems was the same during this period. After 20 p.m., the load is less than 7 kW, and the flexible system started to run the charging mode until the end of the day, while the baseline system was still working with both compressors on. The system was reset on the next day, which means no energy was stored and transferred from one day to the next day to avoid the risk of storage energy leakage and increasing storage costs and complexity.

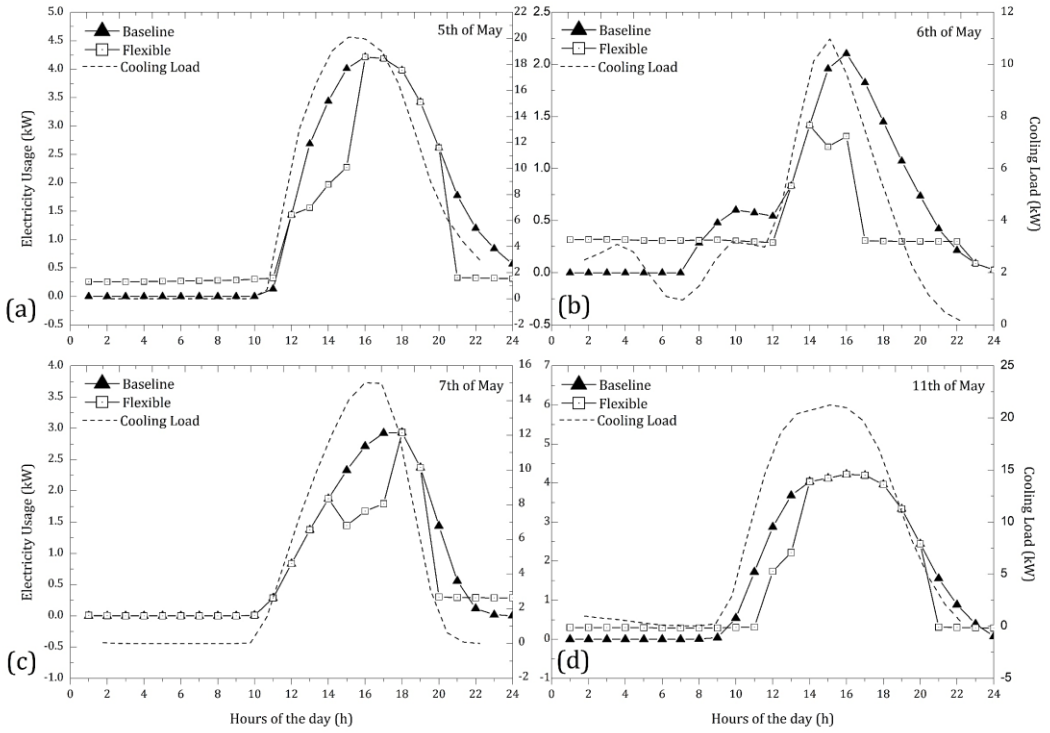

Figure 4.9 Daily electricity usage (left Y axis) for the baseline and proposed flexible two-stage heat pump and cooling loads (right Y axis) for four days in the cooling season of London city.

Table 4.7 shows the results for Rome and reveals that the SCOPs of the flexible single and two-stage heat pumps are 2.55% and 2.33% lower compared to those of the baseline counterparts, respectively. Moreover, the annual price is reduced up to £43 for the two-stage system, while the single-stage system shows a £65 reduction in annual price. The consumed power decreased by 123 kW for the flexible two-stage system, while the flexible single-stage system represented a 202-kW reduction.

Table 4.7 Cooling results for Rome/Italy/ Single and two-stage cycles/ Trigger 10kW.

Cycle type	Model/Load	SCOP	Price	W consumption (kW)
Two-stage	baseline	4.1517	7,501	23,112
	flexible	4.2483	7,458	22,989
Single-stage	baseline	3.7661	8,269	25,479
	flexible	3.8622	8,204	25,277

Table 4.8 shows the results for London weather conditions and two different charging/discharging triggers. As the cooling load is lower in London compared to that in Rome and the trigger is 15% of the maximum cooling load, the trigger value is lower in London (3-7 kW) compared to Rome's (10 kW). It is revealed that the SCOP of the systems running in London is higher compared to those operating in Rome, because heat pumps

generally work more efficiently in milder weather. As a result, the prices and power consumption are lower. Moreover, it indicates that more load contributed to charging will lead to a better result: higher SCOP, lower power consumption and lower price. When using the 7-kW trigger, the SCOP of the flexible two-stage heat pump was 21.3% higher than that of the baseline pump, while with the 3-kW trigger, the flexible two-stage heat pump obtained 20.99% higher SCOP compared to the baseline counterparts. However, the 3-kW trigger is not enough for a flexible two-stage cycle, as the electricity usage and annual price are even higher than the baseline heat pump. Therefore, the trigger plays a key role in controlling the energy performance of the flexible heat pump. In comparison of the single-stage baseline, the flexible single-stage system with the 7-kW trigger has 34.14% higher SCOP, £216 (17.18%) less annual price, and 626 kW (16.97%) less electricity usage, whilst with the 3-kW trigger has 31.22% higher SCOP, £166 (13.21%) less annual price, and 465 kW (12.61%) less electricity usage. It demonstrates that milder weather leads to higher SCOP, less electricity usage and lower prices, even in the baseline system; however, the trigger value would significantly affect the performance.

Table 4.8 Cooling results for London/UK/ Single and two-stage cycles/ Trigger 7kW and 3 kW.

Cycle type	Model/Load	SCOP (-)	Price (£)	W consumption (kW)
	baseline	4.7967	1,154	3,388
Two-stage	Flexible- 7kW trigger	5.8183	1,118	3,303
	Flexible- 3kW trigger	5.8035	1,165	3,447
	Baseline	4.4055	1,257	3,689
Single-stage	Flexible- 7kW trigger	5.9095	1,041	3,063
	Flexible- 3kW trigger	5.7809	1,091	3,224

In addition, another configuration for the flexible two-stage heat pump, named config. 2, is compared with the proposed two-stage configuration (config. 1). The results of different configurations are shown in Table 4.9. The same working conditions are applied to the second configuration, except the interstage temperature. The difference between the two configurations is that the PCM tank in the second configuration does not provide the cooling loads directly during discharging, and both compressors are working, whereas in the config. 1, only one of the compressors is working during charging and discharging. Therefore, the second configuration has higher energy consumption and price than those of the config. 1 of the flexible two-stage system.

Table 4.9 Cooling results for first (config. 1) and second flexible configuration (config. 2) working in London and Rome.

Cycle type	Model/Load	SCOP	Price	W consumption (kW)
London (3 KW)	Flexible V1	5.8035	1,165	3,447
	Flexible V2	4.0863	1,326	4,004
London (7 KW)	Flexible V1	5.8183	1,118	3,303
	Flexible V2	4.0938	1,281	3,853
Rome (10 kW)	Flexible V1	4.2483	7,458	22,989
	Flexible V2	4.0670	7,571	23,409

4.4 Summary of the chapter

This work introduces a new configuration of a flexible two-stage heat pump system (config. 1) for cooling applications and compared it with the second configuration common in literature (config. 2). This new system is investigated in comparison with the other four systems under identical operating conditions: a baseline two-stage heat pump, a baseline single-stage heat pump, and a flexible single-stage heat pump and a second configuration of the flexible two-stage heat pump. A control strategy is developed to regulate four operational modes- normal operation, charging, discharging, and standby, depending on the cooling load, hour of the day, and status of the storage tank. The weather data of London, UK, and Rome, Italy have been used to acquire the variable hourly cooling loads of a typical 4-story residential block via IESVE software. The results show that the flexible two-stage system and flexible single-stage system achieve seasonal coefficients of performance (SCOP) 2.33% and 2.55% higher than the two baseline systems of two-stage and single-stage heat pumps, respectively. Furthermore, the heat pump demonstrates enhanced results in milder weather in London than in Rome. The newly proposed system in this study shows an overall higher SCOP than the other four compared heat pump systems.

Chapter 5

Heat exchanger design and Techno-economic analysis of the flexible two-stage heat pump

5.1 Introduction

Using the thermodynamic rules, the authors have previously worked on a flexible two-stage system for a residential building of 40 flats with 40 separate heat pumps, recently published in *Mokarram, et al.* [116]. This chapter presents a comprehensive techno-economic analysis (TEA) of a newly developed two-stage flexible heat pump system designed for residential applications. The proposed system is capable of operating in three distinct modes: (1) normal operation, (2) thermal charging, and (3) thermal discharging, enabling enhanced operational flexibility and energy management. The heat pump incorporates aluminium-extruded tube micro-channel heat exchangers for both the evaporator and condenser, engineered to maximise heat transfer performance while maintaining compactness. Thermodynamic and heat transfer analyses were conducted to characterise system performance, followed by a TEA to evaluate economic feasibility. The condenser and evaporator achieve heat transfer rates of 106.28 kW and 76.34 kW, respectively, with corresponding heat transfer coefficients of 1,790.8 W/m²·K and 1,011.8 W/m²·K. Economic performance was assessed using standard financial indicators including annual profit (AP), net present value (NPV), payback period (PP), internal rate of return (IRR), and multiple on invested capital (MOIC). Results indicate strong economic viability for deployment in a 40-flat residential building, with an NPV of £177,903, IRR of 16.4%, and a payback period of 7.8 years. The total capital investment required is £163,880, resulting in a MOIC of 2.08. These findings support the feasibility of the proposed heat pump system as a cost-effective and energyefficient solution for low-carbon residential heating applications.

5.2 Methodology

In this section, the simulation logic will be explained in the following sub-sections. In section 5.2.1, thermodynamic analysis will be reviewed, as it is required for the next two sections. Second, the evaporator and condenser design will be elaborated. Two Al-extruded tube micro-channel heat exchangers are designed as the evaporator and condenser of the system. Heat transfer design will be covered in section 5.2.2. In 5.2.3 and 5.2.4, two-phase boiling and condensing heat transfer coefficients are explained, respectively. In 5.2.5, the air-side

convection heat transfer coefficient has been elaborated for a rectangular air channel. Section 5.2.6 explained the validation of the heat transfer section. The heat exchanger design is added based on a work by *Mokarram et al.* [115], which is a study to design a three-fluid AL-extruded tube micro-channel heat exchanger for an air-conditioning cooling system. In the current study, a two-fluid two-phase micro-channel heat exchanger has been considered. In the third phase, a techno-economic analysis will be presented, which has been performed by using the cost function correlations per component of the system. In the end, the results will be explained in the results and discussion section, shown in section 5.4.

For a flexible two-stage heat pump introduced in *Mokarram, et al.* [116] (chapter 3 of this thesis) which is shown in Fig. 5.1, a techno-economic analysis is performed in this chapter. The whole thermodynamic analysis has been performed *in Mokarram, et al.* [116]. Being an air-source heat pump, it draws heat from the surrounding air and has an expansion valve and compressor at each step. A flash tank is connected to work in between the condenser and evaporator in the upper and lower stages, respectively. A fluidic circuit connects a PCM tank to the flash tank. The system operation modes are controlled by four valves that are installed before the compressors and expansion valves. The heated stream from the evaporator is the ambient air. By heating the evaporator's cold working fluid stream, it will transform the fluid into a saturated vapour state.

The core code controls the three phases, and their inputs and outputs, which are written as M-File functions in MATLAB [106]. Fig. 5.2 shows the schematic figure of the functions to calculate the final results. Different parameters have been calculated to analyse the flexible two-stage heat pump in three phases. It has been shown that the order of the study, which starts with a thermodynamic viewpoint, is followed by heat transfer and then techno-economic phases. In the Thermodynamic analysis phase, the work and heat transfer rates of the components are required to be determined. In the second phase, heat exchanger design, the heat exchangers will be sized based on the details of their physical properties, depending on the type of heat exchanger. In the third phase, techno-economic analysis, the key economic parameters are of importance, as the system is meant to be realistic. All the phases will be elaborated in the next sub-sections.

5.2.1 System description

The flexible two-stage heat pump was proposed in our previous work *Mokarram, et al.* [116] for heating application in comparison with the conventional two-stage heat pump. This novel

flexible two-stage air-source heat pump, integrated with a phase-change material (PCM) thermal energy storage system, and is designed to improve heating efficiency and reduce electricity costs. The system has four modes, normal operating, charging, discharging, and standby, based on heating demands and PCM status. Simulations using real and sinusoidal load profiles for two cities in UK show that the system achieves 1.67% and up to 5.31% higher seasonal coefficient of performance (SCOP) with real loads and sinusoidal loads respectively, compared to conventional two-stage heat pumps. Moreover, it lowers annual electricity costs by leveraging stored energy during peak demand.

As an air-source heat pump, this system incorporates a compressor and an expansion valve at every stage and absorbs heat from the atmosphere around it. The condenser and evaporator are located at the top and lower stages, respectively, and both are connected to a flash tank. A fluidic circuit connects the flash tank to a PCM tank. Compressors and expansion valves are controlled by four valves that regulate the operation modes of the system. The evaporator uses two fluids. Ambient air is heated in the evaporator and becomes the hot stream, which will heat the cold working fluid stream to a saturated vapor state. The saturated vapour at the evaporator's outlet is compressed by the compressor at the bottom stage, and becomes superheated vapour. The flash tank evacuates the flash gas at the intermediate pressure in order to prevent it vaporising due to potential pressure drop and thus saves energy for recompression. The flash tank further intercools the vapour from Compressor I (the lower stage compressor), reducing the compression power required by Compressor II (the high-pressure stage compressor). Consequently, the system's COP is significantly higher than that of a single-stage operating at the same temperature lift.

The two-stage heat pump with PCM storage operates in four modes, charging, normal operation, discharging, and standby, controlled by four valves as shown in Fig. 5.1. In normal operating mode (Mode 1), the compressor runs to warm the indoor air (process of refrigerant-air heat transfer) when all the four valves are open. The compressor runs in charging mode (Mode 2) with only valve 3 and 4 (V3 and V4) open to store off-peak electricity energy into PCM-stored energy in the storage tank using hot stream 2-3.; and in discharging mode (Mode 3), the system operates with only V1 and V2 open to cool the indoor air using stored PCM energy. The entire thermodynamic analysis of this system has been performed in our previous work [116].

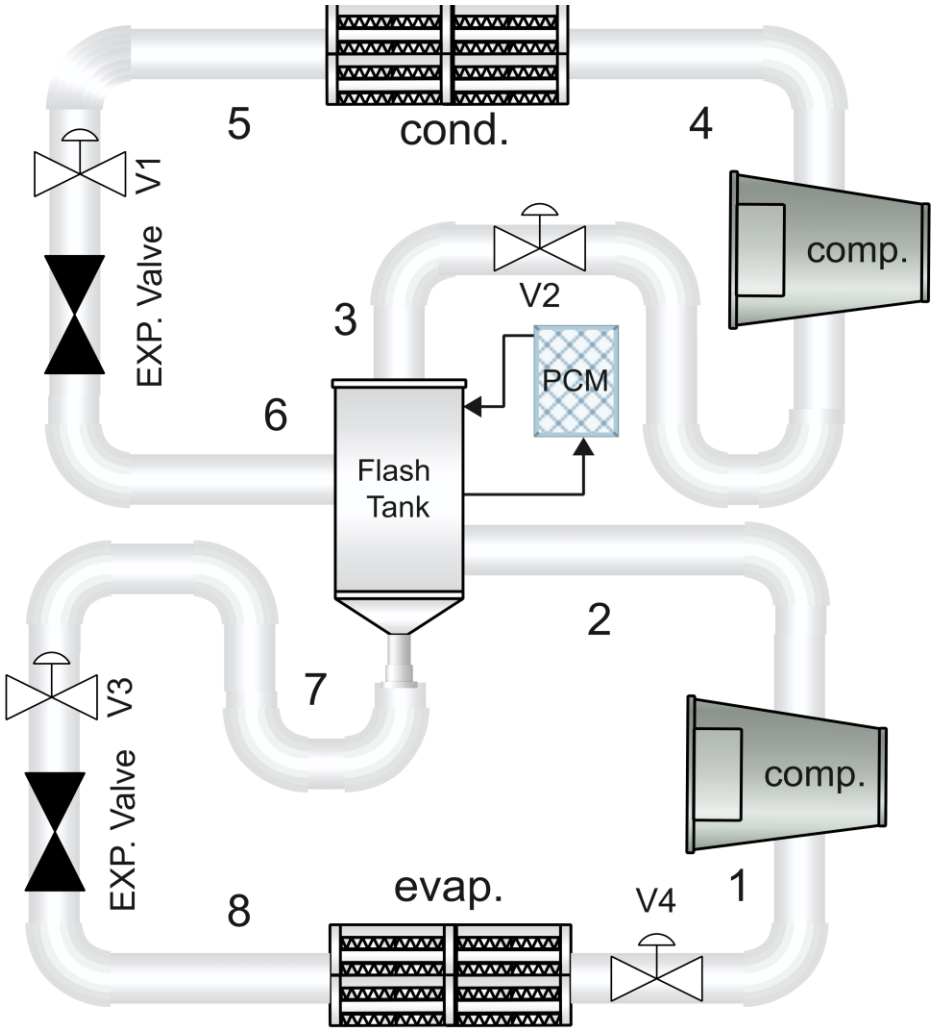

Figure 5.1 A flexible two stage HP cycle with PCM TES.

Fig. 5.2 shows the diagram of the functions to calculate the final results. Different parameters are calculated to simulate the flexible two-stage heat pump in three phases in sequence, thermodynamic analysis, heat transfer, and TEA (techno-economic analysis). The core code controls the three phases, and their inputs and outputs, which are written as M-File functions in MATLAB [106]. In the Thermodynamic analysis phase, the work and heat transfer rates of the components are required to attain for the next phase. In the second phase, heat exchanger design, the heat exchangers will be sized, according to their physical properties and the type of heat exchangers. In the third phase, TEA the key economic parameters are of importance, as the system is meant to be realistic. Based on the results of first and second phase of analysis, thermodynamics and heat transfer analysis, the economic parameters including Annual Profit (AP), Total Capital Investment (TCI), Net Present Value (NPV),

Multiple on Invested Capital (MOIC), Interest Rate of Return (IRR), Period Payback (PP) will be calculated.

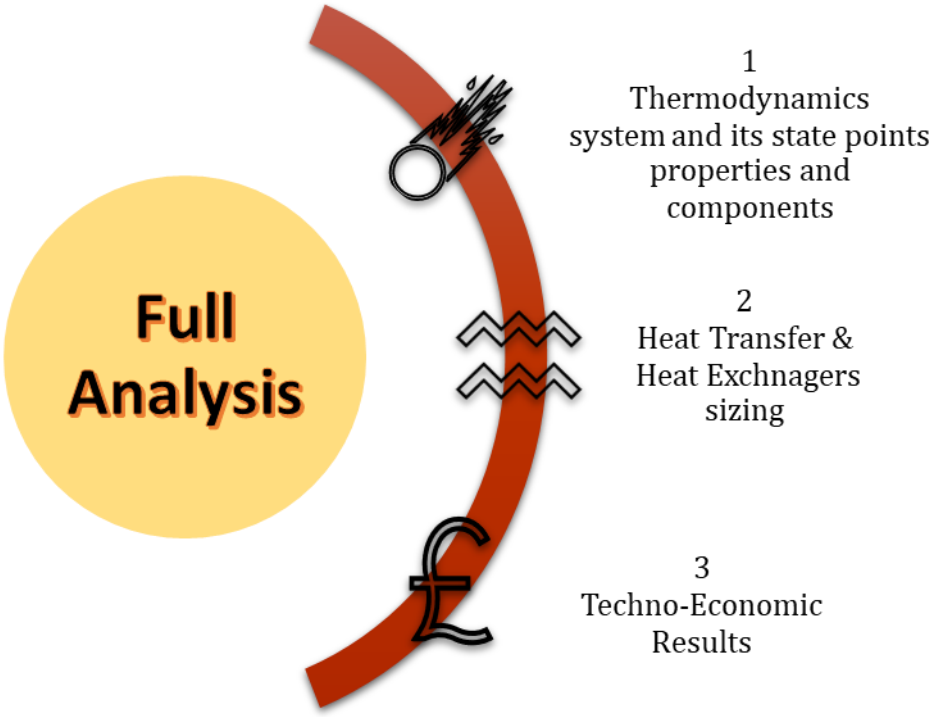

Figure 5.2 Three functions in-order, feeding in each other in this study.

5.2.2 Thermodynamic analysis

The thermodynamic properties to calculate the state points of the cycle are obtained. All are needed to perform components' sizing and economic investigation. Table 5.1 shows the assumptions of the thermodynamic study of this system, which have been used in chapter 3.

The thermodynamic properties to calculate the state points of the cycle are obtained. They are needed to perform thermodynamic analysis and then feed in the results to components' sizing and economic investigation phases. Table 5.1 shows the assumptions of thermodynamic study of this system. Also, the heating loads have been extracted from IESVE software and used as input in thermodynamic phase of analysis. The hourly variable loads of a residential block in Glaswegian weather are shown in Fig. 5.3. For more details regards to the loads, please refer to the previous study by *Mokarram, et al.* [116], chapter 3 and 4 of this thesis and Appendix A.

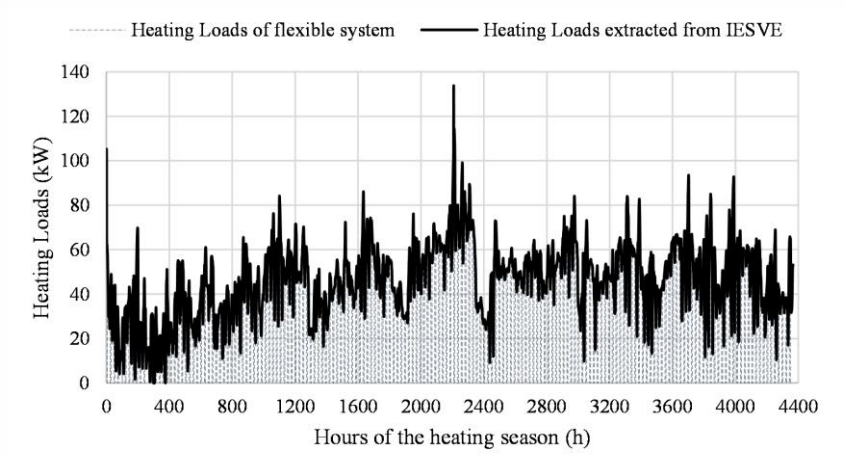

Figure 5.3 Heating loads fitted to control strategy versus the IESVE loads input for Glasgow, Scotland, UK.

The first and second law of thermodynamics are applied to analyse the thermodynamic performance of the systems in MATLAB, and each component is assumed to be a control volume. The corresponding mass and energy balances of each component are given in Eq. 5-1 and 5-2

$$\sum \dot{m}_{in} = \sum \dot{m}_{out} \qquad \textbf{Equation 5-1}$$

$$\sum \dot{m}_{in} h_{in} + \dot{Q} = \sum \dot{m}_{out} h_{out} + \dot{W} \qquad \textbf{Equation 5-2}$$

$\dot{m}$ is the mass flow rate ($kg.s^{-1}$), while h refers to enthalpy (kJ.kg^{-1}.K^{-1}). $\dot{Q}$ is the heat transfer into or out of this control volume (kW), while $\dot{W}$ is the work done (kW). More detailed explanation can be found in *Mokarram, et al.* [116], and chapter 3 and 4 of this thesis.

Table 5.1 Simulation assumptions for heating application.

Parameters	Value	Unit
Condenser Temperature	40	℃
Evaporator Temperature [116]	$T_{atm} - 10$	℃
PCM Melting Temperature [49]	20	℃
Weather Data	Glasgow, UK	-
$\boldsymbol{\eta_{comp}}$	80%	-

5.2.3 Heat Transfer viewpoint

To design two-phase three-fluid micro-channel heat exchangers, the entire design process is described in full detail in Mokarram and Wang [115], and for heat transfer of micro-channels in general in Lee and Mudawar [117,118-120], but the key correlations are included in the following paragraphs for a two-fluid micro-channel evaporator and condenser. In this

chapter, the evaporator and condenser are designed using the same process and reasoning, except that the heat exchangers are two-fluid.

This system is designed to use a two-fluid AL-extruded tube micro-channel condenser and the same evaporator. The schematic figure of an AL-extruded tube micro-channel heat exchanger is shown in Fig. 5.4. The cross-sectional view of the tube itself is presented in Fig. 5.5. Due to a crossflow design, air will flow over the micro-channel tube, via the rectangular air-channels shown in Fig. 5.4 while refrigerant will flow via parallel micro-channel tubes in a counterflow design at both of the evaporator and condenser. The physical properties of the present evaporator and condenser designs are displayed in Table 5.2 with their values.

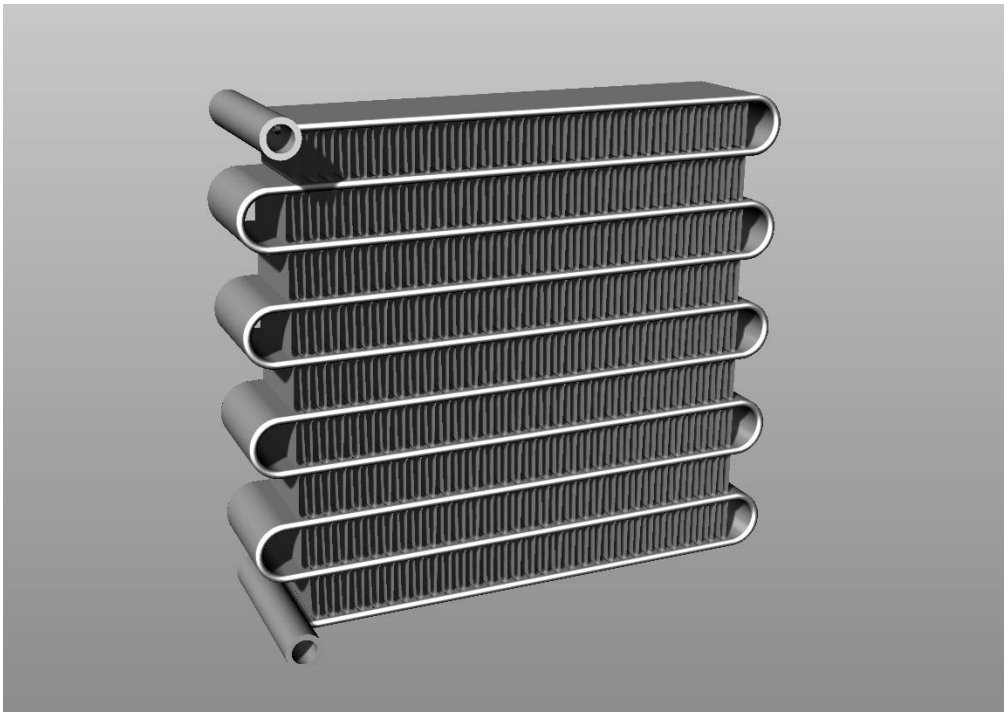

Figure 5.4 3D model of an AL- Extruded tube micro-channel Heat exchanger [121]

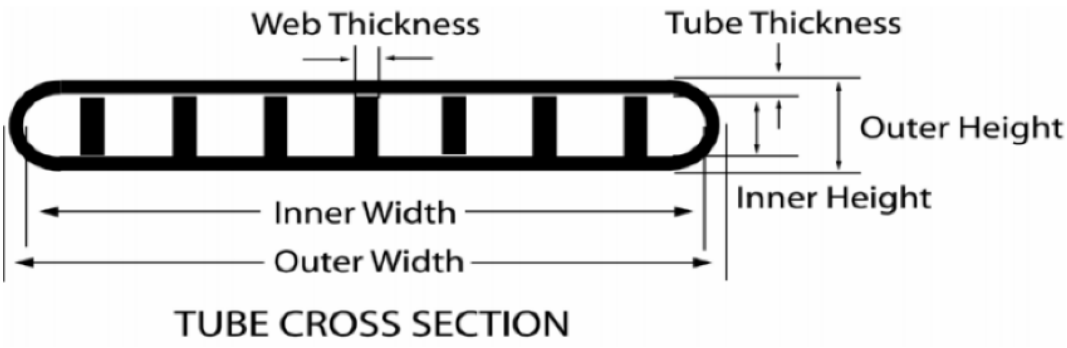

Figure 5.5 A general cross-sectional view of an Al-Extruded Micro-channel [115]

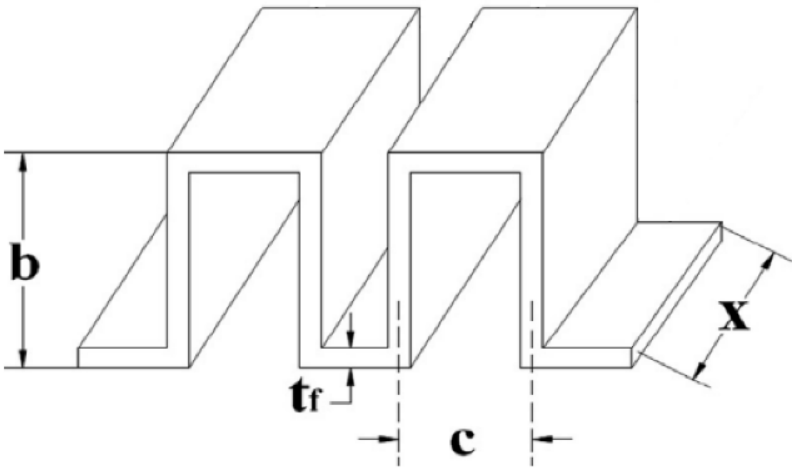

Figure 5.6 One-layer rectangular offset strip fin pattern of air-channel adapted from reference [122].

Channel width, wall thickness, channel hydraulic diameter, tube numbers, and micro-channel numbers are the required information to perform the heat transfer analysis of heat exchangers' design.

Table 5.2 Physical properties assumptions to design heat exchangers [115]

Parameter	Description	Value
N_{ch}	Micro-Channel Numbers in one tube	15
N_{tube}	Number of Al-Extruded micro-Channel tubes	17
w	Width of the Aluminium extruded tube (cm)	4
d_h	Hydraulic diameter (mm)	1.46
th_{fin}	Fin thickness (mm)	0.25
th_{wall}	Wall thickness of tubes (mm)	0.5
s_{fin}	Air fin distances	3
H_{fin}	Air fin height (m)	0.01
k_{wall}	Tube walls thermal conductivity (Aluminium Alloy)	177

Determining the length of the heat exchanger (L) requires computing the overall heat transfer coefficient (U), which is obtained by calculating the thermal resistance between the two fluids (R). It includes the refrigerant's convection resistance and the tube walls' conduction resistance. The refrigerant convection heat transfer coefficient is calculated using the Universal model developed for boiling by Lee and Mudawar [117,118,119] and condensing by *Kim and Mudawar* [118]. The two-phase correlations are expressed in terms of the vapour quality of the fluid. The quality changes along the tube length in both condensation and evaporation phases, which causes variations in the heat exchanger's overall heat transfer coefficient (U value) in the model. Therefore, it is required to divide the heat exchanger into some sections and calculate the length of each section based on the fluids' thermophysical properties and sum them up. In this chapter, there are 50 sections. As there are two fluids in two hot and cold streams, air and working fluid, two types of correlations are required in

each evaporator and condenser. On the other hand, in the evaporator and condenser, two different heat transfer phenomena happen: boiling and condensing, respectively. Therefore, two different convection heat transfer calculation correlations are required, which will be explained in the following sub-sections.

5.2.4 Two-phase boiling heat transfer coefficient in the evaporator (refrigerant side)

Kim et al. [119] developed a generalised correlation to determine the two-phase boiling heat transfer coefficient in the evaporator's microchannels. Convection and nucleate boiling contributions are combined in the correlation. The correlation is created by building a database of 10,805 data points from 37 sources, consisting of 1229 multi-channel points and 9576 single-channel ones.

$$h_{tp} = (h_{nb}{}^2 + h_{cb}{}^2)^{0.5} \quad \textbf{Equation 5-3}$$

$$h_{nb} = [2345\left(Bo\frac{P_H}{P_F}\right)^{0.7} P_R{}^{0.38}(1-x)^{-0.51}](0.023Re_f{}^{0.8}Pr_L{}^{0.4}\frac{K_L}{D_h}) \quad \textbf{Equation 5-4}$$

$$h_{cb} = [5.2\left(Bo\frac{P_H}{P_F}\right)^{0.08} We_{Lo}{}^{-0.54} + 3.5\left(\frac{1}{X_{tt}}\right)^{0.94}\left(\frac{\rho_g}{\rho_L}\right)^{0.25}](0.023Re_L{}^{0.8}Pr_L{}^{0.4}\frac{K_L}{D_h}) \quad \textbf{Equation 5-5}$$

$$X_{tt} = \left(\frac{\mu_f}{\mu_g}\right)^{0.1}\left(\frac{1-x}{x}\right)^{0.9}(\frac{\rho_g}{\rho_L})^{0.5}, Bo = \frac{\ddot{Q}}{\dot{m}_{ref}h_{fg}} = \frac{\dot{Q}/_{2L.w.Ntubes}}{\dot{m}_{ref}h_{fg}} \quad \textbf{Equation 5-6}$$

$$Re_L = \frac{G(1-x)d_h}{\mu_L}, P_R = \frac{P}{P_{crit}}, We_{Lo} = \frac{G^2 d_h}{\rho_L 0\sigma} \quad \textbf{Equation 5-7}$$

The parameters are as follows: h_{tp} the two-phase convection heat transfer coefficient, h_{nb} nucleate boiling dominant heat transfer, h_{cb} convective boiling dominant heat transfer, Bo boiling number, P_H heated perimeter of channel, P_F wetted perimeter of channel, P_R reduced pressure, x thermodynamic equilibrium quality, Re_f liquid-only Reynolds number, Pr_L Prandtl number K_L thermal conductivity, We_{Lo} liquid-only Weber number, X_{tt} Lockhart–Martinelli parameter (X) based on turbulent liquid-turbulent vapour flows, $\ddot{Q}$ effective heat flux averaged over heated perimeter of channel, $\dot{m}$ mass flow rate, h_{fg} latent heat of vaporisation, Re_L superficial liquid Reynolds number, G mass velocity, μ_L dynamic viscosity surface tension, and ρ density. For more details, please refer to [119].

5.2.5 Two-phase condensing heat transfer coefficient in the condenser (refrigerant side)

In order to build the two-fluid micro-channel condenser, the convective heat transfer coefficient of refrigerant is described using the generalised condensing two-phase heat

transfer correlation by *Kim et al.* [120]. The universal correlation of condensation is constructed using a database that contains 4045 data points from 28 sources, including single-channel and multi-channel data points. Depending on the flow regime, the correlation is divided into two parts: one for annular flow and another for slug and bubbly flow, which are shown in Eqs. 5-8 and 5-9.

$h_{tp,annu} = 0.048Re^{0.69}Pr^{0.34}\frac{\emptyset_g}{X_{tt}}, \quad 7X_{tt}^{0.2} < We^*$	**Equation 5-8**
$h_{tp,non-annu} = \left[\left(0.048Re^{0.69}Pr^{0.34}\frac{\emptyset_g}{X_{tt}}\right)^2 + \left(3.2\times10^{-7}Re_L^{-0.38}Su_{go}^{1.39}\right)^2\right]^{0.2}, \quad 7X_{tt}^{0.2} > We^*$	**Equation 5-9**
$X_{tt} = \left(\frac{\mu_L}{\mu_g}\right)^{0.1}\left(\frac{1-x}{x}\right)^{0.9}\left(\frac{\rho_g}{\rho_L}\right)^{0.5}$	**Equation 5-10**
$Re_{Lo} = \frac{Gd_h}{\mu_L}, Re_{go} = \frac{Gd_h}{\mu_g},$ $We = \frac{G^2 d_h}{\rho_L \sigma}, \ Re_L = \frac{G(1-x)d_h}{\mu_L}, Re_g = \frac{Gxd_h}{\mu_g},$ $Su_{Lo} = \frac{Re_{Lo}^2}{We}, Su_{go} = \frac{Re_{go}^2}{We}$	**Equation 5-11**
$We^* = 2.45\frac{Re_g^{0.64}}{Su_{go}^{0.3}(1+1.09X_{tt}^{0.039})^{0.4}}, \quad Re_L \le 1250$	**Equation 5-12**
$We^* = 0.85\frac{Re_g^{0.79}X_{tt}^{0.157}}{Su_{go}^{0.3}(1+1.09X_{tt}^{0.039})^{0.4}}\left[\left(\frac{\mu_g}{\mu_L}\right)^2\left(\frac{v_g}{v_L}\right)\right]^{0.084}, \ Re_L > 1250$	**Equation 5-13**
$\emptyset_g^2 = 1 + CX + X^2, \emptyset_L^2 = 1 + \frac{C}{X} + \frac{1}{X^2}$	**Equation 5-14**
$C = 0.39Re_{Lo}^{0.03}Su_{go}^{0.1}\left(\frac{\rho_L}{\rho_g}\right)^{0.35}, \ Re_L \ge 2000, Re_g \ge 2000$	**Equation 5-15**
$C = 8.7e-4\ Re_{Lo}^{0.17}Su_{go}^{0.5}\left(\frac{\rho_L}{\rho_g}\right)^{0.14}, \ Re_L \ge 2000, Re_g < 2000$	**Equation 5-16**
$C = 0.0015\ Re_{Lo}^{0.59}Su_{go}^{0.19}\left(\frac{\rho_L}{\rho_g}\right)^{0.36}, \ Re_L < 2000, Re_g \ge 2000$	**Equation 5-17**
$C = 3.5e-5\ Re_{Lo}^{0.44}Su_{go}^{0.5}\left(\frac{\rho_L}{\rho_g}\right)^{0.48}, Re_L < 2000, Re_g < 2000$	**Equation 5-18**
$-\left(\frac{dP}{dz}\right)_L = \frac{2f_L v_L G^2(1-x)^2}{d_h}$	**Equation 5-19**
$-\left(\frac{dP}{dz}\right)_g = \frac{2f_g v_g G^2(x)^2}{d_h}$	**Equation 5-20**
$X^2 = \frac{-\left(\frac{dP}{dz}\right)_L}{-\left(\frac{dP}{dz}\right)_g}$	**Equation 5-21**

in which $h_{tp,annu}$ refers to two-phase heat transfer coefficient of annular flow, $h_{tp,non-annu}$ is slug and bubbly flow, $\emptyset_g$ shows two-phase multiplier for saturated vapour, $\emptyset_L$ two-phase multiplier for saturated liquid, Su Suratman number, We^*modified Weber number, X Lockhart–Martinelli parameter, C coefficient in Lockhart–Martinelli parameter, $\left(\frac{dP}{dz}\right)$ frictional pressure gradients based on actual flow rates, x thermodynamic equilibrium quality or flow quality, G mass velocity, v specific volume, f Fanning friction factor, d_h hydraulic diameter, and Re refers to Reynolds number.

5.2.6 Air-side heat transfer coefficient [123]

A rectangular Offset Strip Fin concept is used to construct the air side, as illustrated in Fig. 5.6. To determine the convective heat transfer coefficient of the air-side, the following heat transfer correlation is utilised, where α, δ, and γ stand for the width to length, lateral fin spacing to height, and thickness to lateral fin spacing ratios, respectively.

$$h = \left(\frac{j}{Pr^{2/3}}\right)GC_p \quad \textbf{Equation 5-22}$$

$$j = 0.6522(Re^{-0.5403})(\alpha^{-0.1541})(\delta^{0.1499})(\gamma^{-0.0678})[1 + 5.269 \times 10^{-5}(Re^{1.34})(\alpha^{0.504})(\delta^{0.456})(\gamma^{-1.055})]^{0.1} \quad \textbf{Equation 5-23}$$

$$\alpha = \frac{c}{b};\ \delta = \frac{t_f}{w};\ \gamma = \frac{t_{fin}}{c};\ Re = (D_h G)/\mu$$

$$G = \frac{\dot{m}}{A_{flow}} \quad \textbf{Equation 5-24}$$

$$A_{flow} = \frac{D_h A_{flow-corss}}{4L_{flow}} \quad \textbf{Equation 5-25}$$

$$D_h = \frac{4w(c - t_{fin})(b - t_{fin})}{2(c - t_{fin})w + (b - t_{fin})w + t_{fin}(b - t_{fin}) - t_{fin}(c - t_{fin}) - {t_{fin}}^2} \quad \textbf{Equation 5-26}$$

$$c = s_{fin} + t_{fin};\ b = L_{fin} + t_{fin}; \quad \textbf{Equation 5-27}$$

in which h refers to convection heat transfer coefficient, j Colbourn factor, G mass velocity, Re Reynolds number, t_{fin} fin thickness, w Tube width, c Fin pitch, b Fin height, Pr Prandtl number, γ Fin thickness to fin pitch ratio, δ Fin thickness to fin width ratio, α Fin pitch to fin height ratio, $A_{flow-corss}$ Cross-sectional flow area, A_{flow} Minimum free-flow area for air, and L_{flow} Flow length.

5.2.7 Heat Transfer Validation

The study's methodology and simulation codes (in MATLAB) are validated by considering the input parameters from references [118,119]. The Universal correlations from *Kim and Mudawar* [119] and *Kim and Mudawar* [118] are used to compute the heat transfer coefficients for boiling and condensation. The convective and nucleate boiling heat transfer coefficients vs. quality, as well as the Percentage Difference percentage with the main reference *Kim and Mudawar* [119] are shown in Table 5.3. While Table 5.4 shows the same concept, two-phase heat transfer coefficient along the heat exchanger, for condensing, and compared with the results of reference *Kim and Mudawar* [118]. As can be seen from both Tables, the reasonable percentage difference confirms the heat transfer calculation's accuracy.

Table 5.3 Percentage Difference of Calculated two-phase h_{tp}, nucleate boiling h_{nb} and convective boiling h_{cb} heat transfer coefficients and the same parameters in Ref. 119

Quality	0.4			0.6			0.8		
Parameter	calculated	Ref. [119]	Diff. %	calculated	Ref. [119]	Diff. %	calculated	Ref. [119]	Diff. %
h_{tp}	6.7885	6.8380	0.20	6.73	6.77	0.68	6.59	6.64	0.16
h_{nb}	4.2486	5.2747	-0.06	4.7951	4.8906	1.97	5.33	5.41	0.41
h_{cb}	5.2946	4.3465	0.53	4.7184	4.6701	-1.03	3.88	3.83	-0.31

Table 5.4 Calculated two-phase condensation heat transfer coefficient and the same parameter in Ref. 118and their Percentage Difference.

Quality	Calculated	Ref. [118]	Diff. %
0.1	1101.807	1018.22	-7.88
0.2	1261.901	1245.436	-1.31
0.3	1474.356	1461.568	-0.87
0.4	1522.191	1596.589	4.77
0.5	1728.718	1728.747	0.0016
0.6	1941.588	1947.751	0.317
0.7	2173.789	2174.061	0.0125

5.3 Techno-economic analysis (TEA)

In the economic analysis of this study, an overall cost rate balance is applied to the system as written in Eq. 5-28:

$$\dot{Z}_{total} = \dot{Z}_{fuel} + CEPCI \times [\sum_{i=1}^{K} (\dot{Z}_{CI} + \dot{Z}_{OM}) + BOS] \quad \textbf{Equation 5-28}$$

Here, $\dot{Z}_{fuel}$ is the total price of the electricity used annually. The capital investment cost rate for the k-th system component ($\dot{C}_{CI,K}$) can be estimated by correlations presented in Table 5.6. The cost of operating and maintenance costs ($all\ in\ all\ \dot{Z}_{OM}$) and balance of the system (pipes, valves, the separator) (BOS) are considered as 20% and 6% of the components' updated capital cost investment ($CEPCI \times \sum \dot{Z}_{CI}$), respectively [124]. As a result, Eq. 5-29's factor ϕ equals 1.06 [125]. Additionally, *t* represents the system's annual operational hours, which is assumed to be 4000 (for a heating season). The chemical engineering plant index (CEPCI) equals 798.8, updated to June 2024 [126]. For each component, the sum of capital cost and operating and maintenance cost is calculated using the following equation [127]:

$$\dot{Z}_{CI,K} + \dot{Z}_{OM} = \frac{\dot{C}_{CI,K} \times CRF \times \emptyset}{t} \quad \textbf{Equation 5-29}$$

The capital recovery factor (CRF) is a ratio to calculate the present value of a series of equal annual cash flows. Its value can be estimated using Eq. 5-30 [23,128].

$$CRF = \frac{i(i+1)^n}{(1+i)^n - 1}$$ **Equation 5-30**

Here, i is the interest rate and is assumed to be 5%, and n represents the project lifetime, which is considered 15 years [125]. Assumptions are gathered together in Table 5.5.

Table 5.5 Techno-economic analysis assumptions.

Parameter	sign	Value
Annual interest rate	i	0.05
System lifetime [125]	n	15
Maintenance factor [125,129]	ϕ	1.06
Operational hours in a year (for a heating system)	t	4000

Table 5.6 Cost functions of the components in the recovery cycles [103,130-132]

components	Cost functions ($\dot{C}_{CI,K}$)	No. of Eq.
compressor	$\dot{C}_{comp} = \frac{39.5\dot{m}\left(P_o/P_i\right)\log\left(P_o/P_i\right)}{0.9 - \eta_{is,comp}}$	**Equation 5-31**
evaporator	$C_{evap} = 516.62.A_{evap} + 268.45$	**Equation 5-32**
condenser	$\dot{C}_{cond} = 268.45 + 516.621A_{cond}$	**Equation 5-33**
Flash chamber	$\dot{C}_{FT} = 280.3 \times (\dot{m}_1^{0.67} + \dot{m}_2^{0.67})$	**Equation 5-34**
Expansion valve	$\dot{C}_{exp} = 114.5\,\dot{m}$	**Equation 5-35**

Additional costs should be accounted for the PCM tank. The cost of the storage tank, stored material and encapsulation cost are required to calculate the total cost of PCM-related costs. The following correlations in Table 5.7 are used to calculate the cost of PCM tank manufacturing, the cost of PCM material, the cost of PCM storage (Encapsulation cost of the PCM material), and the total cost. The assumptions required to calculate PCM cost, the tank cost and the details of the parameters are shown in Table 5.8.

Table 5.7 PCM cost functions [133]

correlation	Calculated parameter	No of Eq.
$C_{sm} = [\rho_{PCM}(1-\varepsilon)C_{PCM} + \rho_f \varepsilon C_f]\,\pi R^2 H_b$	PCM material cost	**Equation 5-36**
$C_{EN} = C_{en} \times (\frac{R_{PCM}}{0.005})^{0.3}$	Encapsulation cost of the PCM material	**Equation 5-37**
$C_{st} = \rho_{ms} H\,[\pi(R + w_{th})^2 - \pi R^2]C_{MS} + \pi R^2 C_{pf} + 2\pi R H_b C_{in}$	Cost of mild steel for the storage tank body	**Equation 5-38**

Table 5.8 Assumptions of PCM cost calculation [133].

Parameter	Explanation	Value	Unit
ρ_{PCM}	Density of PCM material	1530	$kg.m^{-3}$
H_b	Height of the PCM tank	0.5	m
ε	void fraction- empty space in between PCM capsules	0.3	-
C_{PCM}	Unit price of PCM per kg	2.5	$\$.kg^{-1}$
C_{R134a}	Unit cost of working fluid per kg	24 (19)	$\$.kg^{-1}$ ($£.kg^{-1}$)
ρ_f	Density of working fluid	511.89	$kg.m^{-3}$
D_{PCM}	PCM spheres diameter	38	mm
C_{en}	Unit cost of encapsulation	2.4	$\$.kg^{-1}$
ρ_{ms}	Density of Mild Steel (tank)	7860	$kg.m^{-3}$
C_{ms}	Unit cost of mild steel	1.5	$\$.kg^{-1}$
w_{tank}	Thickness of PCm tank	1	mm
c_c	Unit cost of Concrete (PCM tank platform)	0.75	$\$.kg^{-1}$
H_p	Concrete platform height of PCM tank	10	cm
ρ_c	Density of concrete	2000	$kg.m^{-3}$
c_{in}	Unit cost of PCM tank insulation	16	$\$.m^{-3}$

The techno-economic approach is applied via calculating some economic concepts such as NPV (Net present value), IRR (internal rate of return), PP (payback period) and MOIC (multiple of invested capital), which are defined as Eqs. 5-39 - 5-45.

The current value of the potential net cash flow from an investment is shown by a standard economic indicator known as net present value (NPV). For the investment period, it contains the annualised cash flow cost estimations, both positive and negative. For a project to be considered acceptable, its NPV must be positive, which means that the cash inflow must exceed the cash outflow. PP is the amount of time required to recover the cost of an initial investment. Stated differently, it is the amount of time required for the NPV to gradually drop to zero. However, IRR has a different perspective on the return of investment. The interest rate at which the cash flow's NPV equals zero is known as the internal rate of return (IRR). MOIC differs from IRR as an investment return metric in that it emphasises *how much* rather than *when*. It compares the current value of the anticipated profit flows over the course of the project with the initial investment [134]. Eq. 5-41 is used to estimate AP, which stands for the plant's annual profit [125]. It is equivalent to the yearly sale of thermal energy minus the recurring yearly costs, like the operation and maintenance charges. After determining the annual profit, further economic metrics such as the multiple of invested capital (MOIC), internal rate of return (IRR), and (dynamic) payback period (PP) have been determined.

In addition, it should be noted that the economic analysis of this study is predicated on the assumption that no loan or subsidy has been secured.

$$TCI = 1.43 \times PEC$$ **Equation 5-39**

$$PEC_{total} = \sum_{i=1}^{k} \dot{Z}_{CI,K} + \dot{Z}_{OM}$$ **Equation 5-40**

$$AP = ((\dot{Q}_{cond} \times t \times C_{heat}) - \dot{Z}_{OM})$$ **Equation 5-41**

$$0 = -TCI + \sum_{t=1}^{n} \frac{AP}{(1+IRR)^t}$$ **Equation 5-42**

$$NPV = -TCI + \sum_{t=1}^{n} \frac{AP}{(1+i)^t}$$ **Equation 5-43**

$$PP = \frac{ln\left(1 - \frac{TCI \times i}{AP}\right)}{ln\left(\frac{1}{1+i}\right)}$$ **Equation 5-44**

$$MOIC = \sum_{t=1}^{n} \frac{AP}{(1+i)^t} \Big/ TCI$$ **Equation 5-45**

TCI refers to *total capital investment. PEC shows the purchased equipment cost.* One piece of a correlation $\sum_{t=1}^{n} \frac{AP}{(1+IRR)^t}$ has been repeated in all of the equations. AP refers to annual profit, C_{heat} the cost per kWh of heat, t Operational hours in a year (for a heating system), and i means annual interest rate.

To calculate the summation of the mentioned series, the geometric progression summation for finite terms is used. AP assumed as (a) in the general form of geometric progression summation of the mentioned series: $S_n = a\left(\frac{1-r^n}{1-r}\right)$, and $\frac{1}{1+i}$ or $\frac{1}{1+IRR}$ is as (r).

Only a portion of the *total capital investment* (TCI) is included in the *purchased equipment cost (*PEC), meaning that additional expenses will be added, including labour costs, the cost of additional miscellaneous equipment, and costs associated with assembling the cycles and combining them with the heat source, etc. Using a constant multiplication factor is a popular technique for obtaining the TCI from the PEC. Numerous similar criteria have been proposed in the literature. The total expenditures listed will be regarded as 43 percent of the PEC,

according to Kolahi, et al. [135]. The results of the heat transfer and economic analysis have been addressed in the following section, results and discussion.

5.4 Results and discussion

A flexible two-stage heat pump has been studied based on techno-economic principles. The first step is to calculate the component's energy/power usage or production. Then, the heat transfer areas of the heat exchangers have been calculated based on heat transfer fundamentals. Then, based on cost functions, the capital costs of the components have been calculated, which leads to measuring the total cost of the system. In the end, the techno-economic parameters have been calculated to have a vision of the system's economic feasibility. Four functions in MATLAB have been created to calculate the results in each step. Table 5.9 shows the heat transfer design results of the evaporator and the condenser. The overall heat transfer coefficient, required length, and total heat transfer area have been shown in this Table. In the residential block, there are 40 flats, and there will be 1 heat pump per flat. However, the heat transfer area and length shown in the Table below are for per flat. Evaporator and condenser heat transfer rates are included in Table 5.9 as well, which resulted from the thermodynamic analysis phase.

Table 5.9 Heat exchanger design result for flexible two-stage heat pump (sizing per heat pump- 40 heat pump in total).

Parameter	Description	Value
$\dot{Q}_{evap}$ total	Evaporator maximum heat transfer rate of the whole block(kW)	76.98
U_{evap}	Evaporator overall heat transfer coefficient (W m^{-2} K^{-1})	1,011.8
L_{evap} per each	Length of the designed Al-Extruded micro-channel Evaporator (cm)	27.06
A_{evap} per each	Heat transfer area of the designed Al-Extruded micro-channel Evaporator (m^2)	1.88
$\dot{Q}_{cond}$ total	Condenser maximum heat transfer rate (kW)	106.28
U_{cond}	Condenser overall heat transfer coefficient of the whole block (W m^{-2} K^{-1})	1,790.7
L_{cond} per each	Length of the designed Al-Extruded micro-channel condenser (cm)	6.5
A_{cond} per each	Heat transfer area of the designed Al-Extruded micro-channel condenser (m^2)	0.80

Figures 5.7 and 5.8 represent the temperature profile of the evaporator and condenser, respectively. The figures have been created within the discretization method. As mentioned before, the properties of the hot and cold fluids, including temperature, should be calculated in each section of the heat exchangers. Therefore, the temperature of all sections in both heat

exchangers is added to create the temperature profiles. In the evaporator shown in Fig. 5.7, the heat is transferred from the air (heat source) to the working fluid, assuming no heat loss in the cycle, therefore the temperature of the hot stream is decreased while the temperature of the cold stream is fixed, as it's going through the two-phase temperature constant evaporating process. On the contrary, in a condenser, the roles of the working fluid and the room air are exchanged, as shown in Fig. 5.8. The working fluid is hot stream, losing energy due to condensing two-phase temperature-constant process, while the temperature of cold stream is increasing as the flows moving through the fluid channels. Also, the pinch point happened at one end of the heat exchangers.

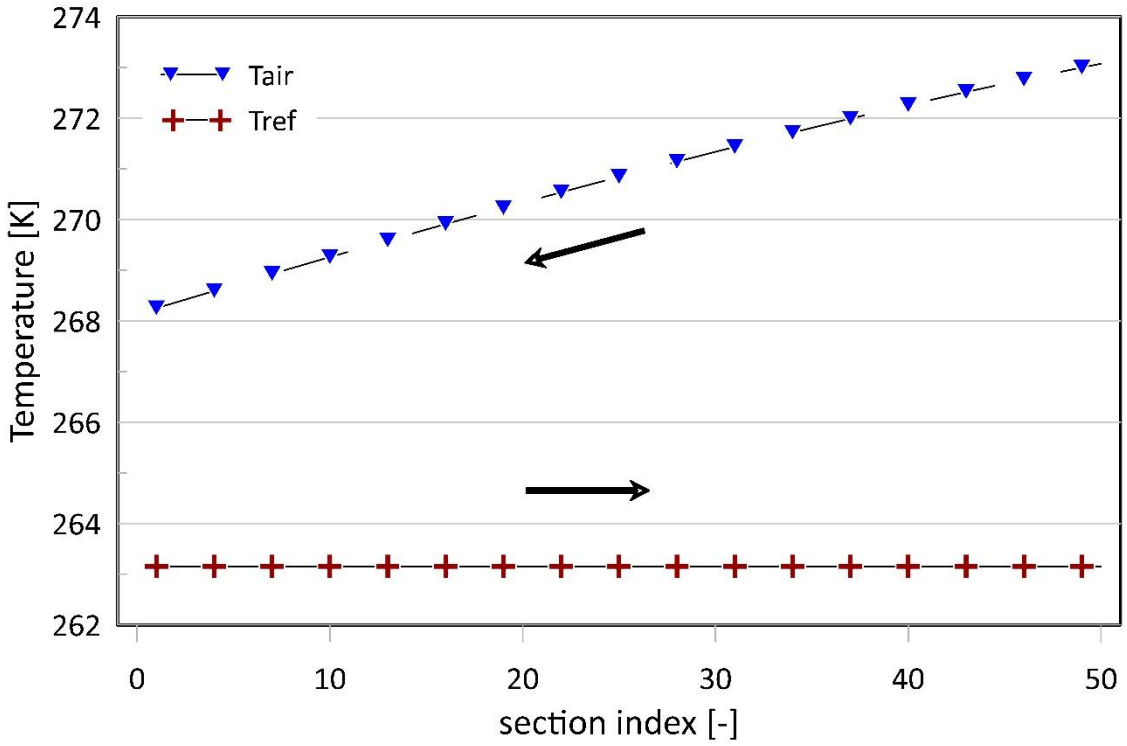

Figure 5.7 Temperature profile of the evaporator in the flexible two-stage system

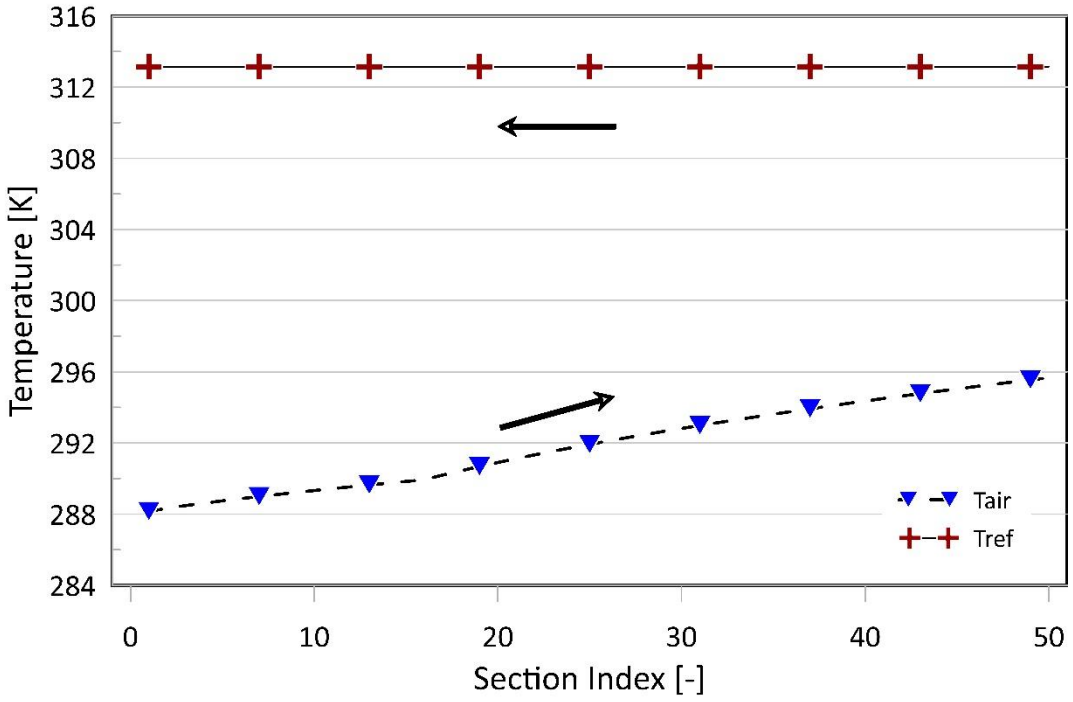

Figure 5.8 Temperature profile of the condenser in the flexible two-stage system

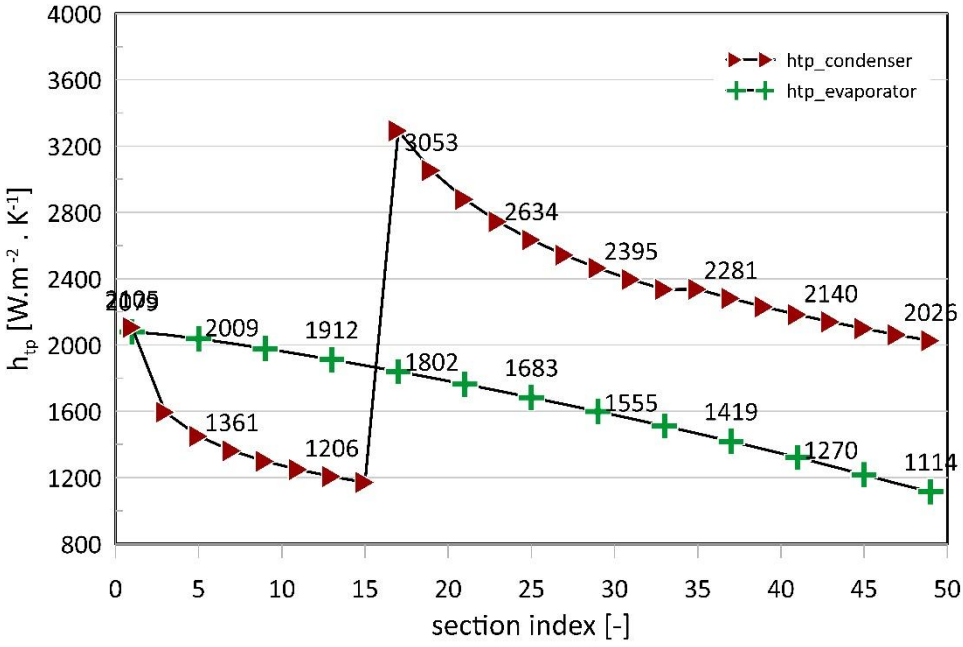

Figure 5.9 two-phase convective heat transfer coefficient of boiling (evaporator) and condensing (condenser) through the length of the evaporator and condenser, respectively.

Convective two-phase heat transfer rate of boiling and condensing for the working fluid passing through the evaporator and the condenser are shown in Fig. 5.9. The boiling heat transfer coefficient declines gradually from effective nucleate boiling at the inlet to convective boiling vapour-dominated flow close to the outlet, where dry-out and decreased liquid film decrease the heat transfer coefficient. The condenser, on the other hand, exhibits an initial plummeting, a sharp peak, and then a slow decline. When vapour condenses, the liquid content increases, decreasing heat transfer and turbulence. This causes the initial

reduction. The rise signifies a shift in the flow regime that momentarily improves the heat transfer coefficient. It's noteworthy that the condensing heat transfer coefficient is higher than the boiling one at the outlet. In contrast to boiling at the exit, which suffers from vapour dominance and loss of liquid film on the pipe inner wall, condensation preserves a thin liquid film on the surface, allowing for more efficient heat transfer. However, both boiling and condensing heat transfer coefficients are decreasing while the flow is moving through the pipe. As condensation proceeds and the liquid fraction increases, the flow becomes more annular and less turbulence, reducing heat transfer. In the evaporator, the reason for reduction toward the exit of the pipe is that as more vapour forms and the liquid film thins, dry-out or film boiling may occur, which reduces heat transfer. Less turbulence and more vapour dominance decrease the boiling heat transfer coefficient through the micro-pipe of the evaporator.

Fig. 5.10 shows the convection heat transfer coefficient of boiling in the evaporator, which in turn contains the convective and nucleate boiling coefficients. As seen from Eq. 5-3, the total boiling heat transfer behaviour and trend during the micro-pipe length depend on the behaviour and trend of the convective or nucleate boiling heat transfer coefficient. It could be decreasing or increasing due to the variation of convective or nucleate boiling heat transfer coefficient. Based on Ref. [115], it depends on the mass flux. At lower mass fluxes, the convective boiling coefficient reduces as the fluid inside the pipe becomes saturated vapour, because the fluid molecules do not obtain enough energy during their movement. While at higher mass fluxes, the molecules absorb more energy to move during their movement which leads to an increase in the convective boiling coefficient in the pipe. This case is the first case (lower mass flux) where the convective boiling factor is getting lower as the quality of the fluid increases.

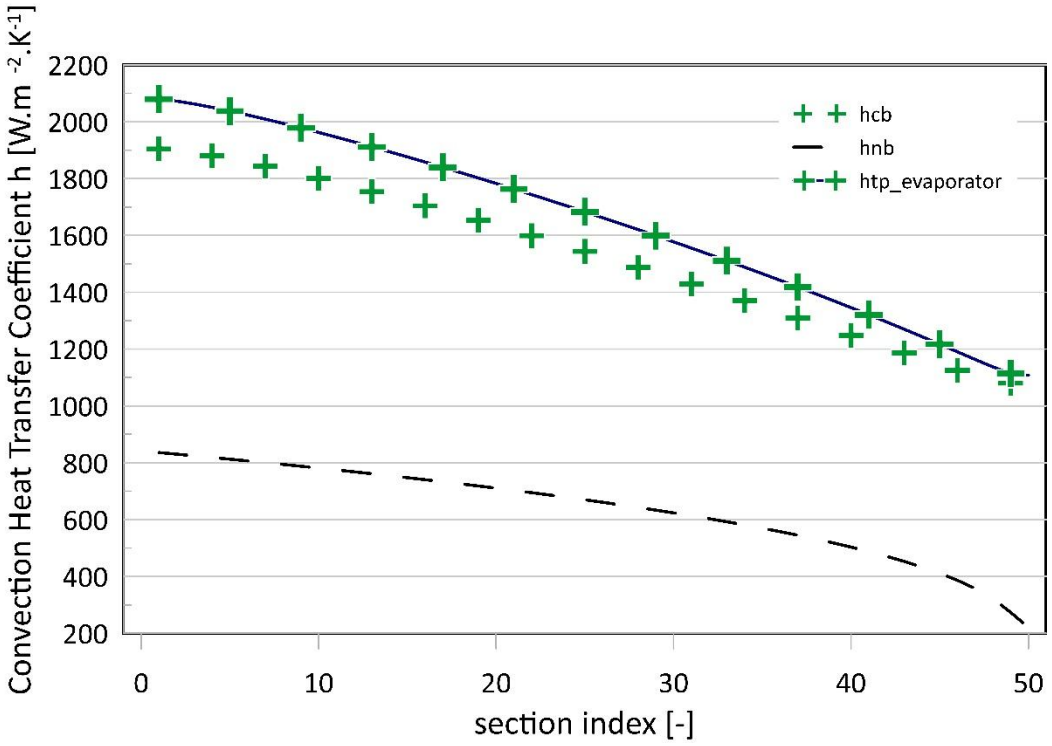

Figure 5.10 convective boiling, nucleate boiling and two-phase convection heat transfer coefficients of the evaporator.

Fig. 5.11 compares the capital cost of the components in the heating system studied. Table 5.10 summarises the costs in Fig. 5.11 and their percentages of the total cost. They both illustrate that the evaporator and condenser are the most expensive components of the system, followed by the PCM storage tank and the Compressor II. As the evaporator of this system is bigger than the condenser, its price is higher compared to the condenser. Because the heat transfer area and the price of the heat exchangers are related based on Eq. 5-30 and Eq. 5-31 from Table 5.6. Also, the PCM storage tank, considering every detail of the storage tank construction and PCM cost and storage cost, shows the third most expensive component of the cycle. The rest of the costs are 1% or less, compared to the total initial investment of the components.

Table 5.10 capital cost of the components for flexible two-stage heat pump.

components	Cost 2016	Cost 2024	Percentage ratio compared to the total
Compressor I	247.82	498.63	0%
Compressor II	642.21	1292.19	1%
Evaporator	39117.76	78708.48	48%
Condenser	16855.01	33913.8	21%
Expansion valve I	72.67	146.21	0%
Expansion valve II	91.45	184	0%
Flash chamber	447.79	900.99	1%
PCM storage tank	13784.97	27736.61	17%
Total updated to 2024	247.82	498.63	0%

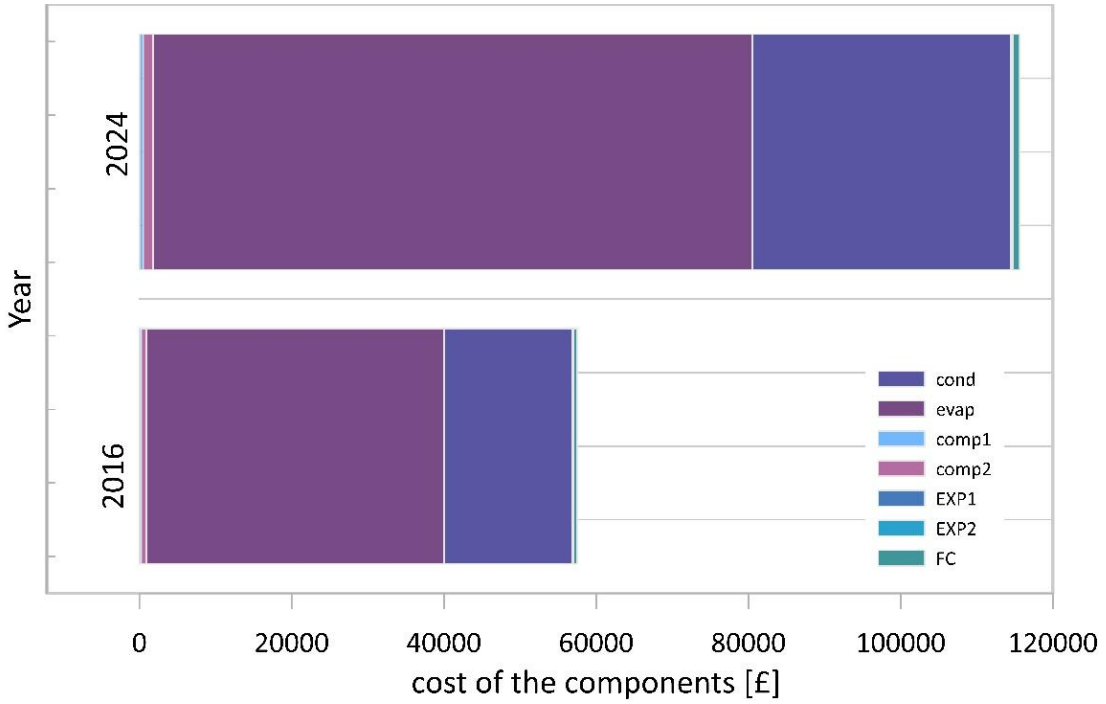

Figure 5.11 capital cost of the components in the flexible two-stage heat pump.

Finally, to show the feasibility of this system, the techno-economic parameters have been calculated using Eq. 5-39-5-45. The summarised results in Table 5.11 reveal that the techno-economic parameters are within a reasonable range. The table presents a techno-economic comparison between a flexible two-stage heating heat pump system and a single-stage heating system. It outlines several key financial performance parameters for each system, including annual profit, total capital investment, net present value, multiple on invested capital, internal rate of return, and payback period. These metrics are commonly used in economic evaluations to assess the feasibility and profitability of engineering investments, particularly in energy-related projects.

Annual profit (AP) represents the net income generated from operating each system per year. The single-stage system demonstrates a slightly higher annual profit of £26,298 compared to £26,122 for the two-stage system. This suggests that, from an operational standpoint, the single-stage system performs marginally better in terms of yearly financial returns. However, this difference is relatively small and might not be significant when viewed over a longer investment horizon.

Total capital investment (TCI) indicates the upfront cost required to implement each system. The two-stage system demands a slightly larger investment of £163,880, while the single-stage system requires £160,220. This cost difference, though modest, could influence the choice of system, especially for investors or projects constrained by initial budgets. Despite

the higher investment, the two-stage system still performs competitively across several indicators.

When evaluating long-term profitability, the net present value (NPV) becomes a critical parameter. It reflects the value of future profits discounted to their present value. The single-stage system yields a higher NPV of £183,900, compared to £177,930 for the two-stage alternative. This suggests that, over time, the single-stage system is expected to deliver more economic value. A similar conclusion can be drawn from the multiple on invested capital (MOIC), where the single-stage system again slightly outperforms with a value of 2.14, meaning it returns more than double the initial investment, compared to 2.08 for the two-stage system.

The internal rate of return (IRR), another key profitability indicator, is also higher for the single-stage system at 17.61%, compared to 16.8% for the two-stage option. This metric represents the rate at which the investment breaks even in net present value terms, with a higher percentage indicating a more favorable return. Additionally, the payback period (PP), or the number of years required to recover the initial investment, is slightly shorter for the single-stage system at 7.4 years, while the two-stage system takes 7.7 years.

In summary, the single-stage heating system demonstrates slightly better performance across all economic indicators. It offers higher annual profits, requires a lower capital investment, and promises better long-term financial returns with a quicker payback period. However, the differences between the two systems are relatively small. Therefore, while the single-stage system may appear more economically attractive, the final decision should also consider other non-economic factors such as energy efficiency, system flexibility, maintenance requirements, and environmental impact, which are not captured in Table 5.11.

Therefore, a single stage shows delicately better techno-economic results, however not too different than those of two-stage. Depends on the objectives of a project and the costumer type, the decision could be different. If we are dealing with a mass-production, the difference between single and two-stage would not too much, but for a private costumer, the initial costs could be beneficial in single-stage case.

Table 5.11 Techno-Economic results of the flexible two-stage heat pump in heating

Parameter	Value	unit
Two-stage		
Annual profit (AP)	26,122	£
Total Capital Investment (TCI)	163,880	£
Net Present Value (NPV)	177,930	£
MOIC	2.08	-
Interest Rate of Return (IRR)	16.8%	-
Period Payback (PP)	7.7	year
Single-stage		
Annual profit (AP)	26,298	£
Total Capital Investment (TCI)	160,220	£
Net Present Value (NPV)	183,900	£
MOIC	2.14	-
Interest Rate of Return (IRR)	17.61%	-
Period Payback (PP)	7.4	year

5.5 summary of the chapter

The two-stage flexible heat pump is studied via techno-economic concept in this chapter. To perform an economic analysis, the heat transfer areas of the heat exchangers are necessary. To design the evaporator and condenser, the type of heat exchanger is assumed as an Al-Extruded Tube micro-channel heat exchanger. Due to compactness of these heat exchangers, they're getting more attention in HVAC systems. One of the issues with heat pumps is their bulkiness, therefore it's not easy to retrofit and substitute with a gas-boiler. Therefore, having Al-extruded tube micro-channel heat exchanger will help the compactness of a heat pump and will solve the retrofitting issues. Using the two-phase correlations to calculate the convection heat transfer coefficient, the heat transfer areas and the length of evaporator and condenser have been calculated. The results of HEX design showed that the condenser and evaporator are quite compact, and the length is only 7 and 27 cm, respectively. Also, economic parameters have been calculated. The initial investment will be gained back to the investor in 7-8 years, the investment is safe, as the IRR is more than 17%, which is higher than interest rate of the UK. However, single-stage shows better results compared to the two-stage, but thermodynamic results were the other side as well, which needs to be considered. Flexible Two-stage system got higher SCOPs compared to the single-stage cycles. For the future works a multi-objective optimization would be helpful to decide in between different objectives for a heating/cooling system.

.

Chapter 6 Conclusions

As the heating and cooling industry moves towards low-emission technology, heat pumps are becoming more popular as a substitute for fossil fuel systems. However, their portion of the market for heating and cooling, as a whole, is still rather small. Although air-source heat pumps are a viable alternative for gas-boilers of individual homes in the UK, their operation is fraught with difficulties. These systems should be able to handle significant temperature increases during peak winter demand while still offering flexibility and cost saving. Energy usage rises and efficiency is frequently decreased under such circumstances, reducing competitiveness and compromising dependability, compared to gas boilers. In light of this, the main research issue is: how can air-source heat pumps be improved to overcome these obstacles at a reasonable cost? A flexible two-stage, multi-valve air-source heat pump with thermal storage is introduced in the thesis to investigate this, for both heating and cooling applications. This study lays the groundwork for upcoming improvements and the creation of optimised designs. In comparison to traditional single- and two-stage heat pump systems, the main goal was to investigate if the addition of flexibility and thermal storage may increase energy efficiency, allow peak shaving, and improve economic performance. Across both heating and cooling case studies, the results consistently highlighted the benefits of flexibility when combined with advanced control strategies and real-world load profiles. The flexible two-stage configuration performed better compared to both baseline systems and the second alternative flexible configuration, demonstrating that the integration of PCM thermal storage can provide measurable achievements in terms of performance, peak shaving, and cost savings.

In both heating and cooling studies, adopting rule-based control techniques proved crucial for managing PCM charging and discharging cycles. In order to utilise the stored energy and prevent compressor running during peak hours, the systems included load-dependent triggers and state-of-charge (SOC) monitoring. In addition to decreasing the strain on the electrical grid, this demand-side flexibility demonstrated how smart control strategies may help thermal storage systems reach their full potential. The quantitative findings will be explained in more detail in the paragraphs that follow.

For the heating study, work consumption of the flexible two-stage system is lower than that of the baseline two-stage heat pump. Consequently, it has more SCOP and a lower electricity usage price compared to the baseline system. For a residential block in Glasgow under

variable loads, the two-stage baseline heat pump achieved SCOP of 4.4654, with annual electricity usage of 30,314 kW, and a running annual price of £9,668, while the proposed flexible two-stage (config. 1) improved these to a SCOP of 4.5403 (+1.67%), reduced electricity consumption to 29,784 kW (−1.74%), and lowered the annual running cost to £9,505 (−1.68%). In the same conditions, the single-stage baseline system reached SCOP 4.0787, electricity consumption 33,189 kW, and annual cost £10,585, while the flexible single-stage improved to SCOP 4.1108 (+0.78%), electricity usage 32,896 kW (−0.88%), and annual price £10,500 (−0.88%). Under a sinusoidal load profile for Glasgow, the flexible two-stage system further improved SCOP from 4.5276 (baseline) to 4.7679 (+5.31%), with electricity consumption reduced from 29,487 to 28,547 kW (≈−3.2%) and annual running cost from £8,369 to £8,195 (≈−2.1%). The flexible single-stage in the same sinusoidal case achieved SCOP 4.3333 compared to 4.1376 for the baseline (+4.73%), with consumption falling from 32,267 to 31,410 kW (−2.65%) and cost from £9,159 to £9,018 (−1.54%). For warmer weather condition, in Birmingham with real variable loads, the flexible two-stage achieved a SCOP of 4.7278 compared to 4.5835 of baseline (+3.15%), with consumption falling from 22,734 to 22,396 kW (−338 kW) and annual price from £7,241 to £7,112 (−£129). The single-stage systems showed a smaller improvement, from SCOP 4.1900 to 4.2890, electricity consumption 24,866 to 24,687 kW, and cost £7,920 to £7,841, compared to a baseline single-stage heat pump. At compressor level, in Glasgow the flexible system reduced Compressor I work from 20,302 to 16,606 kW, while Compressor II work rose from 10,012 to 12,826 kW, resulting in a net reduction. Overall, the heating results highlight that the flexible two-stage system achieved up to 5.31% higher SCOP, almost 3.2% lower electricity use, and nearly 2.1% lower annual cost, with the largest benefit observed under sinusoidal load conditions. The proposed configuration (config. 1) got better results compared to those of the second configuration (config. 2), which has PCM as the sub-cooler. The PCM tank in the second configuration does not provide the loads and has the role of a superheater, rather than a complete evaporator, providing the loads. It has less SCOP, more work consumption, and a higher price compared to config. 1. Config. 1 shows a 3.2% higher SCOP compared to the SCOP of the config. 2 for a two-stage system working in Glaswegian weather.

While the absolute cost savings were modest (a maximum of 2.1% with sinusoidal loads), the thermodynamic improvements and demand-shaping capabilities represent a meaningful contribution to the decarbonization of heating in residential buildings. The integration of PCM allowed the system to operate in four distinct modes, normal, charging, discharging, and standby, depending on heating load, time of day, and storage status. This operational

flexibility enabled partial shifting of heating demand to off-peak periods and reduced reliance on auxiliary systems during cooler conditions in the heating systems.

In addition, in this study, the novel two-stage heat pump has been studied for cooling. Based on thermodynamics aspects, SOC, electricity usage, and the annual price have been calculated and compared with the results of the baseline system. The following results are the highlights of the research.

For the cooling study, similar trends were observed, though the magnitude depended on climate and trigger selection. In Rome (trigger 10 kW), the two-stage baseline system achieved SCOP 4.1517, electricity usage of 23,112 kW, and annual cost £7,501, while the flexible two-stage increased to SCOP of 4.2483 (+2.33%), reduced annual electricity usage to 22,989 kW (-123 kW), and annual price to £7,458 (−£43). The single-stage baseline achieved SCOP 3.7661, annual electricity usage 25,479 kW, and annual price £8,269, whereas the flexible single-stage reached 3.8622 (+2.55%), 25,277 kW (−202 kW), and £8,204 (−£65) for SCOP, annual electricity usage and annual running price, respectively. In London, the improvements were stronger due to milder weather and different triggers. At a 7-kW trigger, the flexible two-stage outperformed its baseline with SCOP 5.8183 vs 4.7967 (+21.3% improvement), electricity consumption 3,303 kW vs 3,388 kW (−85 kW), and annual running cost £1,118 vs £1,154 (−£36), compared to its baseline system. Under the same trigger, the flexible single-stage achieved SCOP 5.9095 vs 4.4055 baseline (+34.14% improvement), reducing consumption from 3,689 to 3,063 kW (decreased −626 kW, −16.97%) and annual running cost from £1,257 to £1,041 (decreased −£216, −17.18%). With a lower 3 kW trigger in London, SCOP still improved substantially: for a two-stage: increasing from 4.7967 to 5.8035, showing +20.99% improvement ; while for single-stage SCOP improved from 4.4055 to 5.7809, representing +31.22% improvement, but in the two-stage case, electricity use slightly increased compared to baseline system from 3,388 to 3,405 kW; and annual cost from £1,154 to £1,165, respectively, whereas the single-stage still showed clear savings in electricity usage from 3,689 to 3,224 kW, and −465 kW changing; and annual price cut from £1,257 to £1,091, −£166 changing. More load sacrificing (higher trigger) to start charging will lead to higher SCOP, lower price, and lower work consumption. However, sacrificing more in a two-stage system results in less favourable results in price and electricity usage. However, the aim was not to endanger the comfort of the residents, but to provide flexibility. Therefore, a reasonable amount for trigger has been considered for milder weather conditions in London.

Compared to the second flexible configuration (config. 2) where the PCM acted as a sub-cooler), the newly proposed configuration (config. 1) proved more effective in balancing cooling demand, reducing peak loads, and enhancing overall system efficiency. The configuration comparison demonstrated that the newly proposed flexible two-stage system (config. 1) outperformed the conventional flexible two-stage design (config. 2) across cities: in London with a 7-kW trigger, config. 1 achieved SCOP 5.8183, annual running price £1,118- and 3,303 kW electricity use, compared with config. 2's SCOP 4.0938, annual running price £1,281, and electricity usage 3,853 kW. In Rome, config. 1 reached SCOP 4.2483, annual running cost £7,458, and electricity usage 22,989 kW, versus config. 2's SCOP 4.0670, annual cost £7,571, and electricity usage 23,409 kW. Overall, in cooling, the flexible systems provided SCOP gains of 2.33–2.55% in hot climates and 21–34% in milder climates, with cost reductions up to 17.18% and electricity savings up to 16.97%, however trigger settings strongly influenced the balance between SCOP improvement and economic savings.

As the second and third phases of this work, the flexible two-stage heat pump for a residential building of 40 flats has been investigated in this work via heat transfer and techno-economic aspects. Heat exchangers, evaporator and condenser, have been designed as two-phase micro-channel Al-Extruded tube heat exchangers. Then, via techno-economic correlations, a techno-economic analysis has been performed. Therefore, the analysis has been performed in three phases: 1- thermodynamic, 2- heat transfer, and 3- techno-economic aspects. At this phase, the objective of research is to find out the economic feasibility using the economic parameters.

Micro-channel Heat exchangers have been designed and are quite compact. The condenser, which is the interior heat exchanger per heat pump, is around 6.5 cm. The evaporator, which has been designed for a worst-case scenario of 0 outside temperature, is only 27 cm in length. The economic parameters show reasonable values: 2.14 times of the total capital cost will come back to the investor in 15 years.

The investment is safe, as it will stop being profitable at an interest rate of 17.61%, which is higher than the inflation rate of Great Britain. The flexible two-stage shows £3,440 less Total Capital Investment (TCI), 3.89% better PP, and 2.88% better MOIC, compared to the baseline two-stage heat pump.

The findings of this thesis contribute to the growing body of literature advocating for heat pumps as a cornerstone technology in the global transition to net-zero energy buildings. While air-source heat pumps are already recognized as efficient alternatives to fossil-fuel boilers, their performance can be constrained by seasonal temperature variations and peak load demands. By embedding flexibility through PCM storage and advanced control, this work demonstrates that such systems can be made more resilient, more efficient, and better aligned with the dynamics of electricity markets.

Nevertheless, several challenges remain. First, while SCOP improvements are clear, the economic benefits are highly sensitive to electricity tariff structures, PCM costs, and system complexity. In many scenarios, modest reductions in annual energy costs may not be sufficient to offset higher capital investments without supportive policies or incentives. Second, the reliance on simplified assumptions in simulation models (e.g., isothermal heat exchangers, constant thermophysical properties) introduces uncertainties that must be addressed through experimental validation. Third, user comfort and real-world integration with smart grids and dynamic pricing schemes require further exploration before widespread deployment.

In conclusion, the novel flexible two-stage heat pump proposed and analyzed in this thesis demonstrates tangible improvements in both heating and cooling applications, offering a pathway toward higher energy efficiency and demand flexibility in the built environment. While challenges remain in terms of cost-effectiveness and large-scale adoption, the results confirm that flexible thermal systems have strong potential to play a pivotal role in reducing greenhouse gas emissions, alleviating grid stress, and advancing the vision of net-zero energy buildings. In the final chapter, the possible future work will be suggested.

Chapter 7 Future Outlook

Connecting flexible heat pumps to phase change material (PCM) tanks may improve energy efficiency and lessen reliance on the grid during times of high demand. These systems enable load shifting by storing thermal energy for use when electricity is more economical or greener, which is especially helpful in the shift to smart, grid-responsive buildings. In colder climates, conventional air-source heat pumps struggle to function effectively; however, PCM storage enhances their effectiveness and lessens the requirement for backup heating.

Based on the experience gained during this research, it turns out that the particulars of each project greatly influence whether the *right* or *wrong* option is chosen. Case-by-case assessments work better than generalised methods, which frequently fail. There are different studies and claims in different research papers, which require double-check to use in real world, which shows the sensitivity of the results to simulation details and assumptions.

Building on this thesis's contributions, future studies ought to focus on:

- Further testing of flexible heat pumps in real-world settings, including ongoing observation of seasonal performance and occupant comfort, is part of the experimental validation process.

- Going beyond the rule-based tactics employed here and performing simulation based on machine learning and model predictive control (MPC).

- Evaluating if it is feasible to use these systems in district heating and cooling networks, where further grid-level advantages may be obtained via aggregated demand flexibility.

- Assessing modern PCMs and low-GWP refrigerants to make sure they comply with environmental requirements and sustainability goals.

- Another important aspect that could have been studied is to combine the concept of digital twins with flexible heat pumps. Given their potential significance for optimisation and real-time decision-making, this study investigates the coupling of

flexible systems with digital twins. Data, simulation, and real-time decision-making come together to form digital twins. They will probably be crucial in tackling the problems of resource management, urbanisation, and climate change, guiding society towards futures that are not merely decarbonised but also wisely managed. As a result, integrating them with heat pump systems will yield further advantages.

Digital twins are expected to transform several key sectors. In Building sector, digital twin techniques may optimise energy consumption, spot inefficiencies (such heating and cooling at the same time), and gradually enhance building performance. Smarter and more flexible buildings are already being made possible by platforms like Microsoft Azure, Honeywell Forge, and Johnson's OpenBlue. In Cities planning, by combining transportation, utility, environmental, and demographic data, urban digital twins assist planners in addressing issues like pollution, traffic, and the resilience of infrastructure. These techniques are already being tested in cities including New York, Helsinki, Singapore, etc. The Virtual Singapore project, which uses billions of data points to recreate real-time urban activity, is a prime example.

Going forward, decarbonisation will affect more than just heating and cooling. It resides in the creation of intelligent, interconnected systems, especially with the ideas of *smart cities* and *smart buildings*. The digital twin, a real-time virtual representation of a physical system made with sensors and real-time data streams, is a crucial enabling technology. Predictive maintenance, system optimisation, and ongoing monitoring are made possible by digital twins. This suggested option would be highly recommended in UK in near future.

In summary, heating and cooling systems have a very bright future. However, substantial technological and regulatory changes will be needed to meet the Net Zero 2050 goal. The most feasible way to electrify heating and cooling systems is still with heat pumps. Traditional units' retrofitting potential has previously been hampered by their relatively large size, but this issue has since been lessened thanks to the creation of small size heat pump systems by a number of manufacturers, including Nesta, Kensa Shoebox, Sunamap, and NZTS.

Appendix A. IESVE Dynamic Simulation for load calculations

A brief explanation of the heating load calculation is provided below. Step-by-step screenshots have been taken and added, starting from geometry to the results. Fig. A.1 shows the first step of creating the project file in IESVE software by clicking on New Project/ Create from starter geometry/click on Midrise Apartment/Create Project. The geometry of different types of buildings has been created and archived in the software. Rather than starting from scratch, the provided geologies can be used. In this research, the mid-rise apartment is selected.

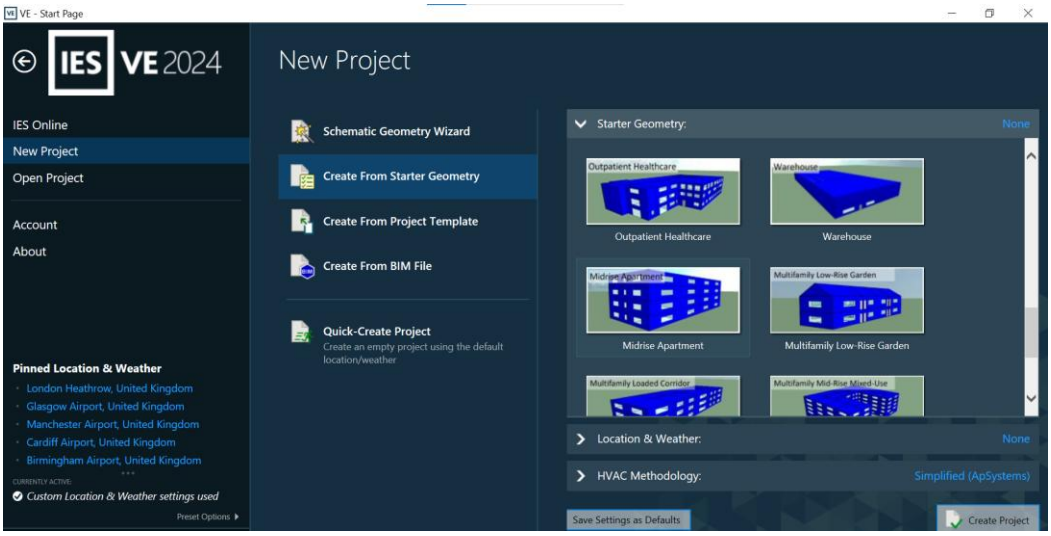

Figure A.1 Geometry selection in IESVE and creating project.

Clicking on the Model Viewer icon, highlighted in red in the figure below, will display a 3D model of the building. Fig. A.2 was extracted from this view of the residential block.

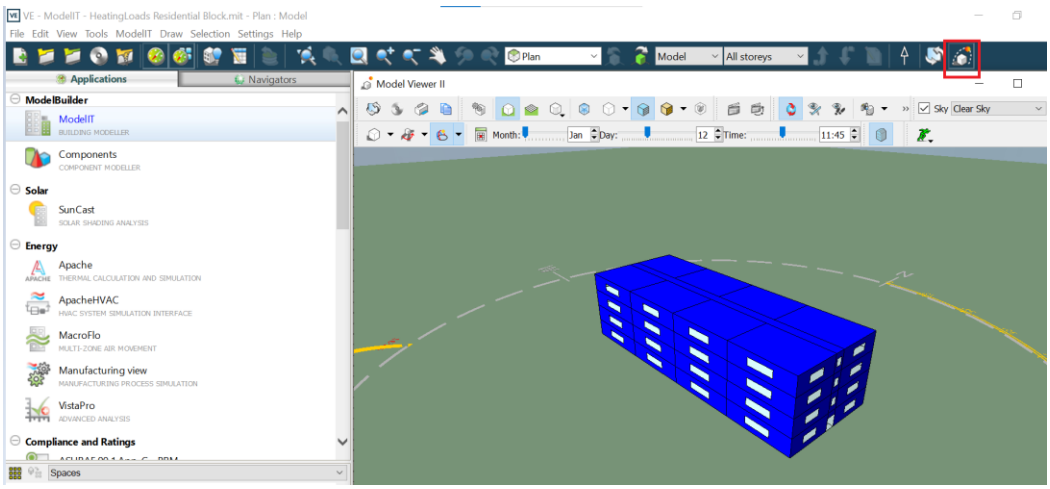

Figure A.2 3D model of the mid-rise apartment in IESVE- Model Viewer view.

The next step is to specify the location of the residential building where the weather data will be attained, as shown in Fig. A.3. By clicking on Tools/APlocate, a new window will be opened, which is shown in Fig. A.4.

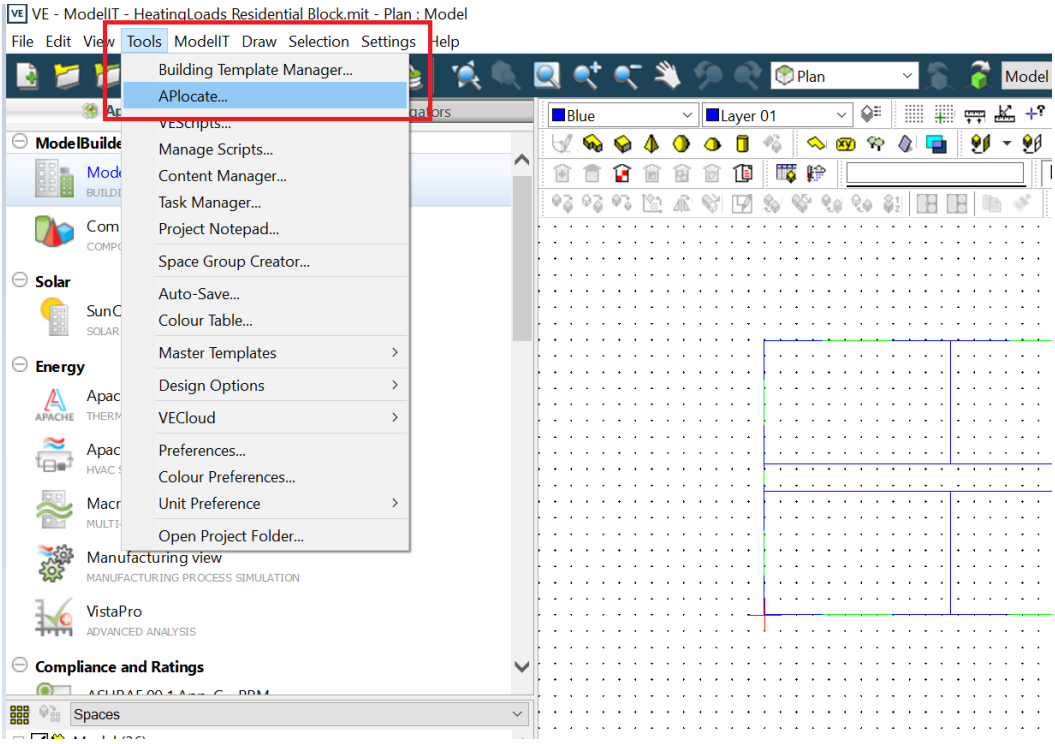

Figure A.3 APlocate section to specify the weather data.

By skipping the other tabs in Fig. A.4, clicking on the simulation weather data tab and then clicking on the select button, a drop-down list will be opened. Glasgow is selected from the drop-down list.

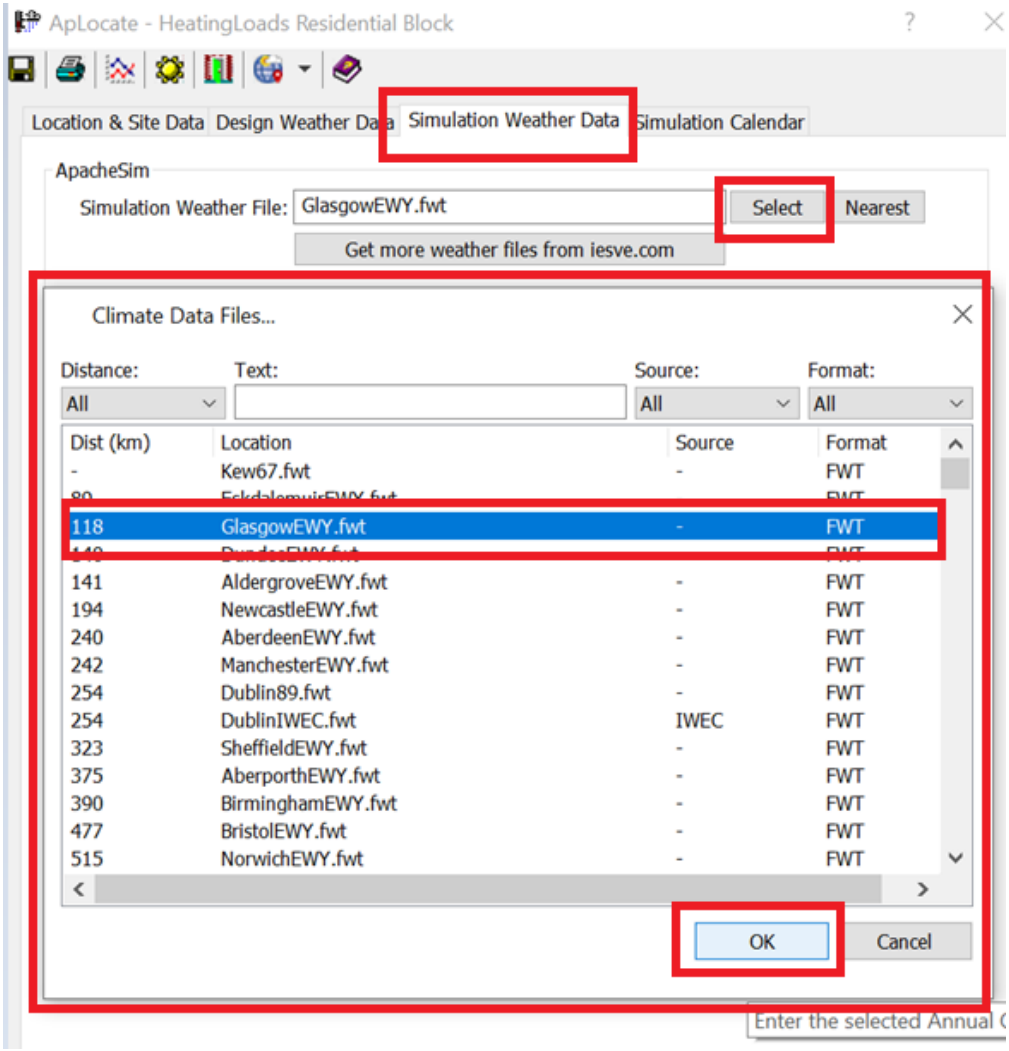

Figure A.4 Selecting the specified cities from the weather data list.

The next step is to specify the details of the building inside (set point temperature, air-exchange, equipment, etc). Click on Building template manager, encircled with red in Fig. A.5.

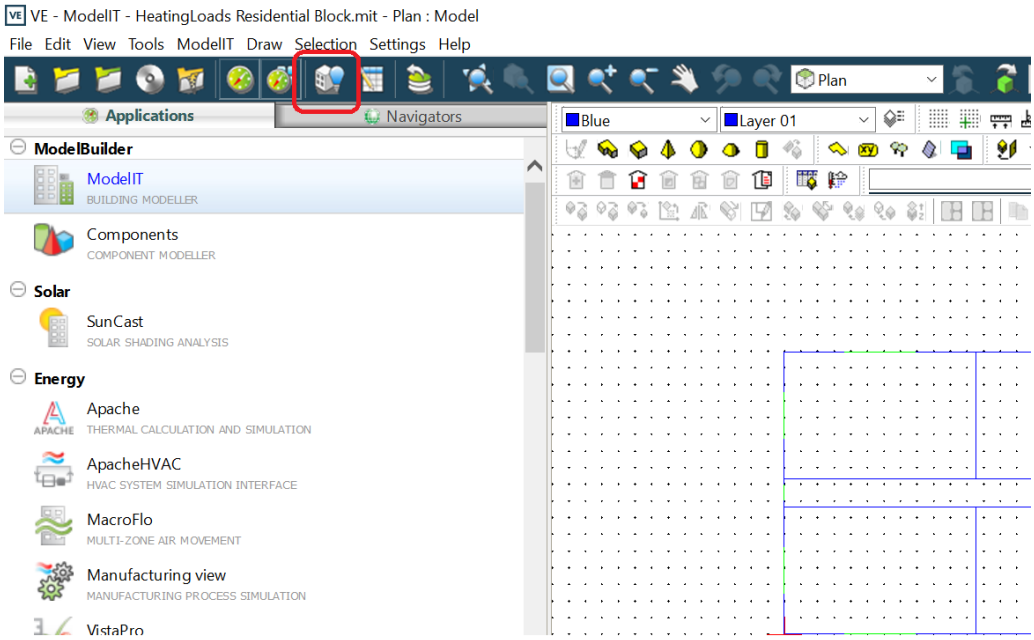

Figure A.5 Building template manager icon in IESVE software.

The following box will be opened, as shown in Fig. A.6. All the tabs shown in red in the following figure should be clicked on and changed one by one if needed.

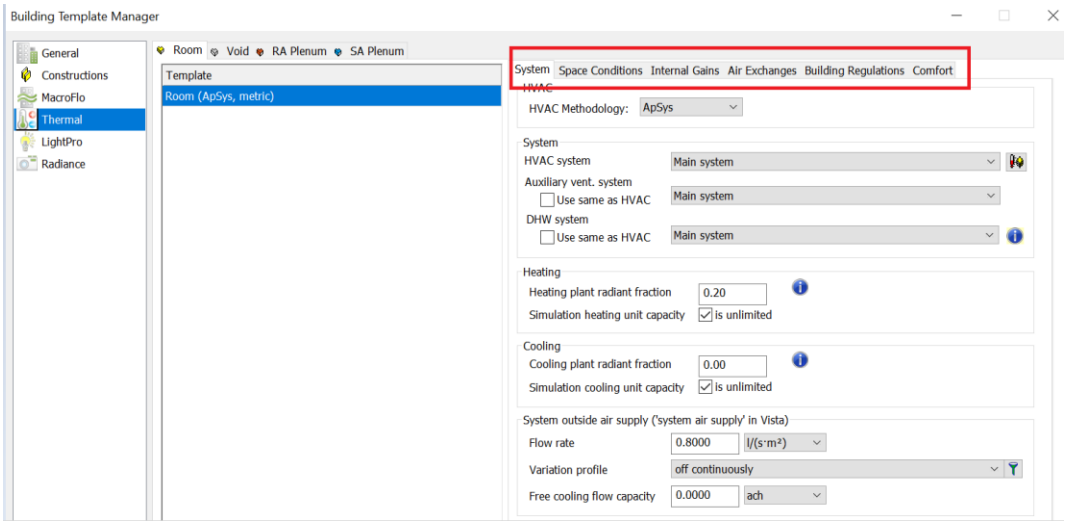

Figure A.6 Tabs in Building template manager window.

The space conditions tab will be set as shown in Fig. A.7. Only heating will be on continuously, and domestic hot water and cooling will be off. The heating loads will be manipulated later. Therefore, there is no need to create any heating load profile. The room set point has been assumed to be 19 ℃ (suitable for UK standards).

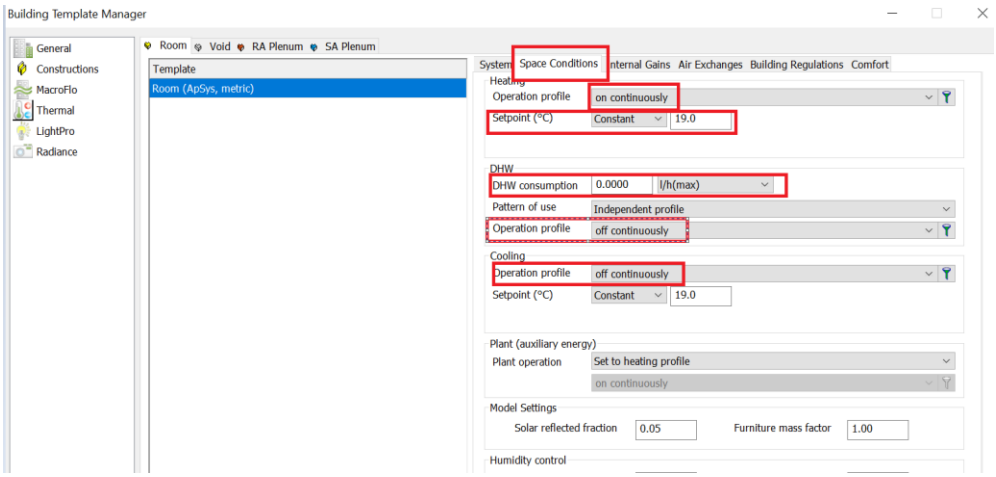

Figure A.7 Space conditions Tab in Building Template Manager Window in IESVE.

In the next Tab shown in Fig. A.8, internal gains, three components have been added: lighting, people, and refrigeration. All three options will be shown in the later figures.

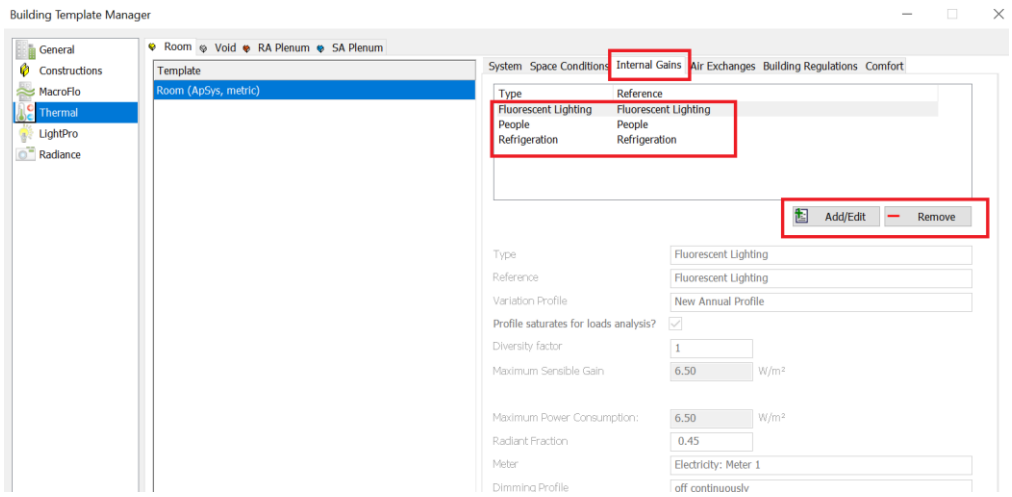

Figure A.8 Internal gains Tab in Building Template Manager of IESVE.

Lighting adjustment is shown in Fig. A.9. The energy gained by turning on the lights will be added to the calculations here. The numbers will be added based on the amounts written in Table 3.4. In any case, that's not mentioned as a parameter; it has been used as its default value.

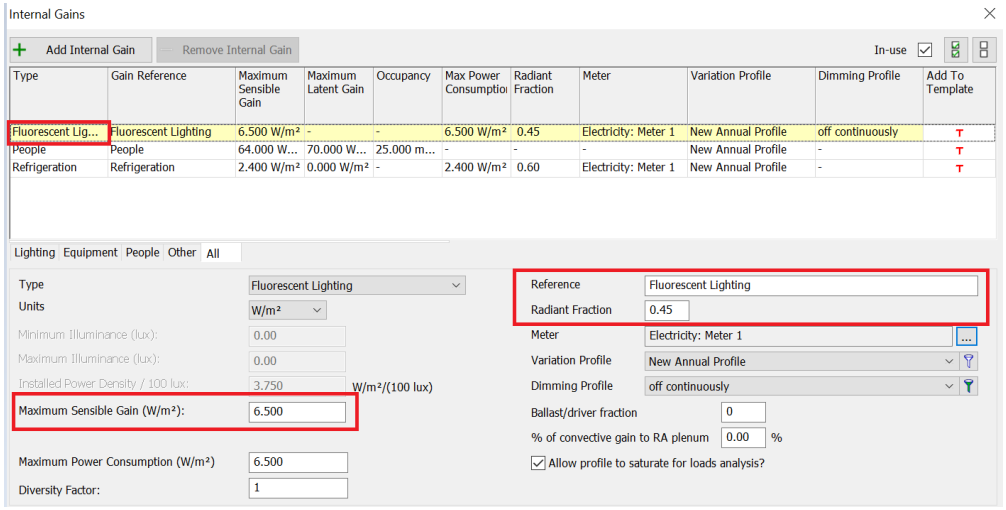

Figure A.9 Internal energy gains via lighting in IESVE.

Internal energy gain by residents is added in this step, shown in Fig. A.10. The number of the people is shown with a parameter named occupancy density with $m^2/person$ unit.

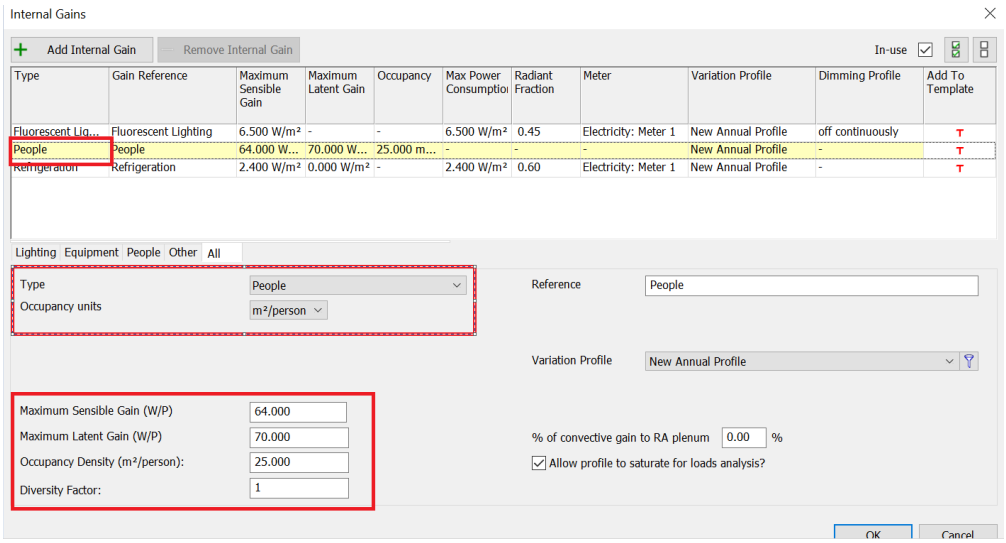

Figure A.10 Internal energy gains via residents in IESVE.

Energy gain via equipment is added, as shown in Fig. A.11. Only refrigeration has been considered here.

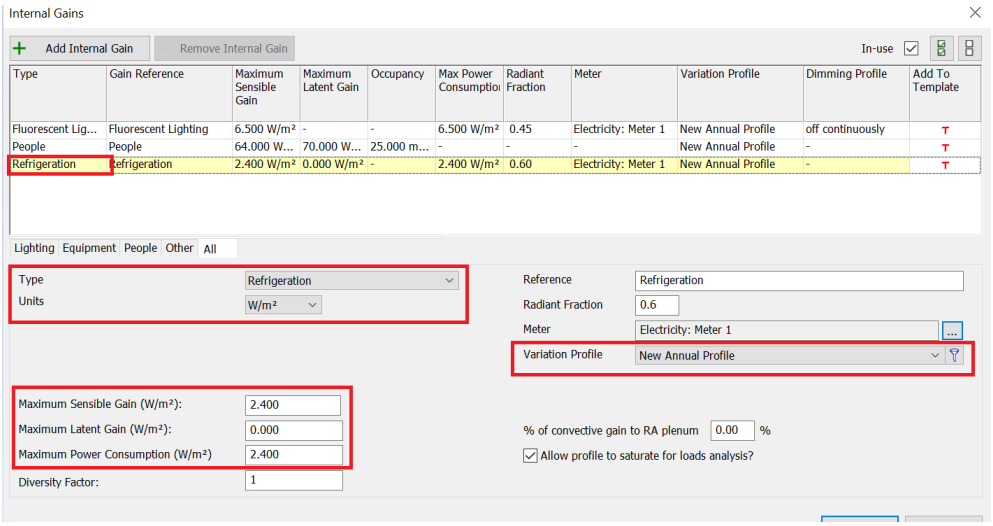

Figure A.11 Internal energy gains via refrigeration in IESVE.

The next Tab in the Building template manager window is the Air Exchange tab, as shown in Fig. A.12. Infiltration and natural ventilation have been adjusted using this window, and the energy loss/gain via air exchange with a unit of air per hour will be added to the calculation. Clicking on the options and then the Add/Edit button will open a new window, which is shown in Figs A.13 and A.14.

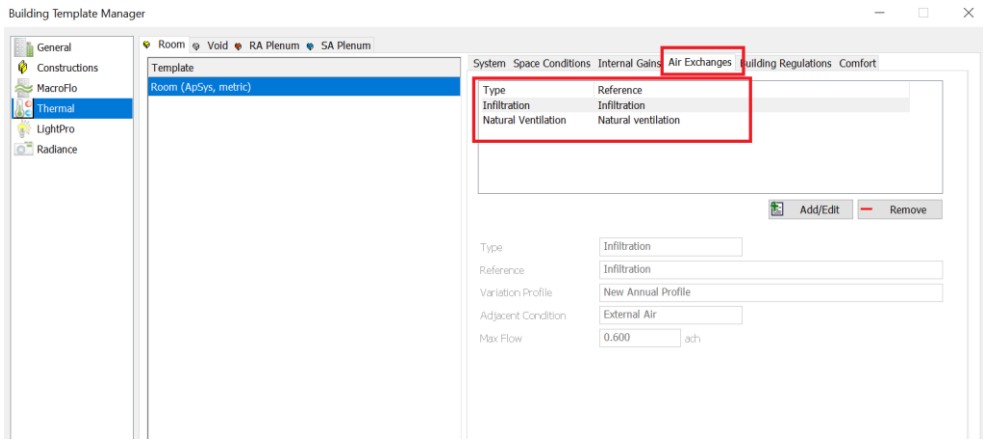

Figure A.12 Tab of Energy loss via Air-exchange in IESVE.

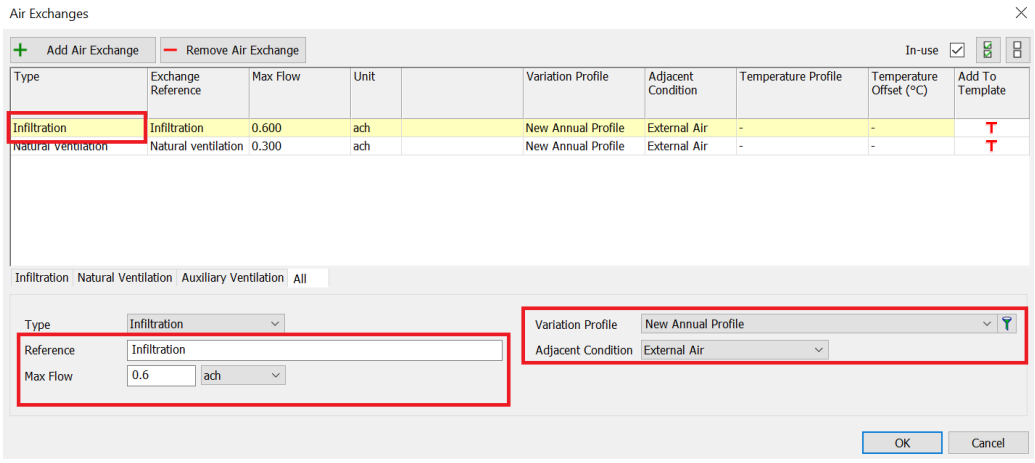

Figure A.13 Air Exchange/Infiltration energy loss in IESVE.

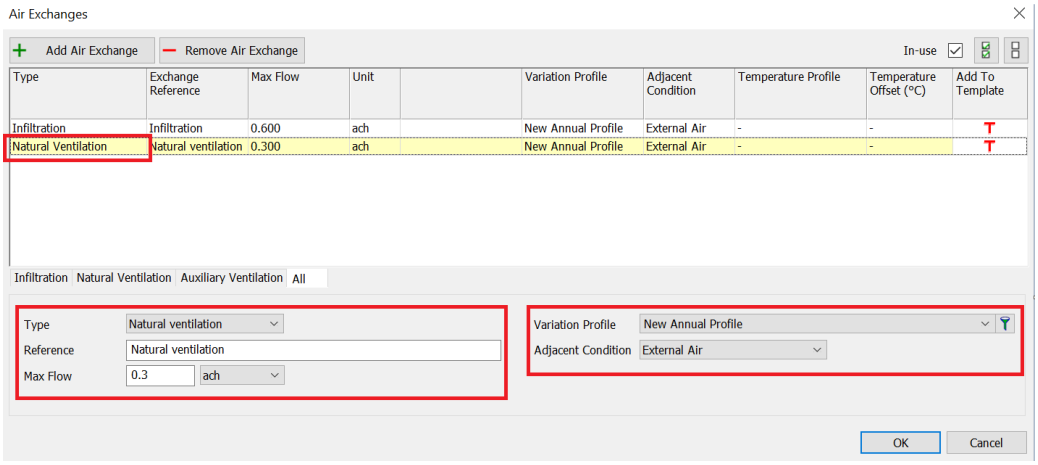

Figure A.14 Air Exchange/natural ventilation energy loss in IESVE.

The next step is to start the simulation. By clicking on Apache, as shown in Fig. A.15, a new box will be opened. The values can be adjusted as below and clicking on Simulate will start the simulation. The whole year has been considered here; however, the heating loads will be zero in a hot season and vice versa.

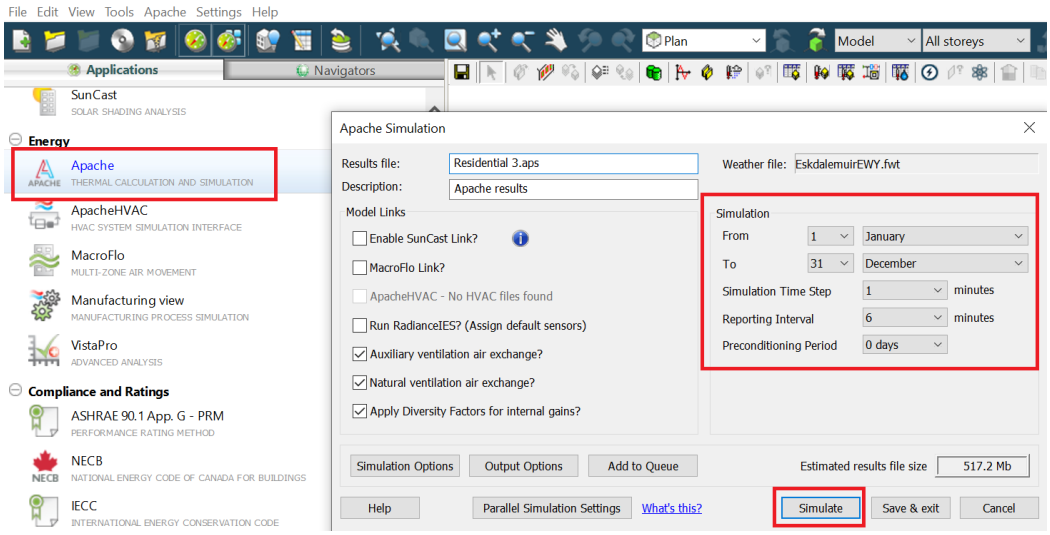

Figure A.15 Simulation starting using Apache IESVE.

The final step is extracting the results that are required for this study: date and time, ambient temperature and heating load. After clicking on VistaPro on the left-hand side, Boilers Load should be selected for the heating load, and Chillers Load for the cooling application. A new window will be opened, showing the selected parameter in a graphic figure. Fig. A.16 shows the result extraction process.

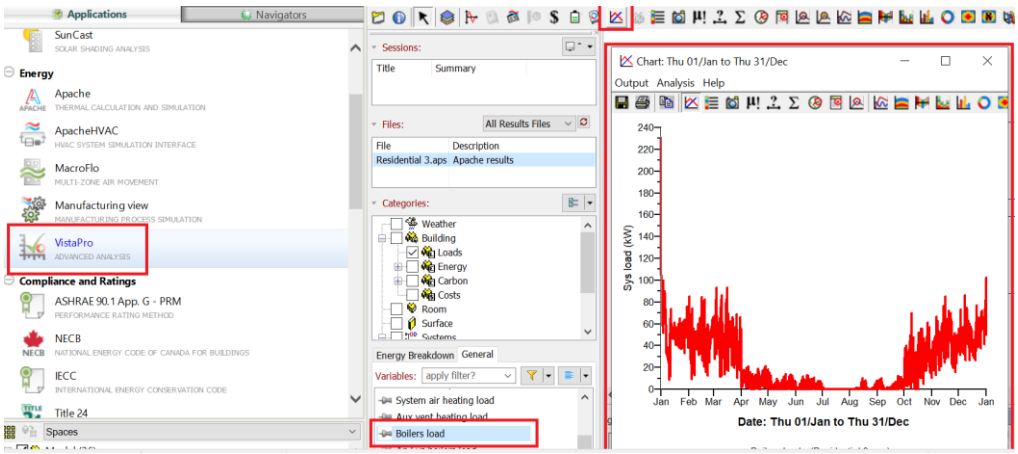

Figure A.16 Graphical representation via VistaPro option in IESVE.

To extract the results in a Table and import it to the MATLAB code, from the window opened to show the graphic result, click on Analysis, and from the list, select Table, as represented in Fig. A.17. The results will be saved in a table and can be saved in a text file. Later, it can be imported as an xlsx/CSV format file.

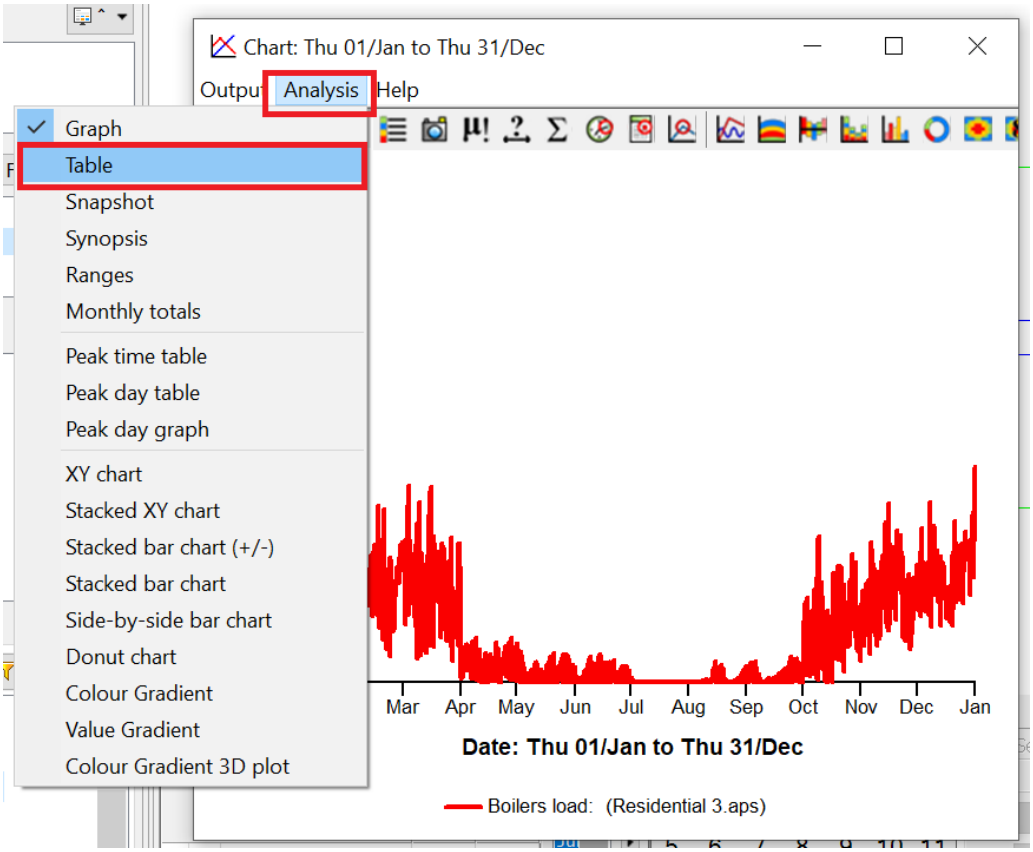

Figure A.17 Saving weather data in a text file using the Table option.

Appendix B. Continued Figure 3.11

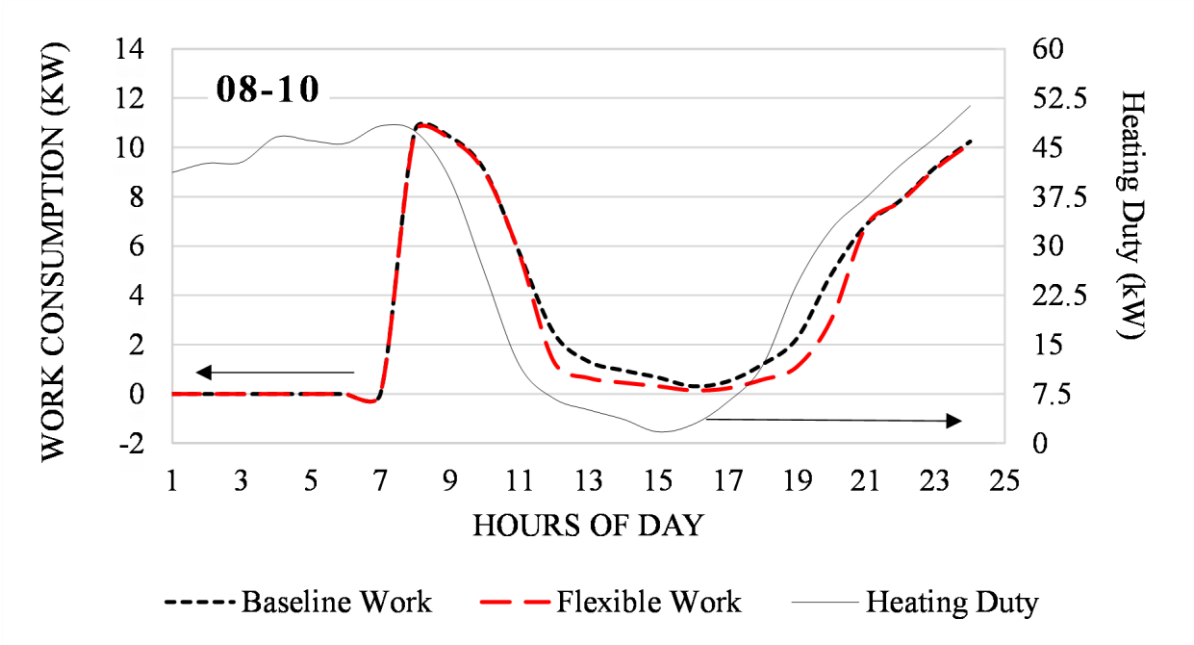

(b)

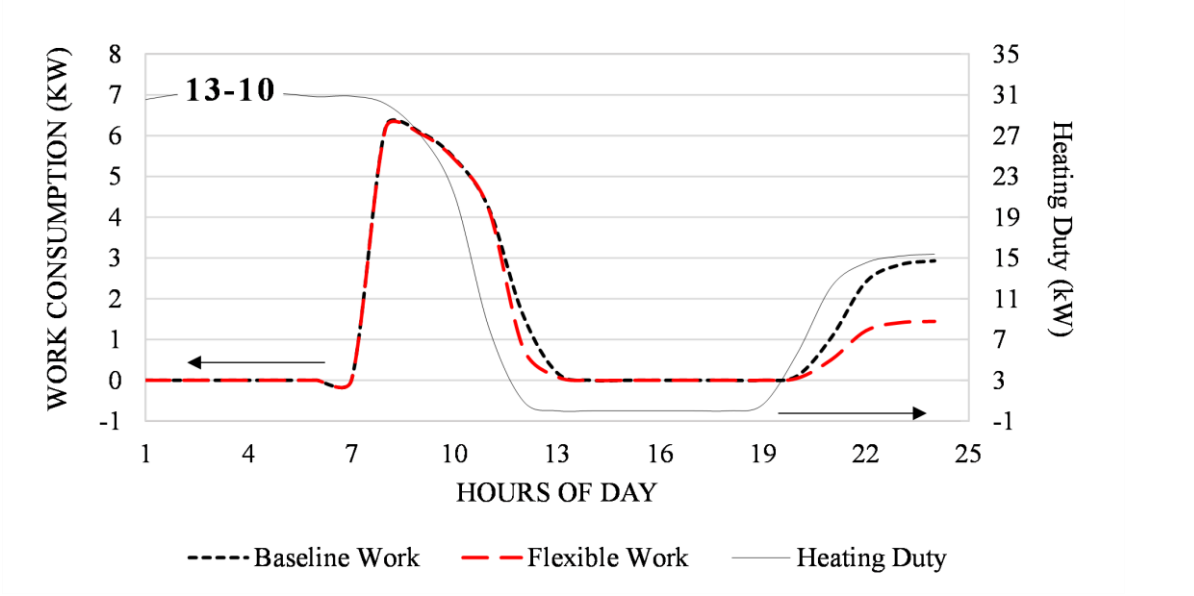

(c)

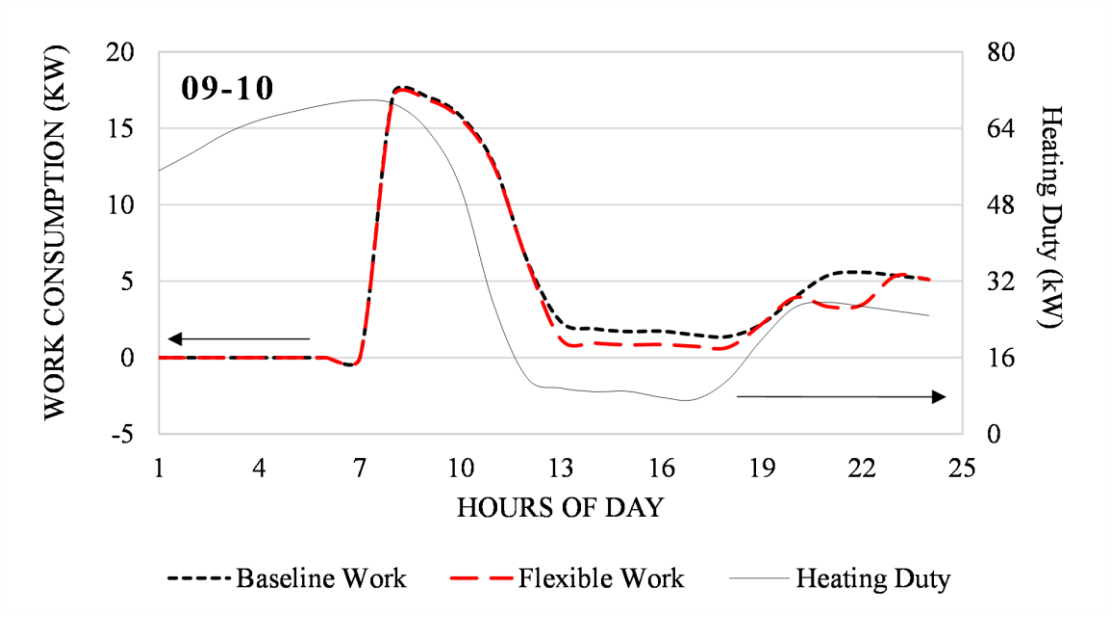
09-10
WORK CONSUMPTION (KW)
Heating Duty (kW)
HOURS OF DAY
Baseline Work
Flexible Work
Heating Duty

(d)

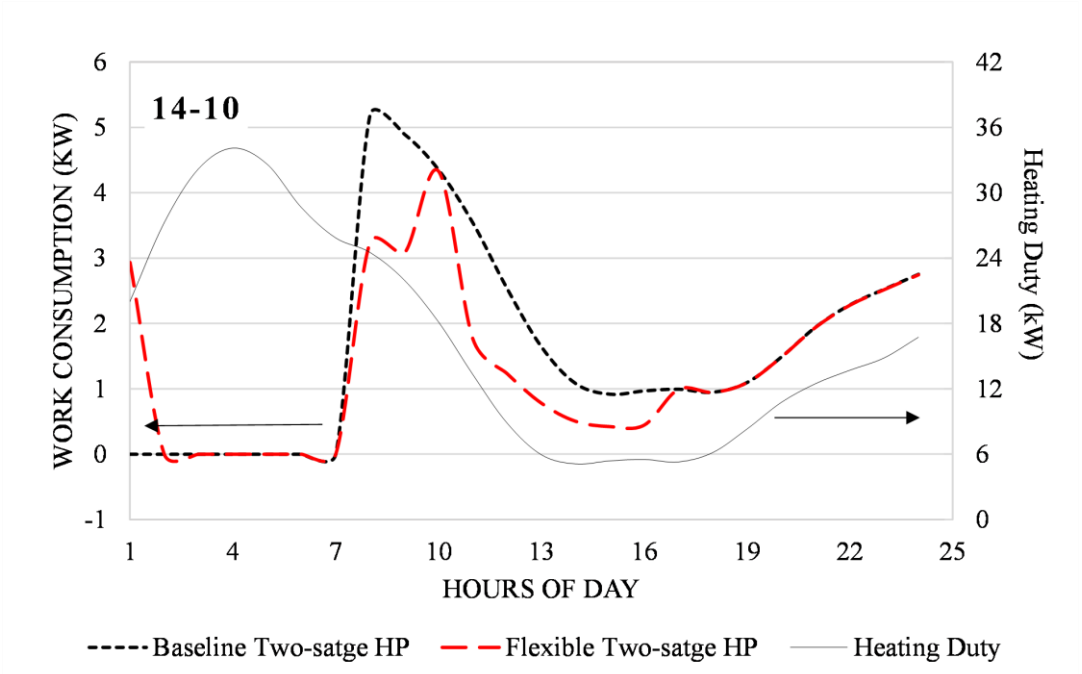
14-10
WORK CONSUMPTION (KW)
Heating Duty (kW)
HOURS OF DAY
Baseline Two-satge HP
Flexible Two-satge HP
Heating Duty

(e)

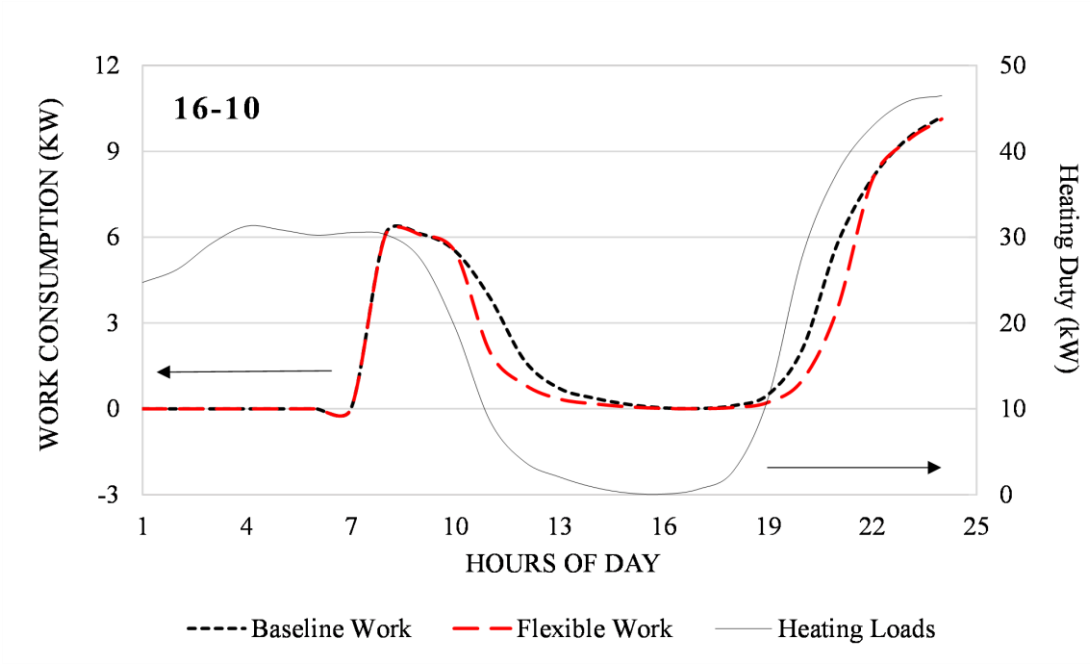
16-10
WORK CONSUMPTION (KW)
Heating Duty (kW)
HOURS OF DAY
Baseline Work
Flexible Work
Heating Loads

(f)

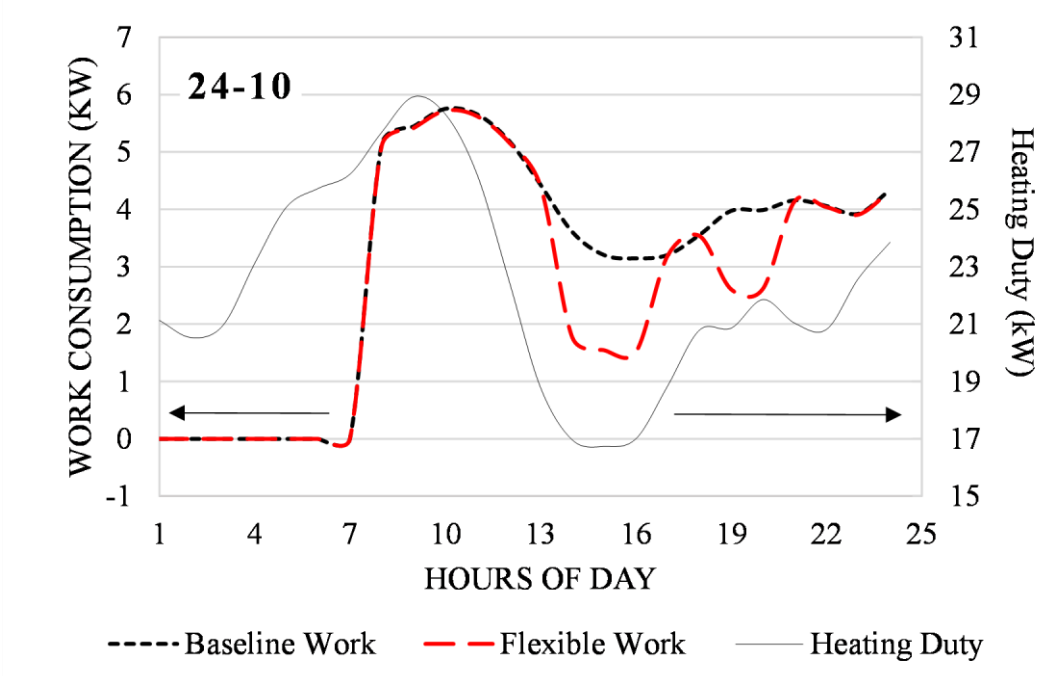
24-10
WORK CONSUMPTION (KW)
Heating Duty (kW)
HOURS OF DAY
Baseline Work
Flexible Work
Heating Duty

(f)

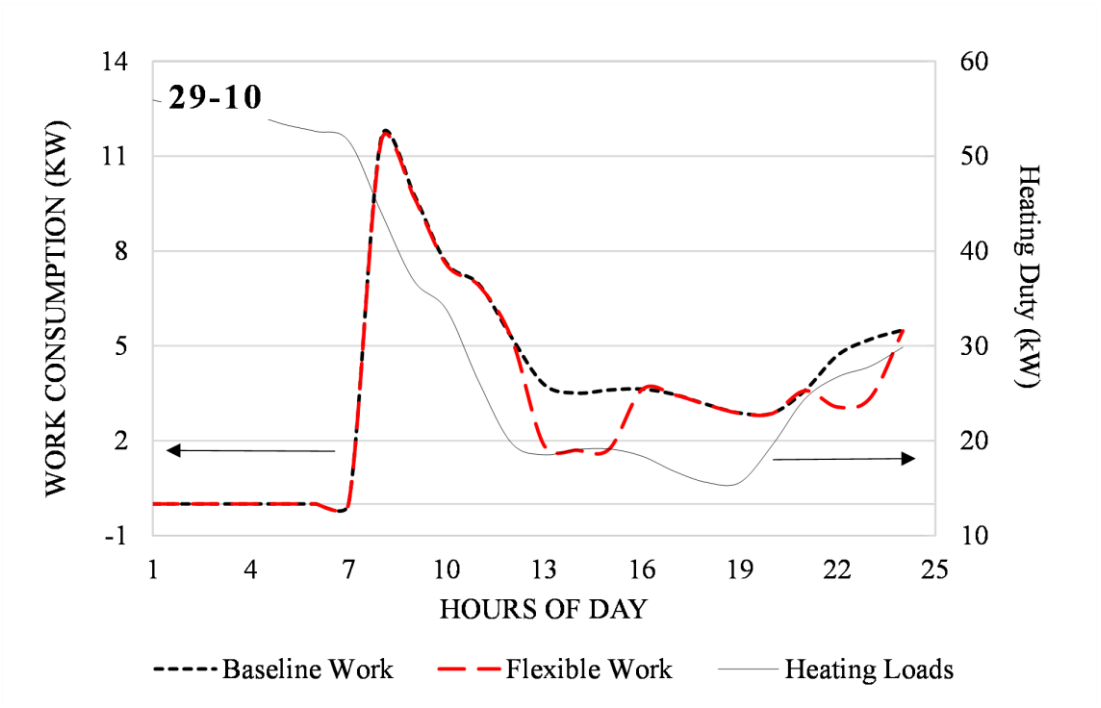
29-10
WORK CONSUMPTION (KW)
Heating Duty (kW)
HOURS OF DAY
Baseline Work
Flexible Work
Heating Loads

(g)

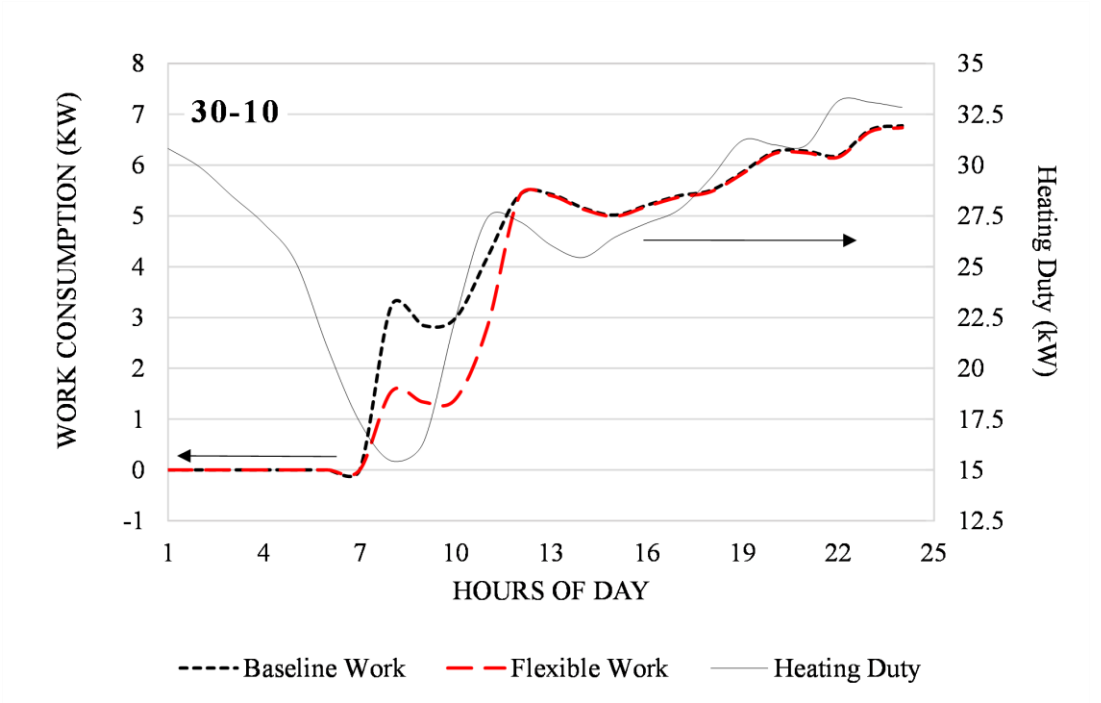
30-10
WORK CONSUMPTION (KW)
Heating Duty (kW)
HOURS OF DAY
Baseline Work
Flexible Work
Heating Duty

(h)

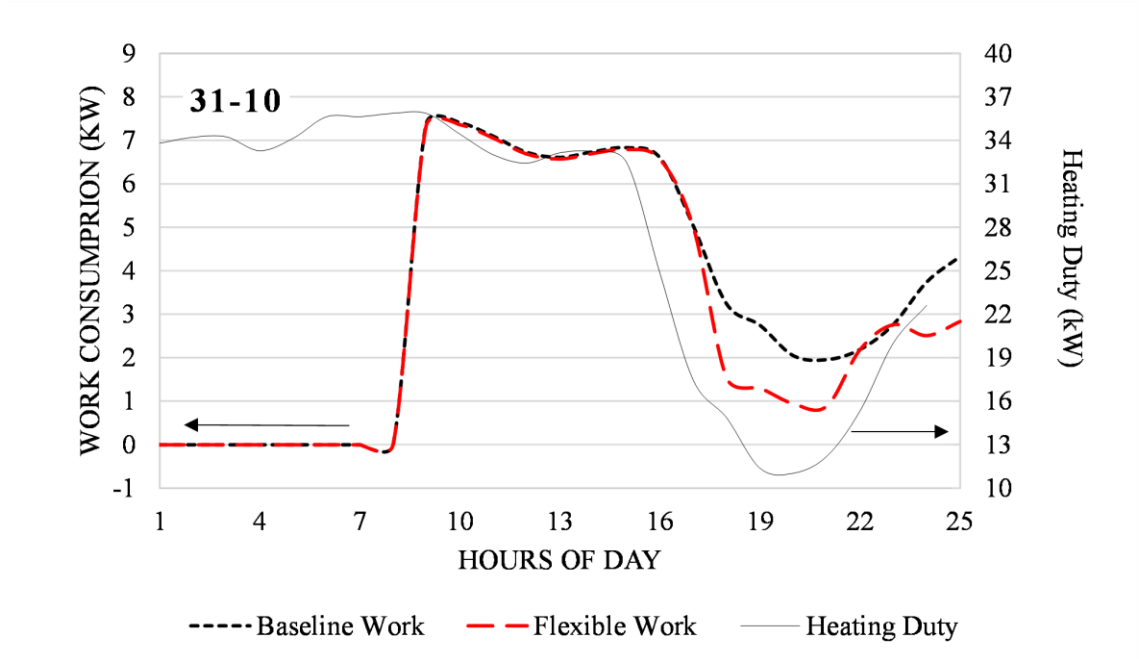

(i)

Figure B.1 Saving Daily electricity usage in heating systems for random days in October

References

1 Alizadeh, M. & Sadrameli, S. M. Development of free cooling based ventilation technology for buildings : Thermal energy storage (TES) unit , performance enhancement techniques and design considerations – A review. *Renewable and Sustainable Energy Reviews* **58**, 619-645 (2016). https://doi.org/10.1016/j.rser.2015.12.168

2 Sarbu, I. & Sebarchievici, C. in *Ground-Source Heat Pumps* (eds Ioan Sarbu & Calin Sebarchievici) 129-165 (Academic Press, 2016).

3 Abergel, T., Dean, B. & Dulac, J. *Towards a zero-emission, efficient, and resilient buildings and construction sector*.

4 Brozovsky, J., Gustavsen, A. & Gaitani, N. in *Sustainable Cities and Society* Vol. 72 (Elsevier Ltd, 2021).

5 Eveloy, V. & Ayou, D. S. Sustainable district cooling systems: Status, challenges, and future opportunities, with emphasis on cooling-dominated regions. *Energies* **12** (2019). https://doi.org/10.3390/en12020235

6 Saffari, M., de Gracia, A., Ushak, S. & Cabeza, L. F. Passive cooling of buildings with phase change materials using whole-building energy simulation tools: A review. *Renewable and Sustainable Energy Reviews* **80**, 1239-1255 (2017). https://doi.org/10.1016/j.rser.2017.05.139

7 Council, D. M. L. E. M. o. Š. C. (European Committee of the Regions, 124th plenary session, 12-13 July 2017).

8 International Energy Agency, I. Market Report Series: Renewables 2018.

9 European, C. Proposal for a DIRECTIVE OF THE EUROPEAN PARLIAMENT AND OF THE COUNCIL amending Directive 2012/27/EU on energy efficiency. (Brussels, 2016).

10 Cop. COP26 THE GLASGOW CLIMATE PACT. (Glasgow, UK, 2021).

11 gov.uk. (2019).

12 Dermentzis, G., Ochs, F. & Franzoi, N. Four years monitoring of heat pump, solar thermal and PV system in two net-zero energy multi-family buildings. *Journal of Building Engineering* **43** (2021). https://doi.org/10.1016/j.jobe.2021.103199

13 Jaysawal, R. K., Chakraborty, S., Elangovan, D. & Padmanaban, S. in *Cleaner Engineering and Technology* Vol. 11 (Elsevier Ltd, 2022).

14 Department for Business, E. & Industrial, S.

15 Zhang, L., Dong, J., Deng, S. & Yan, S. An experimental study on the starting characteristics of an improved radiant-convective air source heat pump system. *Energy and Buildings* **226** (2020). https://doi.org/10.1016/j.enbuild.2020.110384

16 (The International Energy Agency (IEA), Part of Net Zero Roadmap: A Global Pathway to Keep the 1.5 °C Goal in Reach, September 2023).

17 Cao, Y., Dhahad, H. A., Mohamed, A. M. & Anqi, A. E. Thermo-economic investigation and multi-objective optimization of a novel enhanced heat pump system with zeotropic mixture using NSGA-II. *Applied Thermal Engineering* **194** (2021). https://doi.org/10.1016/j.applthermaleng.2020.116374

18 Redko, A., Redko, O. & DiPippo, R. in *Low-Temperature Energy Systems with Applications of Renewable Energy* 1-45 (Elsevier, 2020).

19 Kelly, J. A., Fu, M. & Clinch, J. P. Residential home heating: The potential for air source heat pump technologies as an alternative to solid and liquid fuels. *Energy Policy* **98**, 431-442 (2016). https://doi.org/10.1016/j.enpol.2016.09.016

20 Moran, M. J. *Fundamentals of Engineering Thermodnamics*. (2018).

21 Arora Ramesh, C. *Refrigeration and Air Conditioning*. (PHI Learning, 2012).

22 Bejan, A. *Advanced engineering thermodynamics*. (John Wiley & Sons Inc., 2017).

23 Dincer, I. & Rosen, M. A. *Exergy*. (2012).

24 Tian, C. & Liang, N. State of the Art of Air-source Heat Pump for Cold Regions.

25 Park, C., Lee, H., Hwang, Y. & Radermacher, R. in *International Journal of Refrigeration* Vol. 60 118-134 (Elsevier Ltd, 2015).

26 Liu, J., Chen, X., Shen, J. & Wu, Y. Performance study and multi-objective optimization of two-stage compression single-screw air-source heat pump system. *International Journal of Refrigeration* **177**, 40-53 (2025). https://doi.org/10.1016/j.ijrefrig.2025.05.019

27 Fischer, D., Wolf, T., Wapler, J., Hollinger, R. & Madani, H. Model-based flexibility assessment of a residential heat pump pool. *Energy* **118**, 853-864 (2017). https://doi.org/10.1016/j.energy.2016.10.111

28 Zhang, Y., Kissick, S. & Wang, H. Modeling and Simulation of Building Cooling System With Supercooling-Based Ice Energy Storage. *Journal of Engineering for Sustainable Buildings and Cities* **1** (2020). https://doi.org/10.1115/1.4046788

29 Altuntas, M. & Erdemir, D. An investigation on potential use of ice thermal energy storage system as energy source for heat pumps. *Journal of Energy Storage* **55** (2022). https://doi.org/10.1016/j.est.2022.105588

30 Gado, M. G. & Hassan, H. Energy-saving potential of compression heat pump using thermal energy storage of phase change materials for cooling and heating applications. *Energy* **263** (2023). https://doi.org/10.1016/j.energy.2022.126046

31 Sultan, S. *et al.* PCM Material Selection For Heat Pump Integrated With Thermal PCM Material Selection For Heat Pump Integrated With Thermal Energy Storage For Demand Response in Residential Buildings. (2022).

32 Tang, W., Li, Y., Walker, S. & Keviczky, T. Model Predictive Control for Unlocking Energy Flexibility of Heat Pump and Thermal Energy Storage Systems: Experimental Results. (2025).

33 Gado, M. G. & Hassan, H. Energy-saving potential of compression heat pump using thermal energy storage of phase change materials for cooling and heating applications. *Energy* **263**, 126046 (2023). https://doi.org/https://doi.org/10.1016/j.energy.2022.126046

34 Sultan, S. *et al.* PCM Material Selection For Heat Pump Integrated With Thermal PCM Material Selection For Heat Pump Integrated With Thermal Energy Storage For Demand Response in Residential Buildings Energy Storage For Demand Response in Residential Buildings Authors Authors PCM Selection for Heat Pump Integrated with Thermal Energy Storage for Demand Response in Residential Buildings.

35 Li, G. & Zheng, X. in *Renewable and Sustainable Energy Reviews* Vol. 62 736-757 (Elsevier Ltd, 2016).

36 Lizana, J., Chacartegui, R., Barrios-Padura, A. & Ortiz, C. in *Renewable and Sustainable Energy Reviews* Vol. 82 3705-3749 (Elsevier Ltd, 2018).

37 Socaciu, L. G. Thermal Energy Storage with Phase Change Material Leonardo Electronic Journal of Practices and Technologies Thermal Energy Storage with Phase Change Material.

38 Masood, U., Haggag, M., Hassan, A. & Laghari, M. A Review of Phase Change Materials as a Heat Storage Medium for Cooling Applications in the Built Environment. *Buildings* **13** (2023).

39 Hu, W., Song, M., Jiang, Y., Yao, Y. & Gao, Y. A modeling study on the heat storage and release characteristics of a phase change material based double-spiral coiled heat exchanger in an air source heat pump for defrosting. *Applied Energy* **236**, 877-892 (2019). https://doi.org/10.1016/j.apenergy.2018.12.057

40 Ayalew, B. S. & Andrzejczyk, R. Recent Advancements in Latent Thermal Energy Storage and Their Applications for HVAC Systems in Commercial and Residential Buildings in Europe—Analysis of Different EU Countries' Scenarios. *Energies* **18**, 4000-4000 (2025). https://doi.org/10.3390/en18154000

41 Hosseinnia, S. M. & Sorin, M. Energy targeting approach for optimum solar assisted ground source heat pump integration in buildings. *Energy* **248** (2022). https://doi.org/10.1016/j.energy.2022.123528

42 Zahir, M. H. *et al.* in *Journal of Energy Storage* Vol. 64 (Elsevier Ltd, 2023).

43 Nie, B. *et al.* Development of a heat transfer coefficient based design method of a thermal energy storage device for transport air-conditioning applications. *Energy* **196** (2020). https://doi.org/10.1016/j.energy.2020.117083

44 Hutty, T. D., Patel, N., Dong, S. & Brown, S. in *Energy Reports.* 124-131 (Elsevier Ltd).

45 Real-Fernández, A. *et al.* Modeling of a PCM TES tank used as an alternative heat sink for a water chiller. Analysis of performance and energy savings. *Energies* **12** (2019). https://doi.org/10.3390/en12193652

46 Arteconi, A., Hewitt, N. J. & Polonara, F. Domestic demand-side management (DSM): Role of heat pumps and thermal energy storage (TES) systems. *Applied Thermal Engineering* **51**, 155-165 (2013). https://doi.org/10.1016/j.applthermaleng.2012.09.023

47 Sultan, S. *et al.* Techno-Economic Assessment of Residential Heat Pump Integrated with Thermal Energy Storage. *Energies* **16** (2023). https://doi.org/10.3390/en16104087

48 Lin, Y., Fan, Y., Yu, M., Jiang, L. & Zhang, X. Performance investigation on an air source heat pump system with latent heat thermal energy storage. *Energy* **239** (2022). https://doi.org/10.1016/j.energy.2021.121898

49 Bastani, A. & Tamasauskas, J. 29-46 (2023).

50 Hirschey, J., Li, Z., Gluesenkamp, K. R., LaClair, T. J. & Graham, S. Demand reduction and energy saving potential of thermal energy storage integrated heat pumps. *International Journal of Refrigeration* **148**, 179-192 (2023). https://doi.org/10.1016/j.ijrefrig.2023.01.026

51 Xu, T., Humire, E. N., Chiu, J. N. & Sawalha, S. Latent heat storage integration into heat pump based heating systems for energy-efficient load shifting. *Energy Conversion and Management* **236** (2021). https://doi.org/10.1016/j.enconman.2021.114042

52 Hu, Y. & Shen, B. Development and evaluation of a multi-functional heat pump with embedded thermal storage. *Applied Thermal Engineering* **267** (2025). https://doi.org/10.1016/j.applthermaleng.2025.125862

53 Kelly, N. J., Tuohy, P. G. & Hawkes, A. D. Performance assessment of tariff-based air source heat pump load shifting in a UK detached dwelling featuring phase change-enhanced buffering. *Applied Thermal Engineering* **71**, 809-820 (2014). https://doi.org/10.1016/j.applthermaleng.2013.12.019

54 Kumar, D. M., Catrini, P., Piacentino, A. & Cirrincione, M. Integrated Thermodynamic and Control Modeling of an Air-to-Water Heat Pump for Estimating Energy-Saving Potential and Flexibility in the Building Sector. *Sustainability (Switzerland)* **15** (2023). https://doi.org/10.3390/su15118664

55 Bertsch, S. S. & Groll, E. A. Two-stage air-source heat pump for residential heating and cooling applications in northern U.S. climates. *International Journal of Refrigeration* **31**, 1282-1292 (2008). https://doi.org/10.1016/j.ijrefrig.2008.01.006

56 Roh, C. W. & Kim, M. S. in *International Journal of Refrigeration.*8 edn 1911-1921.

57 Torrella, E., Larumbe, J. A., Cabello, R., Llopis, R. & Sanchez, D. A general methodology for energy comparison of intermediate configurations in two-stage vapour compression refrigeration systems. *Energy* **36**, 4119-4124 (2011). https://doi.org/10.1016/j.energy.2011.04.034

58 Baakeem, S. S., Orfi, J. & Alabdulkarem, A. Optimization of a multistage vapor-compression refrigeration system for various refrigerants. *Applied Thermal Engineering* **136**, 84-96 (2018). https://doi.org/10.1016/j.applthermaleng.2018.02.071

59 Torrella, E., Llopis, R. & Cabello, R. Experimental evaluation of the inter-stage conditions of a two-stage refrigeration cycle using a compound compressor. *International Journal of Refrigeration* **32**, 307-315 (2009). https://doi.org/10.1016/j.ijrefrig.2008.05.006

60 Wang, W. & Li, Y. Intermediate pressure optimization for two-stage air-source heat pump with flash tank cycle vapor injection via extremum seeking. *Applied Energy* **238**, 612-626 (2019). https://doi.org/10.1016/j.apenergy.2019.01.083

61 Lugo-Méndez, H. *et al.* Interstage pressures of a multistage compressor with intercooling. *Entropy* **23** (2021). https://doi.org/10.3390/e23030351

62 Purohit, N., Gupta, D. K. & Dasgupta, M. S. in *Energy Procedia.* 171-178 (Elsevier Ltd).

63 Kapsalis, V. & Karamanis, D. in *Applied Thermal Engineering* Vol. 99 1212-1224 (Elsevier Ltd, 2016).

64 Koşan, M. & Aktaş, M. Experimental investigation of a novel thermal energy storage unit in the heat pump system. *Journal of Cleaner Production* **311** (2021). https://doi.org/10.1016/j.jclepro.2021.127607

65 Jin, X., Zheng, S., Huang, G. & Ck Lai, A. Energy and economic performance of the heat pump integrated with latent heat thermal energy storage for peak demand shifting. *Applied Thermal Engineering* **218** (2023). https://doi.org/10.1016/j.applthermaleng.2022.119337

66 Huang, R. *et al.* Design of Phase-change Thermal Storage Device in a Heat Pump Design of Phase-change Thermal Storage Device in a Heat Pump for Building Electric Peak Load Shaving for Building Electric Peak Load Shaving "Design of Phase-change Thermal Design of A Phase-Change Thermal Storage Device in A Heat Pump for Building Electric Peak Load Shaving.

67 Bahman, A. M., Parikhani, T. & Ziviani, D. Multi-objective optimization of a cold-climate two-stage economized heat pump for residential heating applications. *Journal of Building Engineering* **46** (2022). https://doi.org/10.1016/j.jobe.2021.103799

68 Minglu, Q. *et al.* Experimental analysis of heat coupling during TES based reverse cycle defrosting method for cascade air source heat pumps. *Renewable Energy* **147**, 35-42 (2020). https://doi.org/10.1016/j.renene.2019.08.120

69 Huang, R., Mahvi, A., Kozubal, E. & Woods, J. Design of Phase-Change Thermal Storage Device in a Heat Pump for Building Electric Peak Load Shaving Preprint. (2022).

70 Gholamibozanjani, G. & Farid, M. Application of an active PCM storage system into a building for heating/cooling load reduction. *Energy* **210**, 118572-118572 (2020). https://doi.org/10.1016/j.energy.2020.118572

71 Farah, S., Liu, M. & Saman, W. Numerical investigation of phase change material thermal storage for space cooling. *Applied Energy* **239**, 526-535 (2019). https://doi.org/10.1016/j.apenergy.2019.01.197

72 Chaiyat, N. Energy and economic analysis of a building air-conditioner with a phase change material (PCM). *Energy Conversion and Management* **94**, 150-158 (2015). https://doi.org/10.1016/j.enconman.2015.01.068

73 Li, Y., Zhang, N. & Ding, Z. Investigation on the energy performance of using air-source heat pump to charge PCM storage tank. *Journal of Energy Storage* **28** (2020). https://doi.org/10.1016/j.est.2020.101270

74 Real, A. *et al.* Improvement of a heat pump based HVAC system with PCM thermal storage for cold accumulation and heat dissipation. *Energy and Buildings* **83**, 108-116 (2014). https://doi.org/10.1016/j.enbuild.2014.04.029

75 riahi, A., Mosleh, H. J., Kavian, S. & Shafii, M. B. Performance analysis and transient simulation of a vapor compression cooling system integrated with phase change material as thermal energy storage for electric peak load shaving. *Journal of Energy Storage* **35** (2021). https://doi.org/10.1016/j.est.2021.102316

76 Sanaye, S. & Hekmatian, M. Ice thermal energy storage (ITES) for air-conditioning application in full and partial load operating modes. *International Journal of Refrigeration* **66**, 181-197 (2016). https://doi.org/10.1016/j.ijrefrig.2015.10.014

77 Hoseini Rahdar, M., Emamzadeh, A. & Ataei, A. A comparative study on PCM and ice thermal energy storage tank for air-conditioning systems in office buildings. *Applied Thermal Engineering* **96**, 391-399 (2016). https://doi.org/10.1016/j.applthermaleng.2015.11.107

78 Erdemir, D. & Dincer, I. Potential use of thermal energy storage for shifting cooling and heating load to off‐peak load: A case study for residential building in Canada. *Energy Storage* **2** (2020). https://doi.org/10.1002/est2.125

79 Serale, G., Fiorentini, M. & Noussan, M. in *Start-Up Creation (Second Edition)* (eds Fernando Pacheco-Torgal *et al.*) 267-290 (Woodhead Publishing, 2020).

80 Péan, T. Q., Salom, J. & Costa-Castelló, R. Review of control strategies for improving the energy flexibility provided by heat pump systems in buildings. *Journal of Process Control* **74**, 35-49 (2019). https://doi.org/https://doi.org/10.1016/j.jprocont.2018.03.006

81 Kwadzogah, R., Zhou, M. & Li, S. in *2013 IEEE International Conference on Automation Science and Engineering (CASE)*. 442-447.

82 Epri. Principles and Practice of Demand-Side Management.

83 Hewitt, N. J. Heat pumps and energy storage - The challenges of implementation. *Applied Energy* **89**, 37-44 (2012). https://doi.org/10.1016/j.apenergy.2010.12.028

84 Clark W. Gellings, S. M. The Concept of Demand-Side Management for Electric Utilities. (1985).

85 Alasseri, R., Tripathi, A., Joji Rao, T. & Sreekanth, K. J. in *Renewable and Sustainable Energy Reviews* Vol. 77 617-635 (Elsevier Ltd, 2017).

86 Khalid, H., Amin, F. R. & Chen, C. in *Energy Procedia.* 101-108 (Elsevier Ltd).

87 Sweetnam, T., Fell, M., Oikonomou, E. & Oreszczyn, T. Domestic demand-side response with heat pumps: controls and tariffs. *Building Research and Information* **47**, 344-361 (2019). https://doi.org/10.1080/09613218.2018.1442775

88 Rapucha, A., Narayanan, R. & Jha, M. Heat Pumps with Smart Control in Managing Australian Residential Electrical Load during Transition to Net Zero Emissions. *Energies* **17** (2024). https://doi.org/10.3390/en17122977

89 Wei, W. *et al.* Performance analysis of a quasi-two stage compression air source heat pump in severe cold region with a new control strategy. *Applied Thermal Engineering* **174** (2020). https://doi.org/10.1016/j.applthermaleng.2020.115317

90 Crawley, J. *et al.* Demand response with heat pumps: Practical implementation of three different control options. *Building Services Engineering Research and Technology* **44**, 211-228 (2023). https://doi.org/10.1177/01436244221145871

91 Hanmer, C., Shipworth, D., Shipworth, M. & Johnson, C. Load shifting with smart home heating controls: satisfying thermal comfort preferences.

92 Singh, S. & Sørensen, K. in *Proceedings of The 59th Conference on imulation and Modelling (SIMS 59), 26-28 September 2018, Oslo Metropolitan University, Norway.* 87-94 (Linköping University Electronic Press).

93 Bak-Jensen, B., Sinha, R., Chaudhary, S. K. & Golmohamadi, H. in *7th European GRID SERVICE MARKET Symposium.*

94 Wang, Z., Li, G., Wang, F., Li, K. & Lou, Y. Techno-economic evaluation of a frost-free air source heat pump water heater. *Sustainable Cities and Society* **57** (2020). https://doi.org/10.1016/j.scs.2020.102102

95 Asaee, S. R., Ugursal, V. I. & Beausoleil-Morrison, I. Techno-economic feasibility evaluation of air to water heat pump retrofit in the Canadian housing stock. *Applied Thermal Engineering* **111**, 936-949 (2017). https://doi.org/10.1016/j.applthermaleng.2016.09.117

96 Navidbakhsh, M., Shirazi, A. & Sanaye, S. Four e analysis and multi-objective optimization of an ice storage system incorporating PCM as the partial cold storage for air-conditioning applications. *Applied Thermal Engineering* **58**, 30-41 (2013). https://doi.org/10.1016/j.applthermaleng.2013.04.002

97 Zhang, Q., Zhang, L., Nie, J. & Li, Y. Techno-economic analysis of air source heat pump applied for space heating in northern China. *Applied Energy* **207**, 533-542 (2017). https://doi.org/10.1016/j.apenergy.2017.06.083

98 Nolting, L. & Praktiknjo, A. Techno-economic analysis of flexible heat pump controls. *Applied Energy* **238**, 1417-1433 (2019). https://doi.org/10.1016/j.apenergy.2019.01.177

99 Alshehri, F., Beck, S., Ingham, D., Ma, L. & Pourkashanian, M. Techno-economic analysis of ground and air source heat pumps in hot dry climates. *Journal of Building Engineering* **26** (2019). https://doi.org/10.1016/j.jobe.2019.100825

100 Le, K. X. *et al.* Techno-economic assessment of cascade air-to-water heat pump retrofitted into residential buildings using experimentally validated simulations. *Applied Energy* **250**, 633-652 (2019). https://doi.org/10.1016/j.apenergy.2019.05.041

101 Iqbal, Q. *et al.* Techno-economic comparison of high-temperature and sub-ambient temperature pumped-thermal electricity storage systems integrated with external heat sources. *Journal of Energy Storage* **89** (2024). https://doi.org/10.1016/j.est.2024.111630

102 Li, Z. L., Zhang, C. L., Liu, H. M. & Wang, X. C. Feasibility analysis of thermal storage defrosting method for air source heat pump: From energetic and economic viewpoints.

Applied Thermal Engineering **236** (2024). https://doi.org/10.1016/j.applthermaleng.2023.121828

103 Mosaffa, A. H. & Garousi Farshi, L. Exergoeconomic and environmental analyses of an air conditioning system using thermal energy storage. *Applied Energy* **162**, 515-526 (2016). https://doi.org/10.1016/j.apenergy.2015.10.122

104 de Paula, C. H. *et al.* Thermo-economic and environmental analysis of a small capacity vapor compression refrigeration system using R290, R1234yf, and R600a. *International Journal of Refrigeration* **118**, 250-260 (2020). https://doi.org/10.1016/j.ijrefrig.2020.07.003

105 Mansuriya, K., Patel, V. K., Raja, B. D. & Mudgal, A. Assessment of liquid desiccant dehumidification aided vapor-compression refrigeration system based on thermo-economic approach. *Applied Thermal Engineering* **164** (2020). https://doi.org/10.1016/j.applthermaleng.2019.114542

106 The MathWorks, I. (2021).

107 Lemmon, E. W., Bell, I.H., Huber, M.L., McLinden, M.O. (National Institute of Standards and Technology, Standard Reference Data Program, Gaithersburg, 2018).

108 IESVE Virtual Environment software v. 2025 (IES (Integrated Environmental Solutions). 2025).

109 Xu, L. *et al.* An experimental energy performance investigation and economic analysis on a cascade heat pump for high-temperature water in cold region. *Renewable Energy* **152**, 674-683 (2020). https://doi.org/10.1016/j.renene.2020.01.104

110 Koopman, T., Zhu, T. & Rohlfs, W. Performance evaluation of air-source heat pump based on a pressure drop embedded model. *Heliyon* **10** (2024). https://doi.org/10.1016/j.heliyon.2024.e24634

111 Sundén, B. in *Hydrogen, Batteries and Fuel Cells* 93-110 (Elsevier, 2019).

112 Ballerini, V., Dongellini, M., Rossi Di Schio, E. & Valdiserri, P. in *Journal of Physics: Conference Series.*1 edn (IOP Publishing Ltd).

113 Chris, H. in *Octopus Energy* (https://octopus.energy/order/heat-pump/, 2024).

114 Wang, M., Cheng, Y. & Yu, J. Analysis of a dual-temperature air source heat pump cycle with an ejector. *Applied Thermal Engineering* **193** (2021). https://doi.org/10.1016/j.applthermaleng.2021.116994

115 Mokarram, N. H. & Wang, H. Design and modeling of novel two-phase heat exchangers for a home cooling system with ice energy storage. *Applied Thermal Engineering* **207** (2022). https://doi.org/10.1016/j.applthermaleng.2022.118175

116 Mokarram, N. H., Lu, Y. & Yu, Z. Peak-shaving investigation of a novel flexible two-stage heat pump for heating. *Energy Conversion and Management* **323** (2025). https://doi.org/10.1016/j.enconman.2024.119236

117 Lee, S. & Mudawar, I. Transient characteristics of flow boiling in large micro-channel heat exchangers. *International Journal of Heat and Mass Transfer* **103**, 186-202 (2016). https://doi.org/10.1016/j.ijheatmasstransfer.2016.07.040

118 Kim, S. M. & Mudawar, I. Review of databases and predictive methods for heat transfer in condensing and boiling mini/micro-channel flows. *International Journal of Heat and Mass Transfer* **77**, 627-652 (2014). https://doi.org/10.1016/j.ijheatmasstransfer.2014.05.036

119 Kim, S. M. & Mudawar, I. Universal approach to predicting saturated flow boiling heat transfer in mini/micro-channels – Part II. Two-phase heat transfer coefficient. *International Journal of Heat and Mass Transfer* **64**, 1239-1256 (2013). https://doi.org/10.1016/j.ijheatmasstransfer.2013.04.014

120 Kim, S.-m. & Mudawar, I. International Journal of Heat and Mass Transfer Universal approach to predicting heat transfer coefficient for condensing mini / micro-channel flow. *International Journal of Heat and Mass Transfer* **56**, 238-250 (2013). https://doi.org/10.1016/j.ijheatmasstransfer.2012.09.032

121 Grabcad, C. (GrabCAD, https://grabcad.com/library/micro-channel-heat-exchanger-1, 2021).

122 Hajabdollahi, H. & Seifoori, S. Effect of flow maldistribution on the optimal design of a cross flow heat exchanger. *International Journal of Thermal Sciences* **109**, 242-252 (2016). https://doi.org/10.1016/j.ijthermalsci.2016.06.014

123 Incropera, F. P., Bergman, T. L., DeWitt, D. P. & Lavine, A. S. *Fundamentals of Heat and Mass Transfer*. (Wiley, 2013).

124 Ipakchi, O., Mosaffa, A. H. & Garousi Farshi, L. Ejector based CO2 transcritical combined cooling and power system utilizing waste heat recovery: A thermoeconomic assessment. *Energy Conversion and Management* **186**, 462-472 (2019). https://doi.org/10.1016/j.enconman.2019.03.009

125 Georgousopoulos, S., Braimakis, K., Grimekis, D. & Karellas, S. Thermodynamic and techno-economic assessment of pure and zeotropic fluid ORCs for waste heat recovery in a biomass IGCC plant. *Applied Thermal Engineering* **183** (2021). https://doi.org/10.1016/j.applthermaleng.2020.116202

126 Charles, M. (https://toweringskills.com/financial-analysis/cost-indices/, 2020).

127 Mosaffa, A. H., Mokarram, N. H. & Farshi, L. G. Thermo-economic analysis of combined different ORCs geothermal power plants and LNG cold energy. *Geothermics* **65**, 113-125 (2017). https://doi.org/10.1016/j.geothermics.2016.09.004

128 Hassani Mokarram, N. & Mosaffa, A. H. Investigation of the thermoeconomic improvement of integrating enhanced geothermal single flash with transcritical organic Rankine cycle. *Energy Conversion and Management* **213** (2020). https://doi.org/10.1016/j.enconman.2020.112831

129 Noaman, M., Saade, G., Morosuk, T. & Tsatsaronis, G. Exergoeconomic analysis applied to supercritical CO2 power systems. *Energy* **183**, 756-765 (2019). https://doi.org/10.1016/j.energy.2019.06.161

130 Sanaye, S. & Shirazi, A. Thermo-economic optimization of an ice thermal energy storage system for air-conditioning applications. *Energy and Buildings* **60**, 100-109 (2013). https://doi.org/10.1016/j.enbuild.2012.12.040

131 Hajabdollahi, H. Evaluation of cooling and thermal energy storage tanks in optimization of multi-generation system. *Journal of Energy Storage* **4**, 1-13 (2015). https://doi.org/10.1016/j.est.2015.08.004

132 Sanaye, S. & Hajabdollahi, H. 4E analysis and multi-objective optimization of CCHP using MOPSOA. *Proceedings of the Institution of Mechanical Engineers, Part E: Journal of Process Mechanical Engineering* **228**, 43-60 (2014). https://doi.org/10.1177/0954408912471001

133 Suresh, C., Awasthi, A., Lee, D. & Jeon, Y. Energy and economic evaluation of combined sensible-latent thermal energy storage system with various volume fractions of phase change material. *Alexandria Engineering Journal* **98**, 344-355 (2024). https://doi.org/10.1016/j.aej.2024.04.044

134 Mokarram, N. H., Yu, Z. & Imran, M. A techno-economic survey on high- to low-temperature waste heat recovery cycles for UK glass sector. *International Journal of Green Energy* **20**, 1384-1400 (2023). https://doi.org/10.1080/15435075.2023.2197993

135 Kolahi, M., Yari, M., Mahmoudi, S. M. S. & Mohammadkhani, F. Thermodynamic and economic performance improvement of ORCs through using zeotropic mixtures: Case of waste heat recovery in an offshore platform. *Case Studies in Thermal Engineering* (2016). https://doi.org/10.1016/j.csite.2016.05.001